

Investigating Cancer Cell Dormancy and Recurrence in the Bone Marrow Niche

Jake Casson

(BSc Hons)



Submitted in fulfilment of requirements for the degree of Doctor of Philosophy (PhD)

Centre for the Cellular Microenvironment

Institute of Molecular, Cell and Systems Biology

School of Medical Veterinary and Life Sciences

University of Glasgow

Glasgow, G12 8QQ

August 2019

'There are no facts, only interpretations'

Friedrich Nietzsche

Summary

Breast cancer is the most commonly diagnosed form of cancer in women. The spread of metastatic cancer cells to secondary sites, such as the bone marrow, is the leading cause of mortality. Upon entering the bone marrow, disseminated breast cancer cells enter a period of cycling quiescence, termed dormancy. Here, cells are able to reside in the new environment for years before re-entering a growth phase, known as recurrence.

The relationship between these breast cancer cells and resident mesenchymal stem cells (MSCs) is of clinical importance. MSCs have been implicated in the initiation of breast cancer dormancy. The precise mechanism of recurrence is not known, but there is evidence to suggest the relationship between breast cancer and MSCs is of importance. Research has traditionally used two-dimensional culture techniques, however these models lack the complexity and three-dimensional nature of the bone marrow environment.

The project aimed to develop a novel, bio-responsive *in vitro* three-dimensional bone marrow model. Magnetic nanoparticle-loaded breast cancer and mesenchymal stem cells were levitated using an external magnetic field to form multicellular spheroids. These spheroids were subsequently located within a Type I collagen gel. The breast cancer cells within the spheroid exhibited quiescent behaviour when cultured in the three-dimensional environment when exposed to MSC-derived extracellular vesicles. This quiescent behaviour was reversed when the breast cancer spheroids were exposed to cytokines IL-6 and TGF β , associated with cellular repair.

Table of Contents

Summary	ii
Author’s Declaration	vii
Acknowledgements	ix
Definitions and Abbreviations	x
Units	xv
Publications	xvi
List of Tables	xvii
List of Figures	xviii
1 Introduction	1
1.1 Breast Cancer	1
1.1.i Breast Cancer Subtypes	2
1.2 Breast Cancer Cell Lines	4
1.2.i MDA-MB-231	4
1.2.ii MCF7	5
1.3 The Bone Marrow Niche	7
1.3.i Breast Cancer Metastasis to the Bone Marrow	10
1.3.ii Breast Cancer Dormancy Within The Bone Marrow	15
1.3.iii Breast Cancer Recurrence Within the Bone Marrow	18
1.4 Breast Cancer Cell Interaction with MSCs in The Bone Marrow	19
1.4.i Direct Communication – Gap Junctional Intercellular Communication	20
1.4.ii Indirect Communication – Cytokines	22
1.4.iii Indirect Communication – Extracellular Vesicles	24
1.5 Three-Dimensional Culture	26
1.5.i Scaffold-based Cultures	28
1.5.ii Spheroid Culture	31
1.6 Hypothesis and Project Aims	38
2 Materials and Methods	40

2.1 Cell Culture Solutions	43
2.2 Cell Culture	45
2.3 Cell Freezing/Thawing	46
2.4 Monolayer Culture	46
2.4.i Cell Treatments	46
2.5 Spheroid Synthesis	46
2.6 Collagen Gel Synthesis	47
2.6.i Gels Containing Multiple Spheroids	48
2.7 Collagen Gel Digestion	48
2.8 RNA Extraction	48
2.9 Reverse Transcription	49
2.10 Cell Fluorescent Imaging	50
2.11 BrdU Assay	50
2.12 Live/Dead Viability	51
2.13 Fluidigm Real-Time PCR	51
2.13.i Specific Target Amplification	51
2.13.ii Exonuclease Treatment	54
2.13.iii Sample Pre-Mix Preparation	55
2.13.iv Assay Mix Preparation	55
2.13.v Chip Priming and Loading	55
2.14 Immunofluorescent Staining	57
2.15 In Cell Western	57
2.16 μ -Slide Chemotaxis 2D	57
2.17 Cytokine Array	59
2.18 Electron Microscopy Preparation	59
2.18.i SEM	59
2.18.ii TEM	60
2.19 Conditioned Media Fractionation	60
2.20 Extracellular Vesicle Isolation and Characterisation	61
2.21 Statistical Testing	62
3 Spheroid Characterisation	63

3.1 Introduction	63
3.1.i Objectives	64
3.2 Results	65
3.2.i Cell Seeding Density	65
3.2.ii Electron Microscopy	71
3.2.iii MCF7 Spheroid Viability	77
3.2.iv BrdU Proliferation Assay	79
3.2.v Fluidigm qPCR of Co-Cultured MSC and MCF7 Spheroids	81
3.3 Discussion	87
3.3.i MSC Spheroid Culture	88
3.3.ii MCF7 Cells Generate Stable Spheroids	88
3.3.iii MCF7 Cells Become Quiescent in 3D Spheroid Culture	90
3.3.iv MSC and MCF7 Spheroid Co-Culture	91
3.4 Conclusion	93
4 Paracrine Cell Signalling in MSC/MCF7 Co-Culture	94
4.1 Introduction	94
4.1.i Objectives	96
4.2 Results	97
4.2.i Cytokine Secretions	98
4.2.ii Interleukin-6 Effects on MCF7	104
4.2.iii Transforming Growth Factor B1 Effects on MCF7	108
4.3 Discussion	111
4.3.i Cytokine Secretion Changes Upon Co-Culture of MSC and MCF7 Spheroids	111
4.3.ii IL-6 Stimulates MCF7 Cell Migration	115
4.3.iii MCF7 Migrates in The Presence of TGF β 1	116
4.4 Conclusion	117
5 MSC Migration with Interleukin-6	118
5.1 Introduction	118
5.1.i Objectives	120
5.2 Results	121

5.2.i MSCs Migrate Towards an IL-6 Gradient in Monolayer Culture	121
5.2.ii MMP-1 and MMP-3 Facilitate MSC IL-6-induced Migration in Monolayer	123
5.2.iii MSCs Spheroids Migrate in Response to IL-6	125
5.2.iv MMP-2 and MMP-8 Facilitate MSC IL-6-induced Migration in 3D Spheroid Culture	127
5.3 Discussion	129
5.3.i MSCs Migrate Towards IL-6	129
5.3.ii MSCs Secrete MMPs in Response to IL-6	131
5.4 Conclusion	134
6 Extracellular Vesicles	135
6.1 Introduction	135
6.1.i Extracellular Vesicles in Cell-Cell Communication	135
6.1.ii Cellular Metabolites in EVs	136
6.1.iii Objectives	137
6.2 Results	138
6.2.i Conditioned Media Fractionation	138
6.2.ii Quantification of MSC-Derived EVs from Conditioned Culture Medium	144
6.2.iii Effect of MSC-Derived EVs on MCF7 Migration	146
6.2.iv Effects of MSC-derived EVs on MCF7 Stemness, Proliferation and Adhesion	150
6.2.v Metabolite Analysis of MSC-Derived EV	152
6.2.vi Viability of MCF7 Treated with D-Erythrose or L-Methionine	153
6.2.vii Effects of D-Erythrose and L-Methionine on MCF7 Proliferation	157
6.2.viii Effects of Kinase Inhibitors on D-Erythrose and L-Methionine	159

6.2.ix Proliferative Effects of D-Erythrose and L-Methionine on MCF7 Spheroids	163
6.2.x MCF7 Adhesion Assay with D-Erythrose, L-Methionine and Kinase Inhibitors	168
6.2.xi Fluidigm Real Time PCR of MCF7 Cells Treated with Metabolites	170
6.3 Discussion	176
6.3.i Isolation of Extracellular Vesicles	177
6.3.ii MSC-Derived EVs Slows Growth of MCF7	178
6.3.iii Metabolites from MSC-derived EVs may Influence BCCs	179
6.3.iv Cellular Metabolites Reduce MCF7 Proliferation	181
6.4 Conclusion	183
7 Discussion	185
7.1 Project Summary	185
7.2 Prospective Applications for the in vitro model	187
7.2.i BCC Signalling	187
7.2.ii EV Contents	189
7.2.iii Pharmaceutical Screening	191
7.3 Limitations of the Model	192
7.3.i Additional Bone Marrow Cells Types	192
7.3.ii Modelling Disease Conditions	193
7.4 Conclusion	194
7.4.i Recommendations for Future Work	195
References	196

Author's Declaration

I hereby declare that the research reported within this thesis is my own work, unless otherwise stated, and that at the time of submission is not being considered elsewhere for any other academic qualification.

Jake Casson

August 2019

Acknowledgments

Of course, I should start this by thanking the University of Glasgow for letting me do my undergraduate degree and again for letting me stay, even paying me to do this PhD. I would like to thank my supervisor Dr Catherine Berry for the support and guidance over the past 4 years. I don't think I would've lasted this long with anyone else as my supervisor. Thank you also to Professor Matthew Dalby who has given advice on both the project and on general matters as well as giving me the opportunity to take part in outside engagement events. Thanks to Margaret Mullin for her assistance with electron microscopy, and both Dr Helen Wheadon and Jennifer Cassels from the Paul O'Gorman Leukaemia Research Centre for providing use of their equipment and technical advice for flow cytometry. Thank you to Dr Owen Davies for letting me visit Birmingham and harvest some EVs. Huge thanks to everyone else in CCE, or CeMi, who has provided time and advice; particularly Carol-Anne Smith helping me out and going along with my banter for years. Of course, thanks to Shijoy Mathew for so much, least of all introducing me to Dance Gavin Dance, I hope introducing you to Dragon Soop was a fair trade.

Outside of work, I wouldn't be writing this thesis without the support of Dr Hayley Macfarlane who convinced me not to give up and our rabbits for keeping me reasonably relaxed. Thank you to my mum for supporting me and making sure I get to this point. Thanks to Robert Cook for being my best friend and never saying no to drinking until dawn. Finally, thank you to CMC for giving me a job as a medical writer and saving me from a life of academic research.

Definitions and Abbreviations

2D	Two-dimensional
3D	Three-dimensional
AChE	Acetylcholinesterase
AKT	Protein kinase B
ALDH1	Aldehyde dehydrogenase 1
BAX	B-cell lymphoma 2-associated x protein
BCA	Bicinchoninic acid
BCC	Breast cancer cell
BCL2L2	B-cell lymphoma 2-like protein 2
BLM	Bloom syndrome protein
BM	Bone marrow
BMP	Bone morphogenetic protein
BrdU	5-bromo-2-deoxyuridine
BSA	Bovine serum albumin
CATHD	Cathepsin D
CCL	Chemokine ligand
CCN	Cyclin
CD	Cluster of differentiation
CDK	Cyclin-dependent kinase
cDNA	Complementary deoxyribonucleic acid
CKI	Cyclin-dependent kinase inhibitor
CO ₂	Carbon dioxide
CSC	Cancer stem cell
CTC	Circulating tumour cell
CXCL12	C-X-C motif chemokine ligand 12
CXCR	C-X-C motif chemokine receptor
DAPI	4'-6-diamidino-2-phenylindole

DMEM	Dulbecco's modified Eagle's medium
DMSO	Dimethylsulfoxide
DNA	Deoxyribonucleic acid
DTC	Disseminated tumour cell
ECM	Extracellular matrix
EDTA	Ethylenediaminetetraacetic acid
EGF	Epidermal growth factor
EGFR	Epidermal growth factor receptor
EMT	Epithelial-to-mesenchymal transition
ER	Oestrogen receptor
EV	Extracellular vesicles
FACS	Fluorescence-activated cell sorting
FBS	Foetal bovine serum
FGF	Fibroblast growth factor
FITC	Fluorescein isothiocyanate
FN-1	Fibronectin 1
G ₀	Quiescent phase
G ₁	Gap 1 phase
G ₂	Gap 2 phase
GAPDH	Glyceraldehyde 3-phosphate dehydrogenase
GAS6	Growth arrest-specific 6
G-CSF	Granulocyte colony-stimulating factor
GM-CSF	Granulocyte-macrophage colony-stimulating factor
GRO	C-X-C motif chemokine ligand 9
hBM	Human bone marrow

HEPES	4-(2-hydroxyethyl)-1-piperazineethanesulfonic acid
HER2	human epidermal growth factor receptor 2
HLA-DR	Human leukocyte antigen-DR antigen
hMSC	Human mesenchymal stem cell
HSC	Hematopoietic stem cell
hUC	Human umbilical cord
IL	Interleukin
JAK	Janus kinase
JUP	Junction plakoglobin
KCl	Potassium chloride
kDa	Kilodaltons
M Phase	Mitosis phase
MAPK	Mitogen-activated protein kinase
mBM	Mouse bone marrow
MCF7	Michigan Cancer Foundation 7
MCM	Minichromosome maintenance protein
MCP	Methyl-accepting chemotaxis protein
MDA-MB-231	M D Anderson metastatic breast cancer 2 31
MEM	Modified Eagle's medium
MET	Mesenchymal-to-epithelial transition
MgCl ₂	Magnesium chloride
MIG	C-X-C motif chemokine ligand 9
miR	Microribonucleic acid
mM	Millimolar

MMP	Matrix metalloproteinase
mNP	Magnetic nanoparticles
MSC	Mesenchymal stem cell
MSC-CM	Mesenchymal stem cell conditioned media
NaCl	Sodium chloride
NaOH	Sodium hydroxide
NEAA	Non-essential amino acid
NHS	National health service
O ₂	Oxygen
OPN	Osteopontin
ORC	Origin of recognition complex
OSX	Osterix
PBS	Phosphate buffer saline
PCR	Polymerase chain reaction
PDCD4	Programmed cell death protein 4
PDGR α	Platelet-derived growth factor receptor A
PEA	Polyester amide
PEG	Polyethylene glycol
PI3K	Phosphoinositide 3-kinase
PPAR- γ	Peroxisome proliferator-activated receptor-gamma
PR	Progesterone receptor
p-value	Probability value
RANTES	Chemokine ligand 5
RNA	Ribonucleic acid
Rpm	Revolutions per minute
SCF	Stem cell factor
SEM	Scanning electron microscopy
SNAIL	Zinc finger protein SNAI1

S-phase	DNA synthesis phase
STA	Specific target
STAT	Signal transducer and activator of transcription
STRO-1	Stromal precursor antigen-1
TEM	Transmission electron microscopy
TGFB1	Transforming growth factor beta 1
TIMP	Tissue inhibitor of metalloproteinase
TNF	Tumour necrosis factor
TNP	Triple negative phenotype
TRITC	Texas red isothiocyanate
TYRO	Tyrosine kinase
VCAM	Vascular cell adhesion molecule
VEGF	Vascular endothelial growth factor

Units

g	Gram
g	Acceleration due to gravity
L	Litre
Pa	Pascal
rpm	Revolutions per minute
T	Tesla
V	Volt
n-	nano
μ-	Micro
m-	Milli
k-	Kilo
G-	Giga
°C	Degrees Celsius
%	Percent

Publicatons

Publications authored by the candidate on conducted research relating to this thesis.

Casson, J., O’Kane, S., Smith, C.A., Dalby, M. and Berry, C., 2018. Interleukin 6 plays a role in the migration of magnetically levitated mesenchymal stem cells spheroids. *Applied Sciences*, 8(3), p.412.

Casson, J., Davies, O.G., Smith, C.A., Dalby, M.J. and Berry, C.C., 2018. Mesenchymal stem cell-derived extracellular vesicles may promote breast cancer cell dormancy. *Journal of Tissue Engineering*, 9, p.2041731418810093.

List of Tables

Table 1-1 Breast cancer cell subtypes	3
Table 1-2 Markers used for identification of MSC subpopulations and their function in vivo	8
Table 1-3 EMT markers	11
Table 1-4 Features of 2D and 3D culture.	27
Table 1-5 Summary of studies using 3D cell culture to model MSCs or cancer	28
Table 1-6 Features of different three-dimensional spheroid cell culture techniques	32
Table 2-1 List of materials, reagents and suppliers used throughout all experiments	40
Table 2-2 List of genes and primers tested using Fluidigm real-time PCR, layout for first run	52
Table 2-3 List of genes and primers tested using Fluidigm real-time PCR, layout for second run	53
Table 2-4 Thermocycler program for pre-amplification of cDNA	54
Table 2-5 Thermocycler program for exonuclease treatment of cDNA	54
Table 2-6 Cycling parameters for Fluidigm 48.48 dynamic array IFC	56
Table 2-7 Abcam 23-target cytokine array layout	59
Table 4-1 Abcam 23-target cytokine array layout	98
Table 4-2 Changes in cytokine levels of spheroid co-culture compared with spheroid monoculture at 3 and 7 days	112
Table 6-1 Candidate metabolites derived from MSC EV metabolomics	152
Table 6-2 Summary of results	176

List of Figures

Figure 1-1 Schematic of the breast cancer cell lines MCF7 and MDA-MB-231	6
Figure 1-2 Breast cancer cells within the bone marrow niche	13
Figure 1-3 The cell cycle	17
Figure 1-4 Gap junction communication between MSCs and BCCs	21
Figure 1-5 Extracellular vesicle secretion from MSCs within the bone marrow	25
Figure 1-6 Formation of Multicellular Spheroids	36
Figure 1-7 Bone marrow niche in vitro model	37
Figure 2-1 Fluidigm 48.48 access array chip	56
Figure 3-1 MCF7 spheroids seeded at three cell densities	66
Figure 3-2 MDA-MB-231 spheroids seeded at three cell densities	68
Figure 3-3 MSC spheroids seeded at three cell densities	70
Figure 3-4 Electron microscopy of multicellular MCF7 spheroids	72
Figure 3-5 Electron microscopy of multicellular MDA-MB-231 spheroids	74
Figure 3-6 Electron microscopy of multicellular MSC spheroids	76
Figure 3-7 MCF7 spheroid viability	78
Figure 3-8 BrdU proliferation marker present in MCF7 spheroids	80
Figure 3-9 $\Delta\Delta C_t$ of cell cycle gene expression in MSC spheroids in co-culture with MCF7 spheroids compared with MSC spheroid monoculture	82

Figure 3-10 $\Delta\Delta\text{Ct}$ fold change of EMT marker gene expression in MSC spheroids in co-culture with MCF7 spheroids compared with MSC spheroid monoculture	83
Figure 3-11 $\Delta\Delta\text{Ct}$ fold change of osteogenic differentiation marker gene expression in MSC spheroids in co-culture with MCF7 spheroids compared with MSC spheroid monoculture	84
Figure 3-12 $\Delta\Delta\text{Ct}$ of cell cycle gene expression in MCF7 spheroids in co-culture with MSC spheroids compared with MCF7 spheroid monoculture. Expression normalised to GAPDH	85
Figure 3-13 $\Delta\Delta\text{Ct}$ fold change of EMT marker gene expression in MCF7 spheroids in co-culture with MSC spheroids compared with MCF7 spheroid monoculture	86
Figure 4-1 MCF7 and MSC spheroids co-cultured in a collagen gel	97
Figure 4-2 Cytokine secretion of MCF7 and MSC spheroids cultured alone or together in collagen gel	99
Figure 4-3 Mean cytokine secretion profile of 3-day conditioned culture medium	102
Figure 4-4 Mean cytokine secretion profile of 7-day conditioned culture medium	103
Figure 4-5 MCF7 cell migration in the presence of an IL-6 gradient over 24 hours	105
Figure 4-6 MCF7 spheroids cultured within a collagen gel incubated with 1 ng/mL IL-6	106
Figure 4-7 Relative MCF7 spheroid diameter measurements over 24 hours in culture with IL-6	107
Figure 4-8 MCF7 cell migration in the presence of an TGF β 1 gradient over 24 hours	109
Figure 4-9 Relative MCF7 spheroid diameter measurements over 24 hours in culture with TGF β 1	110

Figure 5-1 A selected montage of six MSC images	122
Figure 5-2 MSC cell migration in the presence of an IL-6 gradient over 24 hours	123
Figure 5-3 MMPs and TIMPs detected in MSC monolayer culture	124
Figure 5-4 MSC spheroids cultured within a collagen gel incubated with 1 ng/mL IL-6.	126
Figure 5-5 MSC spheroid MMP and TIMP secretion	128
Figure 6-1 ALDH1A1 marker fluorescence of MCF7 cells cultured in MSC conditioned media	140
Figure 6-2 MCF7 spheroids cultured in collagen gel with fractioned MSC-conditioned media	142
Figure 6-3 MSC spheroids cultured in collagen gel with fractioned MCF7-conditioned media	143
Figure 6-4 Quantification of the size of MSC-derived EVs	145
Figure 6-5 EV-induced migration of MCF7 cells in monolayer	147
Figure 6-6 MCF7 spheroid cultured with MSC-derived EVs	149
Figure 6-7 The effect of a dilution series of MSC-derived EVs on MCF7 cell stemness	151
Figure 6-8 Viability assay of MCF7 cells cultured with D-erythrose or L-methionine in monolayer	154
Figure 6-9 Viability assay of MCF7 spheroids cultured with D-erythrose or L-methionine in type I collagen gel	156
Figure 6-10 Ki67 fluorescence in MCF7 cells treated with metabolites	158
Figure 6-11 MCF7 cells cultured with p38 inhibitor SB203580 or TGF β receptor kinase inhibitor SB431542	160
Figure 6-12 MCF7 cells cultured with 4 mM D-erythrose and p38 inhibitor SB203580 or TGF β receptor kinase inhibitor SB431542	161

Figure 6-13 MCF7 cells cultured with 67 mM L-methionine and p38 inhibitor SB203580 or TGF β receptor kinase inhibitor SB431542	163
Figure 6-14 MCF7 spheroids cultured with p38 inhibitor SB203580 or TGF β receptor kinase inhibitor SB431542	164
Figure 6-15 MCF7 spheroids cultured with 4 mM erythrose plus either 2 μ M p38 inhibitor SB203580 or 10 μ M TGF β receptor kinase inhibitor SB431542	166
Figure 6-16 MCF7 spheroids cultured with 67 mM L-methionine plus either 2 μ M p38 inhibitor SB203580 or 10 μ M TGF β receptor kinase inhibitor SB431542	167
Figure 6-17 MCF7 adhesion assay with D-erythrose and L-methionine and kinase inhibitors	169
Figure 6-18 $\Delta\Delta$ Ct of cell cycle gene expression in MCF7 cells cultured with 4 mM D-erythrose compared with MCF7 cells cultured without	171
Figure 6-19 $\Delta\Delta$ Ct of EMT marker expression in MCF7 cells cultured with 4mM D-erythrose compared with MCF7 cells cultured without	172
Figure 6-21 $\Delta\Delta$ Ct of EMT marker expression in MCF7 cells cultured with 67 mM L-methionine compared with MCF7 cells cultured without	174
Figure 6-21 $\Delta\Delta$ Ct of EMT marker expression in MCF7 cells cultured with 67 mM L-methionine compared with MCF7 cells cultured without	175
Figure 7-1 Scanning electron microscopy images of MCF7 cells cultured within the CELLine bioreactor	190

1 Introduction

1.1 Breast Cancer

Breast cancer is the most commonly diagnosed form of cancer in women in the UK, with around 55,000 women every year being diagnosed (Breast Cancer Now, 2016). It is forecast that as many as 1 in 8 women in the UK will develop breast cancer in their lifetime. Although it primarily affects women, annually, 350 men are also diagnosed in the UK. Despite increased awareness, 1000 women still die from the disease every month, in the UK (Breast Cancer Now, 2016). Breast cancer commonly metastasises, from the original tumour site to distant organs; this is a major factor in disease prognosis. It is estimated that 20-30% of those diagnosed will develop tumours at secondary sites (Breast Cancer Now, 2016). This spread of metastatic tumour cells throughout the body is the eventual cause of the vast majority of breast cancer-related mortality (Cancer.net, 2018). Following mastectomy or lumpectomy many patients will still go on to develop secondary tumours many years later after the initial diagnosis and therapy, demonstrating that breast cancer cells (BCCs) have a prolonged dormant phase. Whilst both improved screening methods and an increase in the number of effective drugs will help patients with relapsed cancer, research into this dormancy phenomenon is urgently required (American Cancer Society, 2017).

The most common form of breast cancer is a type of carcinoma, termed adenocarcinoma, is derived from epithelial cells and originates in the glandular tissue often in the milk ducts or milk-producing tissue (American Cancer Society, 2017). Whilst the actual causes of breast cancer are not fully understood, there are a range of contributing factors including age, family history, age during first birth and obesity (NHS, 2016; MacMahon et al, 1973).

1.1.i Breast Cancer Subtypes

There are five major breast cancer subtypes, which can be determined by the expression of several markers (table 1-1), in particular several receptor proteins expressed on the cell surface: Oestrogen receptor (ER), progesterone receptor (PR), and human epidermal growth factor receptor 2 (HER2). These subtypes can be further divided into three classes: luminal, HER2 over-expression and triple negative phenotypic (TNP; tumours lacking all three previously described surface receptors) tumours (MacMahon et, 1973). Luminal-type carcinomas are more often found within older patients, with the converse being true for basal TNP-type carcinomas (Carey et al, 2006). TNP-type carcinomas are also noted as being more aggressive and readily metastatic as they often derive from differentiated primary tumours, unlike luminal-type carcinomas, which are often poorly differentiated (Scully et al, 2012).

Table 1-1 Breast cancer cell subtypes. Five commonly recognised breast cancer subtypes and their immunohistochemical markers. Oestrogen receptor (ER), progesterone receptor (PR), human epidermal growth factor receptor 2 (HER2). Basal markers cytokeratin 5/14 or epidermal growth factor receptor (EGFR).

Subtype	Markers
Luminal A	[ER+ PR+] HER2-KI67-
Luminal B	ER+ PR+] HER2-KI67+ ER+ PR+] HER2+KI67+
HER2 over-expression	[ER-PR-] HER2+
Basal	[ER-PR-] HER2-, basal marker +
Normal-like	[ER+ PR+] HER2- KI67-

1.2 Breast Cancer Cell Lines

1.2.i MDA-MB-231

MDA-MB-231 is a triple negative cell line, lacking expression of the oestrogen and progesterone receptors (ER and PR respectively), and HER2 on the cell surface. However epidermal growth factor receptor (EGFR) is expressed (Subik et al, 2010). This cell line has several surface marker variations that contribute to its invasive phenotype; (i) low expression of claudin-3 and claudin-4, proteins associated with the formation of tight junctions between cells, thus reducing cell-cell adhesion (Herschkowitz et al, 2007); (ii) increased expression of N-cadherin on the cell surface, associated with increased motility and invasiveness (Nieman et al, 1999). Unlike E-cadherin, expression of N-cadherin reduces cell-cell contact enabling cell motility, leading to metastasis. This metastatic phenotype gives cells a long, thin appearance (Figure 1-1). MDA-MB-231 is often used as a cell model for aggressive breast cancer *in vitro*, however it is poorly invasive unless directly introduced to the circulation *in vivo* (Adorno et al, 2009). Ki67 is a marker protein for active cell cycle, expressed at all stages of the cell cycle except G₀; MDA-MB-231 expresses this at low levels as it is a slower growing cell line compared with others, also expressing marker profiles associated with cancer stem cells, namely CD44⁺/CD24^{-/low} (Holliday and Spiers, 2011).

1.2.ii MCF7

The MCF7 cell line is derived from the pleural effusion of a patient by the Michigan Cancer Foundation in the 1970s. This breast cancer cell line is well established and commonly used in research (Soule et al, 1973). It is a luminal-type cell line that expresses both ER and PR on the cell surface (figure 1-1), but does not express HER2 (Subik et al, 2010). This hormone-dependency has made this cell line ideally suited for studying the relationship between breast cancer and hormones since its isolation (Katzenellenbogen et al, 1987; Masiakowski et al, 1982; Vickers et al, 1988; Wilder et al, 2018).

E-cadherin is strongly expressed in MCF7 cells, causing cells to tightly bind together giving the cell an epithelial phenotype (figure 1-1). These cells are therefore not considered highly invasive. However, MCF7 cells exhibit high expression (~ 90%) of the prognostic factor Ki67, indicating that the cells are readily proliferate *in vitro* (Subik et al, 2010).

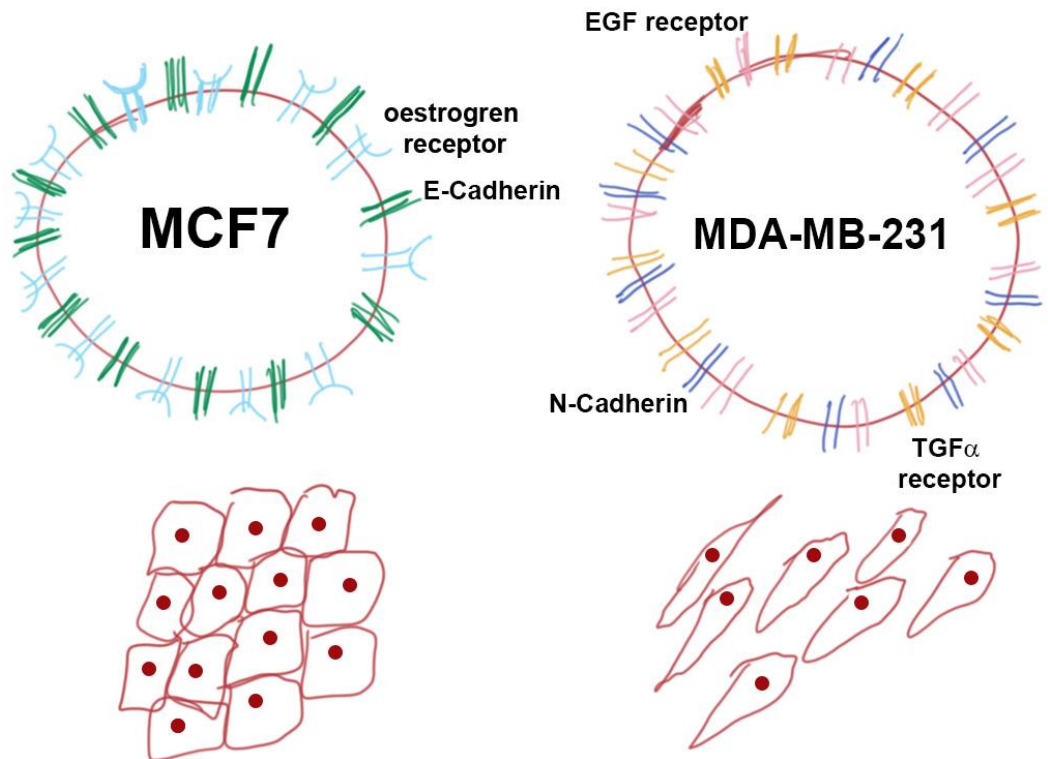


Figure 1-1 Schematic of the breast cancer cell lines MCF7 and MDA-MB-231. Luminal A type MCF7 expresses ER and PR, along with E-cadherin leading to a epithelial-like phenotype. Basal TNP MDA-MB-231 does not express ER or PR, in addition expression of N-cadherin prevents tight cell-cell binding causing the mesenchymal-like phenotype and giving this cell line a more aggressive behaviour.

1.3 The Bone Marrow Niche

The bone marrow microenvironment is richly populated with a range of different cell types. In particular, are the mesenchymal and haematopoietic stem cells (MSC and HSC respectively).

MSCs are adult stem cells that reside in many organs of the body, including the bone marrow (BM). MSCs are multipotent and are able to self-renew; producing mesenchymal lineage cells, including chondrocytes, adipocytes, osteoblasts, and myoblasts dependent on signalling cues from the environment (Baksh et al., 2007). MSCs play an important role in the healing and regeneration process, have immunomodulatory capacity, and are a key support of HSCs, the progenitors of blood and immune cells (Seita and Weissmann, 2010). MSCs can be obtained from multiple tissue sources, and several subsets exist with subtly different biological activities, making identification a complex process. The International Society for Cellular Therapy defines the minimal criteria for MSCs as follows: (1) cells must be plastic adherent under standard culture conditions; (2) cells must be positive for CD105, CD73, and CD90; negative for CD45, CD34, CD14 or CD11b, CD79 α or CD19, and HLA-DR surface molecules; and (3) cells must have the ability to differentiate into osteoblasts, adipocytes, and chondroblasts *in vitro* (Dominici et al., 2006). These properties can be validated by quantitative RNA analysis, functional analysis of relevant surface markers, and proteomic analysis (Galipeau et al., 2015).

It has been widely accepted that all MSCs express STRO-1 and CD271 (Casado-Díaz et al., 2016); many subpopulations of MSCs can be identified by the presence of marker proteins (table 1-2).

Table 1-2 Markers used for identification of MSC subpopulations and their function *in vivo*.

Marker	Source	Function	Reference
STRO-1 ⁺	BM	Promote angiogenesis. May not support HSC engraftment. Also expressed by erythroid cells.	Mo et al., 2016; Lv et al., 2014
CD271 ⁺	BM, Adipose tissue	Express higher levels of differentiation related genes than cells isolated by plastic adherence. Enhanced chondral repair. Express higher levels of immunosuppressive cytokines. Enhance HSC engraftment ability.	Álvarez-Viejo, 2015; Mo et al., 2016; Lv et al., 2014
CD105 ⁺	BM, Umbilical cord blood, Wharton's jelly	Enhanced myogenic differentiation.	Mo et al., 2016
CD146 ⁺	BM, Skeletal muscle pericytes	Enhanced osteogenic differentiation. Produce cardiomyocytes and proangiogenic factors.	Mo et al., 2016
CD44 ⁺	BM	Increased proliferation and homing capacity.	Mo et al., 2016

Nestin ⁺	BM	HSC niche and cellular support.	Mo et al., 2016
CXCR4 ⁺	BM	Enhanced migration and engraftment.	Mo et al., 2016
PDGFR α ⁺	Fetal BM	HSC supportive. Express nestin.	Pinho et al., 2013
CD51 ⁺	Fetal BM	HSC supportive. Express nestin.	Pinho et al., 2013
CD49f ⁺	BM	Multipotent, CFU-Fs. Knock-down causes HSC differentiation.	Lv et al., 2014

MSCs and other key cell types reside together within the bone marrow in two distinct niches: the endosteal niche at the edge of the bone marrow; lined with osteoblasts and remodelled by osteoclasts, and the perivascular niche situated towards the centre of the marrow where these cells line the vessels. CXCL12 is a chemokine highly expressed by MSCs and CXCL12-abundant reticular (CAR) cells within the perivascular niche (Mueller et al, 2001). CAR cells are located adjacent to sinusoids in the BM, and have been found to have a role in haematopoiesis, predominantly in supporting B cells (Eltoukhy et al. 2016). CXCL12 is recognised by the cell surface receptor CXCR4 and is required for colonisation of the bone marrow niche by HSCs. This receptor-ligand relationship leads to physical contact between HSCs and MSCs within each niche (Kiel et al, 2005).

1.3.i Breast Cancer Metastasis to the Bone Marrow

Metastasis occurs when cancer cells leave the primary tumour site and disseminate to the lymph nodes and distant organs. To enable metastasis, cells within the tumour go through an epithelial-to-mesenchymal transition (EMT) (Chaffer et al, 2016) and are able to circulate throughout the patient; at this point they are considered circulating tumour cells (CTCs). Ordinarily the immobile tumour cells at the primary site exhibit an adherent phenotype *via* proteins such as E-cadherin, and integrin family members, but upon initiation of EMT a downregulation of E-cadherin in favour of N-cadherin in addition to the upregulation of mesenchymal markers such as vimentin and fibronectin (table 1-3), promotes cell migration away from the tumour and into the local tissue and circulation (Poste and Fidler, 1980). Most of these cells will not establish secondary tumours, often being destroyed upon entry into the bloodstream by high shearing forces (Kumar and Weaver, 2009). However, cells which survive the mechanical forces present in the bloodstream induce a dramatic reorganisation of the cytoskeleton, strengthening the cell integrity; by doing so these cells persist through the transition stage, allowing adherence of cells to the vascular wall before properly exiting the blood flow (Wendt et al, 2011).

Table 1-3 EMT markers. Regulation of marker genes as cells undergo epithelial-to-mesenchymal transition, with the reverse true of mesenchymal-to-epithelial transition (adapted from Logullo et al., 2010 and Kasimir-Bauer et al., 2012).

Marker	Regulation in EMT
E-Cadherin	↓
N-Cadherin	↑
TGFB1	↑
Snail	↑
Occludin	↓
Vimentin	↑
ALDH1	↑

Upon successful transfer into a distant tissue, these CTCs become known as disseminated tumour cells (DTCs). In the case of the bone marrow, breast cancer DTCs have been found to home in on specific areas rich in E-selectin (figure 1-2; Kang et al, 2016), a protein expressed by endothelial cells that promotes shear-resistant adhesion. Once through the vessel wall, the DTCs will encounter the extracellular matrix (ECM); a three-dimensional network of extracellular macromolecules comprised largely of collagens, but additionally fibronectin, elastins and laminins. These structures support surrounding cells through binding focal adhesions - transmembrane integrins and associated protein complexes that attach to the internal cytoskeleton (Buck and Horwitz, 1987). Surviving the initial entry into this new tissue requires the DTCs to upregulate expression of integrin genes to adhere to the surrounding ECM (Mego et al, 2010). Simply binding the ECM would provide the DTC with physical support in the new environment, but local chemistry will cause it to home to areas where it might be maintained. This movement requires the DTC to degrade the ECM components using a family of endopeptidases known as matrix metalloproteinases (MMPs). Simply, these are proteins that break down

the amine bonds within ECM components to weaken the matrix and permit the cell through (Dano et al, 2005) and may be secreted or membrane-bound (Klein and Bischoff, 2011).

Once *in situ* the DTC is now able to reverse the EMT process and revert to a stationary epithelial-type cell; known as mesenchymal-to-epithelial transition (MET). The DTC requires external stimuli to initiate MET and in the case of entry into the bone marrow, much of this comes from resident MSCs. In particular, the CXCR4-CXCL12 signalling axis is used to detect a hospitable secondary site (Ray et al, 2015). DTCs express CXCR4, the cognate receptor for the ligand CXCL12, on their surface (figure 1-2). Silencing of this removes the metastatic potential of the DTC as it is unable to respond to the concentration gradient of CXCL12 produced by MSCs and cancer-associated fibroblasts (Liang et al, 2005).

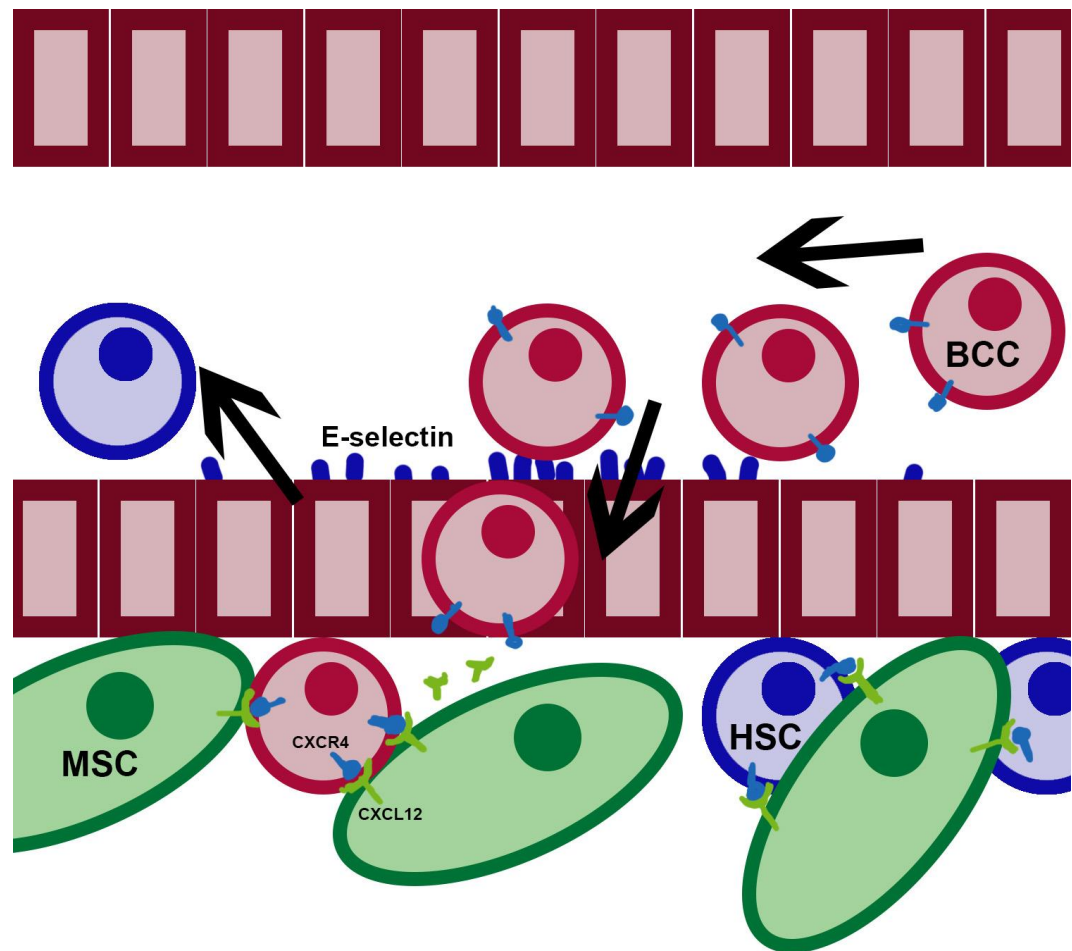


Figure 1-2 Breast cancer cells within the bone marrow niche. Circulating breast cancer cells are disseminated from the primary tumour site into the blood stream. These cells begin to adhere to the vessel walls in response to E-selectin and move between the endothelial cells, entering the BM. Reacting to environmental CXCL12 via surface CXCR4 receptors, BCCs are able to home in on MSC-maintained niches, excluding HSCs and taking residence in the BM.

Approximately 10-15% of patients are diagnosed with an aggressive type of breast cancer and will develop metastases within 3 years of detection of the primary tumour (Weigelt et al, 2005; American Cancer Society, 2017). Breast cancer does not successfully metastasise throughout the body; instead tumour cells tend to favour a suitable microenvironment that will protect them from the body's immune response. In this regard, BCCs preferentially disseminate to the bone marrow, lung and liver (Lee, 1985); tissues that confer an environment favourable for breast cancer growth (Psaila et al, 2009). The BM is the most common site of BCC metastasis, with DTCs preferentially locating to the spine, pelvis and long bones of the limbs. This is believed to be due to their expression of osteomimetic genes, such as osteocalcin and osteopontin (Rucci and Teti, 2010) permitting the DTCs survival in the new environment. These factors alter the bone microenvironment, not only affecting the remodelling of bone through induced apoptosis of osteoblasts (Standal et al, 2004), but impairing the osteogenesis of MSCs by ectopic expression of Runx2 (Pratap et al, 2008). This allows the DTCs to remain in the bone marrow microenvironment, protected by MSCs drawn to them through the CXCR4-CXCL12 axis. Macrophages within the bone marrow will be polarised to an anti-inflammatory, tumour-supporting phenotype through the secretion of cytokines (Sinha et al, 2005; Sica et al, 2006), thus will be unable to remove invading DTCs. Morbidity following metastasis to the bone is due to the effects the DTCs have on the surrounding tissue; hypercalcaemia, a condition indicated by an increase in the calcium levels in the blood, leads to a weakening of the bones as calcium leeches out into the environment (Coleman and Rubens, 1987).

1.3.ii Breast Cancer Dormancy Within The Bone Marrow

Once relocated in favourable tissue sites such as the bone marrow, DTCs can become dormant, causing no pathology. Dormancy also enables the cells to avoid both detection (due to their negligible size) and drug treatments (chemotherapy), due to their reduced proliferation and decreased metabolism. Cancer stem cells (CSCs) make up a proportion of the cells within a dormant tumour. These cells are defined as able to self-renew and initiate new tumours (McDermott and Wicha, 2010). Similar to a tumour-initiating cell, a DTC that forms new tumours, these CSCs can develop new tumours, with the major difference being the time scale (Velasco-Velázquez et al, 2012).

The phenomenon of dormancy can be described as DTCs that maintain a presence at a secondary site without forming into a detectable tumour. These dormant cells have exited the active cell cycle so do not behave like traditional cancer cells that are metabolically overactive, thus are not responsive to traditional chemotherapies (Aguirre-Ghiso, 2007). In addition dormant cells are often unable to initiate angiogenesis, actively suppressing it thereby maintaining a population by a balance of cell death and division (Holmgren et al, 1995).

To achieve dormancy, cells must exit the cell cycle and enter G_0 phase (figure 1-3). Each stage in the cell cycle is regulated by cyclins and cyclin-dependent kinases, which in turn are regulated cyclin-dependent kinase inhibitors (CKIs), such as p21 and p27. The inability for cells to move into G_1 phase can be confirmed in breast cancer cells with an increase in the expression of CDK inhibitors p21 and p27 as well as inhibiting the expression of cyclins, checkpoint proteins required for successful progression of the cell cycle (Kim et al., 2010). A common

prognostic marker for breast cancer is the proliferative protein Ki67, which is present at all stages of cell cycle except for G₀ (Bruno and Darzynkiewicz, 1992).

Dormancy is essential for cancer cells to survive in a new environment, following metastasis. Once in a dormant state, breast cancer cells are able to resist chemotherapies. Chemotherapies, such as the breast cancer-specific lapatinib, work through exploiting the high proliferative rate of cancer cells, meaning dormant cancers are unaffected (Peyvandi et al., 2019). It is believed that treatment with anti-proliferative agents can select for these resistant cells (Roesch et al., 2013). In later stage tumours, dormancy has been shown to represent an important hallmark that facilitates immune evasion (Malladi et al., 2016). The current strategy to combat the existence of dormant cancer is to reawaken the cells, thereby making them vulnerable to chemotherapy and immune destruction. This is done by targeting dormancy-promoting components secreted into the microenvironment. In the case of breast cancer this can be done with cytokines such as IL-6 or TGF β 1 (Tivari et al., 2018). This is thought to recreate the conditions seen in tissue injury; damaged cells secrete these molecules into their environment to promote division of nearby cells to repair injured areas.

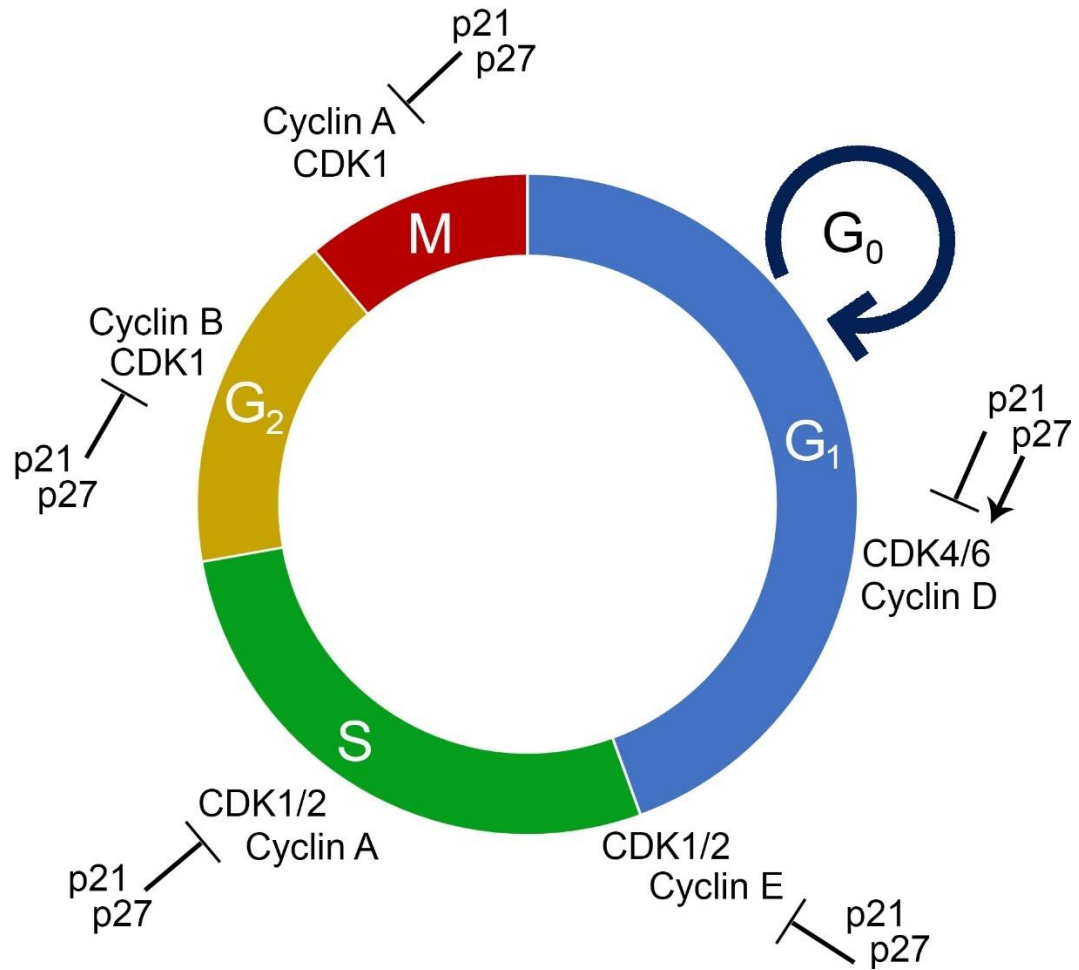


Figure 1-3 The cell cycle. The phases of cell cycle regulation; G_0 indicates a quiescent state. A dividing cell passes through a series of stages described as the cell cycle. There are two gap phases (G_1 and G_2); S (DNA synthesis) phase, when the genetic material is duplicated; and M phase, where cellular mitosis separates the genetic material and the cell divides. Each stage is regulated by cyclins and cyclin-dependent kinases, which in turn are regulated by p21 and p27 (adapted from Yoon et al., 2012).

1.3.iii Breast Cancer Recurrence Within the Bone Marrow

Cancer recurrence at secondary sites can occur years, on occasion decades, after declaration of remission. Recurrence is due to the re-entry into the cell cycle of the dormant micrometastases, which then proliferate and form tumours at the secondary site, such as the bone marrow. This is known as distant recurrence and is classed as stage IV cancer, with 34% patients living up to 5 years following this diagnosis; it is ultimately terminal (Susan G Komen Breast Cancer Foundation, 2018).

Dormant DTCs that form a micrometastasis possess a balance between pro- (vascular endothelial growth factor (VEGF), fibroblast growth factor (FGF)) and anti-angiogenic (thrombospondin, angiostatin) factors (Geleo et al., 2013). An imbalance reducing the effect of the anti-angiogenic factors will result in the micrometastasis becoming vascularised, enabling growth out to tertiary sites. Tissue inhibitor of metalloproteinases 2 (TIMP-2) normally inhibits the effect of FGF on angiogenic initiation (Murphy et al., 1993). The tumour will then grow, initiating angiogenesis so that the inner cells can receive nutrients; it will continue to expand with the possibility of a secondary metastasis to a tertiary site. The exact cause of recurrence is unknown. There is a suggestion that the advancing age of the patient may play a role. For example, in osteoporotic patients, where a bone breakage will initiate release of injury signals that activate the dormant cells, causing them to leave G_0 phase of the cell cycle and reinitiate cell division (Knupfer and PreiB, 2007) and migration through a downregulation of E-cadherin expression (Asgeirsson et al, 1998). When considering both the onset of breast cancer cell dormancy and recurrence, the cellular microenvironment and the interaction between cancer cells and resident cells within the bone marrow is critical.

1.4 Breast Cancer Cell Interaction with MSCs in The Bone Marrow

There is an evolving understanding of how the bone marrow stem cell niche operates, with several signalling axes being identified as fundamental to MSC communication. MSCs use soluble factors such as stem cell factor (SDF), vascular cell adhesion molecule (VCAM), stem cell factor (SCF), angiopoietin-1 (ang1) and chemokines such as CXCL12 to enable cellular homing and cell-cell adhesion (Anthony et al., 2014; Tamplin et al., 2015). Evidence suggests that crosstalk emerges between the tumour cells, vascular endothelia and MSCs (Ridge et al., 2017).

The interaction between resident MSCs and invading BCCs are integral to BCC long-term survival. Whilst there is a large body of literature on the communication between these two cell types within the tumour microenvironment, there is less information regarding communication within the marrow. This section will describe the various ways in which MSCs and BCCs are able to communicate and interact within the BM, which may ultimately be responsible for BCC dormancy and/or recurrence. Such communication can be indirect (eg. via cytokines, chemokines, growth factors and microvesicles) or direct (eg. via gap junctions).

1.4.i Direct Communication – Gap Junctional Intercellular Communication

Gap junctions connect adjacent cells allowing direct cell-cell contact. Gap junctions are channels, formed of a hexamer of connexin proteins, able to cross lipid membranes (Li et al, 2008). Typically, small molecules are transported through gap junctions. For example, it has been demonstrated that MSCs utilise gap junctions to transmit microRNAs (miRs) in order to influence HSC proliferation (Lim et al, 2011). These short miR nucleotides (19-23 bases) regulate gene expression through binding and subsequent degradation of intracellular mRNAs. Likewise, once BCCs have invaded the BM niche, they are also capable of developing gap junctions with MSCs (Walker et al., 2015), potentially allowing MSCs to transmit miRs that cause reduced BCC proliferation (figure 1-4; Gregory et al., 2011). For example, Lim et al (2011) demonstrated that miR-127, -197, -222 and -223 are increased in BCCs co-cultured with MSCs, affecting CXCL12 protein levels. This decrease of CXCL12 in BCCs provides an advantage to adapt dormancy within the bone marrow niche. The miRs delivered to BCCs are not limited to influencing proliferation; miR-21 has been documented as a strong tumour promoting miRNA (Sergina et al, 2007) able to interfere with the expression of the apoptotic factor Bcl-2. In addition to this, miR-21 affects the p53 pathway (Frankel et al, 2008) and cellular proliferation.

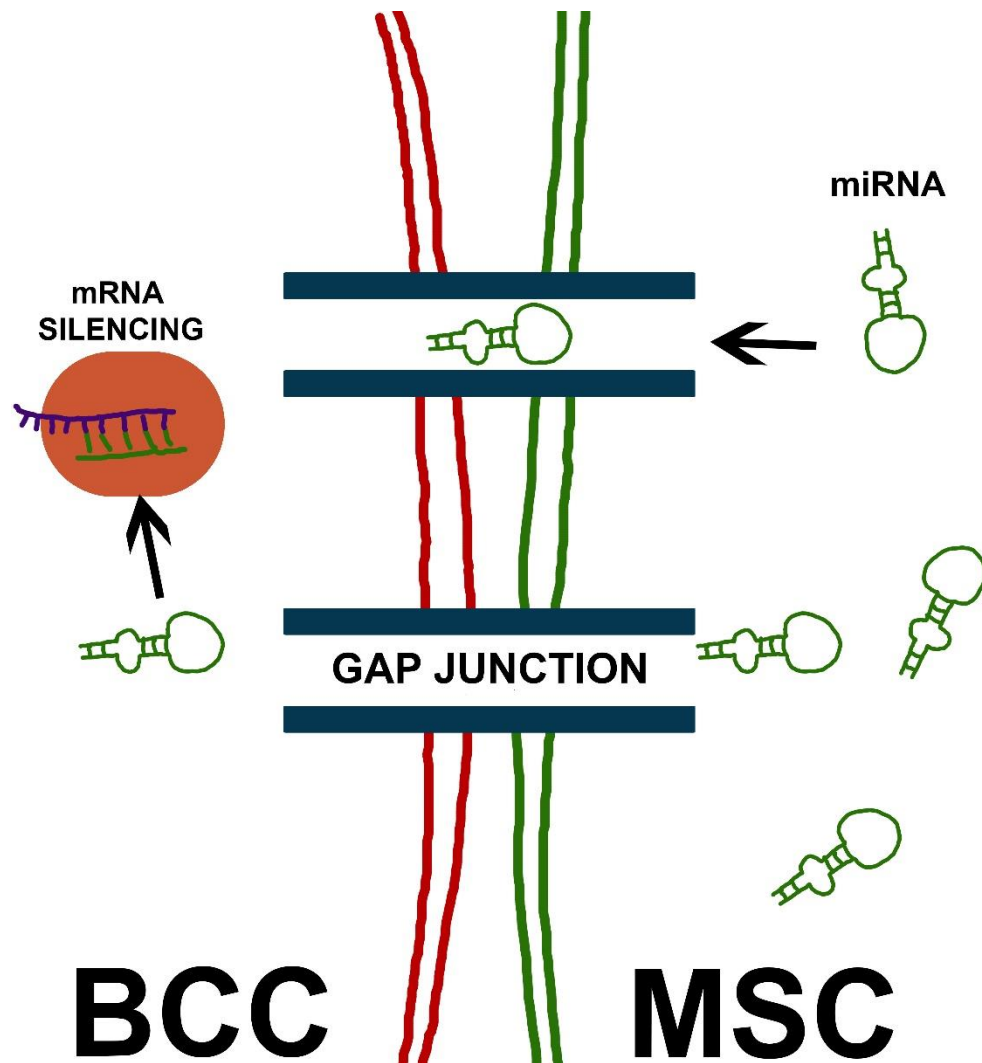


Figure 1-4 Gap junction communication between MSCs and BCCs. The formation of a gap junction between MSCs and BCCs in close proximity allows the movement of small molecules such as miRs from one cell to another. In this scenario, MSC-derived miRs may be able to translocate into BCCs where they can prevent translation of mRNAs leading to a reduction in protein expressed.

1.4.ii Indirect Communication – Cytokines

Cytokines are small proteins usually around 20 kDa, principally secreted by immune cells, which are involved in paracrine (and autocrine) signalling. Paracrine signalling is a form of cell-cell communication, whereby a cell will secrete a signal, such as a cytokine, to induce changes in a neighbouring or nearby cell. Inflammation or injury causes cellular release of cytokines such as transforming growth factor- β (TGF β), tumour necrosis factor- α (TNF- α), interleukins (including IL-1, IL-6, IL-10) and the interferons (Yagi et al, 2012). The release of proinflammatory cytokines, such as IL-6, into the primary tumour environment can lead to EMT and metastasis (Castellana et al., 2015); conversely, the release of anti-inflammatory cytokines can have the opposite effect upon BCCs and this action is key in initiating MET in metastatic BCCs, allowing them to take up residence in distant tissues such as the BM.

The release of cytokines by MSCs in the BM can influence immune cells in close proximity and allows for maintenance of their niche, communicating with other cell types such as HSCs; invading BCCs are able to take advantage of the immune tolerant features and chemotactic properties of MSCs to support cell survival (Psaila et al, 2009). MSCs secrete immunomodulatory molecules, such as IL-8, that inhibit the maturation of cytotoxic T cells and attenuate the effect of inflammatory macrophages by causing naïve cells to preferentially become the anti-inflammatory M2 subtype (Caplan and Sorrell, 2015; Vasandan et al, 2016). Where DTCs would ordinarily be cleared away from tissue by these immune cells, the presence of MSCs prevents this clearance and allows the DTCs to establish themselves within the niche. These invading BCCs express high levels of CXCR4, similar to resident HSCs, and use this to home in on MSCs (figure 1-5). Using this signalling axis, the DTCs are able to outcompete many of the HSCs, preventing them from maintaining their

position in the niche, excluding them from the BM and forcing them to circulate in the bloodstream (figure 1-2). Once in the bloodstream, HSCs will differentiate and are unable to self-renew to maintain their population in the bone marrow. This affects the ability for the patient to generate progenitor cells, such as immune cells, worsening prognosis (Scheuttpelz and Link, 2013).

Whilst the CXCL12/CXCR4 signalling axis is an important maintenance factor of the stem cell niche, aside from enabling BC homing to MSCs in the marrow, it can also aid survival once the DTCs reach their destination (Corcoran et al, 2008), Binding of CXCL12 to surface CXCR4 leads to activation of downstream AKT (Zhang et al, 2009), a signalling pathway known to inhibit apoptosis, promoting cell survival.

MSCs secrete cytokines, such as CXCL12, into their environment to maintain the stem cell niche, in particular the nearby HSCs. DTCs entering into the BM use these cytokines as concentration gradient to home towards the stem cell niche in the bone marrow (figure 1-2), where they can be protected from the immune response by the resident MSCs. The cancer cells can then alter their phenotype through the downregulation of cell cycle proteins and the upregulation of adhesion proteins such as E-cadherin, resulting in cycling quiescence.

1.4.iii Indirect Communication – Extracellular Vesicles

Another form of indirect cell-cell communication is via the release of extracellular vesicles (EVs). EVs are small membrane-bound packets of signalling molecules secreted by cells into the local environment, capable of influencing nearby cells (Ono et al, 2014). EVs are mainly comprised of microvesicles and exosomes (figure 1-5). Microvesicles are large vesicles (50-1000nm in diameter), which are formed through the compartmentalisation of the plasma membrane during cell membrane remodelling, thereby entrapping cytoplasmic molecules (Komalska et al, 2015) (figure 1-6). Following release from the parent cell, the microvesicles can subsequently fuse with neighbouring cells, transferring information directly into the cytoplasm. Exosomes are smaller vesicles (<150nm), which are created when early endosomes form multivesicellular bodies.

Both microvesicles and exosomes contain a multitude of molecules including miRs, cellular metabolites, cytoplasmic proteins and nucleic acids. These molecules are trafficked into neighbouring cells through endocytosis. Released in larger numbers than microvesicles, due to their small size, exosomes will readily enter neighbouring cells. It is possible to see a reduction in proliferation in BCCs as a result of MSC exosome exposure (Walker et al., 2015). Ono et al. (2014) have shown that exosomes derived from MSC-BCC co-cultures contain multiple miRNAs. One such miRNA is miR-23b, which when overexpressed in BCCs suppresses the gene *MARCKS* (Myristoylated alanine-rich C-kinase substrate), important in cell cycle. Further to this, Ota et al. (2011) report that accumulation of miR-21 and miR-181a cause recurrence by affecting *PDCD4* (programmed cell death protein 4) translation, preventing cell death.

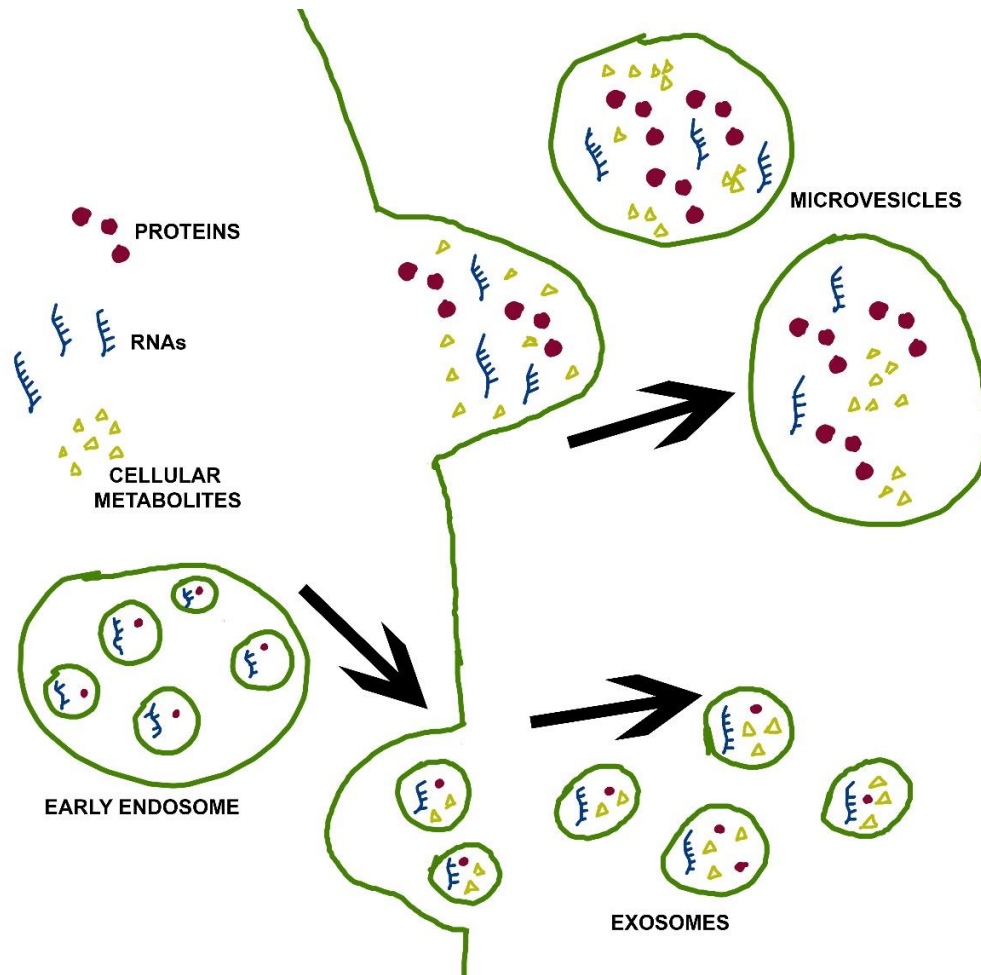


Figure 1-5 Extracellular vesicle secretion from MSCs within the bone marrow. MSCs transmit packets of signalling molecules through the formation of vesicles. Microvesicles (50-1000nm) form at the cell surface capturing internal cellular components (including RNAs, metabolites and proteins) these vesicles are excreted and fuse with neighbouring cells. Exosomes (<150nm) are formed through a combination of the repackaging of molecules brought into the cell and stored in early endosomes and molecules passed through the Golgi complex. Exosomes fuse with the parent cell membrane, exocytose and interact with neighbouring cells (adapted from Hessvik and Lorente, 2018).

1.5 Three-Dimensional Culture

In order to determine the mechanisms that underlie BCC dormancy and recurrence within the bone marrow, focused studies on the microenvironment and cellular signals that mediate the fate of these BCCs are urgently required. Therefore, bioengineered, *in vitro* approaches to model the bone marrow niche are becoming important research tools. Advances in tissue-engineered platforms to induce, model and monitor BCC dormancy and recurrence may provide much needed insight into the regulation of these processes and potentially serve as drug testing platforms (Pradham et al., 2018).

The BM has a complex architecture; organ structures such as the endosteum, ECM components such as collagen, vascular structures including sinusoids and several different cell types. This contributes to a unique physiochemistry that cannot be easily reproduced *ex vivo*. *In vitro* modelling of the BM niche requires consideration of matrix stiffness, topography and local chemistry, as alteration of these factors can affect MSC differentiation (Dalby et al. 2007; Kilian et al. 2010; He et al., 2016). Whilst there are advantages to culturing cells in two-dimensions, culturing on hard plastic surfaces will affect many aspects of the cell (table 1-4), particularly when attempting to model the BM. The stiffness of culture plastic is many orders of magnitude higher than the softer ECM of the BM.

To date, there have been many attempts to recreate metastasis of breast cancer cells to the bone marrow. For example, Bersini and colleagues (2014) attempted to use microfluidics to recreate the extravasation of breast cancer cells as they enter the bone marrow environment, showing that the metastatic cells homed in to MSCs through sensing of cytokines secreted into the environment. MSCs resident in the bone marrow microenvironment have also shown to positively affect the

growth of incoming breast cancer cells. It is the paracrine secretions of MSCs that are primarily able to enhance the proliferation of oestrogen receptor positive breast cancers such as MCF7 (Sasser et al., 2007).

Table 1-4 Features of 2D and 3D culture. Comparison of two and three dimensional cell culture with respect to cells cultured in the native bone marrow (adapted from Nath and Devi, 2016).

Features	2D	3D
Spatial restriction of cells	✓	✗
Concentration gradient of O ₂ , nutrients, and metabolic wastes	✗	✓
Heterogenous clonal subpopulations	✗	✓
Hypoxic core	✗	✓
Biological zones – proliferative, quiescent and necrotic zones	✗	✓
Nutrient diffusion	Low	High
Gene expression profile	Different	Similar

1.5.i Scaffold-based Cultures

To date, there have been many studies developing 3D culture techniques for both MSCs and cancer cells, in an attempt to recapitulate the *in vivo* situation. These are summarised in tables 1-5. These techniques commonly involve the use of a matrix or scaffold to physically support cell growth. Scaffolds can either be biocompatible synthetic materials, such as polycaprolactone and polyethylene glycol, or components natively found in the ECM; collagen, gelatin, or hyaluronan. MSCs grown in 3D environments, whether it be scaffolds, sponges or gels, demonstrate enhanced differentiation capacity and self-renewal, and have potential for scalability (Hong et al., 2015). There are limitations to these scaffolds, as the *in vivo* environment is more complicated than we are able to recapitulate *in vitro*, the whole picture is not represented. Whilst we may be able to recreate the stiffness of any given environment, the material may not be an exact match. However these 3D environments are still an improvement of the traditional 2D cell culture methods.

Table 1-5 Summary of studies using 3D cell culture to model MSCs or cancer (adapted from Hong et al., 2015; Nath and Devi, 2016).

Technique/ Material	Cells	Results	Reference
Hanging drop	hBM-MSCs	Apoptosis Model in fibrin hydrogel. Resistance to apoptosis and enhanced proangiogenic potential	Murphy et al., 2014
	Rat MSCs	Brain injury Comparison of MSCs derived from monolayer and 3D spheroids	Guo et al., 2014

	hMSCs and Breast Cancer	BCCs cannibalise MSCs to enter dormancy	Bartosh et al., 2016
	hBM-MSCs	Spheroids enhance anti-inflammatory properties	Bartosh et al. 2010
Low adherence forced aggregation	MSCs	MSC expansion (scale up) Serum free media optimised	Alimperti et al. 2014
	mBM-MSCs	Enhance utility of MSCs for therapies No necrosis, enhanced multilineage potential	Baraniak & McDevitt 2012
	hBM-MSCs	Investigate role of the cytoskeleton 3D aggregation alters mitochondrial function, and induces functional activation, and cellular stress response	Tsai et al., 2015
Polydimethylsiloxane (PDMS)	Breast cancer	3D spheroids more resistant than 2D-cultured cells to TRAIL-mediated apoptosis and have stem-like characteristics	Chandrasekaran et al., 2014
	Prostate Cancer	3D spheroids are more resistant to chemotherapy than 2D-cultured cells	Chambers et al., 2014

Matrigel	Breast Cancer	Comparative analysis of gene expression and signalling of 2D and 3D cultures.	Kenny et al., 2007
Microfluidics micromasses	hBM-MSCs	'Developmental engineering' for skeletal tissue regeneration. Exposure to morphogens identified chondrogenic concentrations	Occhetta et al., 2015
Micropatterned substrates	hMSCs	Assess potential for tissue engineering greater differentiation capacity: downregulation of self-renewal genes	Wang et al. 2009
Collagen/hyaluronic acid/ 1-ethyl-3(3-dimethylaminopropyl) carbodiimide scaffold	hMSCs	3D elastic modulus Human MSC Brain/spinal cord Stiffness induced differentiation	Her et al., 2013
Magnetic Levitation in type 1 collagen gel	hBM-MSCs	Characterise MSCs in magnetically levitated; more quiescent in spheroids	Lewis et al., 2017
	hBM-MSCs	Probe wound healing response MSCs migrate from spheroid in response to co-culture wounding	Lewis et al., 2016
Chambered slides	Synovial CD105+ MSCs	Chondrogenesis Chondrocytes were produced by spheroids	Arufe et al., 2009

Agar	Ovarian Cancer	Growth and radiation sensitivity was measured in 3D spheroids	Rofstad and Sutherland, 1989
Chitosan	hUC-MSCs	Cell-matrix interaction Calcium signalling inside spheroid	Yeh et al. 2014
	hMSCs/ endothelial progenitors	Angiogenesis. Sphere morphology influenced by cell-substrate interaction	Hsu et al., 2014
	Adipose tissue MSCs	Maintain stemness Upregulation of pluripotency genes, enhanced differentiation	Cheng et al., 2012

1.5.ii Spheroid Culture

More recently, 3D MSC culture techniques have involved creating cellular aggregates, termed spheroids. These cell spheroids facilitate cell-cell interactions, replicate gradients of nutrients and oxygen that would be observed *in vivo*, and can generate their own ECM (Cesarz & Tamama 2016). Traditional methods of spheroid generation include the using hanging drops of culture medium and non-adherent conditions, both of which force cells to aggregate. However further techniques have been recently reported, such as aggregating cells via magnetic levitation utilising magnetic nanoparticles.

The use of spheroids over traditional monolayer culture allows the recapitulation of *in vivo* characteristics; growth kinetics, cellular heterogeneity, cell signalling and gene expression mimic that of the native

physiology (table 1-4). The use of spheroid culture for MSCs has gained attention more recently, with benefits including retention of stem cell markers when compared to corresponding monolayer cultured cells and cell quiescence (Sart et al, 2014), vastly different gene expression profiles (Potapova et al, 2007) and providing new targets to combat autoimmune disease (Bartosh et al, 2010) (table 1-6).

Table 1-6 Features of different three-dimensional spheroid cell culture techniques (adapted from Nath and Devi, 2016).

Technique	Advantages	Disadvantages
Matrix-on-top and matrix-embedded	Cells can be recovered post culture if self-aggregating protein-based hydrogel is used	Hydrogel requires special handling. Yields heterogenous spheroids requiring sorting before assay Challenging to stain and image matrix-embedded spheroids
Matrix encapsulation (microfluidic device)	Yields homogenous spheroids circumventing sorting prior to assay	Slower growth rate due to confinement. Capsule may burst if the matrix shell is thin. Increased occurrence of necrosis due to confinement
Micropatterned plates	Spheroids can be imaged with relative ease. Post culture recovery is possible ECM component is present	Well needs to be coated to create low adhesion surface. Generates spheroids of variable sizes.

		Multiple spheroids in a well can overwhelm assay chemistry.
Hanging drop	<p>Large number of spheroids obtained in a limited space</p> <p>Ideal for studying invasive potential of cancer cells</p> <p>Reduced reagent consumption</p> <p>Post-culture recovery is possible</p>	<p>Labour-intensive</p> <p>Spheroids must be transferred from the hanging drop to a second, higher volume plate for long-term culture</p> <p>Spheroids are transferred to a secondary plate for endpoint analysis.</p>
Ultra-low attachment plates	<p>Inexpensive and easy to handle</p> <p>Large number of spheroids can be obtained in a limited space (96 well or 384 well)</p> <p>Endpoint analysis can be done on the same plate</p> <p>Post-culture recovery is easy</p> <p>Can be multiplexed with imaging and other biochemical assays.</p>	<p>Generates spheroids of variable sizes</p> <p>May have a mixture of attached cells and spheroids</p>
Magnetic levitation and	Can be multiplexed with imaging and other biochemical assays	<p>Limited number of spheroids</p> <p>Beads are expensive</p>

magnetic bioprinting	Endpoint analysis can be done on the same plate.	Cells need to be pre-treated with magnetic beads.
----------------------	--	---

With respect to cancer cells, a large spheroid (>500 μm in diameter) will behave in the same way as micrometastases and avascular tumours *in vivo*; central cells will experience hypoxic conditions due to the limited diffusion of oxygen and nutrients into the mass, in addition to the difficulty in disposing of metabolic waste. Therefore, a large spheroid is ideal to study the effects of physiochemical gradients on tumour cells *in vitro* (Groebe and Muller-Kleiser, 1991; Mehta et al., 2012). Depending on the size of the spheroid, it will comprise a heterogeneous cell population arranged into layers: an innermost necrotic core where cells are able to exchange nutrients; a layer of viable, quiescent cells, able to receive nutrients from the environment, but compressed by the outermost cells; and a peripheral layer of proliferating cells able to migrate into the environment (Bell et al., 2001; Hirschhaeuser et al., 2010). Spheroid culture is therefore advantageous for breast cancer dormancy/recurrence research (Korah et al, 2004; Smith et al, 2010; Child et al, 2011; Dejardin et al, 2011; Marlow et al, 2013; Ono et al, 2014; Cesarz & Tamama, 2015; Romero-Moreno et al, 2018).

These recent studies involving multicellular spheroids have used many methods of forming the 3D structures (Table 1-6), of which a common method is the use of low-attachment culture plates. These have a rounded bottom that allows cells to roll as they attempt to attach themselves to the plastic surface. These can produce large spheroids, however, it can also lead to variable sizes, dependent on the number of cells seeded at the beginning. Another disadvantage of this method is analysis of the spheroids themselves. Unlike other methods, formation requires gravity alone, so analysis of cells within the central mass is

difficult without slicing the spheroids into sections to expose the central cells to immunohistochemical stains or similar. Another method used involves chitosan membranes to prevent cells from spreading on a surface, forcing them to form into 3D masses. However, similar to other methods, spheroids produced can be of variable size, making experimentation difficult (Cesarz & Tomama, 2015).

Spheroid culture has been routinely used for tumour research, for example demonstrating how ovarian cancers become chemotherapy-resistant through changes in metabolism (Liao et al, 2014; Sato et al, 2015), assessing how local stress affects growth of primary breast cancer (Cheng et al, 2009) in addition to facilitating high-throughput screening of drugs (Benton et al, 2015). The formation of spheroids in the study of cancers can also be used to mimic circulating tumours and micrometastases that have broken away from the primary tumour and have been able to enter to circulation or a secondary site, such as the bone marrow (Cho et al., 2012).

The technique used in studies herein involves using fluorescently labelled magnetic nanoparticles (mNPs) to label cells and subsequently levitating them to form multicellular spheroids. The spheroids generated are robust and readily visualised using the fluorescent properties associated with the mNPs.

Although mNPs are available in a range sizes, this project will utilise particles of 200 nm as previously work has determined them to be ideally suited for spheroid generation (Lewis et al., 2016) as the cells readily internalise and retain them. These NPs will freely enter cells through multiple pathways; exposure to a magnetic source aids this endocytosis and generates cells that will be drawn towards a magnet. This phenomenon is then exploited to force the individual cells into

multicellular spheroids (figure 1-6). Over a period of 24 hours, cells are brought together under the force of a magnet and associative bonds form, giving robust multicellular spheroids that can be moved without damaging the three-dimensional structure. These can then be cultured in collagen gel that has a stiffness resembling the native BM. Levitating the spheroid through the gelation process will surround the spheroid in the three-dimensional environment preventing adhesion to the culture plastic underneath (figure 1-7).

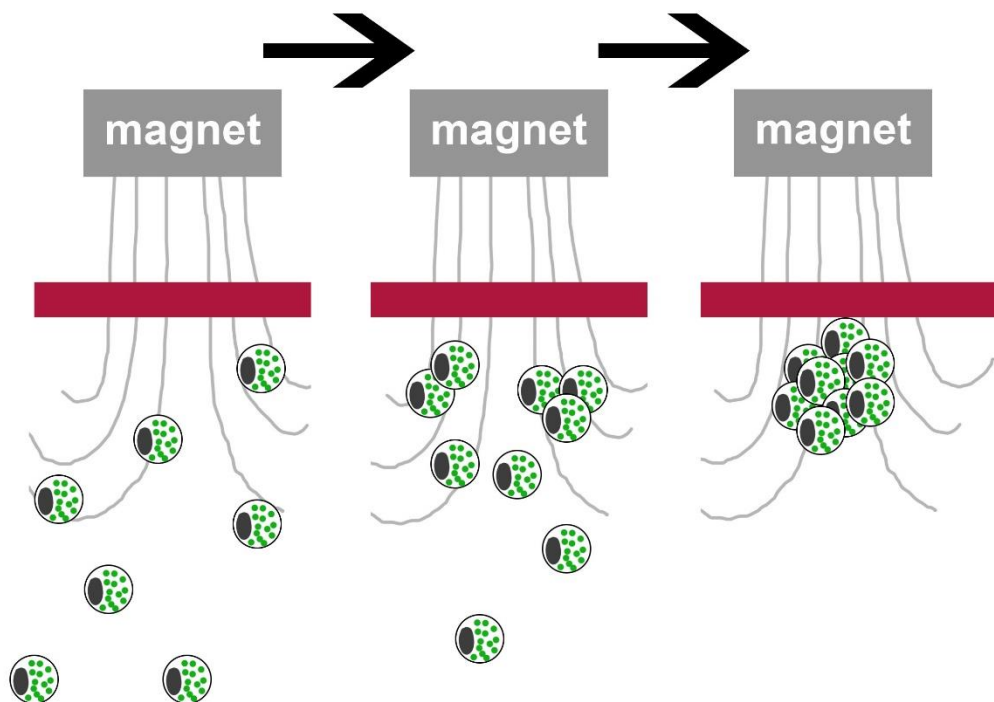


Figure 1-6 Formation of multicellular spheroids. Cells containing magnetic nanoparticles are reseeded into 6-well plates containing 4 mL of culture medium. 350 mT magnets are placed on the lid, approximately 1 cm from the surface of the liquid, sufficient distance from which to influence cells in the media. Cells are drawn towards the magnet, but prevented from leaving the culture medium by surface tension. This phenomenon forces the cells to be in close proximity with one another. Over a 24 hour period, cells move close enough that they may form cell-cell contacts through mechanisms such as E-cadherin dimerisation. This is

similar to a method originally published by Souza et al in 2010. The multicellular spheroids can then be transferred from the culture medium into collagen gels, without damaging the 3D superstructure.

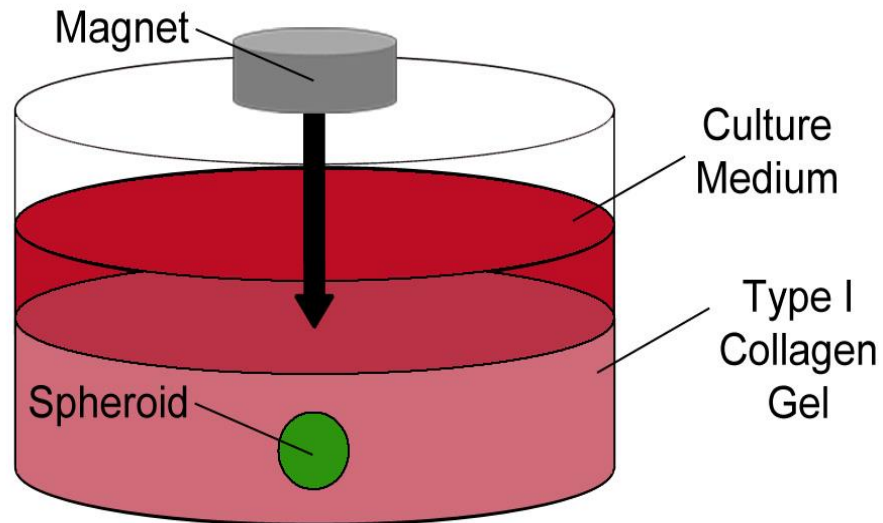


Figure 1-7 Bone marrow niche *in vitro* model. Simplification of the bone marrow niche *in vitro*. Spheroids formed as in figure 1-7 are transferred into new wells and type I collagen gel solution is added. Adding a 350 mT magnet to the lid of the well, as the gel solidifies, causes the spheroids to be levitated to prevent surface adherence. The environment will now closely mimic the stiffness of the bone marrow causing the cell cytoskeleton to be remodelled changing the mechanophysical properties of the cell. This cells within the spheroid will enter a quiescent state where division slows and can be maintained for long periods of time if no external stimuli are experienced.

1.6 Hypothesis and Project Aims

In order to better understand the mechanisms involved in breast cancer dormancy and recurrence within the bone marrow, it is evident that there is a need to study the relationship between BCCs and MSCs. This PhD aims to study potential indirect cell-cell communication, including key cytokines and EVs, both of which have recently been identified as playing a role in dormancy and/or recurrence. This will be done through the creations of a functional *in vitro* model for metastatic breast cancer in the bone marrow niche, to subsequently assess how these BCCs may become quiescent following entry into the bone marrow microenvironment. The initial stage of the project will determine how these breast cancer cells interact with MSCs residing in this microenvironment. Implantation of these cells into the type I collagen gel will approximate the stiffness of the bone marrow to mimic any mechanical processes the cells might encounter that would otherwise be absent in a two-dimensional model. In our lab, we have recently developed a 3D model of the bone marrow (Lewis et al., 2016; Lewis et al., 2017; Lewis et al., 2018; Figure 1-7). This model will be employed in this project to allow the study of both individual and MSC/BCC co-cultures.

The hypothesis of this study is that culture within an *in vitro* BM niche model influences cell phenotype and behaviour in such a way as to more accurately represent *in vivo* cell phenotype and behaviour compared with traditional tissue culture. Primarily, the commercially available BCC lines, MCF7 and MDA-MB-231, will be used to form cell spheroids following the uptake of fluorescently labelled mNPs. This will mimic the presence of DTCs within the BM. In addition to the BCC spheroids, MSC spheroids will also be generated and co-cultured within the collagen gel. To test

this hypothesis and assess cell-cell communication in these two cell types, the aims of this project are as follows:

- Optimisation and characterisation of BCC and MSC spheroid formation to produce consistent three-dimensional structures, using an existing magnetically levitated MSC spheroid model (figure 1-8; Lewis et al., 2016). This part of the project is described in Chapter 3.
- Study of the MSC response to cytokine IL-6, produced by local injury (Lewis et al., 2016). MSC migration through the collagen gel model will be assessed by analysing matrix metalloproteinase expression. This part of the project is described in Chapter 4.
- Co-culture of MSCs and BCCs will be assessed in Chapter 5; how it affects the cytokine secretion profile of the cell types and how cytokines secreted into the BM affect BCC growth and motility.
- Finally Chapter 6 will study the effect MSC-derived EVs have on BCCs in the hope of determining how incoming tumour cells enter dormancy.

2 Materials and Methods

This chapter describes the materials and methods used to carry out all studies detailed in subsequent chapters.

Table 2-1 List of materials, reagents and suppliers used throughout all experiments.

Materials/Reagents	Supplier
1. Cells	
MSCs	Promocell
MCF7	ATCC
MDA-MB-231	ATCC
MG63	Sigma-Aldrich
hTERT	Clontech Laboratories
hOBs	Promocell
HUVECs	Promocell
2. Nanoparticles	
200nm mNPs coated in PEA	Chemicell
200nm mNPs coated in PEA-FITC tag	Chemicell
200nm mNPs coated in PEA-TRITC tag	Chemicell
3. Cell Culture	
DMEM	Sigma-Aldrich
FBS	Sigma-Aldrich
Penicillin-Streptomycin	Sigma-Aldrich
L-glutamine 200 mM	Invitrogen
NEAAs	Life Technologies
Sodium Pyruvate	Life Technologies
Trypsin	Sigma-Aldrich
Versene	In House

NaCl	Fisher Scientific
KCl	Fisher Scientific
HEPES	Fisher Scientific
EDTA	Sigma-Aldrich
DMSO	Sigma-Aldrich
Phenol Red 0.5%	Sigma-Aldrich
Rat Tail Collagen Type I, >2 mg/mL	First Link
10x MEM	First Link
NaOH 0.1M	Sigma-Aldrich
Collagenase D	Roche
4. Electron Microscopy	
Gluteraldehyde (25% aq pure, EM Grade)	Sigma-Aldrich
Sodium cacodylate	Agar Scientific
Osmium tetroxide	Agar Scientific
Aqueous uranyl acetate	Agar Scientific
Ethanol	VWR Chemicals
Methanol	VWR Chemicals
Propylene oxide	VWR Chemicals
Epon resin araldite (812 Kit E202)	TAAB Lab Equipment
Uranyl acetate	Sigma-Aldrich
Reynolds lead citrate	Agar Scientific
5. Cell Staining	
PBS	Sigma-Aldrich
Formaldehyde (38%)	Fisher Scientific
MgCl ₂ (hexahydrate)	VWR Chemicals
Triton X	Sigma-Aldrich
LIVE/DEAD® Viability/Cytotoxicity kit	Invitrogen
BSA	Sigma-Aldrich
BrdU	Sigma-Aldrich
BrdU antibody kit	GE Healthcare

Rhodamine-phalloidin	Invitrogen
Vectashield-DAPI	Vector Laboratories
Anti-Ki67 anti-rabbit primary antibody	Abcam
Anti-ALDH1A1 anti-rabbit primary antibody	Abcam
Unbiotinylated secondary antibodies-Texas Red	Vector Laboratories
CellTag®	Li-Cor
IRDye® Goat Anti-rabbit 800CW	Li-Cor
Tween 20	Sigma-Aldrich
Cytokine array membrane kit	Abcam
6. EV Collection	
Particle-free PBS	Sigma-Aldrich
Pierce BCA Protein Assay Kit	ThermoFisher Scientific
Fluorocet Exosome Quantification kit	New England Biolabs
7. RNA Quantification	
RNeasy Mini Kit	Qiagen
Quantitect Reverse Transcription Kit	Qiagen
Fluidigm Primers	Eurofins Genomics
2x TaqMan PreAmp Master Mix	Applied Biosystems
2x SsoFast EvaGreen Supermix	Bio-Rad
RNaseOUT Recombinant RNase Inhibitor	Invitrogen
DNA Suspension Buffer	Life Technologies
Exonuclease I Reaction Buffer	New England Biolabs
Exonuclease	New England Biolabs
Biomark 20x DNA Binding Dye Sample Loading Reagent	Fluidigm
8. Cell Treatments	
IL-6	Abcam
TGF-β	Abcam

D-Erythrose	Sigma-Aldrich
L-Methionine	Sigma-Aldrich

2.1 Cell Culture Solutions

Modified DMEM (Standard Growth Media)

DMEM	400 mL
Medium-199	100 mL
FBS	50 mL
Penicillin-streptomycin	10 mL
Sodium pyruvate	5 mL
L-glutamine 200 mM	5 mL

Modified Alpha-MEM (Stem Cell Growth Media)

DMEM	400 mL
FBS	50 mL
Penicillin-streptomycin	10 mL
Sodium pyruvate	5 mL
NEAA	5 mL

Versene

Water	1 L
NaCl	8 g
KCl	0.4 g
Glucose	1 g
HEPES	2.38 g
EDTA	0.2 g
0.5% Phenol Red	2 mL

Adjusted to pH 7.5

Trypsin/Versene

Versene	20 mL
Trypsin	0.7 mL

10x PBS Solution

PBS	1 Tablet
Water	200 mL

1% PBS Solution

10x PBS Solution	10 mL
Water	90 mL

Cell Fixation Buffer

Formaldehyde (38%)	10 mL
1% PBS Solution	90 mL
Sucrose	2 g

Cell Permeabilising Buffer

1% PBS Solution	100 mL
Sucrose	10.3 g
NaCl	0.292 g
MgCl ₂ hexahydrate	0.06 g
HEPES	0.476 g
Adjusted to pH 7.2	
Triton X	0.5 mL

Blocking Buffer

1% PBS Solution	100 mL
BSA	1 g

Wash Buffer

1% PBS Solution	100 mL
Tween 20	0.5 mL

Cell Freezing Solution

FBS	50 mL
DMEM	40 mL
DMSO	10 mL

2.2 Cell Culture

The MSCs were cultured in T75 flask with modified alpha-MEM media at 37 °C with 5% CO₂. Once the cells were confluent, the media was removed and the cells were washed with HEPES solution. Cells were detached from the surface using 5 mL trypsin/versene (<5 minutes at 37 °C). 5mL Fresh media was added to the flask to neutralise the active trypsin, and the cell suspension was centrifuged for 4 minutes at 1400 rpm. After centrifugation, the supernatant was removed leaving a cell pellet. The cells were re-suspended in 5 mL fresh media and seeded into appropriate wells for experiments. An appropriate volume of remaining cell suspension was added to new T75 flask containing 10 mL of fresh media to maintain cell supply. The same protocol was followed for other cells types including MCF7 and MDA-MB-231, where modified DMEM was used instead.

2.3 Cell Freezing/Thawing

Cells pelleted as per section 2.1 and resuspended in 1 mL cell freezing solution before being frozen at -80 °C overnight then transferred to liquid nitrogen for storage. Cells were thawed by removing from liquid nitrogen and adding the cell suspension dropwise to fresh media warmed to 37 °C and centrifuging at 1400 rpm for 4 minutes. Cell pellet was resuspended in 5 mL fresh media and cells seeded in several T75 flasks containing 10 mL fresh media.

2.4 Monolayer Culture

Cells were removed from the surface of T75 flask as in section 2.2 before seeding in a 24-well plate and cultured overnight at 37 °C with 5% CO₂ to allow cell adhesion.

2.4.i Cell Treatments

Fresh media doped with additional materials (such as cytokines or metabolites) depending on study, were added after cells had adhered to the surface of the well plate for 24 hours.

2.5 Spheroid Synthesis

Cells were seeded at a density of 1×10^4 cells/ml and incubated overnight (37 °C with 5% CO₂). mNPs (Chemicell) were added to BCCs or

MSCs at a working concentration of 0.1 mg/mL and incubated for 30 minutes (37 °C with 5% CO₂) on a magnet array plate. Wells were washed with HEPES to remove excess mNPs and cells were then detached from the surface using 200 µL trypsin/versene (<5 minutes at 37 °C). 300 µL fresh media was then added to each well to neutralise the active trypsin. Cell suspension was then centrifuged at 1400 rpm for 4 minutes. The supernatant was discarded and cell pellet was resuspended in 500 µL/well. 500 µL cells containing mNPs were then seeded in 6 well plate containing 4mL of fresh media and incubated overnight (37 °C with 5% CO₂) under an external magnetic field (350 mT).

2.6 Collagen Gel Synthesis

0.5 mL fresh DMEM, 0.5 mL FBS and 0.5 mL 10x MEM were mixed on. In a separate universal tube, 2.5 mL acetic acid-stabilised type I rat tail collagen (2 mg/mL) was mixed with 1mL 0.1 M NaCl. The contents of both tubes were combined on ice and NaOH was added dropwise until the solution changed from yellow to pink (via phenol red indicator in media). 500 µL of this solution was added to each well of a 24-well plate containing spheroids synthesised in section 2.4, to produce a gel 5mm thick. A 350 mT magnet was then placed on the lid of the well plate to levitate the spheroid within the gel before it solidified. Gels were incubated at 37°C until solidified. 1mL of fresh media was then applied to the gel and spheroids were incubated as per experiment.

2.6.i Gels Containing Multiple Spheroids

Where gels contain multiple spheroids of different cell types, the protocol above was followed and spheroids generated separately as in section 2.5 were added to new wells prior to addition of collagen gel.

2.7 Collagen Gel Digestion

Media was removed from collagen gels and equal volume 2.5 mg/mL Collagenase D in 1x PBS solution was added and incubated at 37 °C for 90 mins. Solution was then pipetted vigorously before the addition of ice cold 10 mM EDTA to quench the reaction. This solution was pelleted in a centrifuge and supernatant removed. Spheroid pellet could then be used in further experiments.

2.8 RNA extraction

RNA extractions from cell pellets were performed using a QIAGEN RNeasy mini kit, according to the manufacturer's protocol. All centrifuge runs were at 8000 g for 15 seconds unless otherwise stated. 350 µL buffer RLT was added to each pellet, and the sample was homogenised by pipetting. 350 µL 70% ethanol was added to the lysate and mixed by pipetting. The sample was immediately transferred to an Rneasy MinElute spin column in a 2mL collection tube, and centrifuged. The flow-through was discarded from the collection tube. 350 µL buffer RW1 was added to the spin column and centrifuged. 80 µL DNase I in buffer RDD was added directly to the spin column membrane, and incubated at room temperature for 15 minutes. 350 µL buffer RW1 was added and the column

was centrifuged. The collection tube was discarded and replaced, 500 μ L buffer RPE was added and the column was centrifuged again. 500 μ L 80% ethanol was added, and the column was centrifuged for 2 minutes, after which the collection tube was discarded. The spin column was placed into a new collection tube and centrifuged at 13000 g for 5 minutes to dry the membrane. The flow-through and collection tube were discarded. The column was then placed into a 1.5 mL collection tube. 14 μ L RNase-free water was added to the centre of the spin column membrane, and the RNA was eluted by centrifuging at 13000 g for 1 minute. RNA content was quantified using a NanoDrop 2000 spectrophotometer. The samples were either stored at -80 °C or used immediately.

2.9 Reverse Transcription

Reverse transcription was performed using a QuantiTect® Reverse Transcription Kit according to the manufacturer's protocol. Template RNA samples were thawed on ice. The kit reagents (gDNA Wipeout Buffer, Quantiscript® Reverse Transcriptase, Quantiscript RT Buffer, RT Primer Mix, and RNasefree water) were thawed at room temperature. The solutions were gently mixed and centrifuged to collect residual liquid from the sides of the tube. All reactions were prepared on ice. RNA content was normalised so all samples contained equal amounts. The genomic DNA elimination reaction was set up with 2 μ L of gDNA Wipeout Buffer and the appropriate amount of template RNA, made up to 14 μ L with RNase-free water. This reaction was incubated for 2 minutes at 42 °C, and then kept on ice. The reverse transcription reaction was set up with 1 μ L Quantiscript Reverse Transcriptase, 4 μ L Quantiscript RT buffer, 1 μ L RT primer mix, and 14 μ L template RNA from the genomic DNA elimination reaction, to a total reaction volume 20 μ L. This mix was incubated for 15 min at 42 °C,

followed by an incubation for 3 min at 95 °C to inactivate the Quantiscript Reverse Transcriptase. The resulting cDNA was then stored at -20 °C.

2.10 Cell Fluorescent Imaging

After the appropriate incubation period, cell monolayers or cell spheroids levitated in gels were fixed for 15 minutes at room temperature, using cell fixative solution, before being washed three times with 1x PBS solution. In the case of experiments using cell monolayers under gels, a drop of vectashield-DAPI stain was applied to wells for 15mins at room temperature following fixation. Red fluorescence measured at 546nm excitation, 665nm emission. Green fluorescence measured at 440nm excitation, 540nm emission. DAPI blue fluorescence measured at 365nm excitation, 397nm emission. Cell imaged using a Zeiss Axio Vert A1 fluorescent microscope.

2.11 BrdU Assay

10 mg/mL BrdU in DMSO was added to DMEM. Media over collagen gels was replaced with this BrdU-doped DMEM and incubated for 2 6hr at 37 °C. The cells were then stained for immunofluorescence as described in section 2.12.

2.12 Live/Dead Viability Assay

After the appropriate incubation period the cells, in either monolayer or collagen gel, were assessed for cell viability, by preparing 10 mL of fresh DMEM media containing 5 μ L 4 mM calcein AM and 20 μ L 2mM ethidium homodimer, giving working concentrations of 2 μ M and 4 μ M respectively. This media was added to the cultures then incubated for 1 hour at 37°C. Subsequently, the cells or gels were washed three times with fresh media and analysed immediately as in section 2.12.

2.13 Fluidigm Real-Time PCR

2.13.i Specific Target Amplification

Specific target amplification (STA) reactions were performed to increase the cDNA volumes. Primers for the genes listed in Table 2-2 and 2-3 were designed using the Sigma online primer design tool. 1 μ L aliquots of 100 μ M forward and reverse primer sets were pooled and diluted in DNA suspension buffer to create a 500 nM (10x) primer mixture. Pre-mix solutions were made up for each cDNA sample: comprising 2.5 μ L TaqMan PreAmp Master Mix (Applied Biosystems), 0.5 μ L 500 nM pooled primer mix, and 0.75 μ L water. 1.25 μ L cDNA sample was added to the mixture, to a final volume of 5 μ L, mixing by vortex. The samples were then run on a thermocycler under the sequence outlined in Table 2.4.

Table 2-2 List of genes and primers tested using Fluidigm real-time PCR. Layout for first run; shaded cells indicate housekeeping genes.

	Forward Primer 3'-5'	Reverse Primer 3'-5'
B-actin	acggatttggcgtattggg	atthttggagggatctgctc
CCNA2	tcagtaccttagggaagctgaaa	ccagtccaccagaatcgtg
CCNB1	ccatacctcaagtattgcatc	tccagtctttcgtattaatgattcag
CCNC	acatggtgcactttcctcct	aggtaatggttagagttggtgcc
CCND1	tttgctgagctttctgtgga	aatggttgccatctcttttctc
CCND2	tgcattctacaccgacaactcc	cggatgatctgtttgttctccg
CCND3	tacaccgacaactccatcaagc	atgtgctcaatgaagtcagagg
CCND3	tacaccgaccacgctgtct	gaaggccaggaaatcatgtg
CCNE2	acagcttgatttctgtggac	tctgcttctaccgctctgtg
CCNT1	gccattgattcattagagttcca	tgaaatactgtcccactccaaac
CDK1	gaacatgtcatcaaggtagcaca	aatgaccagatcttgaactgttg
ENOX-2	gagctggagggaacctgattt	cactggcactaccaactgca
CDKN1A	aactacaggtcaagtggtagcc	ggaatcctgcataagcacatcc
CDK2	gtggacctggagactctcag	cctcttgagaagatcagccg
CDK4	cctcctgggctgcaaata	cagaatctccaggaataggg
CDK5	agtgttggctgtatctttgag	atctcaggccagtcattcc
CDKN1A	tcttttcccggcaatgat	tctggcagcttggcataga
CDKN1B	ggctaactctgaggacacgc	tgagtagaagaatcgtcggttc
CDC7	attgtcatcaagacgcagggc	gttgcaatcccttcgctgtt
ORC3	tcatcatctgcttattcctt	tgattatctttacatcatcttctg
CDC25B	tgattctctgctcgtgtt	cattcgttcaagtagtcatagt
ORC4	atcaggacacaaggacatc	ctctcacacttccactctc
CCNB2	ggctaactctgaggacacgc	tgagtagaagaatcgtcggttgc
C-MYC	gtggccggacatgtgtagtc	gccgtaattcgagcacatgg
CDK6	gcccttaagtgtcctgtgct	tctcattggtaagagcgcga
N-CAD	ttgctgtcattattctcagtgga	gaggactcagggtggttcag
E-CAD	ggatttgtggacatcctagagagt	acttctgtacatgacgaggt
FN1	acctgcggtcattacacatg	tgctttcgagtccatgctaca
GAS6	agaagacaccaccatcca	tgtagtccaggctgtagaa
AXL	tcttatggcgtagatggag	gagttgagggtggacagat
GAS6	agcatctcaaaattctcaaca	ggtactcctgaatccactt
GAPDH	acggatttggcgtattggg	atthttggagggatctgctc
AXL	aacaagaccctgcccgtgg	cattcagcagaggcattcccgg
JUP	ttctgctggcaagaggttccactc	gtgtttgctcaggtggtcgtt
MER	agacctgtatcgcaggcact	ccactcgtttctggtagtcttcc
TYRO3	agctggatgaccagagtgtc	tgaaattcatggctgtggaa
KERATIN 19	gaagattgggagaaccctca	tgtgggtttatggactgcaa
TWIST 1	gcaatagcactactacactc	ccaacagacctcatcaca
PPARG	gactctgaggaggaacaaga	ttggcagcaggatagtcctt
CXCL12	tgaaatggtcatgggggaac	aaaaagctcctgatgccttg
RUNX2	gaactaggcaagacctacttctga	ggtgggaatccagggttttct
CYCR	ggtgtctcttcaacggaggaa	tagtgaggcatcatcagtgcc
OSX	catcaacaccgagttcaag	atcttattctgctgctcca
BMP2	atctcttgacctcgtgat	cagtcagcatctgtatt
OPN	taagttgccgtctctgaa	gtgtggtgcgttatgtaa
RNF20	cctacctgaagaagaacat	cacggtcagagaatacaga

B2M	ctgatagaagtctgaacagttgt	gattggcagcactcttg
CYC1	ttgtctttcagcaaggactgg	atgcggcatcttcaaactcc

Table 2-3 List of genes and primers tested using Fluidigm real-time PCR, layout for second run; shaded cells indicate housekeeping genes

	Forward Primer 3'-5'	Reverse Primer 3'-5'
ENOX2	gagctggaggaacctgattt	cactggcactaccaaactgca
GAPDH	acggatttggctgattggg	atthttggaggatctgctc
SNAIL1	tcggaagcctaactacagcg	tcccagatgagcayyggcag
SNAIL2	tccttctgggtcaagaagca	ggatgacaggcatggagta
PI3K	cctcaattcacctcatagtagagcaat	ggagaaactattaccagatcaccac
MAPK1	cgtgttgcatccagacca	gccagaatgcagcctacaga
AXL	tcttatggcgtagatggag	gagttgagtgacagat
GAS6	agaagacaccacatcca	tgtagtccaggctgtagaa
MER	gcaatagcactactactc	ccaacagacctcatcaca
JUP	atctcttgacctcgtgat	cagtcagcatcttgatt
TYRO3	taagttgccgtctctgaa	gtgtggcgttatgtaa
OPN	agctggatgaccagagtgct	tgaaattcatggctgtggaa
BMP	agacctgtatcgaggcact	ccactcgtttctggtagttcttcc
RUNX2	aacaagacctgcccgtgg	cattcagcagaggcattccgg
OSX	ttctgaggcaagaggtcactc	gtgtttgctcagggtgctcgtt
CXCL12	agcatctcaaaattctcaaca	ggactcctgaatccactt
Vimentin	catcaacaccgagttcaag	atcttattctgctgctcca
N-Cadherin	tcatcatctgcttattcctt	tgttatctctacatcatcttctg
E-Cadherin	tgattctctgctcgtgtt	cattcgttcaagtagtcatagt
FN-1	atcaggacacaaggacatc	ctctcacacttccactctc
Keratin19	cctacctgaagaagaacat	cacggtcagagaatacaga
TWIST1	ctgatagaagtctgaacagttgt	gattggcagcactcttg
CCN-B2	gaagattgggagaaccctca	tgtgggtttatggactgcaa
UBE2D2	ccatggctctgaagagaatcc	gatagggactgtcatttgccc
B-Actin	gtgggccccttaggcaccag	cactttgatgtcacgcagatttc
CCN-C	tttgctgagctttctgtgga	aatgggtgccatctctttctc
CCND2	tacaccgacaactccatcaagc	atgtgctcaatgaagtcagagg
CCNT1	gaacatgtcatcaaggtagcaca	aatgaccagatctgaacttggtg
CDK4	agtgttggtgtatctttgag	atctcgaggccagtcaccc
CDK5	tcttttcccggcaatgat	tctggcagcttggtcataga
MCM9	ggctaactctgaggacacgc	tgagtagaagaatcgtcgggttc
PPARG	ttgctgtcattattctcagtgga	gaggactcaggggtggttcag
MAPK8	caggactgcaggaacgagtt	ctccatgatgcaccaact
BCL2L2	aagtgcaggagtggatggtg	gtcctcactgatgccagtt
BLM	tccagaaaccagcacagact	gcagttcgttcccacaatcc
CCNA2	tggcggactgaagtccgg	caaggaggaacggtgacatgc
CCNB1	cagctcttggggacattggaac	actggcaccagcataggtacc
CDC25B	ggatttggacatcctagagagt	acttgctgacatgacaggt

CDK1	aactacaggtcaagtggtagcc	ggaatcctgcataagcacatcc
CDK2	cctcctgggctgcaaata	cagaatctccaggggaataggg
CATHEPSIN D	acctgcggtcattacacatg	tgcttcgagtcctgctaca
ORC4	tttccatcagcaggatgtggg	ctgtgggtcttcttccatagc
ORC3	ccagtccttctcagcctg	acttgttcgaatcactgtccca
C-MYB	gaaggtcgaacaggaaggttatct	gtaacgctacagggtatggaaca
BAX	gctgacatgtttctgacgg	atgatggttctgatcagttcc
CDK9	atgaaaaacgagaaggagggg	tagggggaagctttggttcg
CYC1	actgcgggaaggtctctactt	gggtgccatcgtcaaactcta
ATP5B	tccatcctgtcagggactatg	atcaaactggacgtccaccac

Table 2-4 Thermocycler program for pre-amplification of cDNA

Cycles	1	14-22		Hold
Temperatures	95 °C	95 °C	60 °C	4 °C
Times	10 minutes	15 seconds	4 minutes	∞

2.13.ii Exonuclease Treatment

Exonuclease treatment was used to remove unincorporated primers from section 2.9.i. Exonuclease I was diluted to 4 U/μl to a volume of 2 μl per reaction (1.4 μl water, 0.2 μl Exonuclease I reaction buffer, 0.4 μl Exonuclease I at 20 U/μl). This mixture was added to the STA reactions, mixed via vortex, centrifuged briefly to collect entire volume, and run in a thermal cycler as described in Table 2-5. The products were then diluted 5-fold in TE buffer to be used in further steps

Table 2-5 Thermocycler program for exonuclease treatment of cDNA

Temperature	37 °C	80 °C	4 °C
Time	30 minutes	15 minutes	∞

2.13.iii Sample Pre-Mix Preparation

2x SsoFast EvaGreen Supermix was mixed with 20x DNA Binding Dye Sample Loading Reagent in an 11:1 ratio. 2.75 μL pre-mix was added to 2.25 μL of the STA and exonuclease treated cDNA sample. This final mixture was vortexed for 20 seconds and centrifuged for 30 seconds. All reactions were kept on ice.

2.13.iv Assay Mix Preparation

Forward and reverse primer stocks (100 mM) were diluted to a final concentration of 5 μM using 2.5 μL 2x Assay Loading Reagent, 2.25 μL 1x DNA Suspension Buffer and 0.25 μL 100 μM mixed forward and reverse primers. The mixture was vortexed for 20 seconds and centrifuged for 30 seconds.

2.13.v Chip Priming and Loading

The 48.48 Dynamic Array IFC (figure 2-1) was primed with control line fluid, which was injected into each accumulator on the chip. The chip was placed into the IFC controller MX, and the 'Prime (136x)' script was run. Following this, 5 μL each assay mix and sample were pipetted into the wells of the chip. The fully loaded chip was inserted into the IFC Controller and the 'Load Mix (136x)' script was run to load the samples and assays into the chip. The chip was then run in the BioMark HD system using the protocol described in Table 2.6.

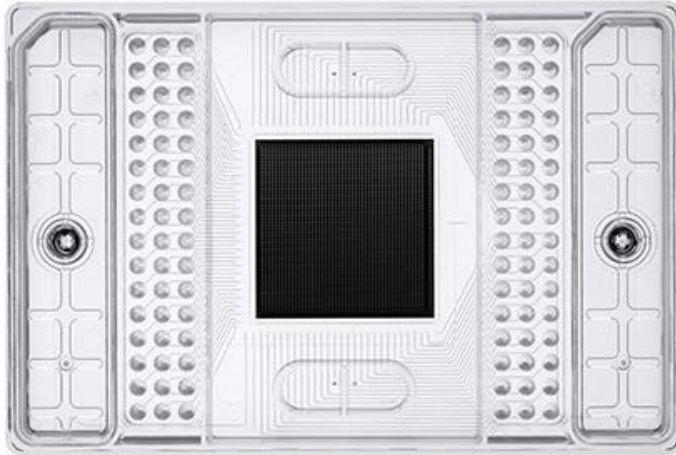


Figure 2-1 Fluidigm 48.48 access array chip. 48 cDNA samples are loaded in the left-hand wells and 48 primer pairs loaded on the right.

Table 2-6 Cycling parameters for Fluidigm 48.48 dynamic array IFC

	Type	Temperature (°C)	Duration (seconds)	BioMark HD Ramp Rate (°C/s)
1	Thermal mix	70	2400	5.5
		60	30	5.5
2	Hot Start	95	60	5.5
3	PCR (30 cycles)	96	5	5.5
		60	20	5.5
4	Melting Curve	60	3	1
		60-95	1	1

2.14 Immunofluorescent Staining

Following a period relevant to specific tests, cells were fixed for 15 minutes at room temperature using cell fixative solution. Fixed cells were incubated in cell permeablising buffer 5 min at 4 °C. Samples were blocked in blocking buffer and stained with primary antibody (Table 2.1), 1:500 in blocking buffer, for 1 hour at 37 °C. After the incubation, they were washed three times in wash buffer. They were then incubated with conjugative secondary antibody (1:50 in blocking buffer) for 1 hour at 37 °C. The samples were then washed three more times in wash buffer and mounted in vectashield-DAPI. Cells could then be imaged using microscope noted in section 2.11.

2.15 In Cell Western

All steps until addition of primary antibodies are as in 2.14. Cells are then washed five times in wash buffer before incubating for 1 hour at 37 °C with CellTag and appropriate conjugative secondary antibody (1:700 and 1:400 respectively). Cells were then washed further using wash buffer and dried prior to imaging using a Li-Cor Odyssey Sa.

2.16 μ -Slide Chemotaxis 2D

The kit provided by Ibidi allows the observation and measurement of directional motility of a group of cells in response to a chemoattractant. Using the set protocol provided with the '3D Chemotaxis Assay Using μ -Slide Chemotaxis - 2.2 2D Chemotaxis experiments without Gel' slides, MSCs were seeded at 1×10^5 . Once both reservoirs were filled with 60 μ L

chemoattractant-free DMEM, 30 μ L of 2 ng/mL IL-6 was aspirated into the left reservoir to begin the chemoattraction for the assay. The plate was then imaged on a 4 times objective lens at 120 second intervals over 24 hours in a 37°C hot room. Results were then analysed using the ImageJ plugin 'manual tracking' and Ibidi's own 'Chemotaxis and Migration' tool.

2.17 Cytokine Array

Following the protocol provided by the supplier samples were incubated overnight on array membranes shaking at 4°C. The following day, media samples were aspirated, membranes washed using the supplied wash buffers and incubated for two hours at room temperature in 1 mL of Biotin-Conjugated Anti-Cytokines. Membranes were then rewashed and incubated in 2 mL HRP-Conjugated Streptavidin shaking overnight at 4°C. Prior to chemiluminescence detection, streptavidin was removed and membranes washed for a final time. Once washed, membranes were transferred printed side up onto provided plastic sheets and detection buffers pipetted onto each sample. After two minutes of incubation, a second plastic sheet was placed on top and membranes were imaged via chemiluminescence detection using an Azure c500 Infrared Western Blot Imaging System. The layout of the array is shown in table 2-7. The pixel density of each dot on the array was recorded using ImageJ and normalised to the mean positive control as per manufacturer's instruction.

Table 2-7 Abcam 23-target cytokine array layout. POS denotes positive control IgG and NEG denotes spots containing buffer only.

POS	POS	NEG	NEG	G-CSF	GM-CSF	GRO	GRO α
POS	POS	NEG	NEG	G-CSF	GM-CSF	GRO	GRO α
IL-1 α	IL-2	IL-3	IL-5	IL-6	IL-7	IL-8	IL-10
IL-1 α	IL-2	IL-3	IL-5	IL-6	IL-7	IL-8	IL-10
IL-13	IL-15	IFN- γ	MCP-1	MCP-2	MCP-3	MIG	RANTES
IL-13	IL-15	IFN- γ	MCP-1	MCP-2	MCP-3	MIG	RANTES
TGFB1	TNF- α	TNF- β	blank	blank	blank	blank	POS
TGFB1	TNF- α	TNF- β	blank	blank	blank	blank	POS

2.18 Electron Microscopy Preparation

Cell spheroids were generated before fixing in 2.5% glutaraldehyde/ 0.1 M phosphate buffer fixative for 1 hour at room temperature before rinsing in buffer three times for 5 minutes. Fixed spheroids were treated in osmium tetroxide/ 0.1 M phosphate buffer for 1 hour and washed with distilled water three times for 10 minutes before being treated in uranyl acetate for 1 hour in the dark. Spheroids were then dehydrated in increasing [ethanol] for 10 minutes until absolute ethanol, which was used twice for 5 minutes.

2.18.i SEM

Scanning EM samples were then dried in hexamethyldisilazane before being mounted on SEM stubs. Mounted samples were then coated with 10 nm gold/palladium using a polaron SCS15 SEM coating system. Samples

were viewed using JOEL 6400 SEM at 10kV. Images were false coloured with Adobe Photoshop CS4.

2.18.ii TEM

Transmission EM sample spheroids were further processed by first washing in propylene oxide three times for 5 minutes then a 1:1 mix of propylene oxide: araldite/epon 812 resin overnight. These samples were then embedded in fresh araldite resin and set in moulds for 48hr to allow the resin to polymerise. 70 nm sections were cut using a Leica Ultracut UCT and a Diatome diamond knife at an angle of 6°. Sections were then mounted on 100 mesh formvar-coated copper grids then contrast stained with 2% methanolic uranyl acetate for 5 minutes and Reynold's lead citrate for a further 5 minutes before imaging on JOEL 1200 TEM TEM at accelerating velocity of 80kV.

2.19 Conditioned Media Fractionation

Culture medium was harvested from cells following an incubation period to allow the secretion of signalling molecules. This was then filtered using a 200 micron filter to remove cells. Media was then sequentially ultrafiltrated using Amicon Ultra filters as per the manufacturer's protocol; reservoir was filled with appropriate volume of media and centrifuged for time depending on rotor and molecular weight of desired filtrate. The runoff containing smaller molecules was then used in the next molecular weight cut off filter to produce filtrates of discrete molecular weights. The media retained in the reservoir was reconstituted

in a volume of fresh culture medium equal to the volume originally filtered to maintain the concentration.

2.20 Extracellular Vesicle Isolation and Characterisation

MSCs and MCF7s were cultured at scale in T150 culture flasks and the medium isolated every two days. Cells were grown in DMEM containing FBS depleted of EVs, through centrifugation at 120000 g for 18 hours. MSC or MCF7-derived EVs were isolated from collected medium by differential centrifugation: 2000 g for 20 minutes to remove cell debris and apoptotic bodies, 10,000 g for 30 minutes to remove micro-vesicles, 120000 g for 70 minutes to pellet EVs. Following the final ultracentrifugation step, the supernatant was removed, the pellet washed in particle-free PBS and further centrifuged at 120,000 g. All ultracentrifugation steps were performed using a Sorvall WX Ultra Series Ultracentrifuge with a Fiberlite, F50L-8 × 39 fixed-angle rotor

The resulting pellet was re-suspended in 200 µL of PBS and the total protein concentration determined using the Pierce BCA protein assay kit. Particle size distribution was analysed using Dynamic Light Scattering (DLS; Malvern Instruments, UK) and quantitated using Fluorocet assays; generating a protein standard then adjusting isolates to the same total protein and measuring fluorescence of acetecylcholinesterase, a known exosomal protein, present within the vesicles. Due to limited supply and assessment of other EV-related studies, the concentration of approximately 2×10^7 /mL was used in each experiment.

2.21 Statistical Testing

Differences between the means of two independent variables in any given case were determined using an unpaired t-test. Where appropriate, an ANOVA was performed to determine differences between whole treatment groups. Statistical significance was determined by $p < 0.05$ indicating a 95% probability of the test hypothesis being correct. All statistical analyses were performed using Graphpad Prism 6.

3 Spheroid Characterisation

3.1 Introduction

Recently there has been interest in the study of dormant cancer cells within the bone marrow (BM) niche; if the factors that cause this phenomenon can be determined then they can be exploited to prevent an exit from this quiescent state (Ono et al., 2014; Zhang et al., 2013; Reddy et al., 2012). There is evidence that entry into the bone marrow stem cell niche leads BCCs to enter dormancy (Lim et al., 2011). This is not necessarily an immediate effect, so incoming cancer cells may begin to form micrometastases before becoming quiescent. Currently the norm for such research is to use two-dimensional environments to test a hypothesis. In the case of recreating a functional bone marrow stem cell niche, ECM proteins such as collagen and fibronectin are utilised, as well as a multitude of expensive growth factors to simulate the *in vivo* niche (Llopis-Hernandez, et al., 2016; Hoshiba, et al. 216; Meads et al., 2008). However, these models could be described as too simplistic as they lack the three-dimensional structure of the BM environment. Both MSCs and BCCs are known to express different surface receptors (Sun et al., 2006; Pickl and Reis, 2009) and exhibit different cell morphologies when cultured in two-dimensional models compared with cells grown in three-dimensional matrices. Therefore, recently there has been a shift towards the use of three-dimensional culture methods, to create a more physiologically relevant model.

There are various methods involved in creating three-dimensional MSC niche models, as described in section 1.x. However, the use of multicellular spheroids has been defined both as an effective and efficient technique. Several protocols for generating spheroids, including hanging drop or mechanical agitation, were summarised in section 1.4. This

chapter aims to utilise a previously described protocol, which causes MSCs to aggregate to create multicellular spheroids using magnetic nanoparticles (mNPs). Through the use of an external magnetic field, cells containing mNPs can be manipulated. Previous studies have shown mNPs incorporated within the MSCs do not affect the characteristic behaviour of these cells (Suh et al., 2009; Markides et al., 2012; Lewis et al., 2016), with the effects on BCCs not as clearly defined. The addition of a type I collagen gel matrix surrounding MSC spheroids further models the bone marrow by approximating the stiffness of the environment where the MSCs reside (Lewis et al., 2017).

3.1.i Objectives

This chapter aims to develop an *in vitro* three-dimensional model, incorporating MSCs and/or BCCs, which effectively mimics the bone marrow stem cell niche. The generation of a more physiologically relevant three-dimensional model may allow native cellular responses and will facilitate the further study of dormancy. If successful, the model will enable the study of initial dormancy signals within BCCs, in addition to paracrine signalling between MSCs and BCCs within the model environment. Understanding these processes may permit the artificial manipulation of BCC dormancy, providing a potential platform for therapy. First, to establish the model, distinct MSC and BCC spheroids are initially generated and cultured in type I collagen gel. Initial assessment of these spheroids will include:

- Determination of optimal cell seeding density number
- Assessment of cell-cell contact within spheroids and spheroid morphology via scanning electron microscopy

- Assessment of internal cellular structures and distribution of mNPs within cells of the spheroids via transmission electron microscopy
- Proliferation analysis of spheroids using BrdU incorporation during DNA synthesis
- Co-culture of MSC and BCC spheroids to assess key gene expression changes

3.2 Results

3.2.i Cell Seeding Density

All results herein used three cell types; MSCs (Promocell), MCF7 (ATCC) or MDA-MB-231 (ATCC). The first stage in generating the *in vitro* model is to create consistently sized spheroid. As described in section 2.5, spheroid generation is a multistep process. The effect of initial cell seeding density with respect to resultant spheroid size was assessed. Each cell type was seeded at three different cell densities; 6×10^3 , 1×10^4 and 2×10^4 cells/mL (figures 3-1 to 3-3), with spheroid cross-sectional area measured after 24hr in collagen gel, using the fluorescent mNPs within the cells as fluorescent tags.

MCF7

MCF7 cells generated the largest spheroids of the cell types tested. As expected, spheroid size increased with increasing cell density; mean areas of MCF7 spheroids seeded at the higher density (2×10^4 cells/mL) were significantly different ($p < 0.05$) from those seeded at lower densities (figure 3-1) and showed a large range of cross-sectional areas, likely due

to the epithelial phenotype of the cells, leading to tighter cell-cell contact. Where the areas of spheroids seeded at the lower density (6×10^3 cells/mL) had the smallest range.

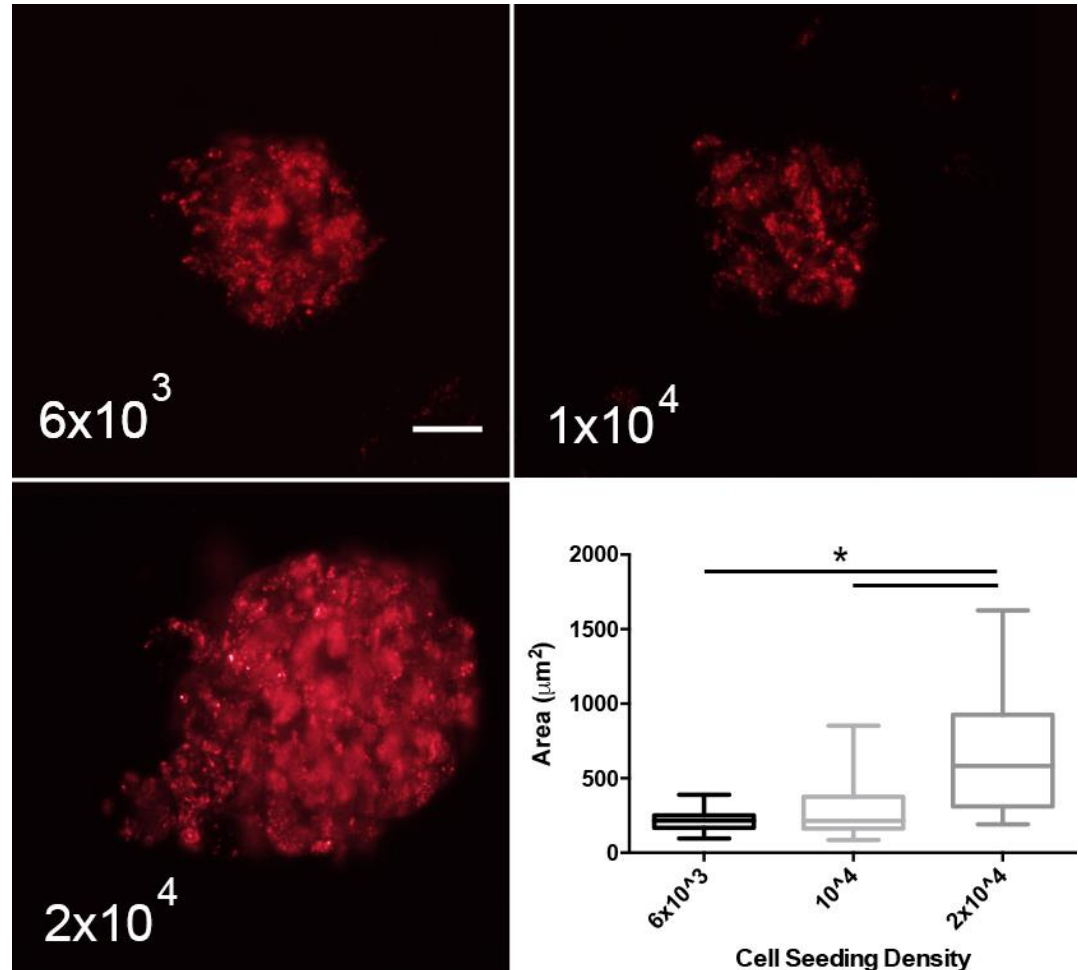


Figure 3-1 MCF7 spheroids seeded at three cell densities. Spheroids cultured for 24 hours in collagen gel, representative of each cell seeding density. Images acquired with Zeiss Axio Vert A1. Red fluorescence derived from mNPs. Scale bar 10 μm . >20 spheroids measured at each cell seeding density across three biological replicates. Spheroid areas measured via pixel count using imageJ. Bars indicate range, asterisk indicates $p < 0.05$.

MDA-MB-231

MDA-MB-231 spheroids generated the smallest spheroids, where seeding at different densities showed no significant change in mean area, with all approximately $200 \mu\text{m}^2$. Each seeding density presented a similar range ($100\text{-}500 \mu\text{m}^2$). Images of these spheroids indicate a loose arrangement of cells, likely due to the more aggressive phenotype of this breast cancer cell line (figure 3-2). These cells are not as tightly bound with one another and appear to be comprised of fewer cells than either MCF7 or MSC spheroids.

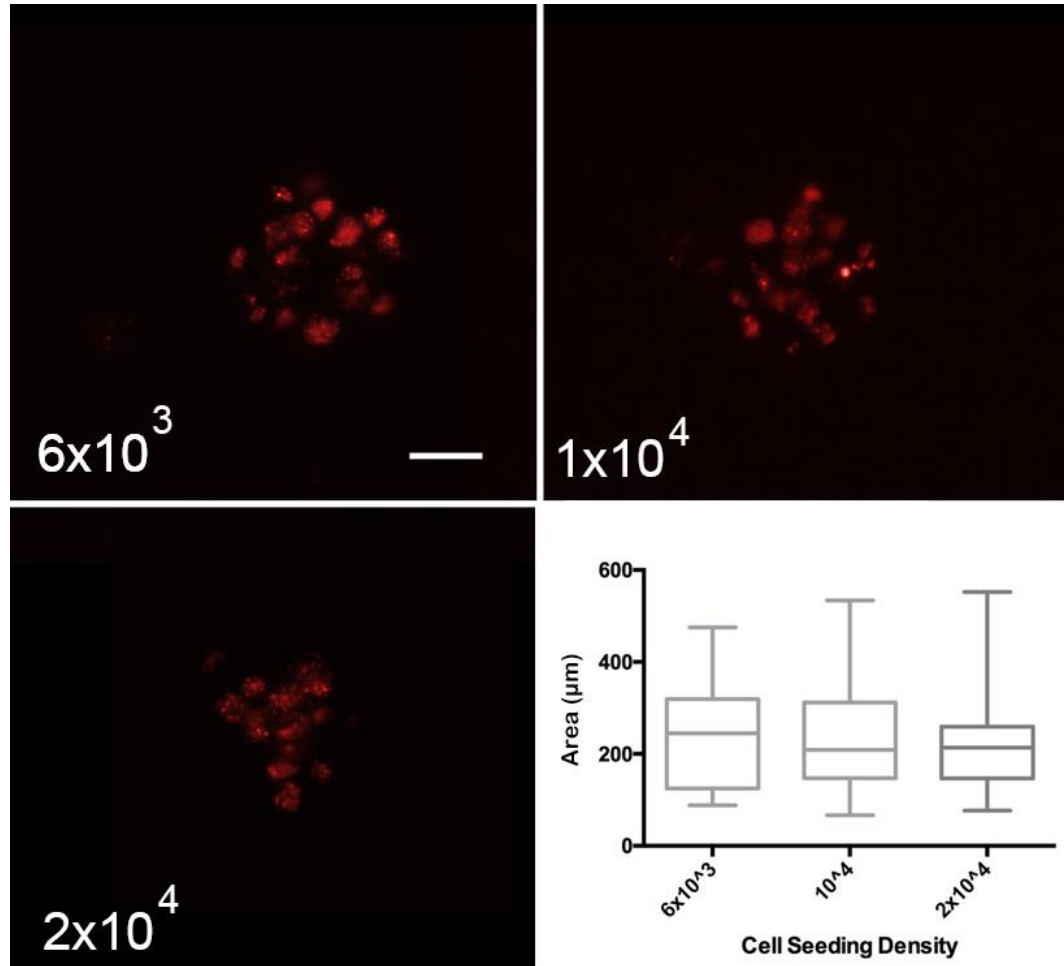


Figure 3-2 MDA-MB-231 spheroids seeded at three cell densities. Spheroids cultured for 24 hours in collagen gel, representative of each cell seeding density. Images acquired with Zeiss Axio Vert A1. Red fluorescence derived from mNPs. Scale bar 10 μm . >20 spheroids measured at each cell seeding density across three biological replicates. Spheroid areas measured via pixel count using imageJ. Bars indicate min and max values.

MSC

MSCs produced mid-range spheroids, where seeding density affected the size of the resulting spheroids. There was a significant difference between cell seeding densities of 6×10^3 cells/mL and the higher 2×10^4 cells/mL, with the mean area of cells seeded at the lower 1×10^4 cells/mL not significantly different from either ($p < 0.05$; figure 3-2). This is reflected in images of these spheroids (figure 3-3). Spheroids derived from cells seeded at 2×10^4 cells/mL appear larger than spheroids derived from lower seeding densities, with a mean area exceeding $200 \mu\text{m}^2$ and a larger range. Spheroids derived from lower cell seeding densities (6×10^3 cells/mL and 1×10^4 cells/mL) appear similar in size, both having a mean area under $200 \mu\text{m}^2$ and a smaller range; cells seeded at 6×10^3 cells/mL having the smallest range likely due to the lower availability of cells.

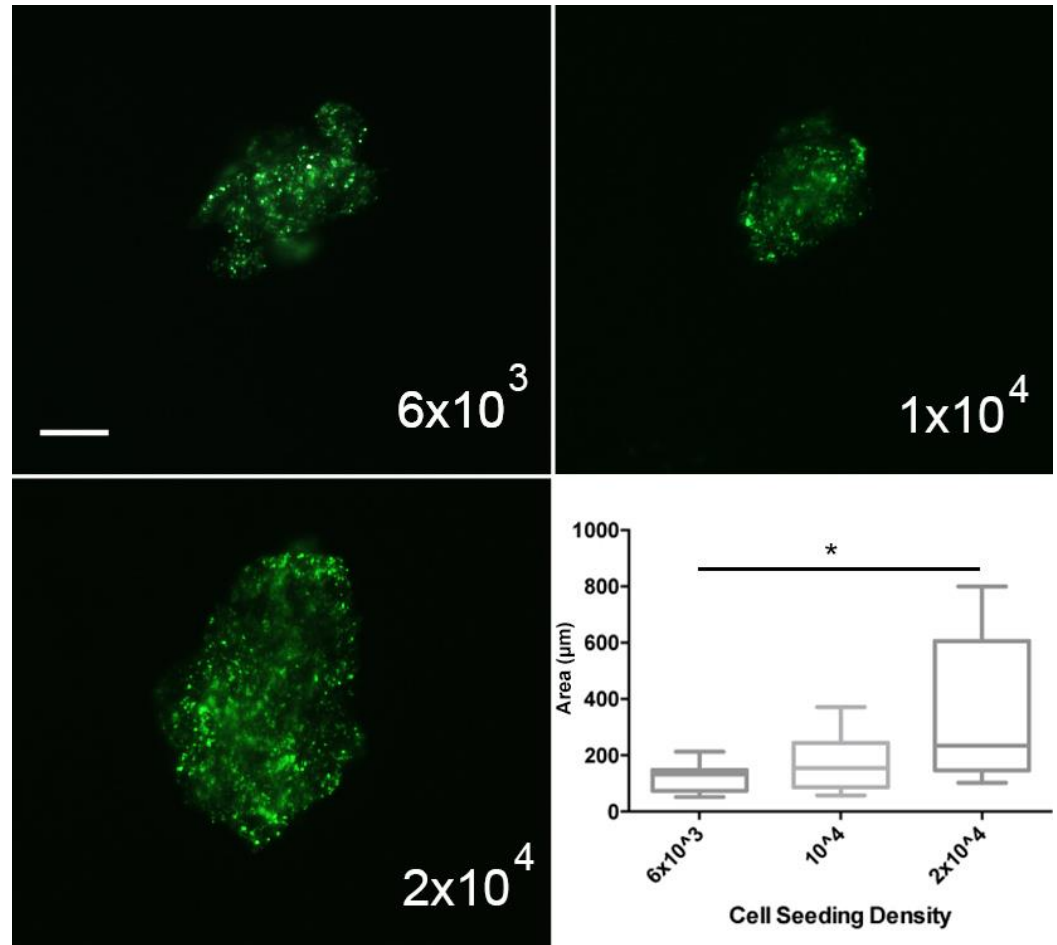


Figure 3-3 MSC spheroids seeded at three cell densities. Spheroids cultured for 24 hours in collagen gel, representative of each cell seeding density. Images acquired with Zeiss Axio Vert A1. Green fluorescence derived from mNPs. Scale bar 10 μm . >20 spheroids measured at each cell seeding density across three biological replicates. Spheroid areas measured via pixel count using imageJ. Bars indicate min and max values asterisk indicates $p < 0.05$.

3.2.ii Electron Microscopy

Following cell density results, all future spheroids were derived from cells seeded at 1×10^4 cells/mL. Spheroids of each cell type were investigated using both scanning and transmission electron microscopy (SEM and TEM respectively). Spheroids were generated as in section 2.5 and prepared for SEM as described in section 2.18.i. TEM was performed to confirm mNP internalisation and to identify the distribution of the mNPs within individual cells in spheroids. Spheroids were sectioned as described in 2.18.ii.

MCF7 spheroids were generated and imaged after 24 hours at 1500x, 2000x and 10000x magnification. The lower magnification shows the whole spheroid (figure 3-4A), providing gross morphology of the entire spheroid, with an approximate spheroid diameter of 50 μm , similar to the cell density study. Increasing the magnification shows the compacted nature of the cells within the spheroid mass (figure 3-4B,C), with approximate cell diameters around 10 μm , and indicates the close relationship between constituent cells. Outer, peripheral, cells appear less compacted; conversely inner cells can be seen compacted to a diameter of ~ 5 μm (figure 3-4B), suggesting peripheral cells experience less force from surrounding cells due to the side exposed to the environment. Further magnification allows the close cell-cell relationships to be seen where protrusions from membranes of neighbouring cells appear to bind to one another forming tight junctions between them.

TEM images of MCF7 spheroids show mNPs are contained within endosomes (figure 3-4D), derived from internalisation via multiple endocytic pathways. No mNPs were detected between cells within a spheroid, suggesting all three cell types are able to retain the mNPs once internalised. Further to this, no mNPs were detected within any

mitochondria. The border of the nucleus can be seen as a double enveloped membrane containing the denser genetic material; No mNPs were present past the nuclear membrane.

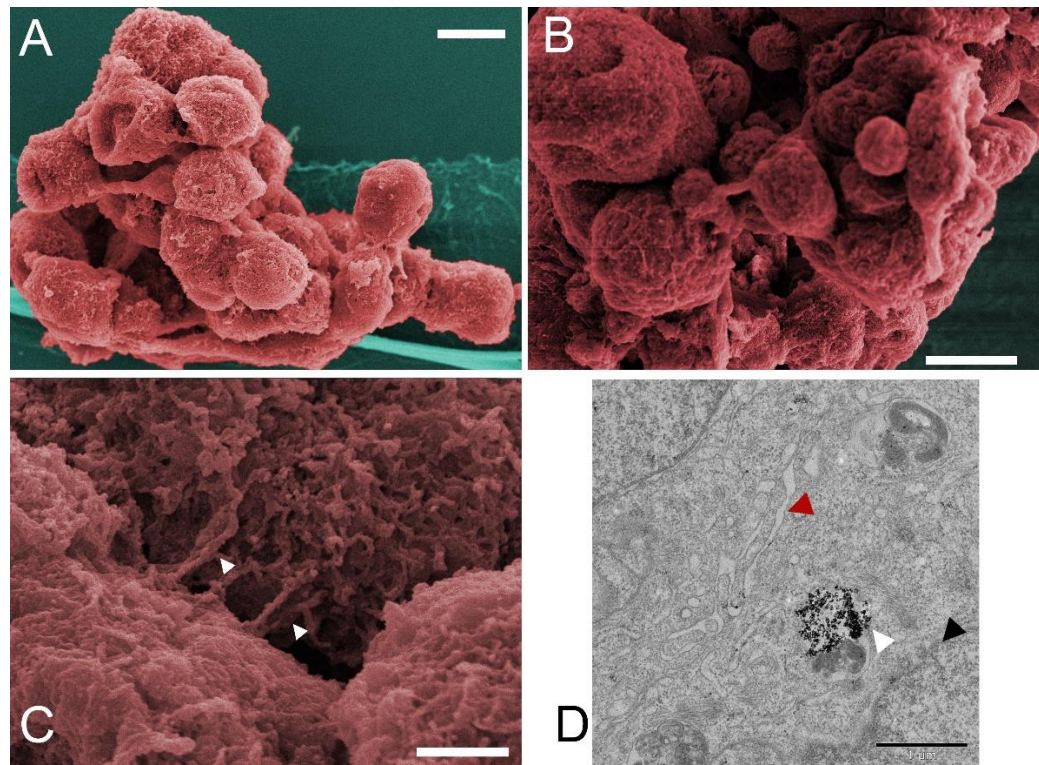


Figure 3-4 Electron microscopy of multicellular MCF7 spheroids. A) 1500X magnification; scale bar 10 μm B) 2000X magnification; scale bar 10 μm C) 10000X magnification; scale bar 2 μm , arrows indicate nanoscale protrusions. Images captured using JEOL JSM-6400 scanning electron microscope at 10kV. D: Transmission electron microscopy of an individual cell within spheroid containing mNPs; black arrow indicates nuclear membrane, red arrow indicates cell membrane, white arrow indicates mNPs. Scale bar 1 μm . Images captured using JEOL 1200 tunnelling electron microscope at 80kV. Spheroids cultured for 24 hours in all cases.

SEM of MDA-MB-231 spheroids incorporating the whole spheroid indicate smaller sized spheroids comprised of fewer cells than those using MCF7, with approximate diameter of 30 μm (figure 3-5A), supporting the cell density study. The MDA-MB-231 cells are compacted, presenting a ball-like phenotype. In a similar fashion to MCF7 cells, these MDA-MB-231 cells have an approximate diameter of around 5-10 μm (figure 3-5B). Higher magnification (figure 3-5C) shows cells within the spheroid are not as tightly bound as MCF7; cell membrane protrusions appear to extending out into the environment and each cell is distinct.

TEM produced images similar to those from MCF7 spheroids; mNPs resided within the cell in endosomes distinct from the cytoplasm and were not present in spaces between cells nor within the nuclei of any cells (figure 3-5D).

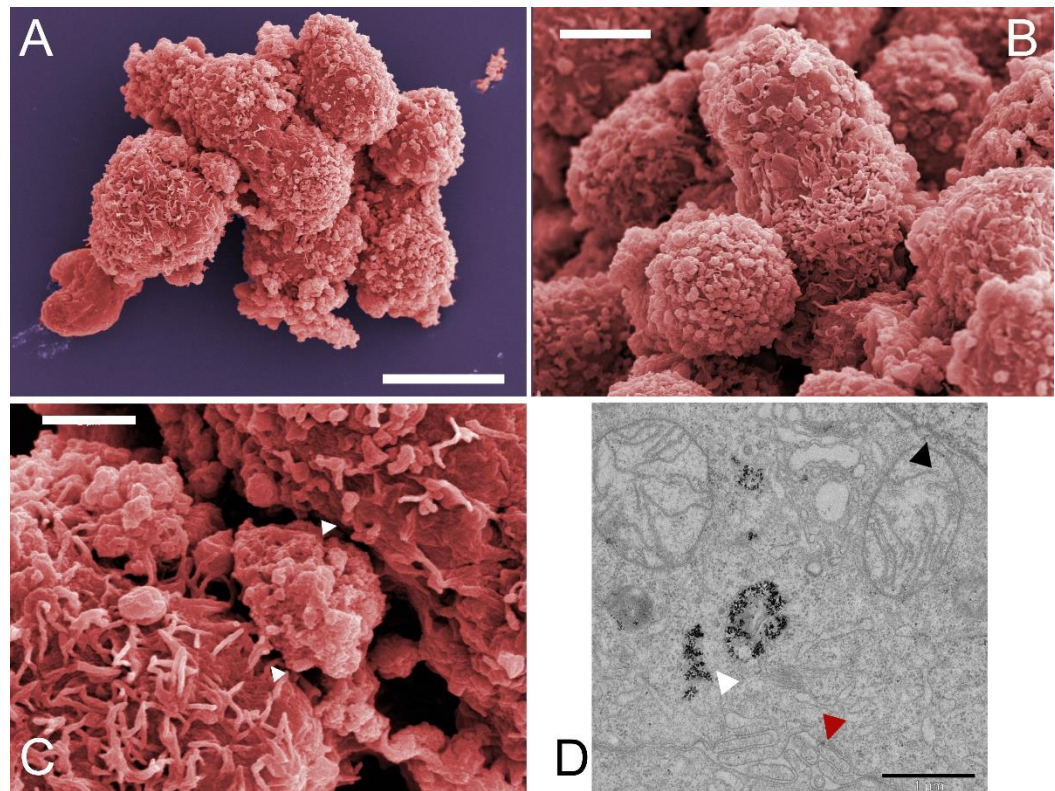


Figure 3-5 Electron microscopy of multicellular MDA-MB-231 spheroids. A) 100X magnification; scale bar 10 μm B) 4000X magnification scale bar 5 μm C) 10000X magnification; scale bar 2 μm , arrows indicate nanoscale protrusions. Images captured using JEOL JSM-6400 scanning electron microscope at 10kV. D: Transmission electron microscopy of an individual cell within spheroid containing mNPs; black arrow indicates nuclear membrane, red arrow indicates cell membrane, white arrow indicates mNPs. Scale bar 1 μm . Images captured using JEOL 1200 tunnelling electron microscope at 80kV. Spheroids cultured for 24 hours in all cases.

MSC spheroids tended to be smaller than MCF7-derived spheroids, despite the same cell seeding density, with spheroid diameters of 40 μm (figure 3-6A) and an overall area approximate to the mean determined in figure 3-2 at 1×10^4 cells/mL. Cells within the spheroid are compacted in a similar way to both BCC lines, with cells measuring approximately 5-10 μm in this three-dimensional environment. Similarly to MCF7 spheroids, increasing the magnification shows the outer membranes of cells comprising the spheroid are indistinct indicating individual cells are tightly associated with one another (figures 3-6B,C).

TEM produced images similar to those from both MCF7 and MDA-MB-231 spheroids; mNPs resided within the cell in endosomes distinct from the cytoplasm and were not present in spaces between cells nor within the nuclei of any cells (figure 3-6D).

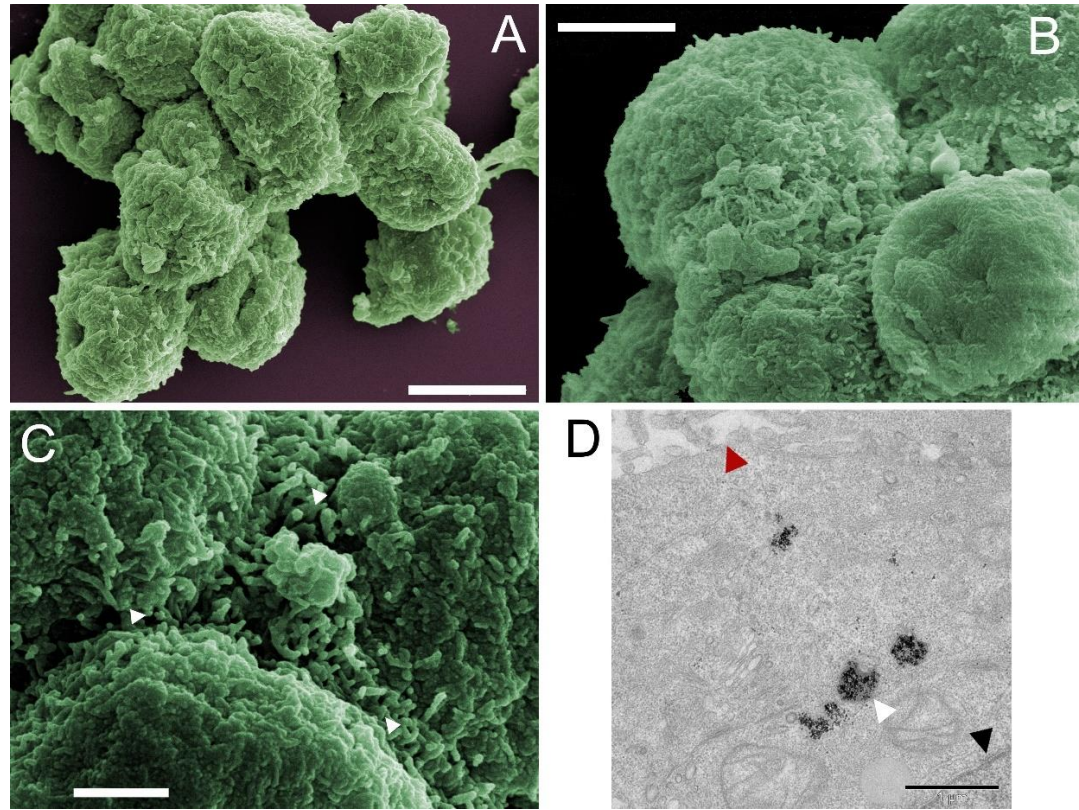


Figure 3-6 Electron microscopy of multicellular MSC spheroids. False colour scanning electron microscopy A) 2500X magnification; scale bar 10 μm B) 5000X magnification; scale bar 5 μm C) 10000X magnification; scale bar 2 μm , arrows indicate nanoscale protrusions. Images captured using JEOL JSM-6400 scanning electron microscope at 10kV. D) Transmission electron microscopy of an individual cell within spheroid containing mNPs; black arrow indicates nuclear membrane, red arrow indicates cell membrane, white arrow indicates mNPs. Scale bar 1 μm . Images captured using JEOL 1200 tunnelling electron microscope at 80kV. Spheroids cultured for 24 hours in all cases.

3.2.iii MCF7 Spheroid Viability

Following the cell density and electron microscopy, all future BCC spheroids were constructed using MCF7 cells as they generated stable spheroids that remained intact over time, where those generated with MDA-MB-231 cells were generally smaller in size, with a large range of sizes. In addition, MDA cells tended to migrate away from the central spheroid mass into the three-dimensional environment of the collagen gel.

The viability of the MCF7 spheroids was subsequently assessed, using the method described in section 2.15, across several days. After both 1 and 7 days there was negligible cell death, indicated by the presence of red fluorescent ethidium (figure 3-7). The majority of the cells within the spheroid were alive, indicated by the presence of green fluorescent calcein.

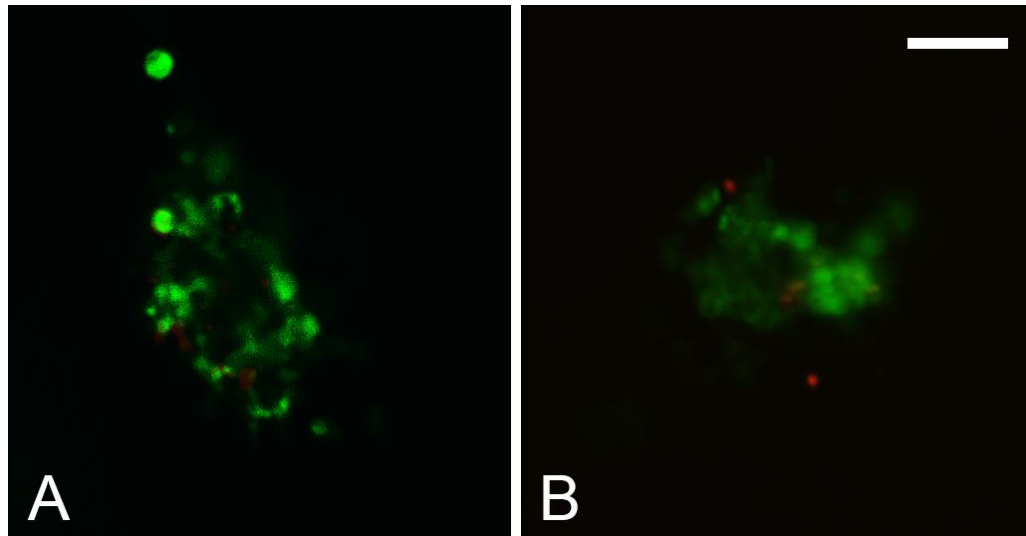


Figure 3-7 MCF7 spheroid viability. Spheroids were cultured in collagen gels for A) 1 day and B) 7 days before being treated with calcein AM to detect live cells (green) and ethidium homodimer to detect dead cells (red). Images acquired with Zeiss Axio Vert A1. Scale bar 10 μm . 3 spheroids imaged with representative spheroid shown.

3.2.iv BrdU Proliferation Assay

The proliferation of MCF7 spheroids was assessed across a 10-day period through BrdU incorporation as described in section 2.13. Peripheral cells in spheroids cultured in collagen gels incorporated BrdU, and were therefore actively synthesising new DNA and proliferating, after 1 and 24 hours (figure 3-8A, B). Proliferation was reduced after 72 hours and absent after 10 days. The cells within the spheroid mass were still partially active at 1 hour (figure 3-8A indicated by the yellow overlap of green mNPs and red antibody-bound BrdU), with only a low level of BrdU fluorescence noted after 72 hours (figure 3-8C). After 10 days in collagen gel the spheroids possessed no red fluorescence (figure 3-8D) indicating no proliferation, suggesting the spheroid had become quiescent between 7 and 10 days.

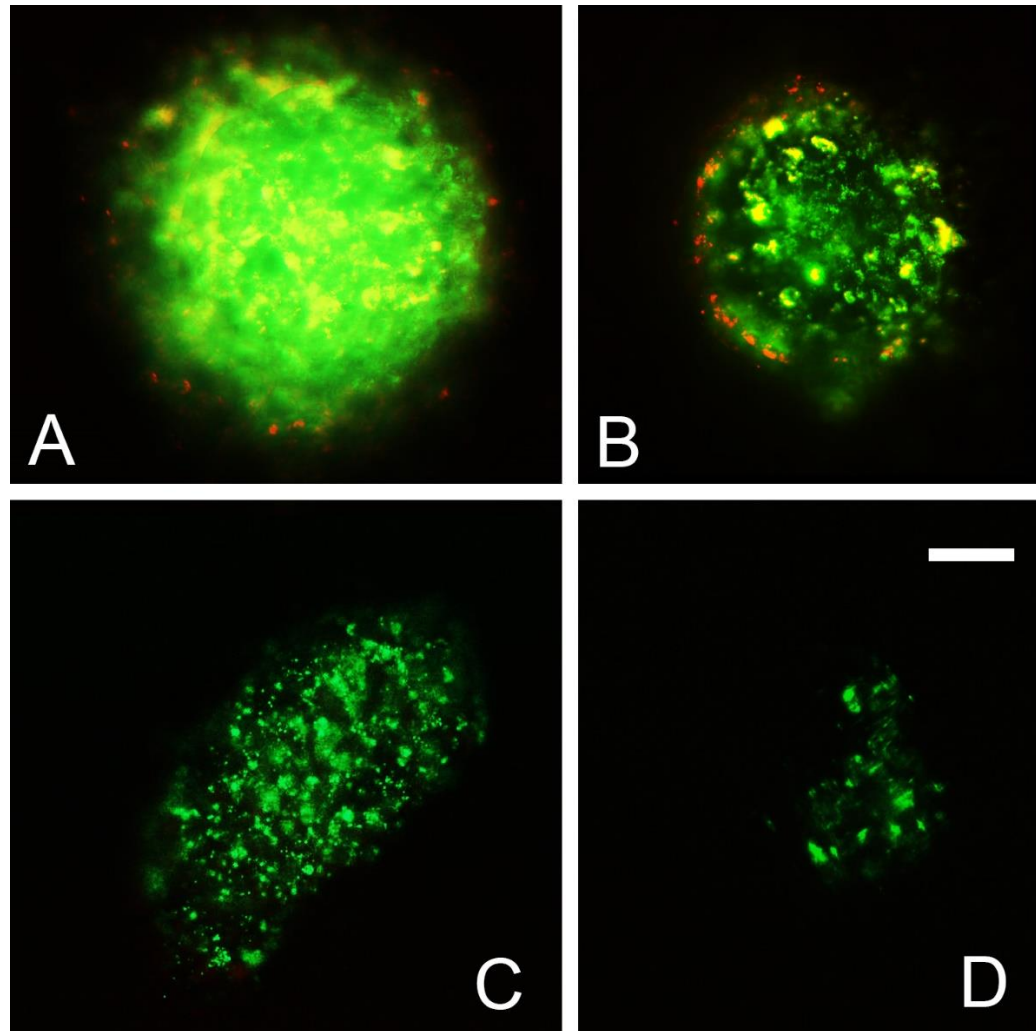


Figure 3-8 BrdU proliferation marker present in MCF7 spheroids. Spheroids cultured in collagen gel for A) 1 hour, B) 24 hours, C) 72 hours and D) 10 days. Images acquired with Zeiss Axio Vert A1. Green fluorescence indicates presence of mNPs, red fluorescence indicates the presence of BrdU probed for using anti-BrdU antibody. Scale bar 10 μm . 3 spheroids imaged at each time point with representative spheroid shown.

3.2.v Fluidigm qPCR of Co-Cultured MSC and MCF7 Spheroids

Following the characterisation of individual MSC and MCF7 spheroid culture, spheroid co-cultures were set-up to determine the influence each cell type has on the other in terms of cell cycle, phenotype and differentiation. MCF7 and MSC spheroids were cultured in collagen gels individually and together; the co-culture was performed as in section 2.6.i and gels were digested as in section 2.7. Where two cell types were present, the cells had to be sorted via FACS as described in section 2.11 to separate the MSCs from MCF7 prior to extracting RNA. Fluidigm real-time PCR was performed as described in section 2.10 and the results herein show the difference in gene expression between spheroids cultured individually and spheroids cultured together. The genes assessed are described in table 2-2.

Effects of Spheroid Co-Culture on MSC Gene Expression

The difference in gene expression of MSC/MCF7 co-cultured spheroids compared with MSCs cultured alone was determined using $\Delta\Delta C_t$. This compared each gene with a housekeeping gene control (GAPDH) to normalise the expression value. These normalised values were then compared to determine how co-culture changes gene expression (figure 3-9).

MSC Cell Cycle : Co-culture downregulated the expression of genes in each stage of the cell cycle several-fold after 7 days in culture. Genes successfully assayed included both cyclins and cyclin-dependent kinases. As shown in figure 1-3, these genes are active at each stage of the cell cycle and several, such as CCNE2 and CDK2 are checkpoints required to pass from G₁ to S phase. The largest decreases are seen in these stages early in the cell cycle, preventing initiation of cell division and DNA synthesis. Whilst CDC7 is upregulated, it acts upon the G₁/S transition where other genes have been downregulated; the overall downregulation will no doubt counter this singular gene.

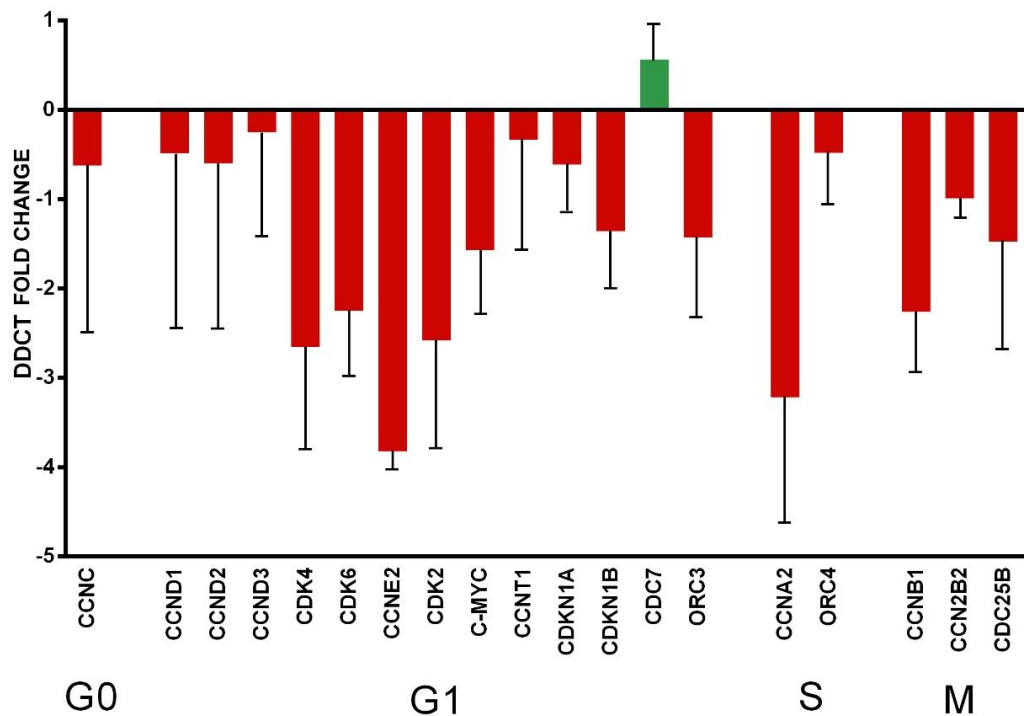


Figure 3-9 $\Delta\Delta C_t$ of cell cycle gene expression in MSC spheroids in co-culture with MCF7 spheroids compared with MSC spheroid monoculture. Expression normalised to GAPDH. Spheroids cultured in collagen gel for 7 days. Error bars indicate standard error mean; n=3 with 3 technical replicates from each.

MSC Phenotype: A panel of epithelial-to-mesenchymal transition (EMT) genes was assessed to determine how co-culture effects the mesenchymal phenotype of MSCs (figure 3-10). Co-culture upregulates N-cadherin and downregulates E-cadherin, suggesting that MSCs will reduce cell-cell adhesion within the spheroid. Other epithelial marker genes assessed such as JUP and Keratin 19 showed over a five-fold reduction indicating an increase in the mesenchymal nature of the MSCs. This is further supported with the upregulation of FN1, a marker of EMT. Successfully assessed genes therefore suggest that MSC/MCF7 spheroid co-culture supported retention of MSC phenotype, with increased migration potential.

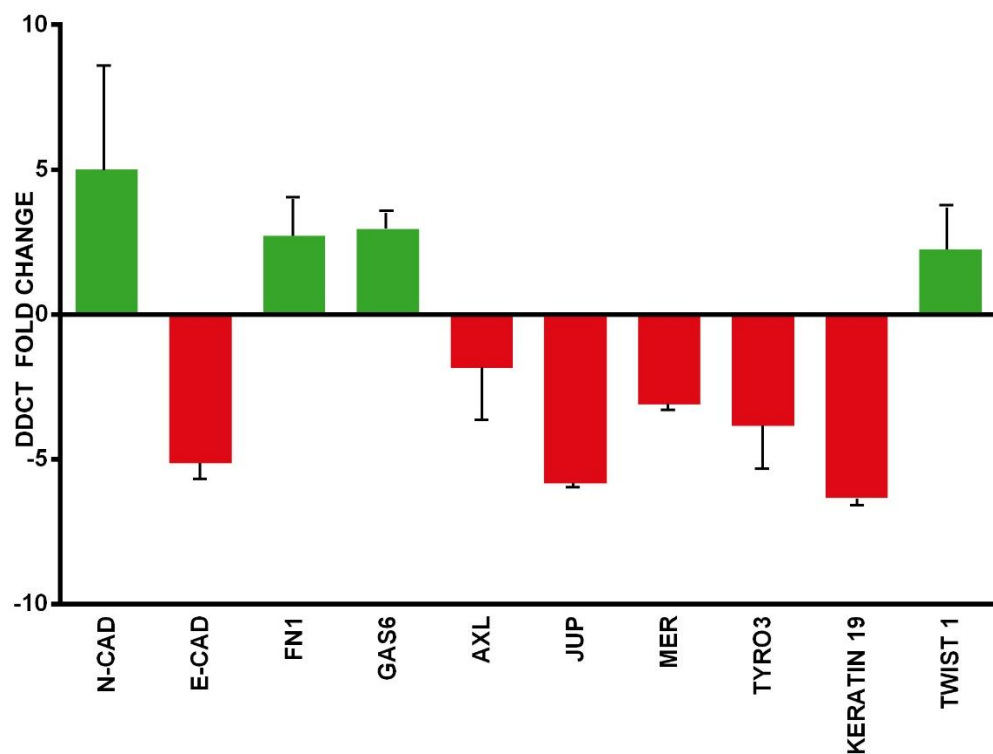


Figure 3-10 $\Delta\Delta C_t$ fold change of EMT marker gene expression in MSC spheroids in co-culture with MCF7 spheroids compared with MSC spheroid monoculture. Expression normalised to GAPDH. Spheroids cultured in collagen gel for 7 days. Error bars indicate standard error mean; n=3 with 3 technical replicates from each.

MSC Differentiation: Several differentiation marker genes were assayed (figure 3-11). Osteopontin (OPN) was upregulated ~3-fold in MSC co-culture reinforcing an MSC migratory phenotype. CXCL12 expression was also upregulated, again indicating increased cell mobility. Differentiation marker genes PPAR γ , RUNX2 and osterix (OSX) are all downregulated in co-culture compared with MSC spheroid monoculture. This may indicate a retention of the stem cell phenotype when co-cultured with MCF7 cells.

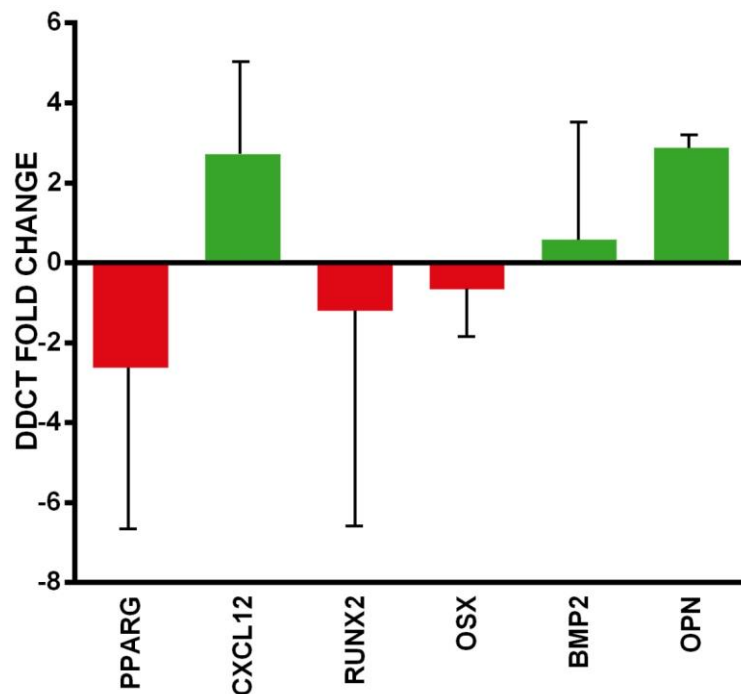


Figure 3-11 $\Delta\Delta C_t$ fold change of osteogenic differentiation marker gene expression in MSC spheroids in co-culture with MCF7 spheroids compared with MSC spheroid monoculture. Expression normalised to GAPDH. Spheroids cultured in collagen gel for 7 days. Error bars indicate standard error mean; n=3 with 3 technical replicates from each.

Effects of Spheroid Co-Culture on MCF7 Gene Expression

The influence of MCF7/MSK spheroids co-culture compared to MCF7 singular spheroid culture in terms of MCF7 gene expression was also assessed (figure 3-12&13).

MCF7 Cell Cycle: BrdU data suggested that MCF7 cells were initially proliferative within spheroid culture, eventually becoming quiescent with time in culture (by day 7-10). However, the proximity with MSCs has upregulated MCF7 cell cycle genes (figure 3-12); each one of the genes successfully assayed was upregulated in each stage of the cell cycle. This suggests that MSC co-culture causes MCF7 cells to either maintain their initial proliferation or become proliferative in the 3D collagen gels (figure 3-12).

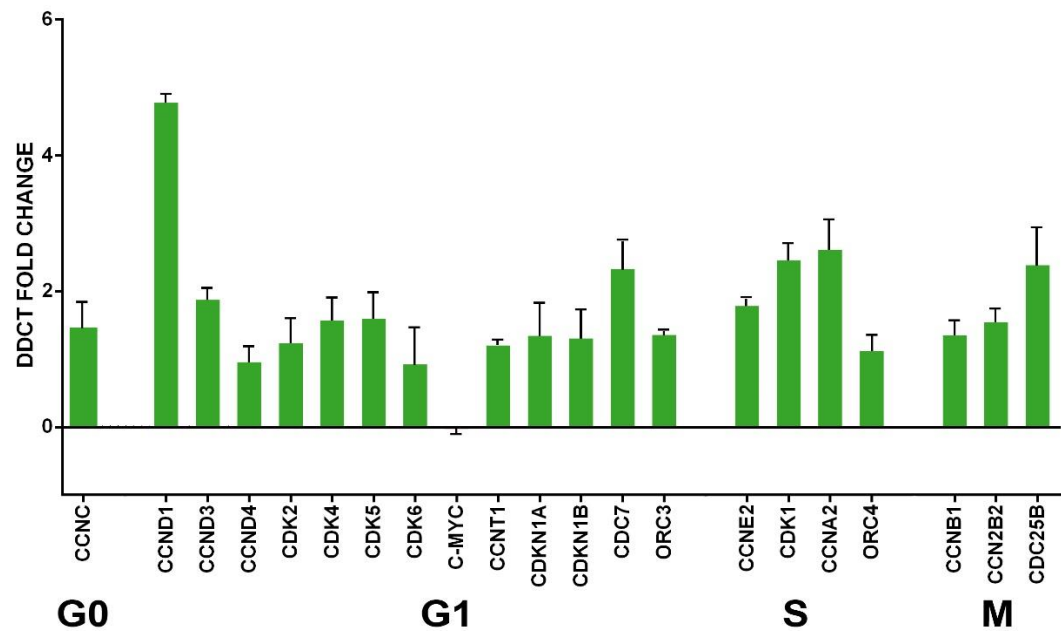


Figure 3-12 $\Delta\Delta C_t$ of cell cycle gene expression in MCF7 spheroids in co-culture with MSC spheroids compared with MCF7 spheroid monoculture. Expression normalised to GAPDH. Spheroids cultured in collagen gel for 7

days. Error bars indicate standard error mean; n=3 with 3 technical replicates from each.

MCF7 Phenotype: A panel of 8 EMT marker genes were successfully assayed (figure 3-13). Whilst N-cadherin assay was unsuccessful, the E-cadherin gene expression increased 4-fold in co-culture suggesting cells become more adherent. Keratin 19, another negative marker for EMT was upregulated. JUP is an important marker of outgrowth and is downregulated here 16-fold. Vimentin and TYRO3 are both highly downregulated (8- and 10-fold respectively) indicating a reinforcement of the epithelial phenotype and a resistance to migrate into the environment when co-cultured with MSCs.

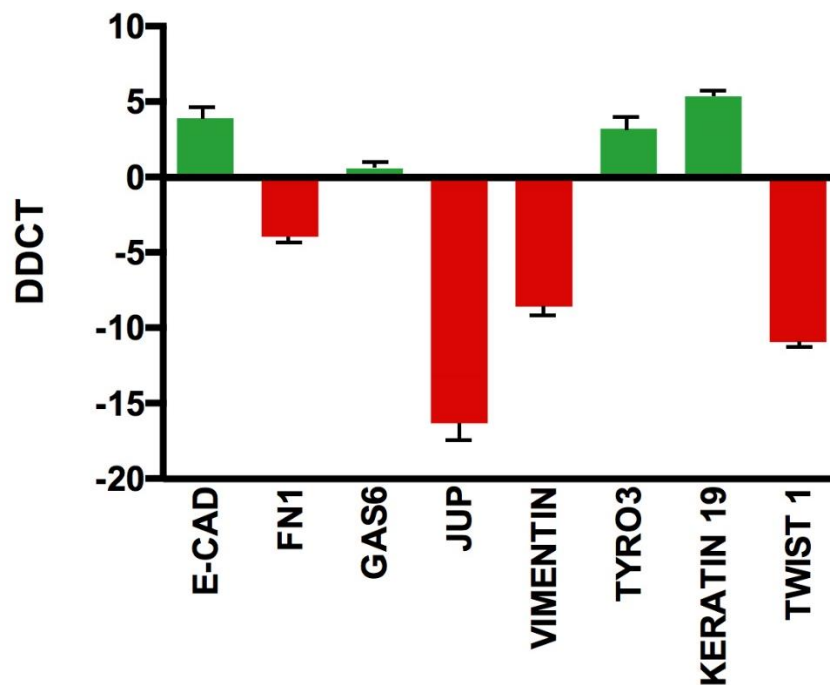


Figure 3-13 $\Delta\Delta C_t$ fold change of EMT marker gene expression in MCF7 spheroids in co-culture with MSC spheroids compared with MCF7 spheroid monoculture. Expression normalised to GAPDH. Spheroids cultured in collagen gel for 7 days. Error bars indicate standard error mean; n=3 with 3 technical replicates from each.

3.3 Discussion

Within the BM niche, resident MSCs remain quiescent until they are required to respond to external signalling cues. Invading BCCs are also able to become quiescent (or dormant) within this environment. This chapter aimed to determine the best BCC line to use in development of a simple *in vitro* model for the BM niche; by co-culturing MSCs and BCCs spheroids within a controlled three-dimensional microenvironment their interactions can be assessed.

Standard two-dimensional monolayer MSC culture generates an artificial environment, unlike the native *in vivo* environment, causing many factors to be lost (Mueller-Klieser et al., 1997). In three-dimensional spheroid culture MSC morphology is vastly different from monolayer culture; instead of adopting a stellate morphology, MSCs will form a ball-like phenotype (figure 3-6) and tightly adhere to neighbouring cells through cadherins (Lee et al., 2012). This morphological change affects MSC proliferation, motility, metabolism and differentiation potential (Bellas and Chen, 2014, McBeath et al., 2004).

The stiffness of the environment also plays a vital role in MSC growth and differentiation. For example, in monolayer culture, the Young's modulus of culture plastic is in the GPa range, whereas the BM environment is several orders of magnitude lower (Baraniak et al., 2012). The type of spheroid culture adopted here, where spheroids are cultured within a type I collagen gel, mimicking the native bone marrow microenvironment, with the collagen gel approximately 10kPa (Lewis et al., 2016). We believe that the stiffness of the environment affects the cell cytoskeleton, thus changing gene expression and causing the MSCs to quiesce (Lewis et al., 2016).

3.3.i MSC Spheroid Culture

MSC spheroid size was dependent on cell seeding density; more cells lead to larger spheroids, but also a greater range of sizes (figure 3-2). It is evident that higher seeding densities permit faster spheroid formation as more cells are present in the same location. Furthermore, as there will be more small spheroids, these are able to accrete to form larger spheroids in the incubation period. This relationship is similar to that seen by Bartosh and colleagues (2010); larger numbers of cells added will produce larger spheroids in a linear fashion. However, the cell numbers are much larger, in some cases 250,000 cells/mL, producing spheroids much larger in size over a period of up to 4 days instead of the 24 hour incubation used within this study.

The results here supported previous finding in our group where Lewis et al. (2016) reported that MSCs remain viable when cultured as spheroids in collagen gels, with increased MSC marker retention and reduced proliferation (i.e. MSCs become quiescent).

3.3.ii MCF7 Cells Generate Stable Spheroids

MCF7 cells form spheroids similar in size to MSCs, whilst MDA-MB-231 cells generate much smaller spheroids. Likewise, MCF7 spheroids increase in size and size range with increasing cell numbers, while MDA spheroids remain of a similar overall size regardless of the cell seeding density. As detailed in section 1.2 there are several key differences between MCF7 and MDA-MB-231 BCCs. MCF7 possesses a strong epithelial phenotype (Yin, 2011); in monolayer these cells will form colonies due to the high native E-cadherin expression (Hazan et al., 2004). The E-cadherin

expression is maintained within 3D culture, potentially enhancing spheroid formation (Yui et al., 2005).

The SEM images of the MCF7 spheroids supports their epithelial phenotype, demonstrating cells closely associated with one another. The lamellipodia on the cells' surfaces can be seen in figure 3-4C; neighbouring cells appear to be joined at these cellular protrusions, likely through E-cadherin (Yui et al., 2005). In the absence of any external cues these bonds will remain strong (Hazan et al., 2004). MCF7 cells adopted a ball-like phenotype as they are compacted within the spheroid (figure 3-4)(Webster et al., 2008). MCF7 spheroids cultured alone in collagen gels are initially proliferative, becoming quiescent by day 7. The rounded cell morphology may encourage cell quiescence as it is believed the cytoplasm:nucleus ratio dictates whether the nucleus enters G_0 or divides (Roca-Cusachs et al., 2004).

Cell phenotype, therefore, appears to play a significant role in spheroid generation. MDA-MB-231 exhibits a mesenchymal phenotype, so is prone to metastasis (Charafe-Jauffret et al., 2006). This phenotype results in a low E-cadherin expression (Theys et al., 2011), with a higher N-cadherin expression increasing cell motility (Nieman et al., 1999). This is likely why spheroids generated using MDA-MB-231 do not aggregate into larger masses when more cells are available (figure 3-3). It is for this reason that MCF7 cells were selected moving forward with MSC co-culture studies, as MCF7 spheroids are stable and appear quiescent in 3D culture.

3.3.iii MCF7 Cells Become Quiescent in 3D Spheroid Culture

Initially the MCF7 spheroids retain their proliferative activity as they are transferred into the collagen gel matrix. Over time in culture this activity is lost and distinct zones become apparent within the cell mass. The core cells lose their proliferative activity, perhaps as they are compacted against neighbouring cells (De Sousa et al., 2013), reducing the availability of nutrients. Meanwhile, the peripheral cells remain proliferative for longer as they have access to the surrounding environment. This proliferation gradient is a key factor when modelling micrometastases, as this occurs in an *in vivo* setting (Mueller-Klieser, 1987). The loss of cell proliferation by day 10 further supports the use of MCF7 cells in further analysis of breast cancer dormancy within the BM environment.

3.3.iv MSC and MCF7 Spheroid Co-Culture

In order to create a 3D bone marrow model of BCC dormancy/recurrence, both MSC and MCF7 cell spheroids were co-cultured together within the collagen gel. Co-culture for 7 days clearly changed several aspects of gene expression within both cell types.

MSC Spheroids are Quiescent and Retain phenotype in Co-culture

As previously stated, MSCs cultured as spheroids within collagen gels enter a quiescent state after several days (Lewis et al., 2016). Whilst there is much research into how MSCs might affect BCC proliferation in 3D co-culture, studies into the converse are much less common. It is interesting then that MCF7 spheroids in close proximity to MSCs enhance their quiescence by actively downregulating many cell cycle genes (figure 3-9).

Conversely the phenotype (EMT) markers expressed by MSCs in co-culture show an upregulation in the mobile mesenchymal phenotype (figure 3-10), perhaps leading to cell migration in the BM environment via signalling axes caused by the proximal BCCs, such as CXCR4-CXCL12 (Wang et al., 2006).

MCF7 spheroids appear to have a positive effect on the long-term stemness of MSCs (Melzer et al., 2016), where key markers are downregulated to prevent a movement towards either osteogenesis or adipogenesis (figure 3-11).

MCF7 Spheroids Re-enter Cell Cycle While Retaining Phenotype in Co-culture

Conversely the MCF7 spheroid cells co-cultured with MSCs experience an upregulation of genes at each stage of the cell cycle, when compared to MCF7 spheroids cultured in isolation (figure 3-12). BCCs co-cultured with MSCs have previously been shown to increase proliferation following both physical contact and paracrine signalling (Daverey et al., 2015; Maffey et al., 2017). MCF7 cells cultured in 3D scaffolds as both multicellular spheroids or discrete cells display an increase in tumourigenicity and secrete pro-angiogenic factors in addition to becoming stem cell-like indicated by CSC markers CD44⁺/CD24^{low/-} (Boo et al., 2016; Chen et al., 2012).

The presence of the MSCs appears to reinforce the epithelial MCF7 phenotype, with an increase in EMT markers present in MCF7 spheroids (figure 3-13); a resistance to metastasise further.

Generating these spheroids separately causes the spheroids to reside within the gel distinctly, with a relatively large distance between them (up to 1 cm in the case of gels generated in 24-well plates). This does not stop the presence of one cell type affecting the other so this would indicate a paracrine signalling effect. This effect could be caused by several agents; cytokines (Karnoub et al., 2007), cellular metabolites (Chiarugi et al., 2016) or exosomes (Bliss et al., 2016). The effects of these will be assessed in future chapters. Direct contact between the two cell types may also be playing a role, through the formation of gap junctions between the cells, then can permit the passage of microRNAs (Gregory et al., 2011), and receptor ligand interactions (Wang et al., 2006).

3.4 Conclusion

In this chapter, the previously described method of spheroid generation using mNPs has been successfully adopted in both MCF7 and MDA-MB-231 BCC lines, in addition to providing further data for MSC-based spheroids. The seeding density of future spheroids in this thesis was determined to be 1×10^4 cells/mL. This study indicated that MDA-MB-231 spheroids were not suitable moving forward with the *in vitro* model, due to their small size and difficulty with maintaining them in collagen gel. Therefore, MCF7 will be used.

The gene expression data obtained from MSC/MCF7 spheroid co-culture suggested active paracrine signalling, with each cell type affecting the other. In subsequent chapters I will look at the type of paracrine signalling that may be responsible, and try to determine whether we can use these cell signals to control MCF7 cell behaviour in culture, with the potential to artificially control cell dormancy and recurrence.

4 Paracrine Cell Signalling in MSC/MCF7 Co-Culture

4.1 Introduction

The mechanism of primary metastasis is well documented (Kang et al., 2003; Weigelt et al., 2005; Hüsemann et al., 2008). However, the mechanism of secondary metastasis within the BM is currently not well understood (Chaffer and Weinberg, 2011). The initiation of cancer cells, in particular BCCs, from dormant to a recurrent, active state has been a focus of much research (Paik et al., 2004; Dent et al., 2007; Korde et al., 2018). It is believed that external environmental stimuli cause dormant cancer cells to re-enter the cell cycle allowing secondary metastasis to occur.

The BM microenvironment contains multiple cell types, including resident MSCs, which secrete many soluble factors, such as cytokines and chemokines, which maintain cellular homeostasis in the BM (Papaccio et al., 2017). On entering the BM environment, invading cancer cells are exposed to these soluble factors (Birbrair and Frenette, 2016). Therefore, paracrine signaling, facilitated by the cytokine secretion of cells residing in the BM, may be key when considering BCC dormancy and recurrence in the marrow.

Of particular relevance are resident MSCs, which govern the homeostasis of the BM microenvironment. As described in chapter 1, MSCs respond to tissue injury via migration and differentiation by using soluble factors as chemical cues. Local inflammation or injury causes immune cells within the BM to release cytokines such as transforming growth factor- β (TGF β 1), tumour necrosis factor- α (TNF- α), several interleukins including IL-1, IL-6, IL-10 and the interferons; all play an important role in controlling the immune system (Yagi et al, 2012). These cytokines also

stimulate the recruitment of MSCs where they are able to initiate tissue repair at the site of wound (Maxson et al, 2012).

In addition to their own response to chemokines, MSCs themselves anchor in the BM and secrete soluble factors to influence other resident cells. For example, MSCs secrete cytokines such as CXCL12 that are integral in maintaining a population of self-renewing HSCs (Mishima et al., 2015). In addition, MSCs secrete a range of anti-inflammatory cytokines such as IL-10 and VEGF, which can affect the polarisation of macrophages (Sridharan et al., 2015); and IL-6, which stimulates tumour growth through the production of tumour-stimulating factors (Spaeth et al., 2013).

When considering BCC invasion into the marrow, the BCCs will therefore also be influenced by soluble factors secreted by MSCs. Indeed, BCCs are attracted towards MSCs via the CXCR4/CXCL12 axis. It is well established that the proliferation and metastatic potential of BCCs is dependent on autocrine signalling of cytokines such as IL-6 and IL-8 (Hartman et al., 2013). Thus it seems appropriate to suggest that MSCs are able to regulate the growth of BCCs within the BM through cytokine networks (Liu et al., 2011).

The *in vitro* model of the BM described in Chapter 3 will provide an excellent platform to study paracrine signaling of MSCs and MCF7 3D co-cultured spheroids. Through the culturing of individual spheroids discretely and also in co-culture, the model provides an opportunity to ascertain how each cell type may affect the other; MSCs may react differently in the presence of BCCs and vice versa.

4.1.i Objectives

This chapter aims to assess paracrine signalling in MSC/MCF7 co-cultures. Initially, the types of cytokines secreted from both cell types will be determined, followed by migration studies on the cells in both monolayer and 3D spheroid culture. In order to achieve this, the following objectives will be met:

- The identification of key cytokine secretions from MSC and MCF7 cell spheroids, from both individual and co-cultures.
- Assessing the effect of two main MSC-derived cytokines, IL-6 and TGF β 1, on MCF7 cell migration.

4.2 Results

Chapter 3 described a co-culture system for MSC and MCF7 spheroids. These co-cultures will be used throughout this chapter to ascertain the influence each cell type may have on the other in terms of paracrine (cytokine) signalling. The spheroids are co-cultured and imaged using the fluorescent properties of the mNPs.

MCF7 and MSC Spheroid Co-cultures

MSC and MCF7 spheroids were co-cultured in collagen gels as described in section 2.6.i. After 3 days' co-culture the MSC and MCF7 spheroids were observed in close proximity (figure 4-1A), but appear to retain their bulk spheroid morphology. Further time in co-culture, however, appears to disturb the distinct spheroid structures, where cells from both MCF7 and MSC spheroids appear to migrate out into the collagen gel environment, interacting with each other (figure 4-1B).

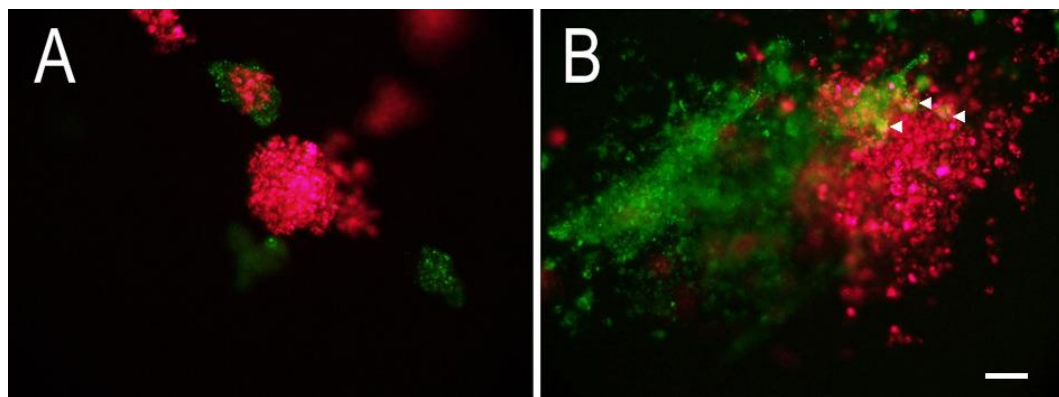


Figure 4-1 MCF7 and MSC spheroids co-cultured in a collagen gel. A) 3 days and B) 7 days. Images acquired using Zeiss Axio Vert A1 fluorescent microscope and colourised using Adobe Photoshop; (n=3, representative spheroid shown, scale bar 10 μ m). Arrows indicate areas of yellow fluorescence where red and green are co-localised, indicating cell interaction.

4.2.i Cytokine Secretions

MSC and MCF7 spheroids were generated as described in section 2.5 and cultured in collagen gels as in section 2.6. In the case of MSC/MCF7 spheroid co-culture, spheroids were generated discretely and cultured in the same gel as described in section 2.6.i. After 3 days, the culture medium was removed from the gel and replaced. This was then removed 4 days later, at day 7 post gel implantation. These conditioned media were then applied to individual 23-target cytokine arrays as described in section 2.17. The targets and array layout are shown in table 2-7 below. Targets were selected based on a literature review to determine which cytokines are key in BM homeostasis. The positive control spots on each array contain the same amount of IgG; the mean pixel density derived from positive controls on each of the six arrays was similar so each array can be fairly compared (figure 4-2).

Table 4-1 Abcam 23-target cytokine array layout. POS denotes positive control IgG and NEG denotes spots containing buffer only.

POS	POS	NEG	NEG	G-CSF	GM-CSF	GRO	GRO α
POS	POS	NEG	NEG	G-CSF	GM-CSF	GRO	GRO α
IL-1 α	IL-2	IL-3	IL-5	IL-6	IL-7	IL-8	IL-10
IL-1 α	IL-2	IL-3	IL-5	IL-6	IL-7	IL-8	IL-10
IL-13	IL-15	IFN- γ	MCP-1	MCP-2	MCP-3	MIG	RANTES
IL-13	IL-15	IFN- γ	MCP-1	MCP-2	MCP-3	MIG	RANTES
TGFB1	TNF- α	TNF- β	blank	blank	blank	blank	POS
TGFB1	TNF- α	TNF- β	blank	blank	blank	blank	POS

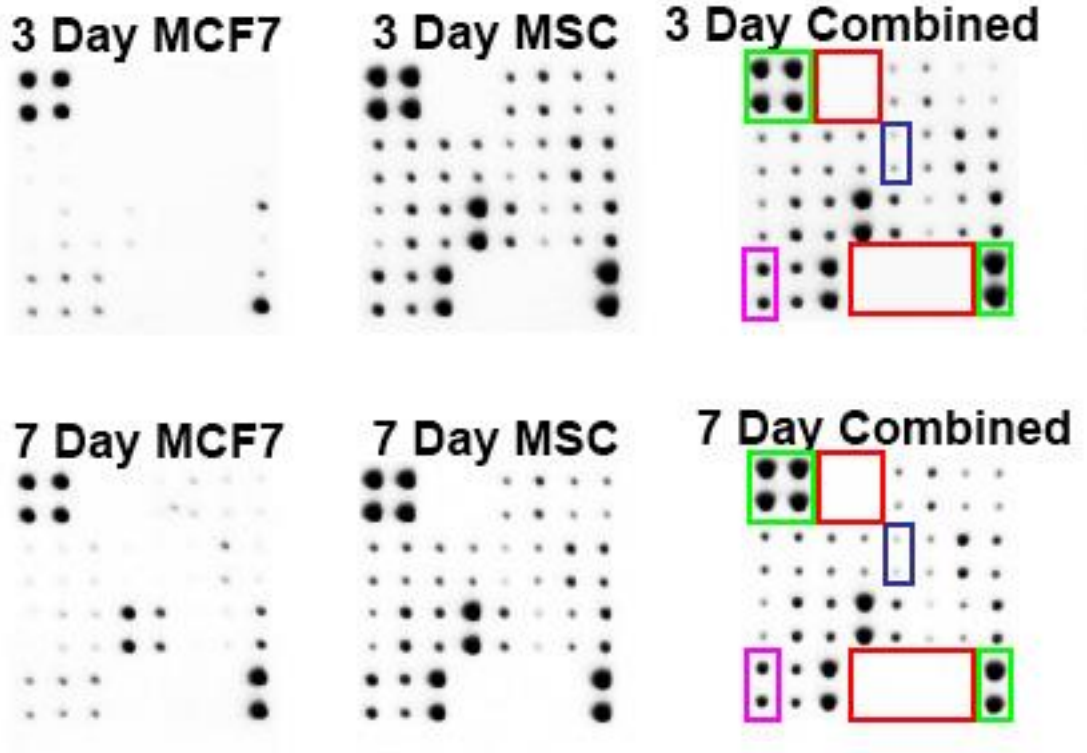


Figure 4-2 Cytokine secretion of MCF7 and MSC spheroids cultured alone or together in collagen gel. DMEM was collected from gels at day 3 and 7 then applied to individual 23 target cytokine arrays. Antibody chemiluminescence detected using Azure c500 Infrared Western Blot Imaging System. Pink box indicates TGFβ and blue IL-6. Green squares indicate positive controls, red negative. *MSC Spheroid Cultures*

Many cytokines assayed by MSC spheroid monocultures did not greatly change between days 3 and 7 (figures 4-3 and 4-4 respectively). However, longer culture did affect the levels of some cytokines secreted into the culture medium both positively and negatively; there was a significant decrease ($p < 0.05$) in IL-8 and MCP-1, with a significant increase in TNFB secretion after 7 days vs 3 days.

When compared with MCF7 cytokine secretion levels, MSCs clearly secrete large levels of many interleukins (eg. IL-3, -5, -6, -7, -8 and -10) at the earlier 3 day time point; however, by day 7, in almost all cases, whilst MSC secretion levels have not changed, MCF7 levels have increased to match the MSCs.

MCF7 Spheroid Cultures

In a similar way to MSC spheroid monoculture, MCF7 spheroids cultured alone do not exhibit large variations in cytokine secretions (figures 4-3 and 4-4 respectively). Whilst many cytokines are reduced after 7 days in culture, IL-8 and MCP-1 are significantly increased and TNFB decreased, the converse to that seen in MSC spheroid monoculture.

MSC/MCF7 Spheroid Co-Cultures

The co-culture environment appears to create a slightly different cytokine profile. Many of the cytokines present in co-culture are significantly different (changes both higher and lower; $p < 0.05$), clearly indicating that the cells are altering their paracrine signalling secretions in response to each other.

Co-culture does not appear to greatly affect the cytokine secretion profile of MSCs, with many levels appearing similar at both time points (figures 4-3 and 4-4 respectively). However, the TNF- β level at 3 days, is greatly reduced when MSCs are co-cultured with MCF7 compared with MSC spheroids alone (figure 4-3), indicating the presence of MCF7 is directly affecting the MSCs. The greater change arises between MCF7 spheroids and MSC/MCF7 co-culture. The nature of the experiment doesn't allow the two cell types to be separated, but the overall level of cytokines released into the environment does not appear not additive (figure 4-3); it is not the concentration secreted by MSC spheroids plus that of MCF7 spheroids.

Proliferative cytokines such as IL-6 and TGF β 1 are increased in the co-culture compared with MCF7 alone, which will alter the behaviour of the breast cancer, likely causing cell division and migration. There is a significant decrease ($p < 0.05$) in the pro-inflammatory cytokines MCP-1 (CCL2), MCP-2 (CCL8) and RANTES (CCL5) after 7 days (figure 4-3). A decrease will slow the recruitment of pro-inflammatory immune cells, protecting the BCCs from destruction. Whilst these aren't decreased until after day 3, TNF α and TGF β are reduced after 3 days in co-culture compared with MCF7 alone, suggesting the MSCs are conferring an immune-protection upon the BCCs.

The changes seen in the interleukins after 7 days (figure 4-3) will contribute to maintaining the immaturity of local immune cells, further protecting the BCCs from destruction. In these cases, it is clear that the presence of MCF7 is reducing the ability of MSCs to produce these cytokines that would ordinarily contribute to niche maintenance. These results suggest that the presence of MCF7 cells causes MSC to alter their secretion profile, which may protect them from the immune cells present in the BM.

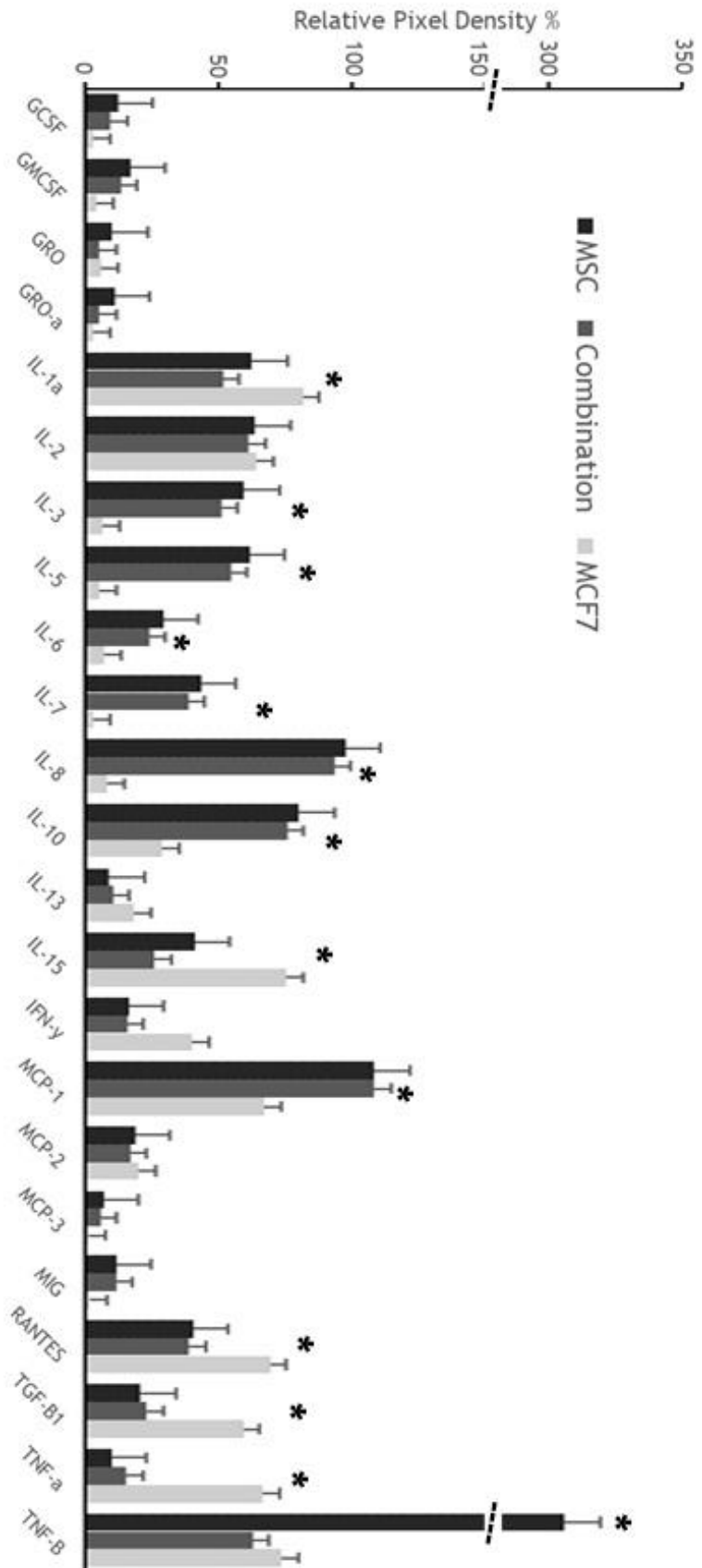


Figure 4-3 Mean cytokine secretion profile of 3-day conditioned culture medium. All values normalised to mean of positive control. Pixel density calculated in ImageJ from 3 day arrays depicted in figure 4-1. Error bars indicate standard error mean; n=2 with 2 replicates on each array. * denotes co-culture change (p<0.05) compared with either MSC or MCF7.

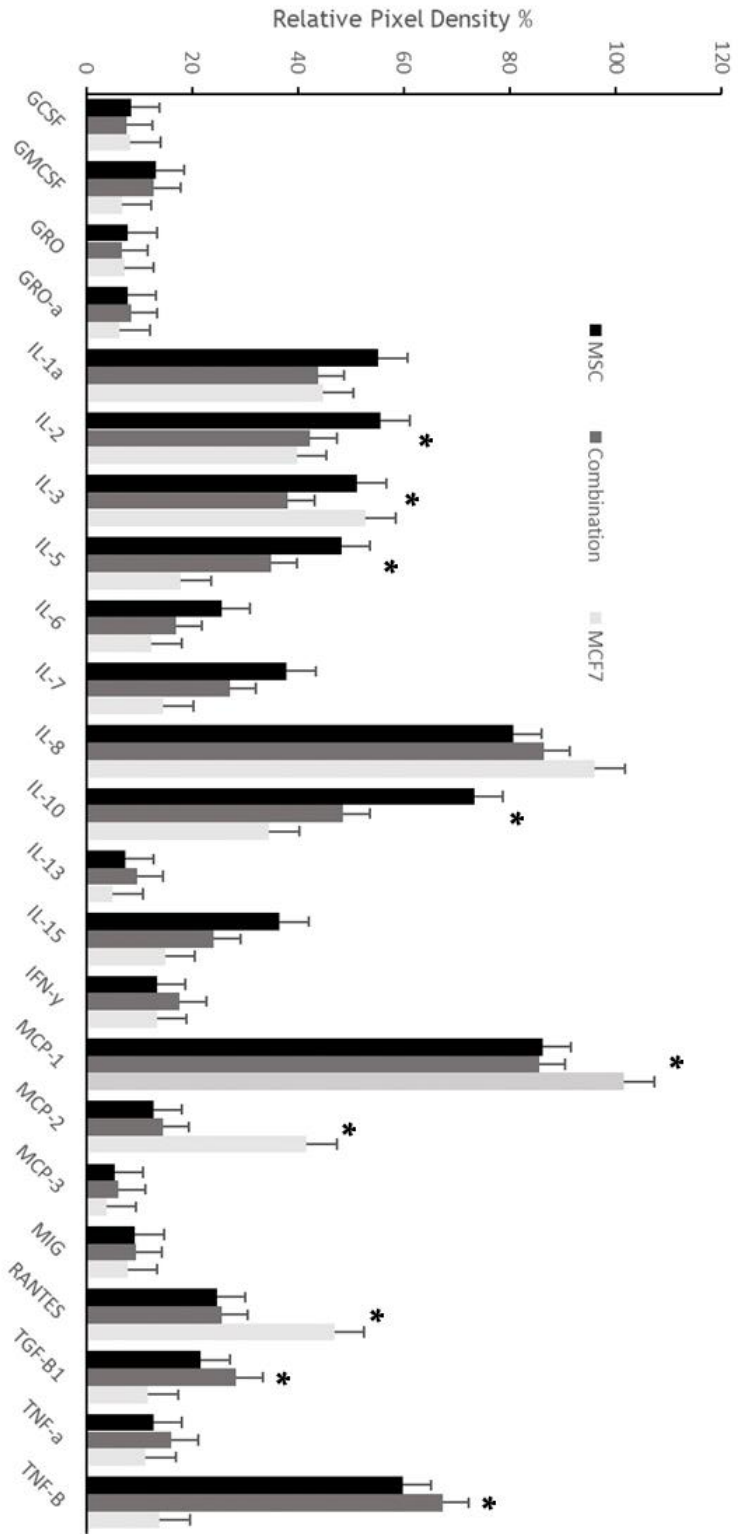


Figure 4-4 Mean cytokine secretion profile of 7-day conditioned culture medium. All values normalised to mean of positive control. Pixel density calculated in ImageJ from 3 day arrays depicted in figure 4-1. Error bars indicate standard error mean; n=2 with 2 replicates on each array. * denotes co-culture change (p<0.05) compared with either MSC or MCF7.

4.2.ii Interleukin-6 Effects on MCF7

During co-culture, it was observed that both MSC and MCF7 cells migrate in 3D spheroid co-cultures at day 7 (figure 4-1). Assuming MCF7 migration is related to MSC-derived cytokines, the cytokine profiling suggested that several cytokines may be responsible for this migration. In this regard, based on our results and the current literature implicating both with increased tumour proliferation and metastasis, IL-6 and TGF β were selected for further study, to determine their effect on MCF7 migration.

MCF7 Cell Migration Response to IL-6 (2D Study)

Purified IL-6 protein was added to culture medium to determine any migratory influence upon MCF7 cells cultured in monolayer. The migration of individual MCF7 cells was assessed using time lapse over a period of 24 hours (figure 4-5). Cell migration was analysed and plotted, indicating preferential migration towards IL-6 (figure 4-8B).

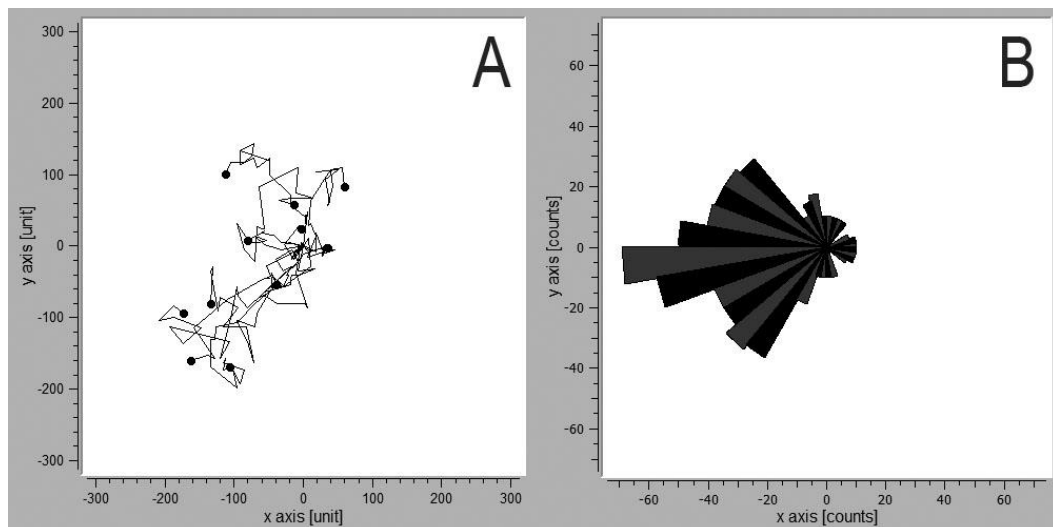


Figure 4-5 MCF7 cell migration in the presence of an IL-6 gradient over 24 hours. A) a vector plot of individual cells tracked, and B) a rose plot summarising overall migration. Coordinates (0,0) reflect the origin of each cell. DMEM containing IL-6 1 ng/mL concentration gradient located on negative x-axis, with undoped DMEM present towards the positive x-axis (12 cells tracked across 3 wells). Cells imaged on Zeiss Axiovert 25, photographed every hour for 24 hours and tracked using ibidi chemotaxis plugin for ImageJ.

MCF7 Cell Migration Response to IL-6 (3D Spheroid Study)

MCF7 spheroids were cultured in collagen gels and incubated with culture medium containing IL-6. Spheroids were imaged 3 hours after the addition of IL-6-doped culture medium and again after 72 hours. No change was noted in spheroids cultured in control culture medium. No MCF7 migration was noted after 3 hour culture (figure 4-6C), however migration was clearly evident in all directions from the spheroid mass after 72 hours culture (figure 4-6D).

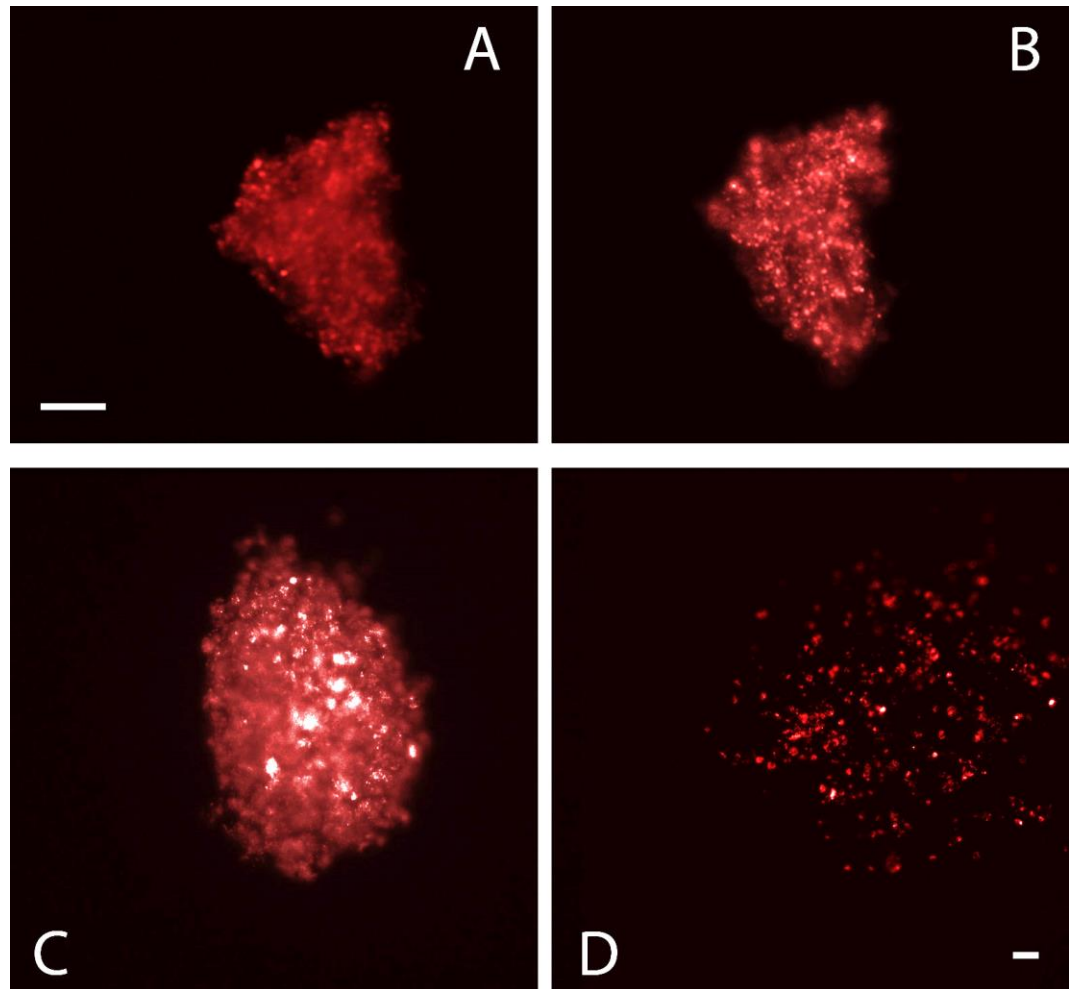


Figure 4-6 MCF7 spheroids cultured within a collagen gel incubated with 1 ng/mL IL-6. MCF7 cultured in collagen gel for A) 3 hours and B) 72 hours. C) MCF7 spheroid cultured for 3 hours and D) 72 hours incubated with IL-6. Images acquired using Zeiss Axio Vert A1 fluorescent microscope and coloured using Adobe Photoshop; (n=3, representative spheroid shown, scale bar 10 μ m).

MCF7 spheroids were subsequently cultured in the presence of IL-6 and imaged hourly, up to 24 hours, to allow a closer study of cell migration from the spheroid. Results indicated that cell migration occurs after

approximately 5 hours, however, it was not until around 10 hours culture that the spheroid diameter significantly differs from time zero (figure 4-7). Spheroids cultured in DMEM only do not exhibit any significant change in cell migration (figure 4-7).

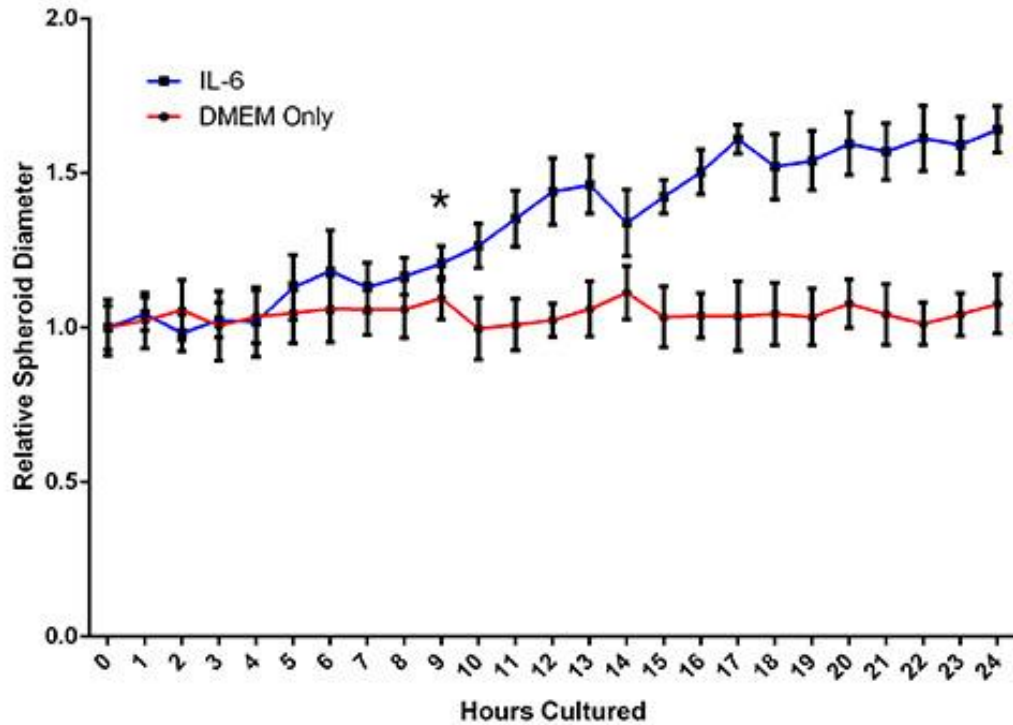


Figure 4-7 Relative MCF7 spheroid diameter measurements over 24 hours in culture with IL-6. MCF7 spheroids cultured in DMEM containing 1 ng/mL IL-6 or DMEM only, imaged every hour for 24 hours. Diameter was measured through centre of the spheroid and normalised to hour 0 (n=4; error bars show standard error mean). * denotes point from which there was a significant change from hour 0, $p < 0.05$. Spheroids imaged on Zeiss Axiovert 25, photographed every hour for 24 hours and measured using ImageJ.

4.2.iii Transforming Growth Factor B1 Effects on MCF7

MCF7 Cell Migration Response to TGF β 1 (2D Study)

Purified TGF β 1 was added to fresh DMEM before culturing MCF7 cells, as in 4.2.iii with IL-6. The effect of TGF β 1 on MCF7 cells in cultured in monolayer was performed using chemotaxis slides, allowing a concentration gradient to be established. Cells cultured in these slides were able to experience an area of TGF β 1 on one side and TGF β 1-free culture medium on the other. Unlike cells exposed to IL-6 (figure 4-5), here MCF7 cells do not preferentially migrate towards TGF β 1 (figure 4-8). Cells do become active, moving through the environment, but in no particular directionality.

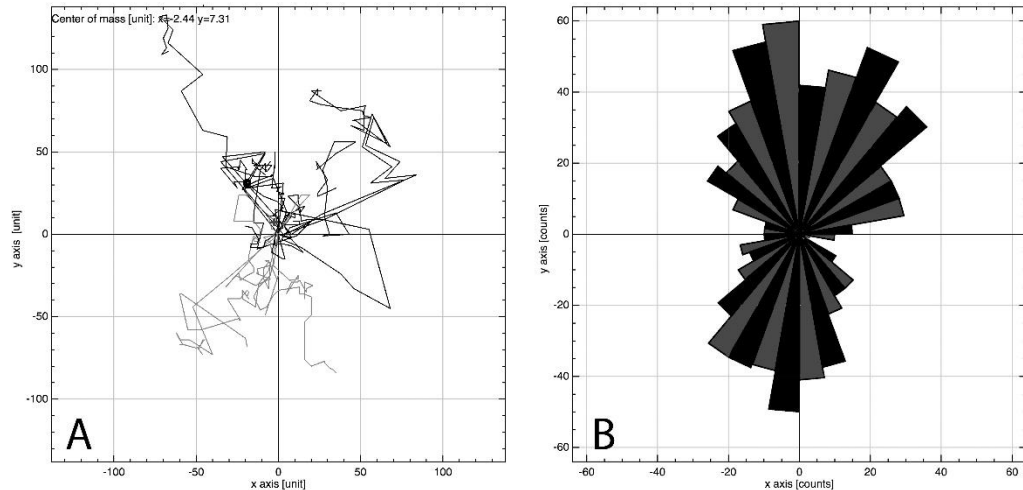


Figure 4-8 MCF7 cell migration in the presence of an TGF β 1 gradient over 24 hours. A) a vector plot of individual cells tracked, and B) a rose plot summarising overall migration. Coordinates (0,0) reflect the origin of each cell. DMEM TGF β 1 2 ng/mL concentration gradient located on negative x-axis, with undoped DMEM present towards the positive x-axis (12 cells tracked across 3 wells). Cells imaged on Zeiss Axiovert 25, photographed every hour for 24 hours and tracked using ibidi chemotaxis plugin for ImageJ.

MCF7 Cell Migration Response to TGF β 1 (3D Spheroid Study)

Spheroid expansion was measured over 24 hours using TGF β 1, exactly as for IL-6. Spheroids appeared relatively unreactive to the TGF β 1 until 9 hours culture, but from this point, MCF7 cells began to react by migration from the spheroid mass (figure 4-9). A steady increase in spheroid diameter was noted until 13 hours, when it becomes significantly larger ($p < 0.05$) than hour 0. There is a much steeper increase in diameter than that seen in the presence of IL-6 (figure 4-7). The cells in the periphery of the spheroid move away several cell lengths over the 24 hour time period. Whilst cells did not appear to move towards the source of

TGFB1 in monolayer (figure 4-8), it is possible that the cytokine caused cells to become more active as is shown here where cells comprising the spheroid move further into the environment over time. The TGFB1 is present everywhere in the environment, whilst the collagen gel will provide a concentration gradient for nutrients, over time this will equilibrate and that is perhaps why the effect of TGFB1 is not seen until around hour 10, as a threshold concentration at the spheroid has not been reached until then.

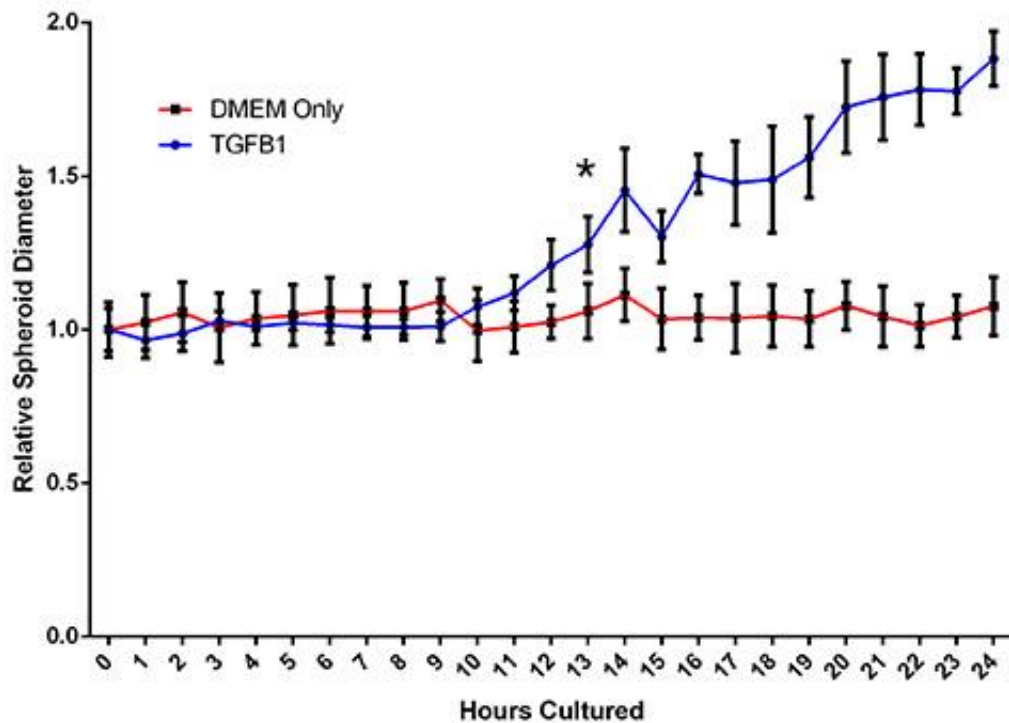


Figure 4-9 Relative MCF7 spheroid diameter measurements over 24 hours in culture with TGFB1. MCF7 spheroids cultured in DMEM containing 2 ng/mL TGFB1 or DMEM only, imaged every hour for 24 hours. Diameter was measured through centre of the spheroid and normalised to hour 0 (n=4; error bars show standard error mean). * denotes point from which there was a significant change from hour 0, $p < 0.05$. Spheroids imaged on Zeiss Axiovert 25, photographed every hour for 24 hours and measured using ImageJ.

4.3 Discussion

Paracrine signalling within the BM is essential to the maintenance of the cells residing there. The cytokines produced by MSCs are vital to the maintenance of the stem cell niche, in addition to affecting the maturation of other local cells such as macrophages (Waterman et al., 2010; Li and Wu, 2011). When BCCs metastasise to the BM they are able to use these paracrine signals within the microenvironment to their advantage. This forms the seed and soil hypothesis put forth by Paget over a century ago; metastatic cancer will only form new populations in tissues where the environment is compatible.

4.3.i Cytokine Secretion Changes Upon Co-Culture of MSC and MCF7 Spheroids

The results presented within this chapter demonstrate that MSCs and MCF7 spheroids do influence each other in 3D co-culture. Cytokine secretions are altered after both 3 and 7 days of co-culture (figures 4-3 and 4-4 respectively). A summary of the significantly changes ($p < 0.05$) is presented in table 4-2.

Table 4-2 Changes in cytokine levels of spheroid co-culture compared with spheroid monoculture at 3 and 7 days. Red = decrease, blue = increase and white no change. Data derived from figures 4-3 and 4-4.

Cytokine	Co-Culture v MSC		Co-Culture v MCF7	
	3 days	7 days	3 days	7 days
TGFB1			Red	Blue
IL-6			Blue	
TNF α			Red	
RANTES			Red	Red
IL-1 α			Red	
IL-2		Red		
IL-3		Red	Blue	Red
IL-5		Red	Blue	Blue
IL-7			Blue	
IL-8			Blue	
IL-10		Red	Blue	Blue
MCP-1			Blue	Red
MCP-2				Red
TNFB	Red			Blue

Cytokine Changes May Increase MCF7 Cell Migration and Proliferation in Co-culture

Many of the cytokine changes observed occurred in the MCF7 spheroids after 3 and 7 days of co-culture; this is reflected in a study by Liu and colleagues (2011), who note how co-culture between BCC and MSC causes an increase in many of the cytokine secretions of both cell types. The main cytokines which are altered in MCF7 co-culture compared with single spheroid culture include RANTES (decreased), TNFB/TGFB1

(increased), a range of interleukins (increased) and MCP-1 (initially increased, then decreased); taken globally, this infers changes in MCF7 cell motility and proliferation, although when individual changes are studied, there is a mixed response. In particular, the co-culture environment sees a reduction in some of the interleukins compared with MSC monoculture. This reduction *in vivo* could lead to a reduction in the number of pro-inflammatory macrophages maturing in the BM through this immunophenotype, protecting the BCCs from removal (Kim and Hematti et al., 2009).

For example, RANTES is involved in cell homing and migration (Khalid et al., 2015). Karnoub and colleagues illustrated how co-culture of MSCs with the MDA-MB-231 cell line can lead to an increase in RANTES signalling, leading to increased motility. However, the results of this study show a decrease in RANTES upon MSC co-culture, perhaps due to a less invasive phenotype of the MCF7 cell type (as described in chapter 1). This therefore suggests a decrease in MCF7 migration potential. Likewise, although MCF7 migration is supported by an initial increase in MCP-1 (day 3), this is decreased by day 7 co-culture. MCP-1 (or CCL2 as it is also referred to as) can stimulate angiogenesis to occur, enabling the development of breast cancer (Bonapace et al., 2014). It has been reported that MCP-1 along with RANTES (CCL5) when expressed by cells in the tumour stroma in the BM, such as MSCs, will promote a more active, malignant phenotype (Soria et al., 2008). Thus the reduction of these cytokines from the environment should inhibit further migration of the BCCs.

Meanwhile, other cytokine changes noted for MCF7 cells in co-culture actually support an increase in cell proliferation and migration, such as the increase in interleukin secretion. In particular IL-3, 5, 7, 8, and 10 are all increased in co-culture at day 3. Il-10 maintained an

increase in secretion over the longer day 7 time point, which is interesting, as Il-10 is implicated in breast cancer progression (with increase mRNA levels in breast cancer cells) and is involved in angiogenesis (Sheikpour et al., 2018). Together, the increase in the interleukins would cause an increase in MCF7 cell proliferation and motility, both of which have been observed in chapter 3 (increased MCF7 proliferation upon co-culture) and in figure 4.1 in this chapter (fluorescent images indicating showing MCF7 cell migration in co-culture).

TNFB/TGFB1 are both increased in MCF7 cells at day 7 co-culture. Both are involved in cell growth and differentiation, whilst also being responsible for increasing cancer cell invasiveness and stimulating angiogenesis (Pang et al., 2016). The fact that both are increase in co-culture again supports an increase in MCF7 cell migration. *In vivo*, the paracrine signalling to macrophages in the environment will cause them to mature into the immunosuppressive M2 subtype (Song et al., 2015). Rey and Colleagues (2018) report an increase in the aggressive phenotype of MCF7 cells cultured with MSCs, where co-culture induced the CSC surface marker CD44⁺/CD24^{low/-} and surface E-cadherin was internalised leading to reduced cell-cell adhesion. Their study had cells seeded freely throughout a collagen gel so lacks the features of a spheroid culture where a concentration gradient can be produced across the cross-section of the mass.

A Decrease in Cytokine Secretions in Co-culture Support Reduced MSC Migration

Several cytokines were decreased when MSCs were co-cultured with MCF7. The effect this has is not necessarily upon the MSCs directly, although the previous chapter suggested MCF7 prevent differentiation;

the effect is more likely to be upon cells residing in close proximity in the BM niche with the MSCs (Dhawan et al., 2013). In particular, the results showed a general decrease in interleukin secretion (IL-2, 3, 5 and 10) by MSCs after 7 days' co-culture with MCF7. Reduced MSC proliferation was maintained in co-culture, as demonstrated by the cell cycle study in chapter 3; a reduction in interleukin secretion would further support this.

When extrapolated to the BM environment, the changes in cytokines observed during MSCs co-culture may lead to a polarisation of macrophages to the M2 subtype (Tripathi et al., 2010). Where M1 macrophages are proinflammatory cells, M2 macrophages will confer the opposite effect. As poor antigen presenting cells, they will prevent any further immune response thereby conferring an immunoprotection upon the BCCs. Paracrine signalling by MSCs is a major contributor to the polarisation of macrophages in the BM and the decrease of cytokines such as CCL2, 5 and 8 (MCP-2) will reduce the homing of pro-inflammatory immune cells to the MSCs. Therefore, if invading BCCs are in close proximity to MSCs, they will be protected from the immune response, subsequently this will allow them to remain in the BM undisturbed.

4.3.ii IL-6 Stimulates MCF7 Cell Migration

IL-6 has been identified as a key paracrine signal for MSC migration within the BM niche model used in this study (Lewis et al., 2016), whilst TGF β 1 has been shown to have an effect on breast cancer metastasis (Yin et al., 1999). In addition, both cytokines have been noted as important factors in the EMT of BCCs (Sullivan et al, 2009; Lamouille et al, 2014) in the BM. Whilst the actual role of TGF β 1 in cancer cell progression is

ambiguous, it may positively affect the growth of hormone responsive cancers, such as MCF7 (Buck and Knabbe, 2006).

There is a body of evidence that IL-6 in the environment causes BCCs to induce EMT and become metastatic (Kim et al., 2003; Knüpfer and Preiß 2007; Sullivan et al., 2009). Hence, IL-6 was assessed in our cell models to determine the effect it had upon MCF7 cells in 2D monolayer and 3D spheroid culture. In both cases MCF7 cells migrated towards [IL-6]. Fierro and colleagues (2004) reported that IL-6 can induce MCF7 cell proliferation and migration. Furthermore, MSC co-culture has been shown to increase MCF7 cell proliferation 2-fold through IL-6-related pathways (Sasser et al., 2007). This suggests that MCF7 cells response to IL-6 through an increase in cell proliferation and migration. The presence of MSC-derived IL-6 in the BM environment may therefore have the potential to stimulate dormant BCCs into recurring.

4.3.iii MCF7 Migrates in The Presence of TGF β 1

TGF β 1 has been cited as pro-metastatic factor (Tang et al., 2003; Meng et al., 2016). The MSCs within the BM may play a role in secreting the cytokine into the environment. As demonstrated in this study, co-culturing MCF7 spheroids with MSC spheroids exposes the BCCs to a higher level of TGF β 1 than when cultured alone. In a study by Xu and Colleagues (2012), co-culture of MCF7 and adipose-derived MSCs stimulated the MCF7 cells to undergo EMT and establish a mesenchymal phenotype; this was regulated by TGF β 1 targeting the ZEB/MiR 200 regulatory loop, a crucial activator of EMT (Brabletz and Brabletz, 2010).

Whilst MSCs play a role in the maintenance of dormancy, other cells will be present around the tumour stroma in the BM. One of these cell

types, cancer-associated fibroblasts (CAFs) are noted as being responsible for TGF β 1 signalling into the tumour environment within the BM leading to EMT (Yu et al., 2014); these CAFs are derived from MSCs. It is clear that TGF β 1 increases the activity/general migration of MCF7, likewise, this suggests that TGF β 1 may be able to activate dormant BCCs within the BM and move out into the environment as a secondary metastasis. This appears to be true for other ER α + BCC lines, where the converse is true for triple negative lines such as MDA-MB-231 (Sasser et al., 2007).

4.4 Conclusion

The seed and soil hypothesis proposed by Paget over a century ago is still very much relevant, as the microenvironment clearly dictates BCC migration and survival. The BM contains a multitude of different cells, each with its own paracrine signalling profile. In this chapter, taking a paracrine perspective, the influence of co-culturing MCF7/MSCs was studied through cytokine secretions.

As BCCs enter the BM and encounter MSCs, they are exposed to MSC-derived cytokines. Many of the cytokines secreted into the BM environment will lead to attenuation of the immune response preventing destruction of the invading cells. In addition, these secretions may lead to BCC dormancy, or be responsible for BCC recurrence. During co-culture, the MCF7 cell cytokine profiles were changed, promoting cell migration (and potentially proliferation). Further migration studies in both 2D and 3D culture demonstrated that two specific cytokines, IL-6 and TGF β 1 (both secreted by MSCs), caused MCF7 cell activation and migration. These simple experiments establish how MSC co-culture and paracrine signalling have the potential to control BC fate and may, in this case, play a role in BCC recurrence.

5 MSC Migration with Interleukin-6

5.1 Introduction

Stem cell-based therapies have the potential of becoming the future of medicine (Ullah et al., 2015); personalised to the patient (Quimby and Borjesson, 2018). MSCs, are of great interest when developing new therapies and technologies (Sohni and Verfaillie, 2013). As described in section 1.3, MSCs derived from the bone marrow niche are multipotent, capable of differentiating into osteoblasts (bone), chondroblasts (cartilage) and adipoblasts (fat) (Baksh et al., 2004). These precursor cells are essential to the formation, maintenance and repair of the skeleton.

MSCs are identified by several cell surface markers including the presence of CD105, CD90 and CD73 and the absence of CD45, CD34, CD14, CD19 and HLA-DR (table 1-2). MSCs grown in monolayer will typically begin to lose differentiation potential from around the 6th passage, demonstrating the vital role cell signalling from other supporting cell types within the bone marrow microenvironment plays in maintaining stemness (Dominici et al., 2006; Bonab et al., 2007). Within the BM microenvironment, the MSC niche can be subdivided into the endosteal and the perivascular niches where MSC populations are maintained by, and communicate via cytokines, with HSCs and other later precursor cells such as osteoblasts and adipoblasts (DaSilva Meirelles et al., 2008; Frenette et al., 2013; Bara et al., 2014).

Upon appropriate signalling cues, MSCs mobilise and migrate out from the niche. MSC mobilisation is often due to either (1) homing to sites of injury (Hannoush et al., 2011) or (2) homing to disseminated tumour cells (Hu et al., 2013); both are of key interest to researchers in terms of

regenerative medicine (ie. replacement of lost skeletal tissue) and potential therapeutics for cancer.

Injury or inflammation cause cellular release of cytokines; transforming growth factor- β (TGF- β), tumour necrosis factor- α (TNF- α), several interleukins (IL) such as IL-1, IL-6, IL-10 and the interferons which all play an important role in controlling the immune response (Yagi et al., 2012). These cytokines also stimulate the recruitment of MSCs where they initiate tissue repair at the site of wound (Maxson et al., 2012). Previously published work from our lab assessed migratory signals produced by artificial wound models; from a panel of several key cytokines (IL-1b, IL-2, TNF α , IL-12p70 and IL-6), only IL-6 was identified as being able to induce MSC migration from the spheroid models (Lewis et al., 2016). Well known for its roles within inflammation, immune response and skeletal maintenance, IL-6 is also a key regulator in cell differentiation, being heavily associated with haematopoiesis and differentiation of both osteoblasts and osteoclasts (Roux and Orcel, 2000; Marriot et al., 2004; Grellner et al., 2000; Yoshitake et al., 2008).

The study carried out in chapter 4 looked at MSC-derived cytokines, with the belief that these can affect the metastasis of nearby BCCs; key cytokines included TGF β 1, TNF α and IL-6. MSCs are also under the influence of their own autocrine signalling via cytokines such as IL10, VEGF and IL-6. MCF7 was noted to migrate towards IL-6 in both 2D and 3D. The Berry lab has previously described how MSCs migrate towards damaged cells - a source of IL-6 (Lewis et al., 2016). This study sought to elucidate the effect of IL-6 upon MSC migration in the same conditions as previously seen in chapter 4.

As well as understanding the role of various cytokines within the BM niche, studies on MSC migration will help inform on potential delivery routes in cancer therapeutics and within the field of regenerative

medicine. Cell migration involves the breakdown of extracellular matrix (ECM); which requires the action of proteolytic enzymes such as matrix metalloproteinases (MMPs). There are several classes of MMPs depending on their substrate specificity; (1) collagenases (MMP-1, -8, -13 and -18) which cleave fibrillar collagens type I, II and III; (2) gelatinases (MMP-2 and -9) which cleave gelatin, but can also degrade other extracellular matrix proteins including collagen and laminin; (3) stromelysins (MMP-3, -10 and -11), which degrade several non-collagenous proteins and (4) membrane-type MMPs (MMP-14, -15, -16, -17, -24 and -25) (Birkedal-Hansen et al., 1993; Page-McCaw et al., 2007). MMP activity is regulated by tissue-specific inhibitors of MMPs (TIMPs). The balance between MMP/TIMPs is critical in ECM remodelling, cell migration, cell differentiation and the regeneration of any tissue (Almalki et al., 2016).

5.1.i Objectives

IL6 was noted as being key to MSC migration in a previous study in our lab. This study aims to assess how MSCs respond to IL-6 in 2D monolayer culture and 3D spheroid model. This will be achieved by:

- Assess monolayer MSC migration response to IL6
- Identify the MMPs and TIMPs secreted by migrating MSC monolayers when exposed to IL-6 using a cytokine blot array
- Monitor MSC spheroids and observe response to IL-6
- Identify the MMPs and TIMPs secreted by MSC spheroids in response to IL-6 using a cytokine blot array

5.2 Results

The presence of a panel of seven human matrix metalloproteinases (MMP-1, MMP-2, MMP-3, MMP-8, MMP-9, MMP-10 and MMP-13) and three tissue inhibitors of metalloproteinases (TIMPs; TIMP-1, TIMP-2 and TIMP-4) was quantified following MSC incubation with IL-6. To complement this analysis, monolayer cell migration was assessed using an Ibidi cell migration plate assay via time lapse microscopy over a 24-hour period in the presence of IL-6. Spheroids were also imaged over a series of days, both in the presence and absence of IL-6.

5.2.i MSCs Migrate Towards an IL-6 Gradient in Monolayer Culture

Upon IL-6 exposure, cells were tracked over 24 hours using time-lapse microscopy. A clear directionality was observed towards the IL-6-spiked DMEM, where large filopodia were noted extending in the direction of IL-6, inducing a leading edge and migration (Figure 4-1). The direction of cell migration was analysed and a vector plot indicated the path of cells incubated in the [IL-6] gradient (Figure 4-2A). A rose plot confirmed MSC preferential migration towards IL-6 (positive axis; figure 4-2B).

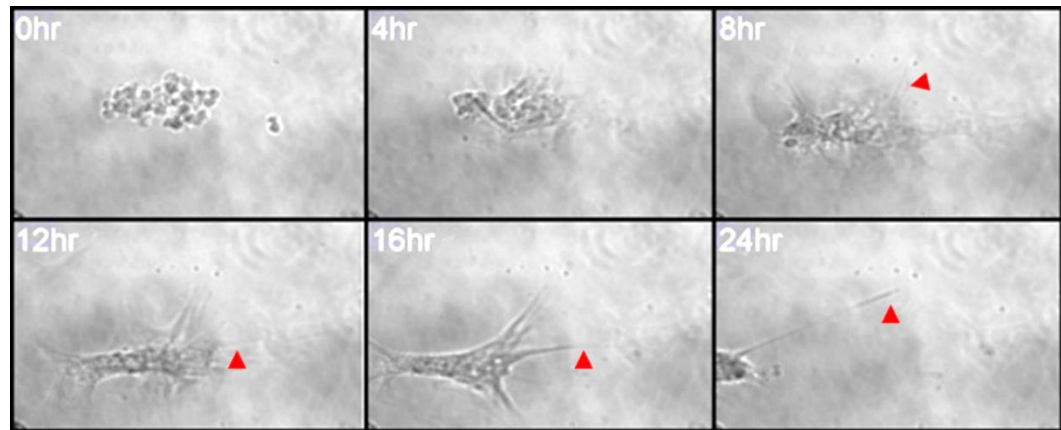


Figure 5-1 A selected montage of six MSC images. Taken from the 24-hour time-lapse following a single MSC cultured within an Ibidi μ -Slide Chemotaxis 2D assay plate with IL-6/DMEM (1 ng/mL) in the first reservoir and culture media alone in the reservoir on the right. Red arrows indicate presence of extending.

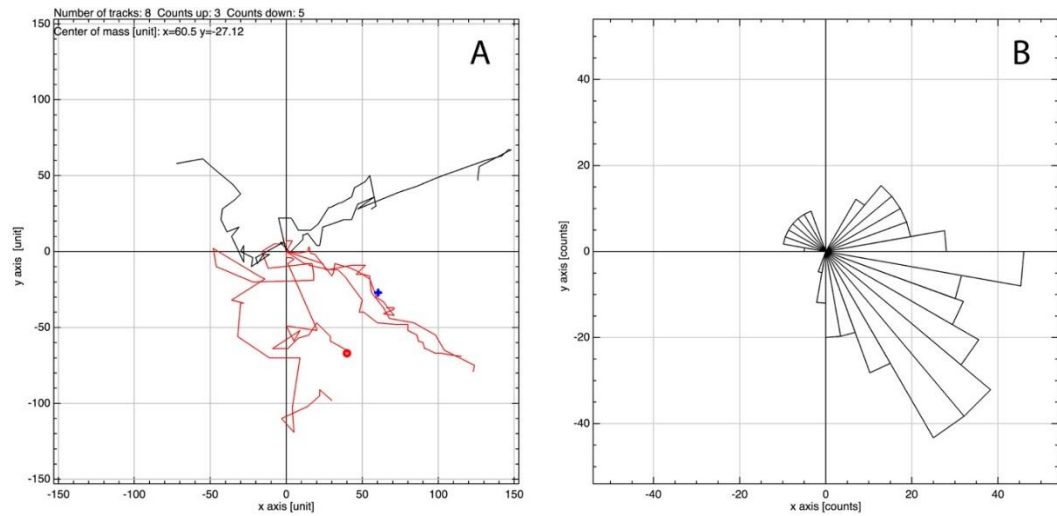


Figure 5-2 MSC cell migration in the presence of an IL-6 gradient over 24 hours. A) a vector plot of 8 individual cells tracked, and B) a rose plot summarising overall migration. Coordinates (0,0) reflect the origin of each cell. DMEM containing IL-6 1 ng/mL concentration gradient located on negative x-axis, with undoped DMEM present towards the positive x-axis (12 cells tracked across 3 wells). Cells imaged on Zeiss Axiovert 25, photographed every hour for 24 hours and tracked using ibidi chemotaxis plugin for ImageJ.

5.2.ii MMP-1 and MMP-3 Facilitate MSC IL-6-induced Migration in Monolayer

MSCs were incubated in IL-6 (1 ng/mL); culture media was then collected after 3hr and 24hr and analysed for the presence of MMPs and their inhibitors, TIMPs. Changes in MMP/TIMP levels were quantified and expressed graphically (Figure 5-3). Collagenases MMP-1 and MMP-3 were increased after 24 hours' incubation, with the corresponding inhibitor, TIMP-1, also upregulated to balance degradation of the local collagen.

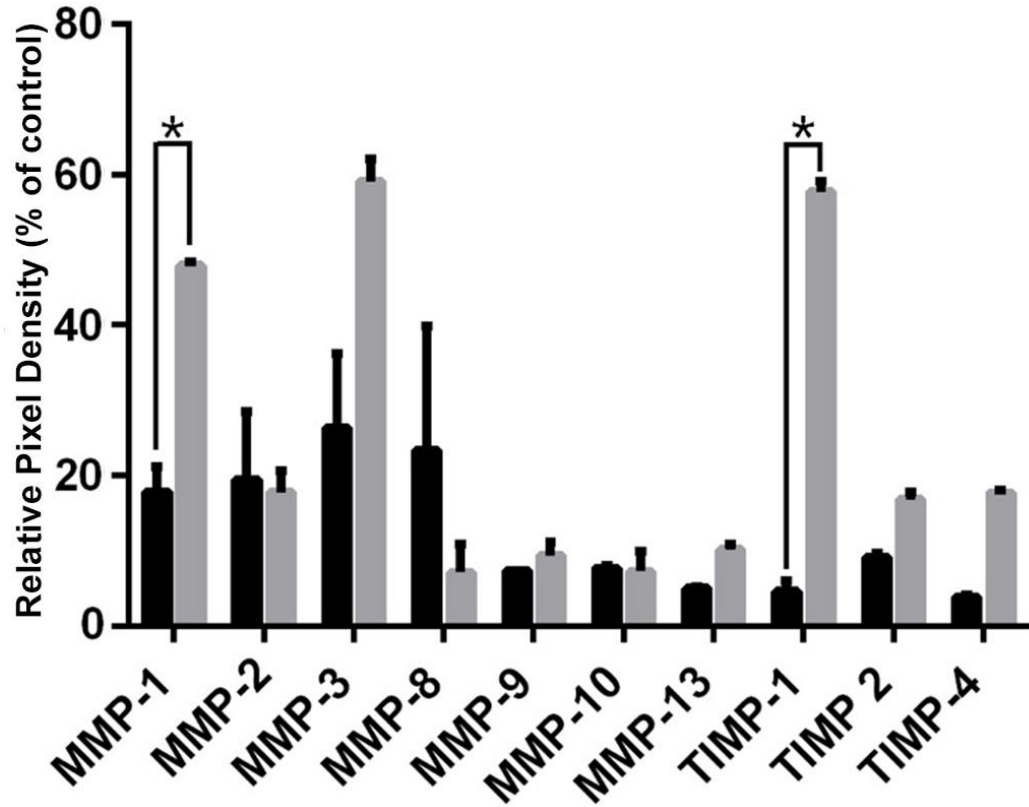


Figure 5-3 MMPs and TIMPs detected in MSC monolayer culture. Mean pixel density, relative to control, of target proteins secreted into culture media by MSCs following IL-6 1 ng/mL incubation for 3hr (black) and 24hr (grey) hour intervals. Culture medium was analysed using Abcam human MMP antibody array membranes, viewed on Agilent 2100 Bioanalyzer, followed by quantification using imageJ; n=2 technical replicates, error bars indicate SEM, * indicates significant change at 24 hours ($p < 0.05$).

5.2.iii MSCs Spheroids Migrate in Response to IL-6

Cell migration was observed in MSC spheroid culture in response to IL-6 over a 3-day period. Spheroids cultured in DMEM alone do not migrate from the central mass in the 72-hour period, as the spheroid morphology remained similar (figure 4-4C). Addition of IL-6 caused MSCs to begin migrating from the spheroid after 3 hours, with peripheral cells beginning to extend filopodia (figure 5-4B) as in the monolayer culture in the previous study (figure 5-1). After 72 hours incubation with IL-6, MSCs have migrated several cell lengths from the spheroid into the collagen gel (figure 5-4D), with migrating cells extending filopodia out into the environment, producing a stellate morphology.

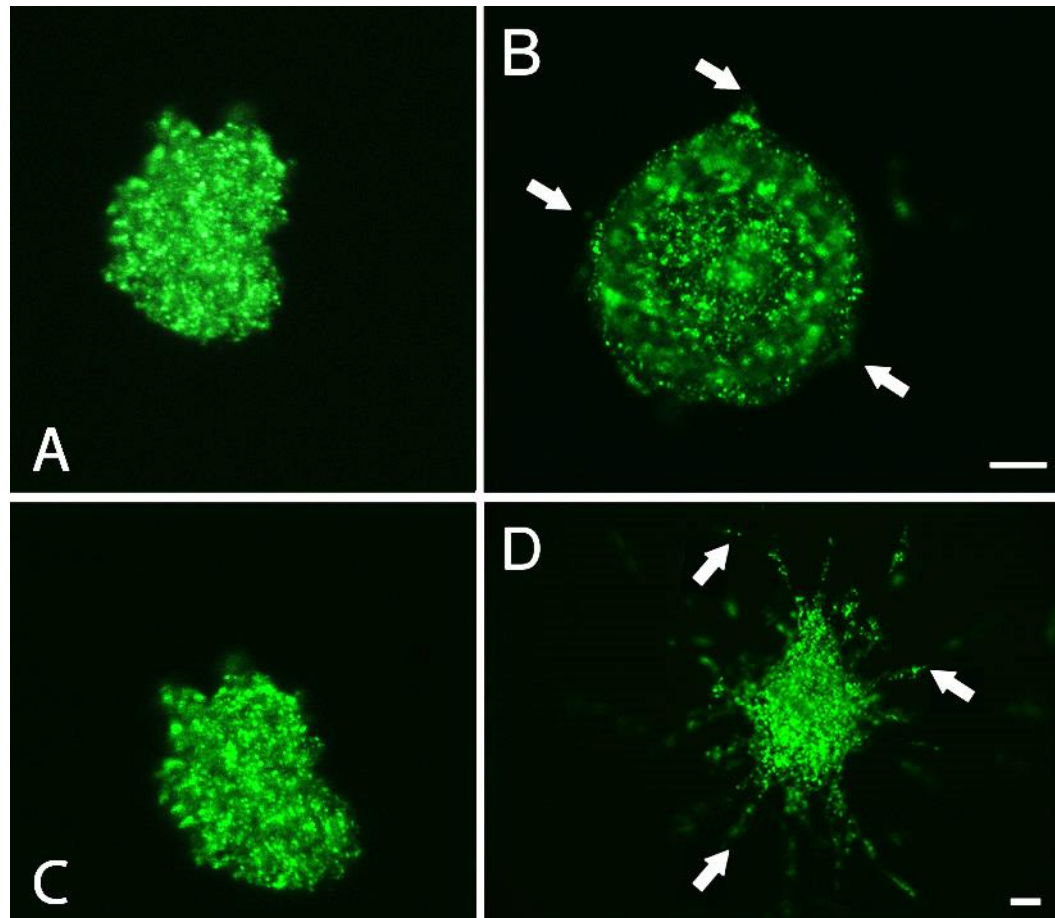


Figure 5-4 MSC spheroids cultured within a collagen gel incubated with 1 ng/mL IL-6. MSC spheroids cultured in collagen gel for 3 hours in A) standard culture medium and B) culture medium containing 1 ng/mL IL-6. MSC spheroid cultured for 72 hours in C) standard culture medium and D) culture medium containing IL-6. Images acquired using Zeiss Axio Vert A1 fluorescent microscope and coloured using Adobe Photoshop. n=3, representative spheroid shown, white arrows indicate migrating cells scale bar 10 μm .

5.2.iv MMP-2 and MMP-8 Facilitate MSC IL-6-induced Migration in 3D Spheroid Culture

MSC spheroids cultured in standard culture medium indicated an overall decrease in both MMP and TIMP secretion from 1 day to 3 days (figure 5-5A). However, the MMP secretion profile for MSC spheroids challenged with 1 ng/mL IL-6 is notably different, as MSCs increase the secretion of some MMPs. The secretion of MMP-8 (a collagenase specific to types I-III) significantly increased ($p < 0.05$) over time (figure 5-5B). Interestingly, other collagenases specific to collagen type I, MMP-1 and MMP-13, showed no significant change following IL-6 treatment. The only significant increase in TIMP secretion was through an increase in TIMP-4 (figure 5-5B). TIMP-1, an inhibitor of MMP-3, significantly decreased ($p < 0.05$) after 72 hours culture with IL-6.

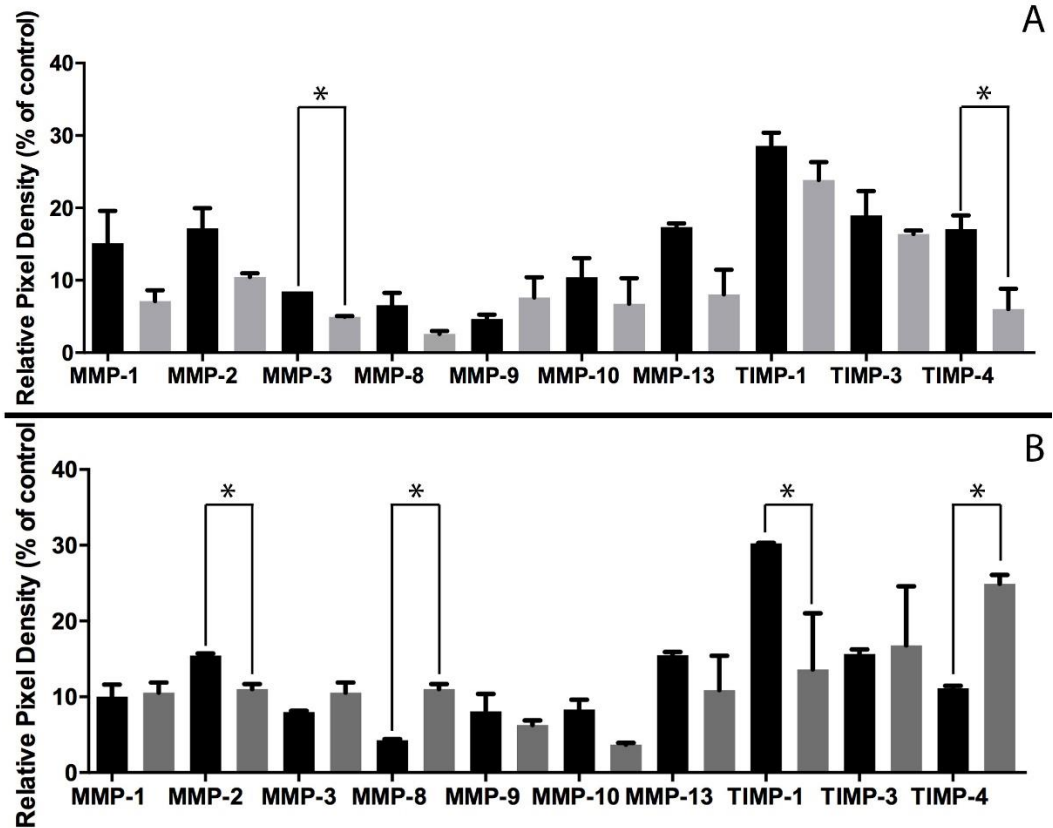


Figure 5-5 MSC spheroid MMP and TIMP secretion. MMPs and TIMPs detected in culture medium at 3hr (black) and 72hr (grey). A) Standard media and B) culture medium with 1 ng/mL IL-6. Culture medium was analysed using Abcam human MMP antibody array membranes, viewed on Agilent 2100 Bioanalyzer, followed by quantification using imageJ; n=2 technical replicates, error bars indicate SEM, * indicates significant change at 24 hours ($p < 0.05$), * indicates significant change at 24 hours ($p < 0.05$).

5.3 Discussion

In this chapter I aimed to assess MSC migration response to IL6 in both 2D and 3D culture. In addition, if cells migrate, I wanted to determine what changes in MMP/TIMP secretion profiles facilitated this migration. The initial study focused on monolayer MSC response, whilst the second part of the study utilised MSC spheroid culture within a collagen gel, to verify whether the migration response can be translated to the 3D environment.

5.3.i MSCs Migrate Towards IL-6

MSCs are known to respond to $TNF\alpha$, $IFN\gamma$, IL-1 and IL-6 concentration gradients (Ren et al., 2008; Lewis et al., 2016) permitting movement towards the site of damaged cells to initiate repair (Maxson et al., 2012). IL-6 activates JAK/STAT and MAPK pathways to permit survival and proliferation of MSCs (Rattigan et al., 2010). This leads to the formation of actin stress fibres to facilitate migration (Menon et al., 2007). In this way, local MSCs act as a source of fibroblasts to permit tumorigenesis of the neoplastic cells (Mishra et al., 2008). Therefore, the response of MSCs to paracrine IL-6 is of importance in understanding the growth patterns of disseminated cancer cells.

2D Study

The initial study to establish how MSCs responded to IL-6 in monolayer indicated the formation of filopodia only in the direction of the IL-6 as the cells attempted to migrate towards the source. There has been much research into the study of MSCs' response to IL-6. An increase in

MSCs migration has previously been described in response to cytokines MCP-1 and IL-8 (Wang et al., 2002). Pricola and colleagues (2009) showed how IL-6 can maintain the stemness of MSCs whilst enhancing both proliferation and wound-healing abilities *in vitro*. The migratory response of MSCs to IL-6 is utilised to repair epithelial damage and suppress further inflammation (Ke et al., 2014). IL-6 is able to induce VEGF production by MSCs, permitting endothelial growth and the development of vasculature in ischemic environments (Herrmann et al., 2011). *In vivo*, cells would migrate towards the source of IL-6 (Heinrich et al., 2003) to initiate repair of damaged tissues, this study showed this migratory response is conserved *in vitro* before moving forward with the 3D spheroid study.

Spheroid Study

The MSC spheroid experienced an IL-6 gradient across the entire spheroid surface, which caused the peripheral cells to migrate away from the central mass in all directions. MSCs within the spheroid therefore appear to sense IL-6, most likely via the cognate cell surface receptor, IL6R (Yagi et al., 2012), with peripheral cells transitioning to a migratory cell phenotype as they lose cell-cell contacts, to move towards the IL-6 (figure 5-4D). The culture of MSCs as 3D multicellular spheroids increases the secretion of immunomodulatory factors, including IL-6 (Zimmermann and McDevitt et al., 2018), leading to an increase in the production of anti-inflammatory molecules, which would support the results of Ke and colleagues (2014) as MSCs repair damaged tissues. The use of 3D culture systems over traditional monolayer culture has indicated that the immunomodulatory effect of MSCs is enhanced through the upregulation of mRNA markers. This phenomenon is beneficial for the future of cell therapy using 'off-the-shelf' MSCs (Chen et al., 2017).

The migratory response of MSCs to IL-6 in the environment did not change from monolayer to spheroid; in both cases MSCs migrated towards IL-6. MSCs in the BM will encounter elevated IL-6 secreted by macrophages that have been polarised to the pro-inflammatory M1 phenotype. These M1 macrophages are able to repress osteogenic markers, preventing MSC differentiation (Gong et al., 2016). Once exposed to environmental IL-6 by M1 macrophages MSCs will begin to secrete their own IL-6 in response. This then prevents further M1 polarisation as MSC-derived IL-6 favours the maturation of naïve macrophages towards to anti-inflammatory M2 phenotype. (Phillipp et al., 2018). The ability of ‘activated’ MSCs to downregulate M1 polarisation will be beneficial to any invading BCCs as this will prevent the inflammatory immune response from clearing them from the BM, allowing their continued proliferation (Weng et al., 2019).

5.3.ii MSCs Secrete MMPs in Response to IL-6

The MMP profiles observed in 2D and 3D MSC culture differ notably, in both the types of MMP secreted and the levels in which they change. This is likely due to the environment surrounding the cells, as the ECM surrounding cells in monolayer will differ from the type I collagen, which the 3D spheroids are cultured within.

2D Study

MMP transcription is regulated by cytokine signalling (Brew et al., 2000), hence as the cell senses IL-6, collagenases MMP-1 and MMP-3 secretion are upregulated. In a 2D environment, BM-derived MSCs secrete large volumes of laminin, in addition to small amounts of collagen I, into

their environment. This ECM component is a target of MMP-3, indicating why this was upregulated in the this 2D study (Amable et al., 2014). Amable and colleagues quantified ECM and MMPs in much the same way as the study within this chapter, using ELISA to analyse the conditioned media.

Secretion of the corresponding inhibitor (Yang et al., 2002), TIMP-1, is also increased in response to upregulation of MMP-1 and MMP-3 to attenuate their effect. As the MSCs migrate they must digest the surrounding ECM in order to progress forward, so a balance between MMP and cognate TIMP allows the cell to move and stop in response to environment cues.

Spheroid Study

In order for MSCs to migrate, they must change from an adherent phenotype to a migratory phenotype. The migratory behaviour of MSCs involves MMP activity, with different MMP profiles depending on the cause of migration (Almalki et al., 2016). Within this model system, focusing on MSC migration in response to IL-6, an increase in collagen I-digesting MMP-8 was seen, whereas MMP-2, able to digest collagen IV, decreased. This profile is different to that seen in the 2D study. In monolayer the cells are laying down their own ECM, in the case of BM-derived MSCs mostly laminin (Amable et al., 2014), whereas the 3D spheroids are implanted within a collagen I gel, there is less need to lay down their own ECM. The change in the makeup of the ECM will change what the MSC needs to secrete in order to move through it; as the surrounding ECM consists of collagen I only, this finding suggests these MSCs are aware of the makeup of their environment.

There have been many recent studies into MMP secretion by MSCs. The ability of MMPs to digest hydrogels has been used to the advantage of studies where cell-mediated remodelling of the 3D structure is required. Fonseca and colleagues (2013) used an alginate hydrogel, containing MMP-sensitive peptides, to culture MSCs and through altering the peptide structure of the hydrogel could direct the movement of the cells. Leight and colleagues (2013) studied the effects of hydrogel stiffness upon MMP expression. The addition of TGF β 1 increased MMP production much in the same way IL-6 did within this study. MSCs cultured in collagen environments require the expression of MMP-1 to migrate. Blocking this results in MSCs that are unable to move through their environment (Lu et al., 2013).

Without IL-6 in the environment, the MSCs remain within the spheroid. This correlates with previous evidence that MSCs become quiescent in collagen gels with time, thus do not migrate (Lewis et al., 2015). The change in behaviour caused by the addition of IL-6 to the model environment is likely due to IL-6R activation by paracrine IL-6 leading to the phosphorylation of STAT3 within the cell (Horwood et al., 2016). This activation, in turn, leads to the expression of migration genes; MMPs are then upregulated by the phosphorylated STAT3 leading to the movement of cells towards sites of high IL-6 concentration, initiating cellular repair (Lukovic et al., 2015).

The upregulation of MMP-8, able to digest collagen type I-III (Nagase et al., 2006) will act upon the type I collagen used to produce the *in vitro* 3D model. TIMP-4 is known to interact with MMP-2 (Heinrich et al., 2003), a gelatinase, which indicates a significant decrease following IL-6 treatment (figure 5-5). The expression level of TIMPs act in a feedback loop with expression of their cognate MMP in order to attenuate the response when the cell needs to cease further migration (Birkedal-Hansen et al., 1993). The upregulation of TIMP-4 in MSC

spheroids cultured in IL-6 for 72 hours indicates the cell is attempting to attenuate the effect of its cognate protein, MMP-2. De Becker and colleagues (2007) found MMP-2 was required for MSC extravasation using endothelial cells embedded in Matrigel, consisting of laminin, collagens and heparan sulphate. As the components differ from the model used within this study, the MMPs required to migrate will also differ; MMP-2 decreased when cells were embedded in collagen I gels. As a consequence of differential MMP expression, a different TIMP was secreted to attenuate the effects. In this case TIMP-4 was upregulated, but De Becker and colleagues saw an increase in TIMP-3. This evidence, again, suggests that MSCs are able to sense their environment and alter the expression of appropriate MMPs to migrate through it.

5.4 Conclusion

The response of MSCs to paracrine IL-6 is of importance in understanding the growth patterns of disseminated cancer cells. This chapter has verified that MSCs migrate towards IL-6 in 2D and 3D culture; a cytokine not only released by the MSCs themselves, but by macrophages during cellular damage, and secreted by invading cancer cells. This migration will both promote breast cancer proliferation and cause MSCs to migrate towards the tumour and become part of the tumour stroma, further supporting the cancerous growth.

6 Extracellular Vesicles Effects on MCF7

6.1 Introduction

There is increasing evidence that MSCs cause metastatic BCCs to enter a dormant state (Ono et al., 2014; Bliss et al., 2016; Walker et al., 2016). Previous studies within this thesis have indicated that MSC spheroids in co-culture with MCF7 spheroids in a three-dimensional environment secrete a wide range of cytokines that differ from MSC spheroids cultured alone. This indicates a paracrine signalling effect emanating from the invading BCCs as they enter the environment that causes the MSCs to change their secretome. Paracrine signalling is not limited to the reception of extracellular proteins within the environment, but includes other agents, in particular extracellular vesicles (EVs).

6.1.i Extracellular Vesicles in Cell-Cell Communication

The relationship between marrow MSCs and invading BCCs has to date focussed on more traditional cell-to-cell communication routes, such as paracrine signalling via soluble proteins including cytokines (Luker et al., 2006; Liu et al., 2011). The studies done in chapters 4 and 5 demonstrated that cytokines released by both cell types within the BM model environment can have a strong effect on the proliferation and migration of both MSCs and BCCs.

However, EVs are also key mediators in cell-cell communication. As described in section 1.4.iii, EVs are small extracellular membrane-enclosed vesicles that contain a variety of molecules including proteins

and RNAs (Davies et al., 2014; Ono et al., 2014; Wu et al., 2017; Yáñez-Mó et al., 2015). Increasing evidence suggests that interactions between MSCs and tumour cells involve the exchange of information via EVs (Ono et al., 2014). EV contents can potentially bypass the cell surface receptors that may ordinarily block their entry (Prada and Meldolesi, 2016). Therefore, the EV contents can enter the host cell either through endosome trafficking or directly into the cytoplasm if the plasma membrane fuses with the membrane of the EV. Once inside, these biomolecules can change host cell behaviour through interference with cellular processes or gene expression. For example, MSC-derived EVs have been reported to contain microRNAs such as miR23b (Vallabhaneni et al., 2015), miR21 and miR34a (Del Fattore et al., 2015), which have been found to have a tumour-suppressive effect through the silencing of proliferative pathways. These EVs also contained tumour-supportive molecules, such as tissue inhibitor of metalloproteases (TIMP)-1 and -2.

6.1.ii Cellular Metabolites in EVs

In addition to microRNAs, MSC-derived EVs contain other biomolecules that may influence BCCs, such as cellular metabolites. These small molecules are products of metabolic processes occurring within the cell, such as sugars and amino acids, and that will exist freely within the cytoplasm and organelles. During the formation of EVs, these free molecules can then be packaged, along with microRNAs and proteins, and trafficked out of the cell through processes described in section 1.4.iii. There is some evidence to suggest that these small molecules can be effective in encouraging a dormant effect in cancer cells (Kim and Park, 2003; Phang et al., 2014), although little research has been carried out to determine which, if any, metabolites may be responsible.

6.1.iii Objectives

There is a current lack of knowledge of the mechanistic events that allow BCCs to adopt a dormant phenotype in the marrow. Within this study, EVs derived from MSC conditioned media (MSC-CM) will be used to assess their influence upon MCF7 cells, both in monolayer and as spheroids. How these EVs impact MCF7 proliferation, migration and adhesion will be assessed. In order to achieve this, the following experiments will be performed in this study:

- MSC-CM will be fractionated depending on molecular weight, each fraction will be incubated with MCF7 cells to determine effects on cell behaviour
- MSC-derived EVs will be isolated from MSC-CM, quantified and incubated with MCF7 cells in 2D monolayer and 3D spheroid culture.
- Metabolomics will be performed on MSC-derived EVs to profile their contents in terms of cellular metabolites
- Metabolites highlighted within the MSC-derived EVs will be used in isolation to assess their potential to induce a dormant phenotype in MCF7

6.2 Results

The results presented within this chapter seek to investigate the effects of MSC-derived EVs upon MCF7 cells, both in monolayer and in spheroid culture. First, MSC-CM was fractionated to contain biomolecules of size determined by filter pores. Of particular interest are the <30 kDa fraction, containing many cytokines including TGF β and IL-6, and the >100 kDa fraction, containing EVs. These MSC-derived EVs contain a combination of biomolecules; metabolomics was performed to determine if any small molecules contained within the vesicles could have an effect upon dormancy.

6.2.i Conditioned Media Fractionation

MSC-CM contained signalling molecules secreted by MSCs into their environment. MSC-CM was collected as described in section 2.20 and was then incubated with MCF7 cells in monolayer. The cancer stem cell marker ALDH1A1 (Marcato et al., 2010) is important in tumour progression and considered a stem cell marker, it was used to determine the ‘stemness’ of the MCF7 cells after 24 hours in culture with MSC-CM. A dilution series of MSC-CM was performed to identify if there was a change in stemness relative to volume (figure 6-1A). This indicated that the ALDH1A1 expression of MCF7 cells was negatively affected as higher concentrations of MSC-CM were present, this indicates a more stem cell-like MCF7.

Following complete MSC-CM studies, MSC-CM was sequentially ultrafiltered as in section 2.20. The filtrates contained molecules of a particular molecular weight range (>30 kDa, 30-50 kDa, 50-100 kDa and >100 kDa). Through fractionating the MSC-CM, distinct effects can be identified. Again, ALDH1A1 fluorescence was assessed to determine

changes in MCF7 stemness caused by the MSC-CM fractions (figure 6-1B). A decrease in ALDH1A1 fluorescence was noted through the MSC-CM fractions, with >100 kDa indicating the greatest change. This fraction, containing MSC-derived EVs, showed the only significant decrease ($p < 0.05$) in ALDH1A1 fluorescence.

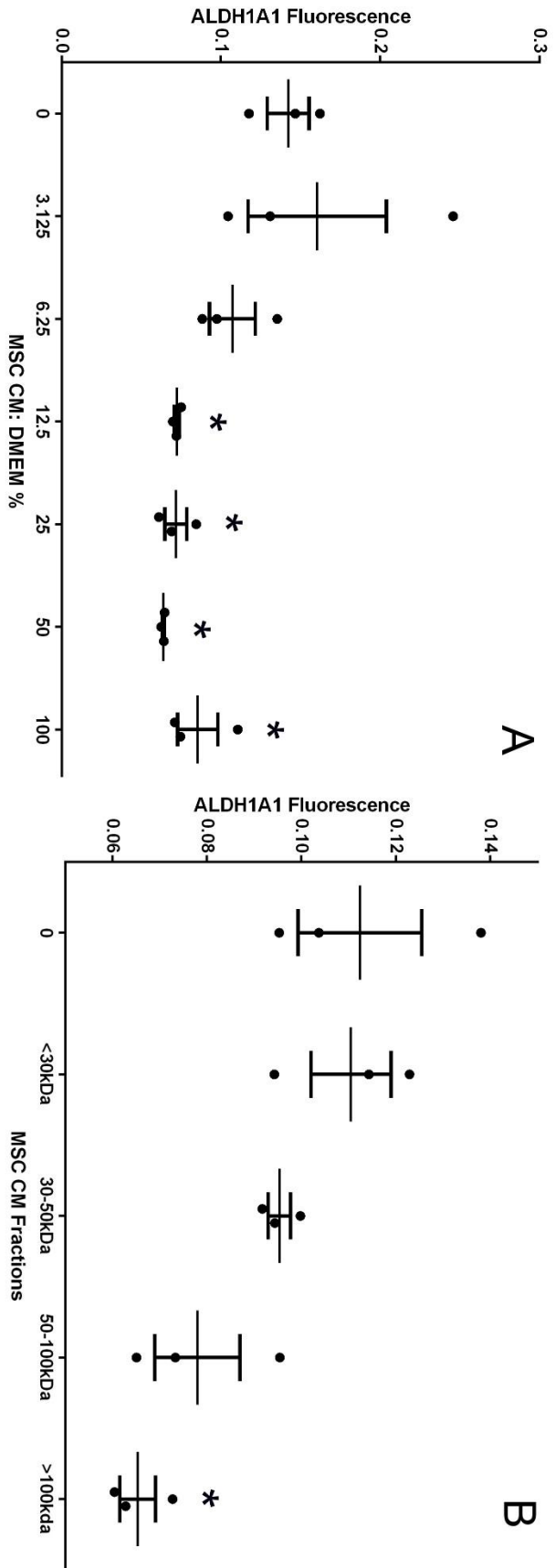


Figure 6-1 ALDH1A1 marker fluorescence of MCF7 cells cultured in MSC conditioned media. A) MSC CM dilution series, diluted in fresh DMEM. B) MSC CM fractionated by size and reconstituted back into fresh DMEM. All cells cultured for 24 hours. ALDH1A1 fluorescence relative to fluorescence of CellTag in whole cell imaged using Odyssey SA; n=3 all points shown, error bars show standard error mean, * denotes significant change compared with 0 (DMEM only).

Effects Upon MCF7 Spheroids

MSC-CM was filtered to separate the molecular weights of signalling molecules. Each fraction was incubated with MCF7 spheroids in collagen gel (BM model). The mean diameter of all spheroids at zero hours was similar, although there was a variation in the range of sizes (figure 6-2). After 24 hours in culture, control spheroids cultured in DMEM alone, saw a significant increase in diameter, with an increase in overall range. MSC-CM fraction containing molecules <30 kDa showed a large increase in mean diameter and range over 24 hours; this fraction will contain many of the cytokines tested in previous sections of this chapter, such as IL-6, TGF β 1 and CCL5. Cells cultured in MSC-CM containing molecules 30-50 kDa and 50-100 kDa exhibit a significant increase in spheroid diameter after 24 hours (figure 6-2). The largest molecules contained in the >100 kDa fraction appear to maintain mean spheroid diameter over 24 hours (figure 6-2). The range of diameters still increases, but the mean does not significantly increase ($p < 0.05$).

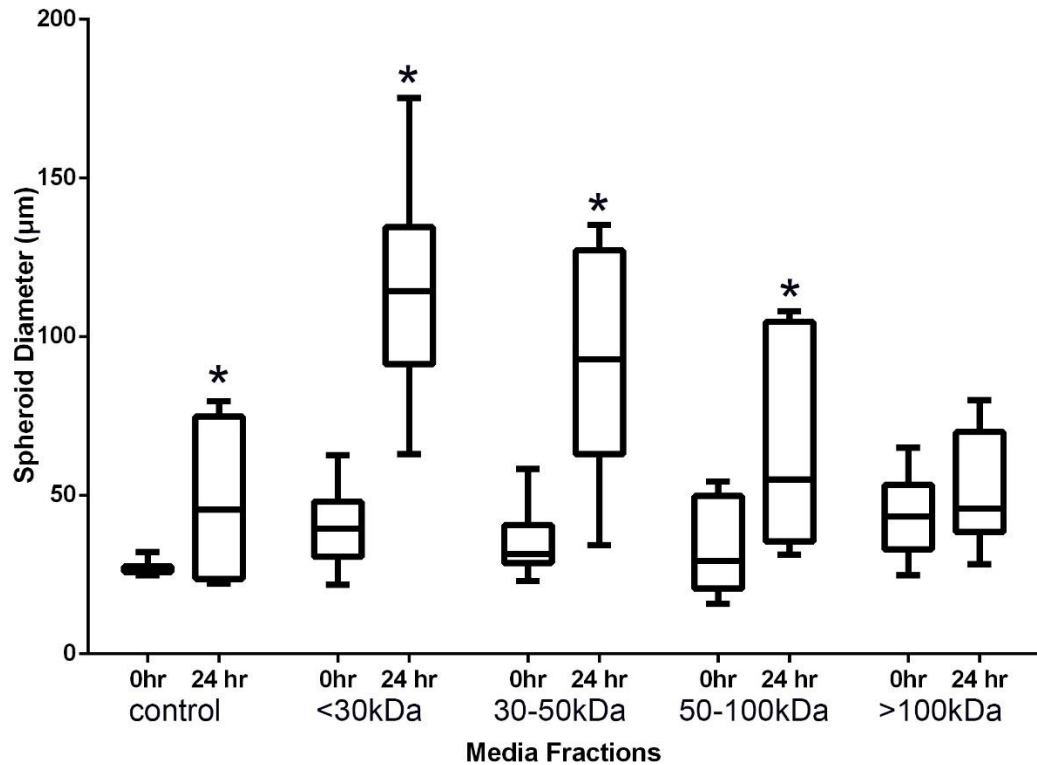


Figure 6-2 MCF7 spheroids cultured in collagen gel with fractioned MSC-conditioned media. Spheroid diameter recorded immediately following collagen gelation and after 24 hours. Spheroid diameter measured using imageJ. * denotes significant change, $p < 0.05$, from 0hr to 24hr; $n \geq 7$ across 3 collagen gels in each condition. Bars indicate diameter range.

MSC Spheroids and MCF7-CM Fractions

The converse experiment was also performed; MCF7 cells were cultured, media collected and fractionated as in section 2.20. This MCF7-conditioned media (MCF7-CM) was then used to culture MSC spheroids in collagen gels. As before spheroids were measured immediately following collagen gelation and 24 hours later to determine if the MCF7-CM had any effect upon cellular outgrowth. Control spheroids, cultured in DMEM only, saw a significant increase ($p < 0.05$) in diameter (figure 6-3), with no

difference in range. No MSC spheroids cultured in any MCF7-CM fractions showed a significant change in diameter over 24 hours, unlike the effects of MSC-CM upon MCF7 spheroids.

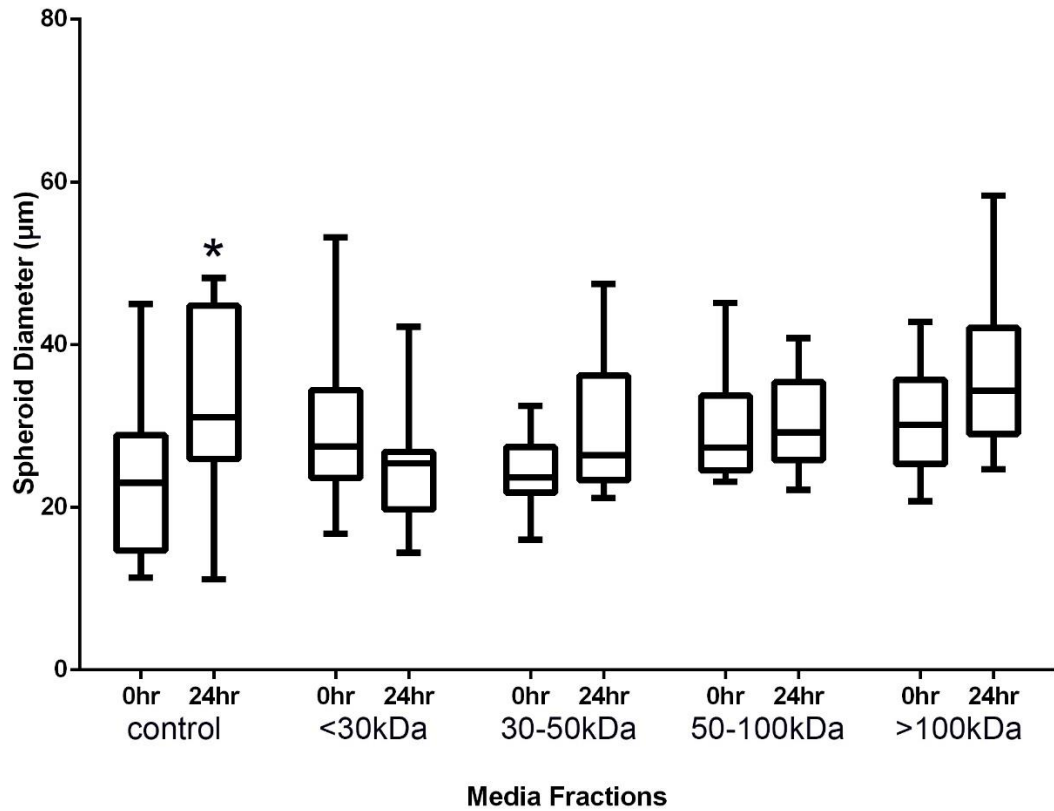


Figure 6-3 MSC spheroids cultured in collagen gel with fractionated MCF7-conditioned media. Spheroid diameter recorded immediately following collagen gelation and after 24 hours. Spheroid diameter measured using imageJ. * denotes significant change, $p < 0.05$, from 0hr to 24hr; $n \geq 7$ across 3 collagen gels in each condition. Bars indicate diameter range.

6.2.ii Quantification of MSC-Derived EVs from Conditioned Culture Medium

In figure 6-1B it was determined that 100 kDa+ fractions, which contain EVs, of MSC-conditioned medium negatively affected the ALDH1A1 expression of MCF7, leading to a more stem cell-like phenotype. This fraction contains EVs; these were purified to remove other large molecules, quantified and used to enrich further MCF7 cultures to assess EV influence on cell behaviour.

EVs isolated from MSC culture medium were quantified using dynamic light scattering and Fluorocet assay. Dynamic light scattering allows the size of particles to be determined (figure 6-4A) indicating highest peak intensities at 91.3nm and 164nm, with a weighted average diameter of 174.4nm (figure 6-4C). This indicates the presence of two vesicle populations; exosomes and larger microvesicles. Acetylcholinesterase (AChE) fluorescence, a marker for EVs, was then assayed to determine the number of MSC-derived EVs present, found to be 1.6×10^9 /mL (figure 6-4C). The presence of MSC-derived EVs using this method of isolation is indicated by TEM (figure 6-4B).

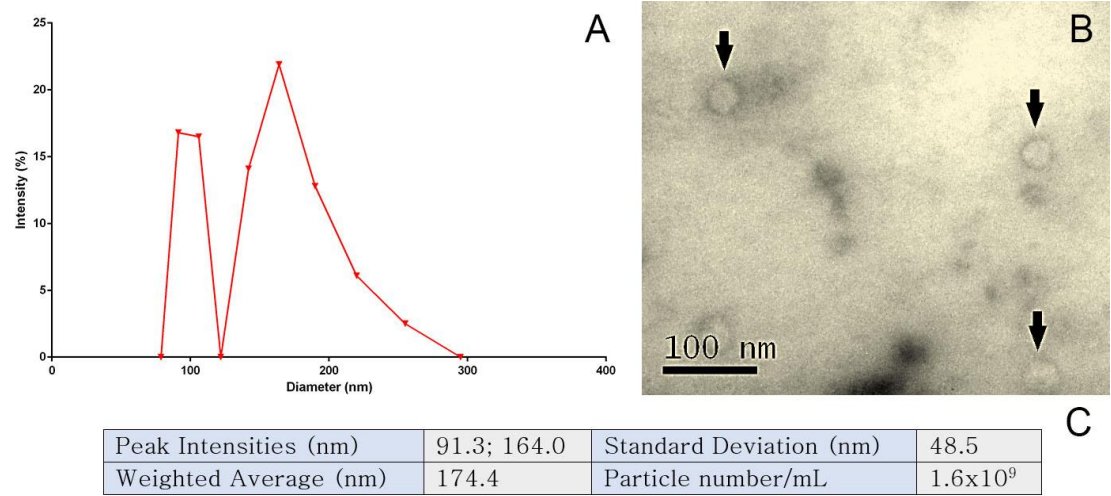


Figure 6-4 Quantification of the size of MSC-derived EVs. A: Measured using dynamic light scattering and average intensities plotted (n=3). B: Transmission Electron Microscope image of MSC-derived EVs; arrows indicate the presence of vesicles. C: A table detailing key data from dynamic light scatter in addition to particle number acquired through measurement of AChE fluorescence using Fluorocet assay.

6.2.iii The Influence of MSC-Derived EVs on MCF7 Migration

The effect of MSC-derived EVs on MCF7 cell motility was assessed in both two- and three-dimensional culture.

Two-Dimensional Culture

MCF7 cells were seeded into ibidi chemotaxis plates, used in previous studies; one side contained DMEM doped with 2×10^7 MSC-derived EVs, whereas the other contained standard DMEM. Within standard monolayer culture, MCF7 cells grown in control culture medium did not migrate preferentially in any direction (figure 6-5B), however, when treated with cell culture medium containing purified MSC-derived EVs they become more mobile. Interestingly, MCF7 cells do not move towards the MSC-derived EVs, but appear to migrate away from them (figure 6-5A). This phenomenon is quite pronounced over 24 hours, with no MCF7 cells migrating towards the MSC-derived EVs. This confirms that MCF7 cells react to the MSC-derived EVs and shows that they do so differently to cytokines, previously examined in chapter 4.

Spheroid culture

MCF7 cells were then cultured as spheroids in collagen gels, as previously described, across 120 hours (5 days) and imaged at several intervals (figure 6-6A-C). Through tracking the same spheroid across this time period, a reduction in size was recorded, with no individual cells surrounding the spheroid, indicating that the cells were not migrating from the central mass. The spheroid tracked in figure 6-6A-C retains a similar morphology, but fluorescence becomes denser over the time period. This appears to mirror the phenomenon seen in monolayer culture as cells move away from the source of MSC-derived EVs (figure 6-5). Hourly measurements of spheroids over a 24 hour period indicate MSC-derived EVs prevent an increase in spheroid diameter (figure 6-6D). However, due to the range of spheroid diameters, there is no significant change ($p < 0.05$) until day 5 (figure 6-6E), where the spheroids treated with MSC-derived EVs are significantly smaller than untreated spheroids.

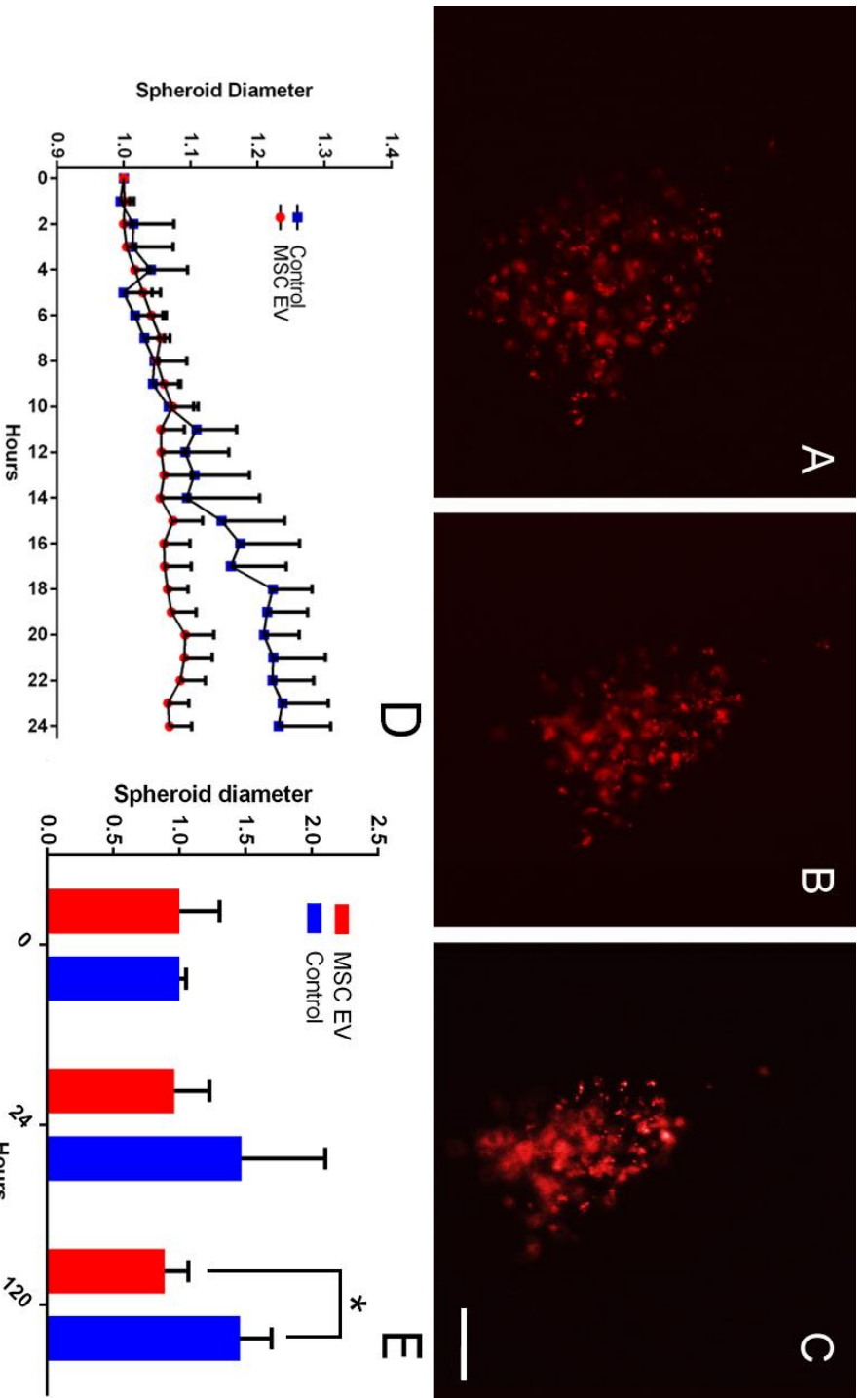
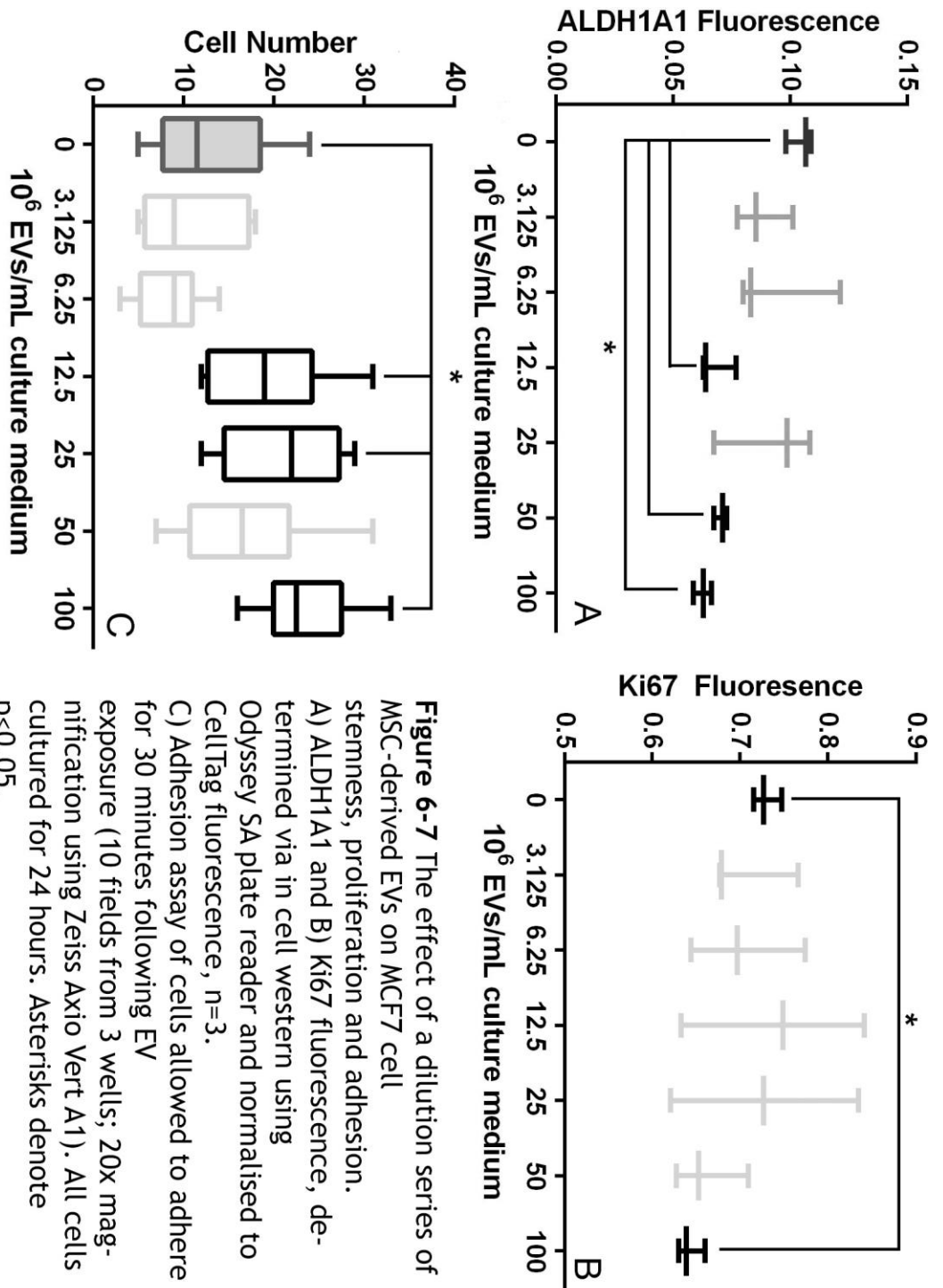


Figure 6-6 MCF7 spheroid cultured with MSC-derived EVs. Spheroids cultured in collagen gel for A) 0 hours, B) 24 hours and C) 120 hours; same representative spheroid measured over time; scale bar = 10μm. D) 24 hour time lapse of spheroids treated with EVs, spheroid diameter normalised to 0 hour, n=3. E) Measurements of MCF7 spheroids at hours 0, 24 and 120.

6.2.iv Effects of MSC-derived EVs on MCF7 Stemness, Proliferation and Adhesion

The influence of MSC-derived EVs on MCF7 growth was assessed via in cell western probing for the cancer stemness marker ALDH1A1, as in 6.2.i, and Ki67, a proliferation marker present throughout the cell cycle except G₀. A reduction in ALDH1A1 expression by MCF7 cells was noted (figure 6-7A), indicating a reduction in tumourigenicity, as cells become less metabolically active. This response is reflected in the Ki67 expression (figure 6-7B); there is a steady decline in fluorescence until 1×10^9 EVs/mL, where this decline is significantly lower ($p < 0.05$) than the 0 EVs/mL treatment. These results indicate MSC-derived EVs have a negative effect on the growth of MCF7 cells.

Cell adhesion following EV treatment was subsequently assessed, using different concentrations of MSC-derived EVs (figure 6-7C). A positive correlation was observed, as increased amounts of MSC-derived EVs present in the culture medium encourage MCF7 adhesion. In fact, relatively small volumes of MSC-derived EVs significantly increase this adhesion (12.5×10^6 EVs/ mL) over 24 hours (figure 6-7C).



6.2.v Metabolite Analysis of MSC-Derived EV

The contents of MSC-derived EVs were assessed by metabolomics. Five samples of 2×10^7 EVs/mL were analysed by Glasgow Polyomics. Metabolites were detected within the EVs and a literature search was performed to determine if any of the metabolites present in high levels were associated with the initiation the cancer cell cycle. Table 6-1 shows a list of candidate metabolites that have evidence supporting their involvement in breast cancer growth.

Table 6-1: Candidate metabolites derived from MSC EV metabolomics

Metabolite	Effect	Source
<i>D-Erythrose</i>	<i>Toxic to breast cancer in high levels</i>	<i>Wang and Wei, 2010</i>
<i>Pyroxidine</i>	<i>Associated with lower ER-breast cancer formation</i>	<i>Smith et al., 1995</i>
<i>L-Proline</i>	<i>Energy source in stress, blocking may slow growth</i>	<i>Phang et al, 2014</i>
<i>L-Phenylalanine</i>	<i>L-PAM, a well-documented chemotherapeutic agent</i>	<i>Fisher et al, 1975</i>
<i>L-Methionine</i>	<i>Significantly suppresses MCF7 growth</i>	<i>Kim and Park, 2003</i>
<i>L-Valine</i>	<i>Glutamine uptake inhibitor. Addition to lapatinib increases effect</i>	<i>Maeng et al. 2014</i>
<i>L-Tryptophan</i>	<i>Deficiency leads to increased risk therefore overdose may suppress.</i>	<i>Travers et al., 2004</i>

6.2.vi Viability of MCF7 Treated with D-Erythrose or L-Methionine

Two candidate metabolites were taken from the literature search performed in section 6.2.v; D-erythrose and L-methionine. A viability assay was performed using a range of concentrations determined from the literature to have an effect on cancer cell growth.

Monolayer Culture

In monolayer neither erythrose nor methionine affect the viability of MCF7 cells over 24 hours (figure 6-8A,B). Therefore, the highest concentration of each was used to further test the effect on cell viability across 5 days (figure 6-5C). Again, these metabolites did not greatly effect MCF7 viability.

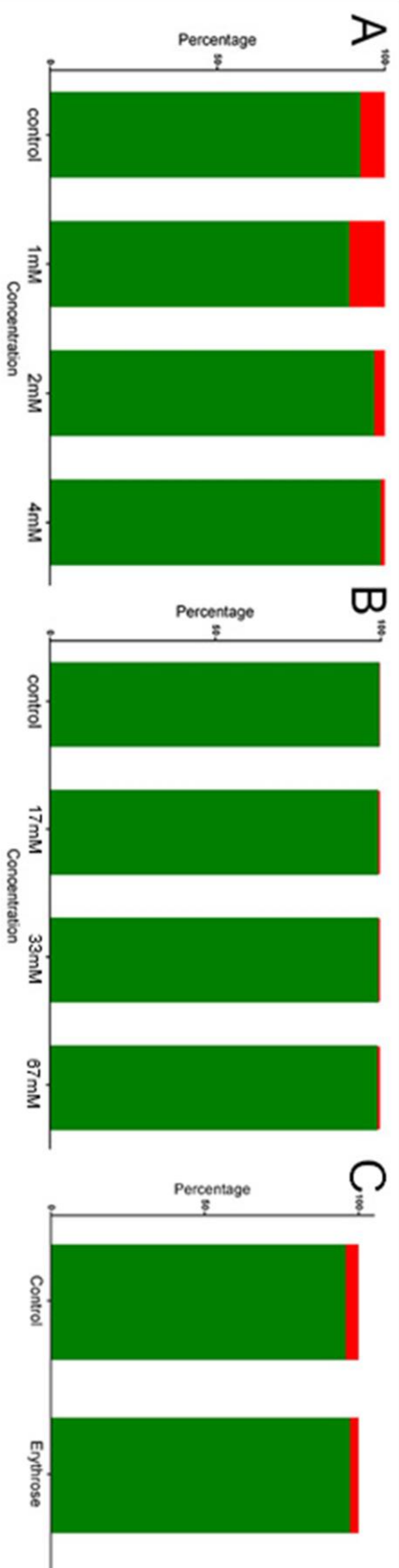


Figure 6-8 Viability assay of MCF7 cells cultured with D-erythrose or L-methionine in monolayer. A) Cells treated with increasing concentrations of D-erythrose in culture medium. B) Cells treated with increasing concentrations of L-methionine in culture medium. Cells were cultured for 24 hours. C) Cells treated with 4 mM erythrose or 67 mM methionine and cultured for 5 days. Following metabolite treatment, cell viability was tested with calcein AM and ethidium homodimer for 30 minutes before imaging using Zeiss Axio Vert A1 fluorescence microscope. Cells were viewed at 10 times magnification, 2 fields counted in each of 3 wells. Green indicates living cells, with red indicating dead.

Spheroid Culture

As it was determined neither erythrore, nor methionine affected the viability of MCF7 in monolayer, metabolites were tested with MCF7 spheroids in collagen gels to determine if the three-dimensional environment affected viability. Spheroids cultured for 24 hours with erythrore or methionine resembled those cultured in DMEM alone controls (figure 6-9 A-C). Spheroids cultured for 72 hours in 4 mM erythrore were also as controls cultures (figure 6-9 D, E), however, spheroids cultured for 72 hours in 67 mM methionine indicate large areas of cell death, reflected by red fluorescence (figure 6-9 F).

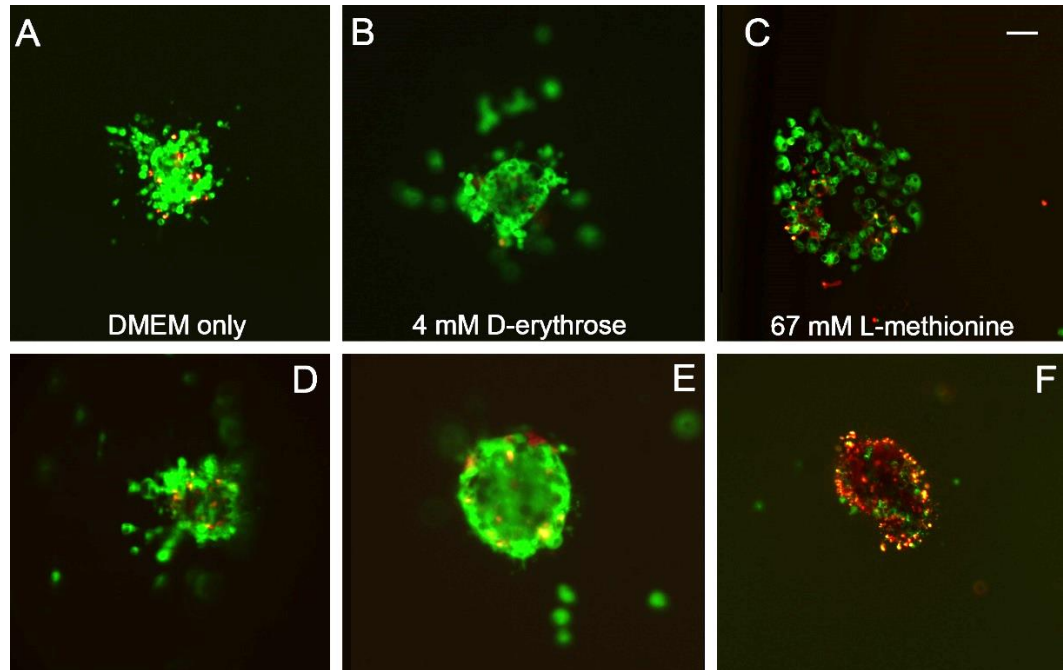


Figure 6-9 Viability assay of MCF7 spheroids cultured with D-erythrose or L-methionine in type I collagen gel. Control spheroids were cultured with DMEM only for A) 24 hr and D) 72 hr; 4 mM D-erythrose for B) 24 hr and E) 72 hr or 67 mM L-methionine for C) 24 hr and F) 72 hr. Cells were then treated with calcein AM (live; green) and ethidium homodimer (dead; red) before imaging using Zeiss Axio Vert A1 fluorescence microscope. Scale bar 10 μ m, n=3, representative image shown.

6.2.vii Effects of D-Erythrose and L-Methionine on MCF7 proliferation

No changes in MCF7 cell viability were noted in spheroid culture when incubated with either metabolite. Here, cell cycle of MCF7 spheroids was assessed, using Ki67 fluorescence, in response to metabolite culture.

Monolayer culture

The Ki67 expression of MCF7 cells treated with increasing concentrations of either D-erythrose or L-methionine was determined using in cell western (figure 6-10). Both metabolites, caused a decrease in proliferation after treatment; 2mM erythrose was sufficient for a significant decrease ($p < 0.05$), with all concentrations of methionine significantly reducing ($p < 0.05$) ki67 fluorescence over 24 hours.

MCF7 cells were then cultured in the highest concentrations of metabolites, 4 mM D-erythrose or 67 mM L-methionine, for 3 and 5 days (figure 6-10C). Control cells showed no change in Ki67 fluorescence, L-methionine indicated a significant decrease ($p < 0.05$) in proliferation after day 3, continuing to day 5. D-erythrose treatment showed a significant decrease ($p < 0.05$) after 1 day, and again after 5 days in culture (figure 6-10C).

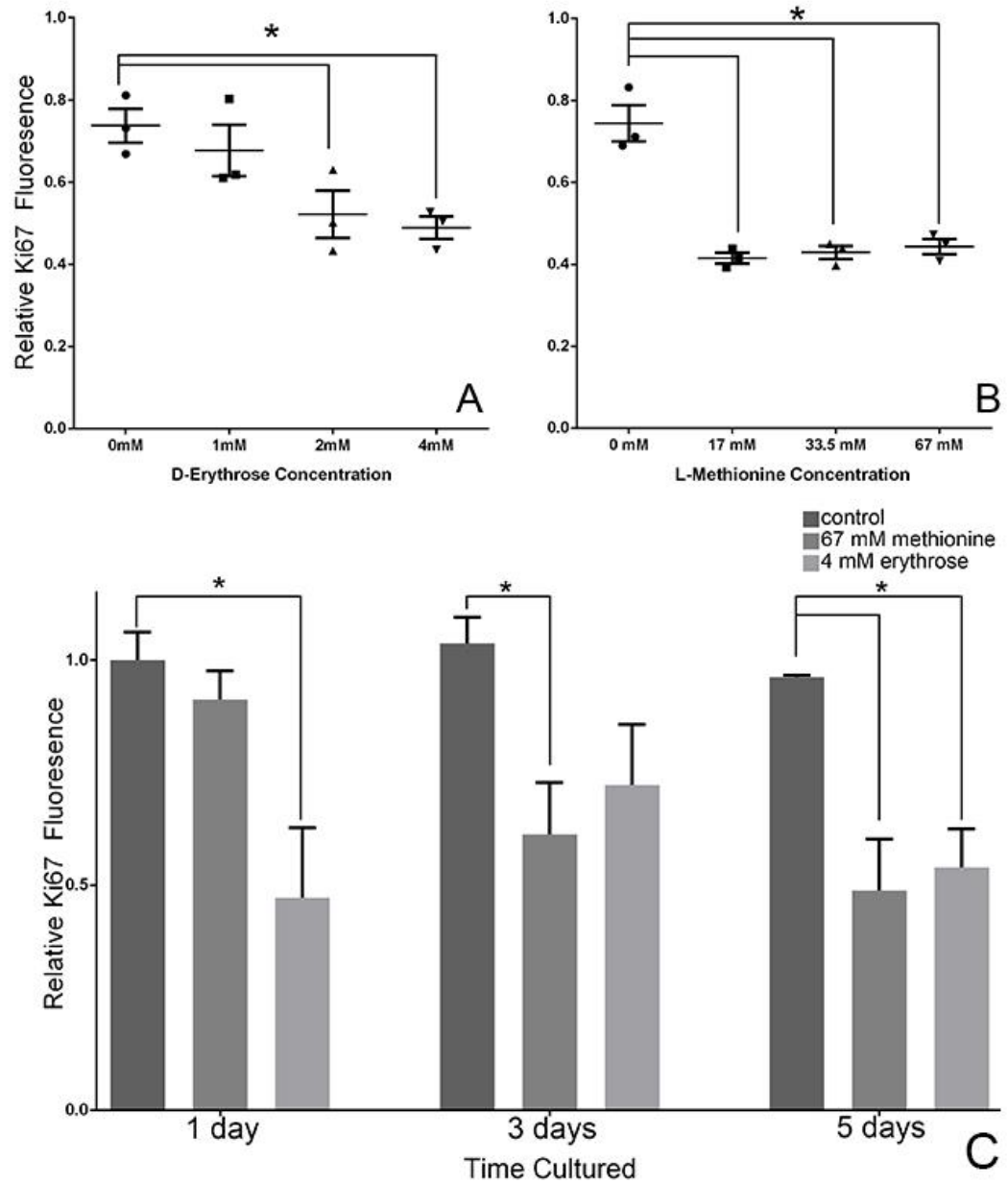


Figure 6-10 Ki67 fluorescence in MCF7 cells treated with metabolites. A) Increasing levels of D-erythrose at 24 hours; B): increasing levels of L-methionine at 24 hours. C): Cells were then incubated with metabolites for 1, 3 and 5 days, imaged on Odyssey SA fluorescence plate reader and Ki67 fluorescence normalised to cell number; n=3. Asterisks denote $p < 0.05$.

6.2.viii Effects of Kinase Inhibitors on D-Erythrose and L-Methionine

Changes seen previously may be linked to specific pathways. In order to determine how D-erythrose and L-methionine may be affecting proliferation, p38 MAP kinase inhibitor SB203580 and TGF β receptor kinase inhibitor SB431542 were added to DMEM. If either of these metabolites act upstream of these inhibitors then their addition will negate the effect of adding D-erythrose or L-methionine. These cells were then cultured in monolayer over 72 hours before Ki67 expression was assessed using in cell western. DMEM only (control) cells show an increase in Ki67 fluorescence across the 3 day test period (Figure 6-11). Whilst both inhibitors lower Ki67 fluorescence, SB203580 treated cells show an increase over time similar to DMEM alone. However, SB431542-treated cells steadily decrease Ki67 fluorescence over the test period.

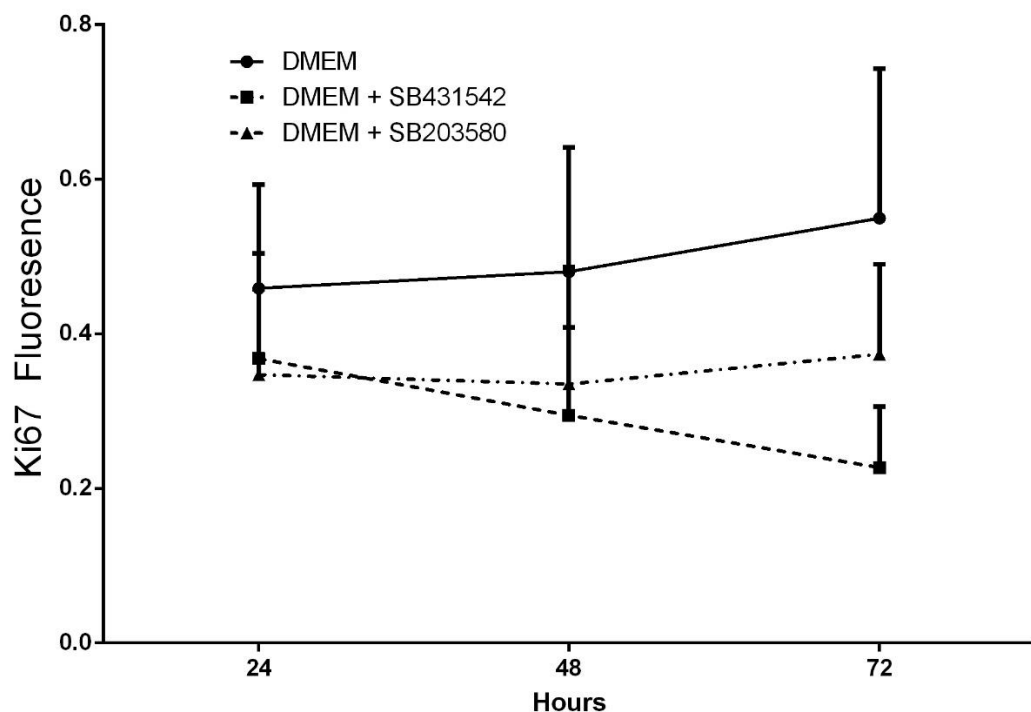


Figure 6-11 MCF7 cells cultured with p38 inhibitor SB203580 or TGF β receptor kinase inhibitor SB431542. DMEM containing 2 μ M SB203580 or 10 μ M SB431542 was used to culture cells over 3 days; n=6. Bars indicate SEM. Cells cultured in 96-well plate and fluorescence of Ki67 measured using Odyssey SA, normalised to Celltag fluorescence.

D-Erythrose

Previously, D-erythrose encouraged a decrease in MCF7 cell proliferation over 5 days in culture. Here, by adding pathway inhibitors, we can determine if it is these pathways being affected. DMEM containing 4 mM D-erythrose was used to culture MCF7 cells in addition to the inhibitors SB203580 or SB431542. Similar to previous results (Figure 6-10), MCF7 cells treated with D-erythrose alone showed a decline in Ki67 fluorescence over time compared with the cells cultured in DMEM alone (red line, figure 6-12). An additional 2 μ M p38 inhibitor SB203580 or 10 μ M

TGF β receptor kinase inhibitor was added to the D-erythrose DMEM to identify if the metabolite affects MCF7 cells through activation of either of their respective pathways. Whilst Ki67 fluorescence is higher in cells treated with the inhibitors, the gradient of lines generated are similar to that of 4 mM D-erythrose (Figure 6-12). However, SB431542 demonstrates a shallower decline over time, which may indicate that this inhibitor is potentially slowing the reduced proliferation effects of D-erythrose on the cell.

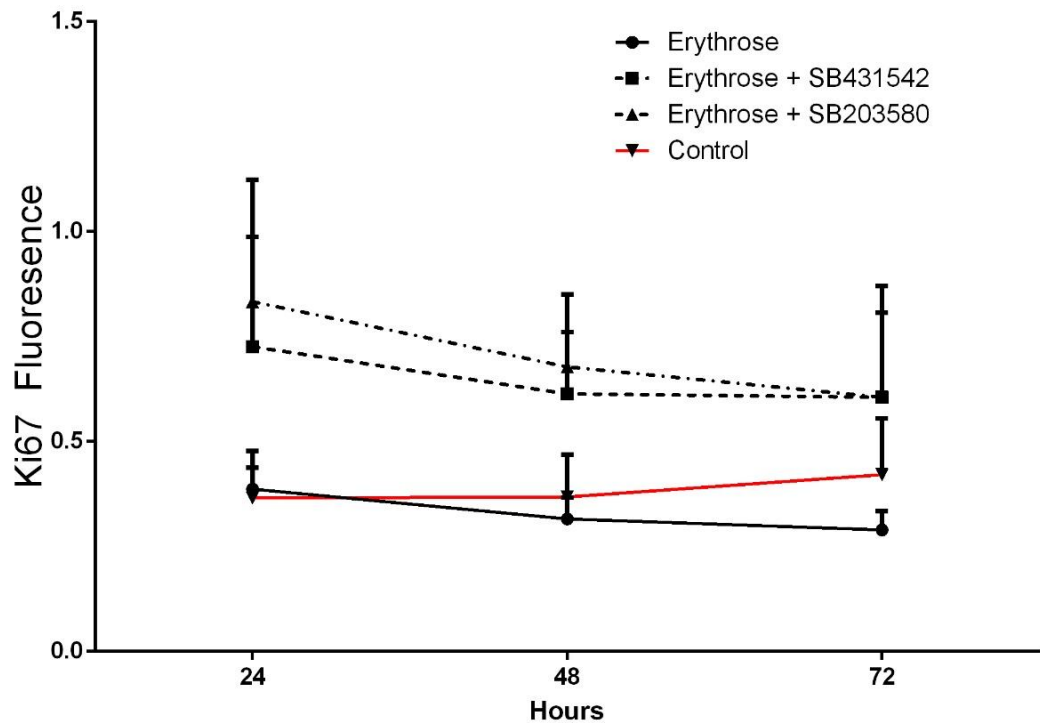


Figure 6-12 MCF7 cells cultured with 4 mM D-erythrose and p38 inhibitor SB203580 or TGF β receptor kinase inhibitor SB431542. DMEM containing 2 μ M SB203580 or 10 μ M SB431542 was used to culture cells over 3 days; n=6. Bars indicate SEM. Cells cultured in 96-well plate and fluorescence of Ki67 measured using Odyssey SA, normalised to Celltag fluorescence.

L-Methionine

Previously, L-methionine significantly reduced MCF7 cell proliferation over 5 days in culture. Here, the effect of the pathway inhibitors did not affect the metabolite's response. Ki67 fluorescence in control cells appears to increase between 24 and 48 hours, but rapidly reduces at 72 hours (figure 6-13). Neither SB203580 nor SB431542 recover Ki67 fluorescence in the presence of L-methionine (figure 6-10). The line generated by SB431542 mirrors that of L-methionine alone, whereas SB203580 shows a steady decline over the time period. Results therefore suggest that these pathways are not affected by L-methionine.

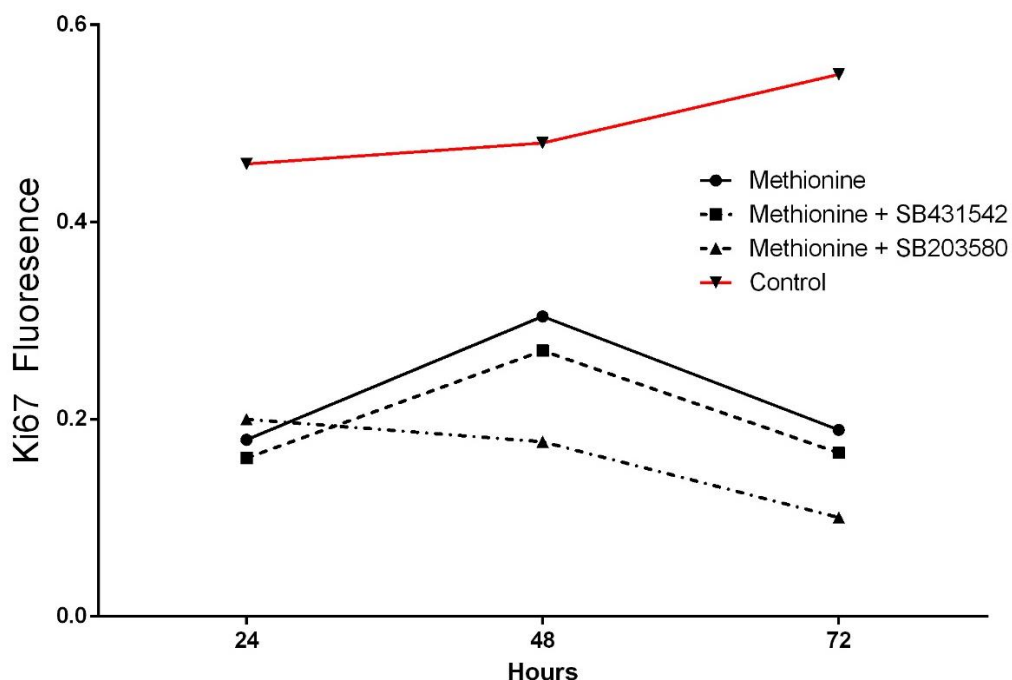


Figure 6-13 MCF7 cells cultured with 67 mM L-methionine and p38 inhibitor SB203580 or TGF β receptor kinase inhibitor SB431542. DMEM containing 2 μ M SB203580 or 10 μ M SB431542 was used to culture cells over 3 days; n=6. Bars indicate SEM. Cells cultured in 96-well plate and fluorescence of Ki67 measured using Odyssey SA, normalised to Celltag fluorescence.

6.2.ix Proliferative Effects of D-Erythrose and L-Methionine on MCF7 Spheroids

Due to differences in the ways cells behave in two and three dimensions, the tests performed in 6.2.viii were repeated in MCF7 spheroids. The fluorescence of mNPs within cells was used to compare the level of ki67 fluorescence in a similar fashion to CellTag used previously.

Both SB203580 or SB431542 were added to DMEM and cultured spheroids were measured daily for 3 days. There was no significant difference between the expansion of spheroids in DMEM alone or in DMEM containing either of the inhibitors (figure 6-14). If either of these metabolites act upstream of these inhibitors then their addition will negate the effect of adding D-erythrose or L-methionine.

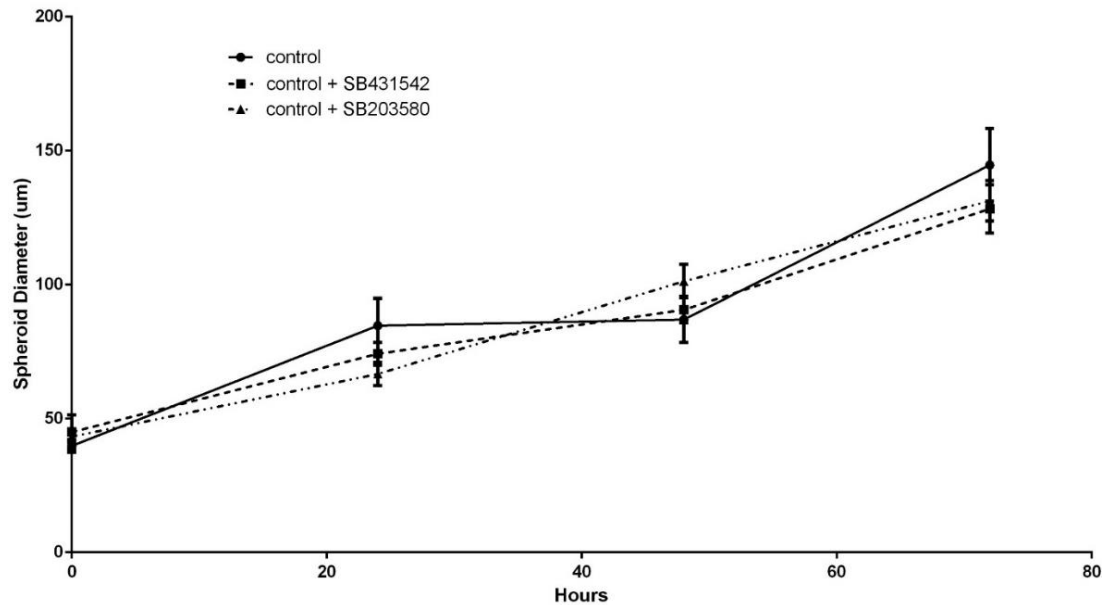


Figure 6-14 MCF7 spheroids cultured with p38 inhibitor SB203580 or TGF β receptor kinase inhibitor SB431542. MCF7 spheroids grown in control DMEM, DMEM plus 2 μ M p38 inhibitor SB203580 or 10 μ M TGF β receptor kinase inhibitor SB431542. Spheroid measurements taken at daily intervals by measuring the cross-section of images using ImageJ; $n \geq 6$. Images captured using Axio Vert A1 fluorescent microscope, utilising green-fluorescent mNPs to detect spheroids.

D-Erythrose

When spheroids are cultured in media containing 4 mM D-erythrose, there is significant reduction in spheroid expansion after 24 hours in culture compared with control spheroids cultured in DMEM alone (figure 6-15). This was also noted at 72 hours. This reflects the earlier reduction in spheroid size noted when MCF7 spheroids were incubated with MSC-derived EVs (figure 6-6D), which contain elevated levels of D-erythrose (table 6-1). This suggests D-erythrose is able to reduce cell migration.

When 2 μ M SB203580 is added to the media, the effects of the erythrose are reversed, and spheroid mass increases again, to significantly higher levels than control spheroids (figure 6-15). This suggests that D-erythrose acts upon some part of the p38 MAPK pathway and inhibiting p38 phosphorylation prevents this action. The SB431542 inhibitor did not influence cell migration.

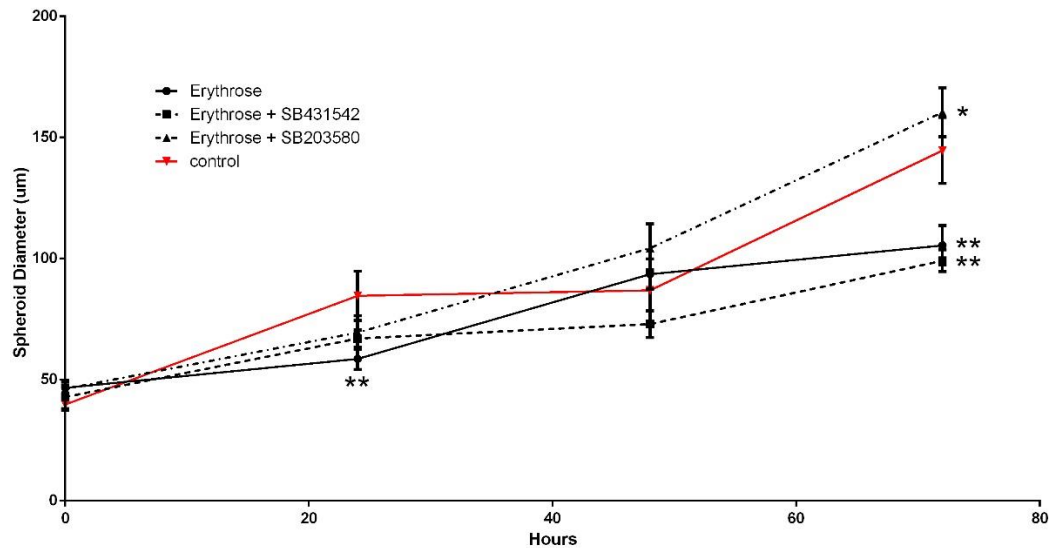


Figure 6-15 MCF7 spheroids cultured with 4 mM erythrose plus either 2 μ M p38 inhibitor SB203580 or 10 μ M TGF β receptor kinase inhibitor SB431542. Spheroid measurements taken at daily intervals by measuring the cross-section of images using ImageJ; $n \geq 12$. Images captured using Axio Vert A1 fluorescent microscope, utilising green-fluorescent mNPs to detect spheroids. * denotes $p < 0.05$ compared with erythrose treatment, ** denotes $p < 0.05$ compared with control.

L-Methionine

Likewise, the effects of L-methionine were assessed in MCF7 spheroid culture. 67 mM L-methionine was added to DMEM and spheroids were cultured for 3 days, recording their diameter each day. In parallel, SB203580 or SB431542 were added to the L-methionine-doped DMEM. Whilst MSC-derived EVS reduced MCF7 spheroid diameter (figure 6-6C), here the metabolite in isolation does not affect spheroid diameter (Figure 6-16). After 24 hours there is a slight decrease in spheroid diameter, but this is not a significant ($p < 0.05$) change. Indeed, from this time point,

spheroids appear to rapidly expand. The addition of either inhibitor in combination with L-methionine reduced spheroid outgrowth, but L-methionine alone does not reduce this so likely does not act through either of the pathways that have been inhibited.

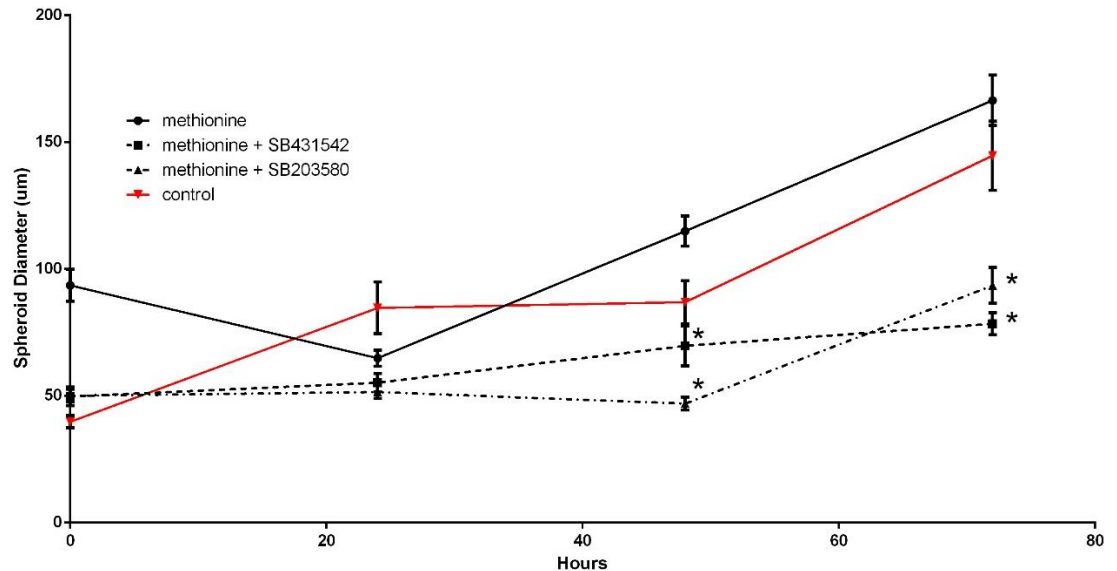


Figure 6-16 MCF7 spheroids cultured with 67 mM L-methionine plus either 2 μ M p38 inhibitor SB203580 or 10 μ M TGF β receptor kinase inhibitor SB431542. Spheroid measurements taken at daily intervals by measuring the cross-section of images using ImageJ; $n \geq 10$. Images captured using Axio Vert A1 fluorescent microscope, utilising green-fluorescent mNPs to detect spheroids. * denotes $p < 0.05$ compared with methionine treatment.

6.2.x MCF7 Adhesion Assay with D-Erythrose, L-Methionine and Kinase Inhibitors

Previously, addition of MSC-derived EVs to MCF7 cultures caused an increase in adhesion (figure 6-7C), suggesting the cells become less migratory. Here, an adhesion assay was performed on MCF7 cells cultured in 4 mM D-erythrose or 67 mM L-methionine for 24 hours. Additionally, either SB203580 or SB431542 was added to determine any influence over control cells and cells incubated with the metabolites.

D-Erythrose

MCF7 cells were cultured for 24 hours in DMEM containing 4 mM D-erythrose. There was no significant change in adhesion of cells compared with control cells in DMEM alone (figure 6-17). The addition of SB203580 did not affect the cell adhesion. There was a significant increase ($p < 0.05$) in adhesion in cells cultured in SB431542, but this increase was also observed in control cells (DMEM) supplemented with SB431542, thus it is unlikely that the inhibitor is driving any increase in the cell adhesion.

L-Methionine

MCF7 cells were cultured for 24 hours in DMEM containing 67 mM L-methionine, causing a significant decrease in MCF7 cell adhesion (figure 6-17). Interestingly, the addition of either SB203580 or SB431542 recovered cell adhesion and significantly increased adhesion ($p < 0.05$) to almost three times the level observed in metabolite alone (figure 6-17).

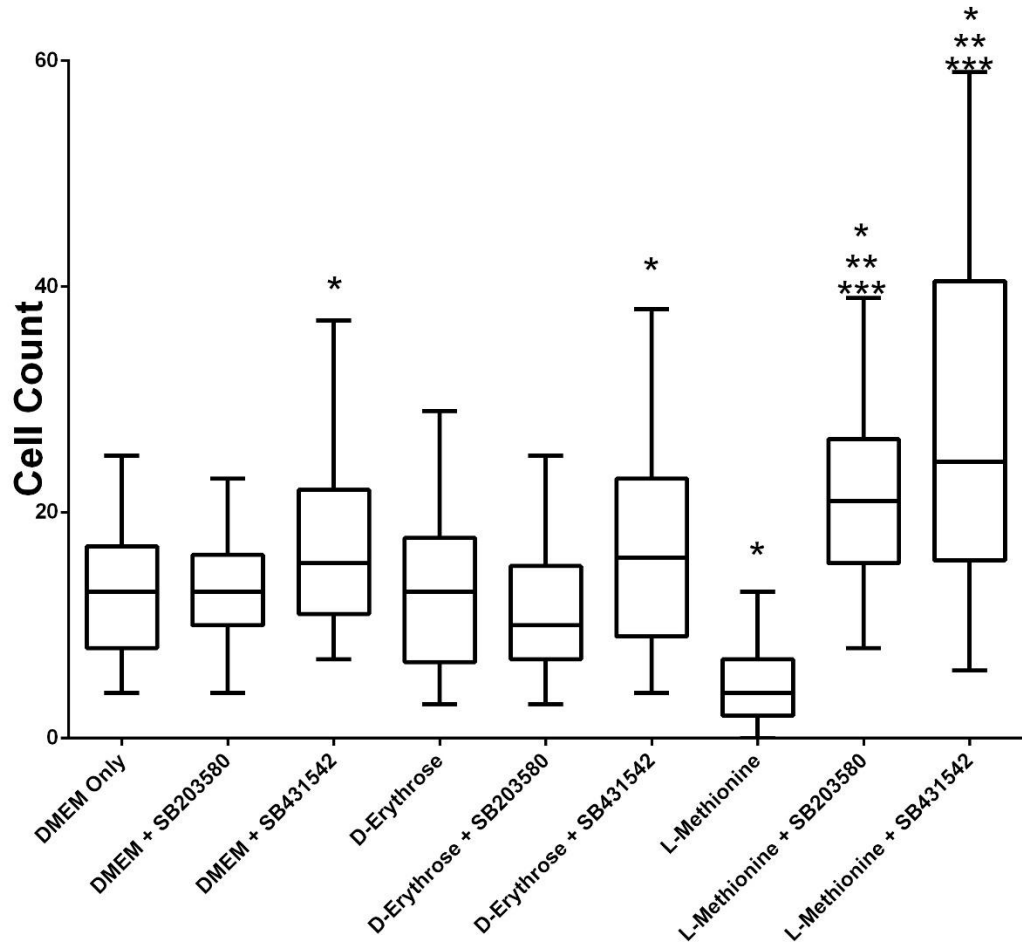


Figure 6-17 MCF7 adhesion assay with D-erythrose and L-methionine and kinase inhibitors. MCF7 monolayers cultured in DMEM alone, DMEM containing 4 mM D-erythrose or 67 mM L-methionine plus either plus 2 μ M p38 MAP kinase inhibitor SB203580 or 10 μ M TGF β receptor kinase inhibitor SB431542. Cells cultured for 24 hours before being reseeded in a new 96-well plate. Cells were able to attach for 30 minutes before being fixed and stained with Vectashield-DAPI. Images captured using Axio Vert A1 fluorescent microscope, 10 fields in 3 wells. Cell nuclei counted using ImageJ cell counter plugin. * denotes $p < 0.05$ compared with DMEM only. ** denotes $p < 0.05$ compared with relevant metabolite only. *** denotes $p < 0.05$ compared with DMEM with relevant inhibitor.

6.2.xi Fluidigm Real Time PCR of MCF7 Cells Treated with Metabolites

Following on from general observations regarding the influence of the two metabolites on MCF7 cell viability, proliferation, migration, 'stemness' and adhesion, the gene expression of various sets of genes in MCF7 cells cultured in either 4 mM D-erythrose or 67 mM L-methionine was assessed using fluidigm real time PCR. Leading on from the previous result investigating proliferation, genes from each stage of the cell cycle were assessed (Figure 6-18, 6-20) to determine how D-erythrose and L-methionine affected the MCF7 proliferation. Following observations of spheroid expansion, genes associated with epithelial-to-mesenchymal transition to determine how the metabolites affected cell adhesion and migration (Figure 6-19, 6-21).

D-Erythrose

Cell cycle: MCF7 cells cultured in 4 mM D-erythrose showed an overall decrease in cell cycle related genes compared with MCF7 cells culture in DMEM alone (figure 6-18). There were several cyclin genes upregulated, however, without cognate cyclin-dependent kinases, the cell cycle will not progress as normal.

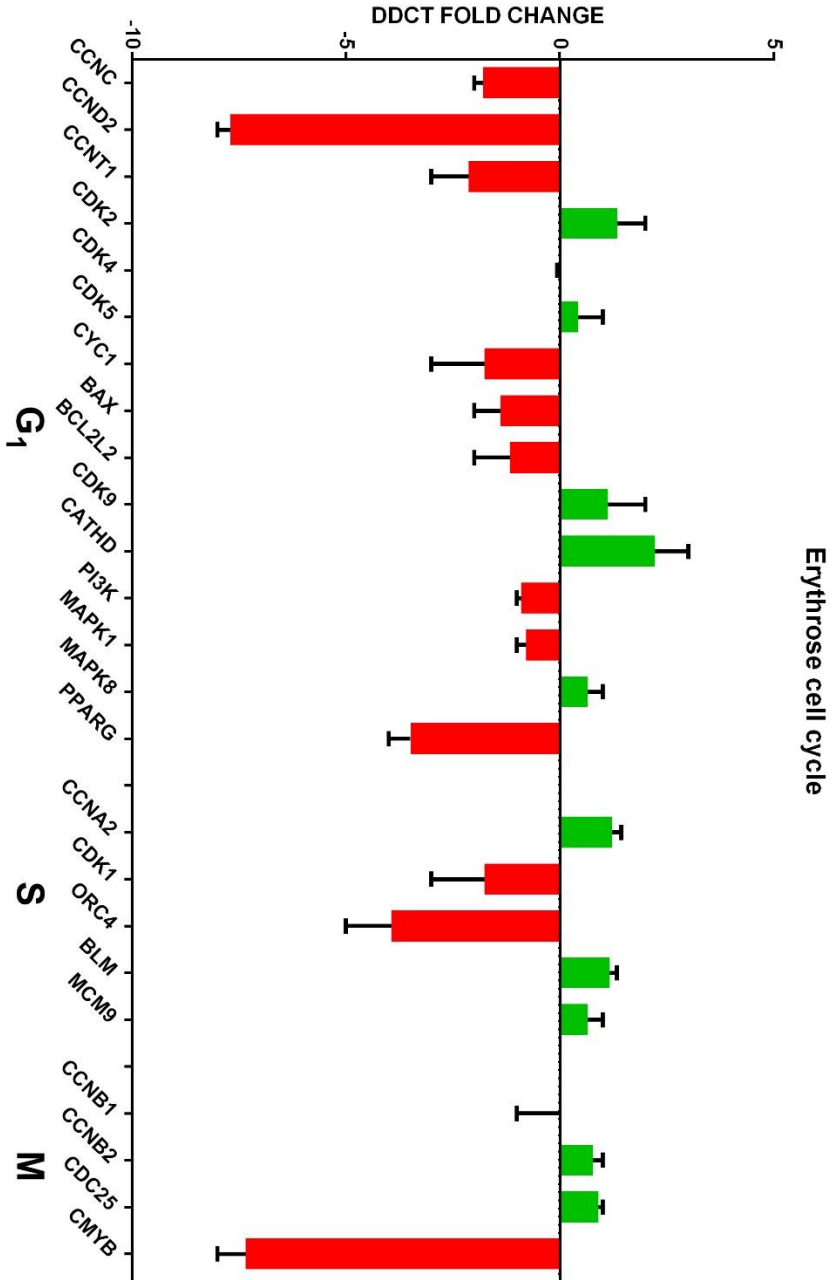


Figure 6-18 Δ DDCT of cell cycle gene expression in MCF7 cells cultured with 4 mM D-erythrose compared with MCF7 cells cultured without. Expression normalised to GAPDH. Cells cultured for 24 hours. Error bars indicate standard error mean; n=3 with 3 technical replicates from each.

EMT markers: MCF7 cells cultured in 4 mM D-erythrose showed downregulation in many of the EMT marker genes assayed, compared with MCF7 cells cultured in DMEM alone. The majority of genes assessed were markers of a mesenchymal phenotype. However several were markers of an epithelial phenotype; E-cadherin, Keratin 19 and JUP (figure 6-19). All of these markers saw a downregulation when exposed to D-erythrose in monolayer. Whilst many cell cycle genes were downregulated, it appears that these MCF7 cells did not experience a reinforcement of their epithelial phenotype.

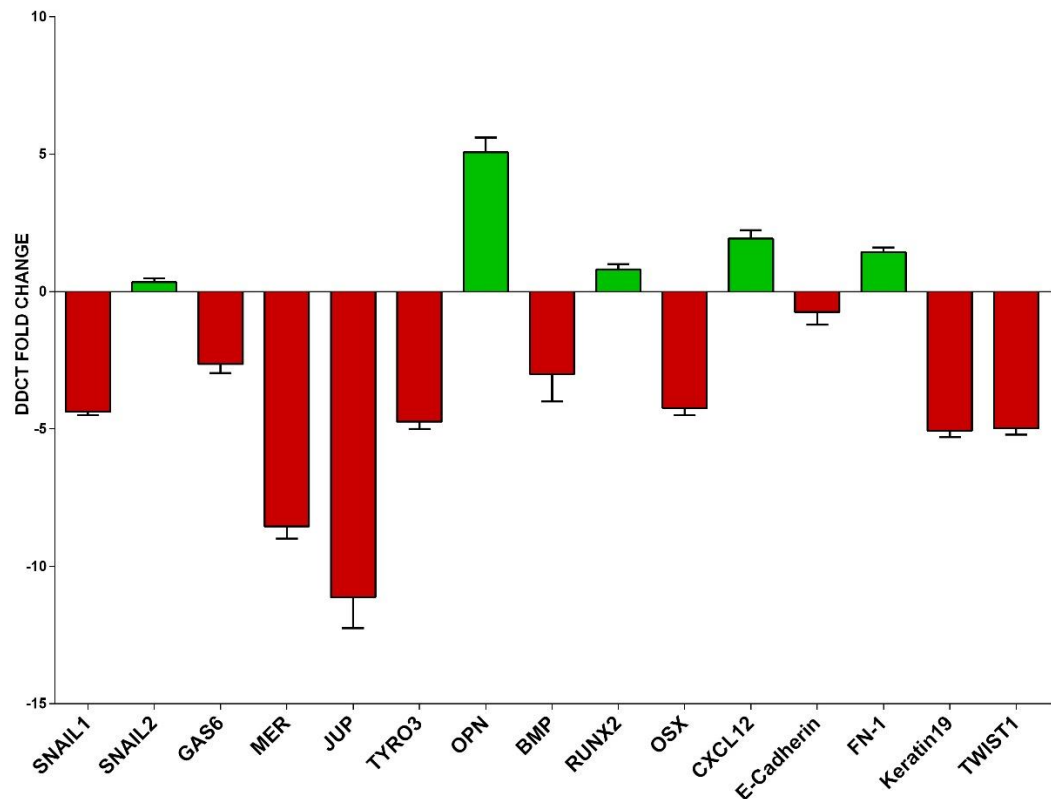


Figure 6-19 $\Delta\Delta C_t$ of EMT marker expression in MCF7 cells cultured with 4mM D-erythrose compared with MCF7 cells cultured without. Expression normalised to GAPDH. Cells cultured for 24 hours. Error bars indicate standard error mean; n=3 with 3 technical replicates from each.

L-Methionine

Cell cycle: MCF7 cells cultured in 67 mM L-methionine indicated the downregulation of some genes in early cell cycle, compared with MCF7 cultured in DMEM alone (figure 6-20). Despite the downregulation of these genes, many of the genes assayed were unaffected by the presence of L-methionine throughout each stage of the cell cycle.

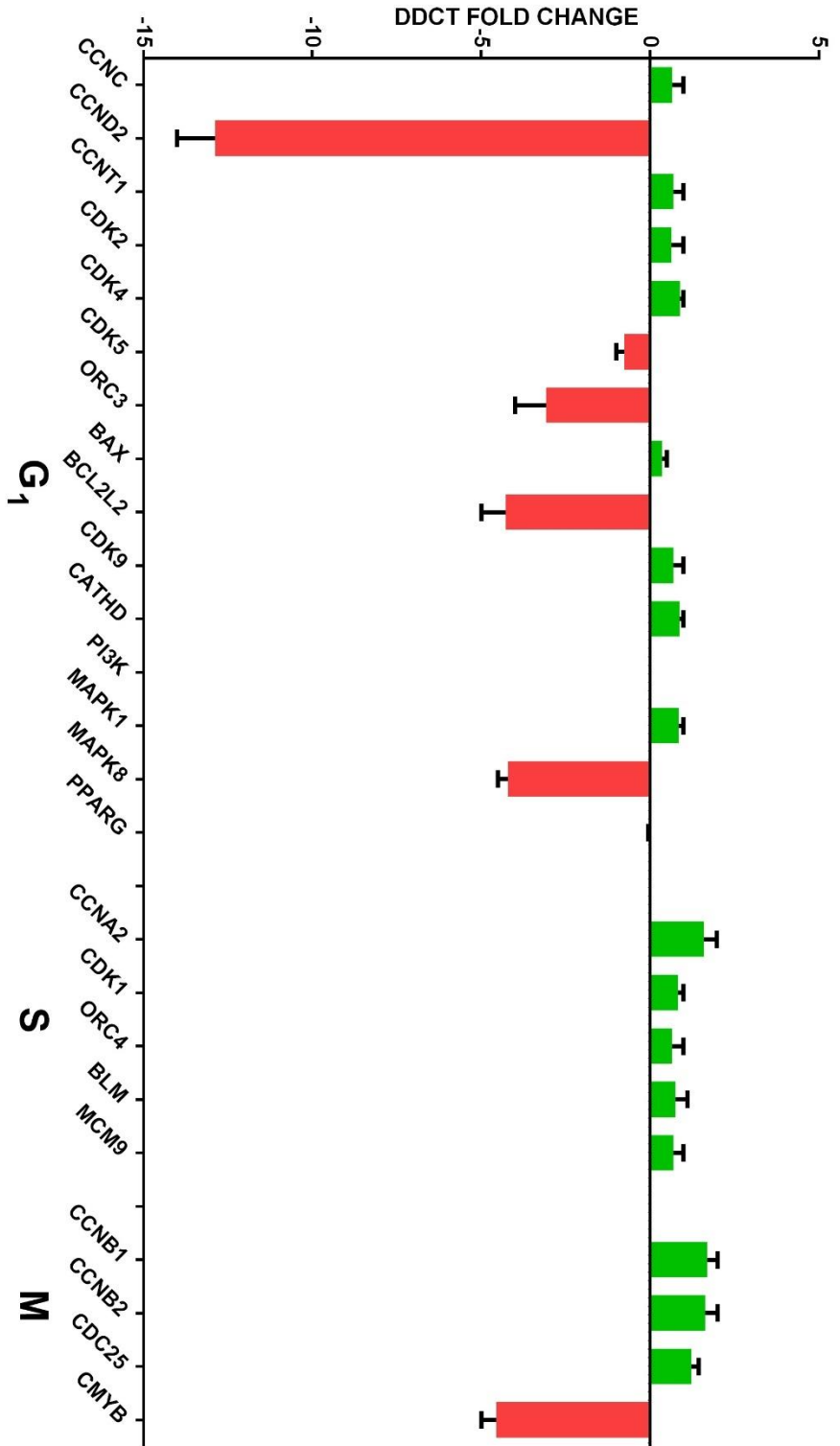


Figure 6-21 $\Delta\Delta$ Ct of EMT marker expression in MCF7 cells cultured with 67 mM L-methionine compared with MCF7 cells cultured without. Expression normalised to GAPDH. Cells cultured for 24 hours. Error bars indicate standard error mean: n=3 with 3 technical replicates from each.

EMT markers: MCF7 cells cultured in 67 mM L-methionine indicate a strong decrease in many EMT marker genes such as Vimentin, TWIST1 and Snail (figure 6-21). The large downregulation of RUNX2 will further prevent metastasis and migration by lowering the expression of some MMPs. Whilst there is a small upregulation in E-cadherin gene expression when cultured with L-methionine, other epithelial markers are reduced, such as JUP and Keratin19. This may lead to an overall reduction in the epithelial phenotype.

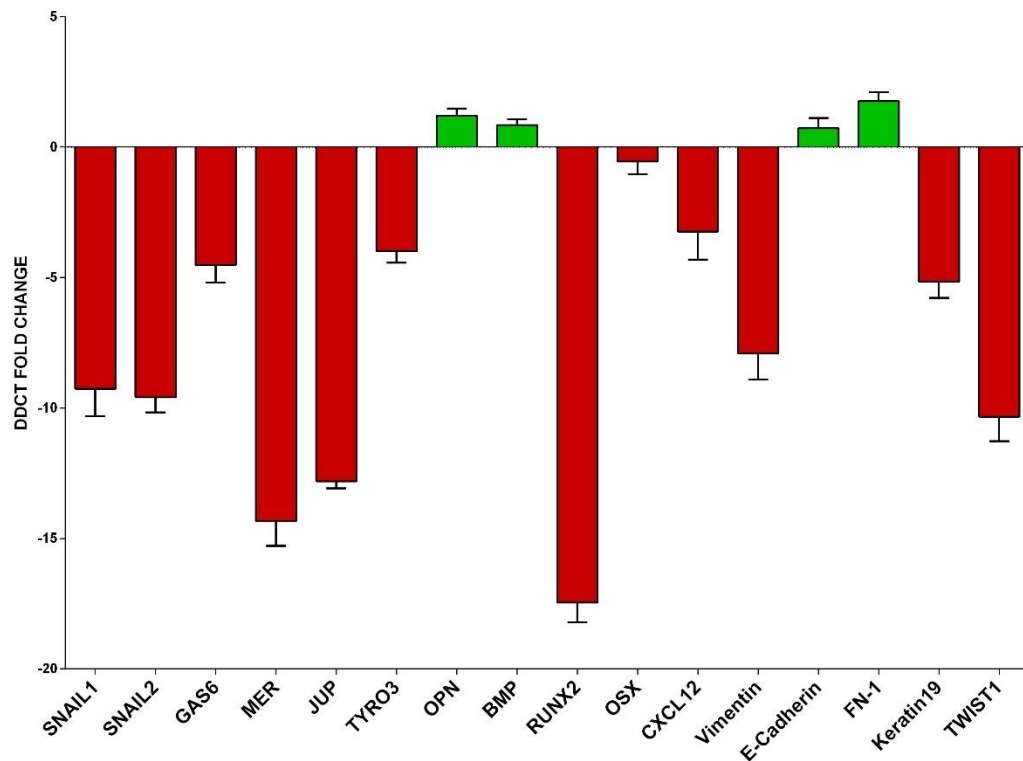


Figure 6-21 $\Delta\Delta C_t$ of EMT marker expression in MCF7 cells cultured with 67 mM L-methionine compared with MCF7 cells cultured without. Expression normalised to GAPDH. Cells cultured for 24 hours. Error bars indicate standard error mean; n=3 with 3 technical replicates from each.

6.3 Discussion

As described previously, paracrine signalling within the BM is essential to the maintenance of the cells residing there. The cytokines produced by MSCs are vital to the maintenance of their niche in addition to affecting the maturation of other local cells such as macrophages (Waterman et al., 2010; Li and Wu, 2011). However, there is increasing evidence to suggest that EVs also play an important role in maintaining the BCCs that have metastasised to the BM (Wu et al., 2017). EVs contain >14,000 biomolecules including nucleic acids, proteins and metabolites; any one of these biomolecules has the potential to affect gene expression and protein function. (Mathivanan et al., 2011). A summary of the results from this chapter are shown in table 6-2.

Table 6-2 Summary of results. Arrows indicate increase, ↑; decrease, ↓; or no change, ↔ from DMEM alone. NR, not recorded.

Media Supplement	Proliferation	Adhesion	EMT markers	Spheroid Migration	Cell cycle
MSC-CM	↓	NR	NR	↓	NR
MSC-derived EVs	↓	↑	NR	↔	NR
D-eythrose	↓	↔	↓	↓	↓
L-methionine	↓	↓	↓	↔	↓
SB203580	↔	↔	NR	↔	NR
SB431542	↔	↑	NR	↔	NR
D-erythrose +SB203580	↔	↔	NR	↔	NR
D-erythrose +SB431542	↓	↑	NR	↓	NR

L- methionine +SB203580	↓	↑	NR	↓	NR
L- methionine +SB431542	↓	↑	NR	↓	NR

6.3.i Isolation of Extracellular Vesicles

EVs are notoriously difficult to purify and the yields are never substantial (Van Deun et al., 2014). MSC-derived EVs used within this study were acquired using ultracentrifugation, which provides a reasonably high yield of EVs, but is a laborious, time-consuming method that requires large volumes of starting material. Additionally, the high-speed centrifugation (in excess of 100,000 g) can damage the smaller exosomes, lowering yield. Purification through the precipitation of EVs requires less expensive equipment and can be done in a smaller time frame. The precipitation method is commercially available as ExoQuick and whilst it is much simpler, producing many orders of magnitude more particles, it may also purify large protein complexes due to the imprecise nature of the method (Thind and Wilson, 2016).

A faster method of isolation using size-exclusion chromatography has been successfully used to yield EVs from the plasma of patients (Hong et al., 2016). This method takes around 30 minutes to complete although there are concerns for the purity of samples as it may also purify lipoproteins in the process (Welton et al., 2015). However, the overall advantages have to be considered against other ‘traditional’ methods. Advances in microfluidics has allowed the development of a method that isolates EVs through antibodies and analyses the resulting vesicles all

within the same system (He et al., 2014); purifying EVs from small volumes quickly, with the potential to scale up the system (Chen et al., 2010). Microfluidics uses a single device so eliminates many of the financial and time costs associated with other purification methods.

Sequential centrifugation of MSC-CM was used to first remove cell debris and smaller particles until all that remained were the EVs. This followed by quantification of EV surface markers allowed for relatively large volumes to be purified. Addition of these EVs into DMEM allowed all the other biomolecules contained within MSC-CM to be excluded.

6.3.ii MSC-Derived EVs Slows Growth of MCF7

Previous studies showed co-culture with MSCs alters the behaviour of MCF7 BCCs. The preliminary study in this chapter assessed how MSC-CM affects the stemness of MCF7 cells. It indicated that a higher concentration of MSC-CM led to a more stem cell-like phenotype, through a reduction in ALDH1 expression (figure 6-1). High levels of ALDH1 correlate with a tumourigenic phenotype (Resetskova et al., 2010). Fractionating the media by molecular weight further affects the stemness of MCF7 cells; only the 100 kDa+ fraction significantly lowers the ALDH1 expression compared with fresh culture medium. These different signalling components explain why there is evidence indicating MSCs can aid growth and migration (De Luca et al., 2012) and as well as inhibiting (Ono et al., 2014). The 100 kDa+ fraction slows MCF7 migration out of spheroids in 3D (table 6-2), more than any of the other media fractions. Whilst this fraction may contain many components such as protein complexes and cellular waste, it will also contain EVs. These have been shown to lead to cycling quiescence in BCCs (Lim et al., 2011; Bliss et al., 2016; Walker et al., 2016).

6.3.iii Metabolites from MSC-derived EVs may Influence BCCs

Whilst it may not be financially practical to utilise MSC-derived EVs in treatment of breast cancer, due to the large volumes of cells required, there is great potential to use the isolated biomolecules contained within EVs. Multiple studies have successfully shown MSCs secrete miRNAs packaged into EVs which alter the behaviour of BCCs: miR-16 confers a silencing effect upon VEGF mRNA in BCCs reducing angiogenesis and therefore proliferation in BCCs (Lee et al., 2013); miR-23 inhibited MARCKS expression, vital to cell cycle progression through activation of downstream components (Ono et al., 2014); Lim and colleagues (2011) showed multiple EV-derived miRNAs (miR-127, miR-197, miR-222, and miR-223) elicited a phenotype of cycling quiescence in BCCs. These are just a small subset of the biomolecules contained within MSC-derived EVs; it is clear many components of these EVs lead to a phenotype of cycling quiescence in BCCs. Here we focused on metabolites, where it was evident that one or more key metabolites appear to cause BCCs to slow proliferation.

There is evidence to suggest that EVs (both exosomes and the larger MVs) may play a considerable role in establishing a dormant phenotype in invading BCCs; much of which focuses upon the study of miRNAs to bring about changes in gene expression (Ono et al., 2014; Bliss et al., 2016). As previously discussed, the EVs contain >14,000 biomolecules and whilst these miRNAs are abundant within EVs (Graveel et al., 2015), they are expensive to synthesise and use in clinic. Here we explored whether small cellular metabolites could have an effect upon MCF7 proliferation.

A preliminary metabolomics assay was performed to identify metabolites contained within the MSC-derived EVs; a literature search

hoped to find evidence of dormant effects caused by any of the metabolites detected (table 6-1). From this list of candidates D-erythrose and L-methionine were selected as possible candidates because there was evidence of slowing growth in BCCs, where others were tested in different cancer types.

From a diagnostic perspective, the presence of EVs derived from BCCs within the blood plasma of a patient, receptor-negative types in particular, could lead to early detection of tumours traditionally too small to notice through testing for cancer-specific miRNAs (Eichelser et al., 2014). EVs derived from HER2⁺ tumours will also express the protein on their surface, attenuating the effect of antibody-based treatments, such as Trastuzumab. These HER2-expressing EVs will bind the antibody, allowing further progression of the tumour (Ciravolo et al., 2012). The improvement in EV purification techniques will make detection possible as small volumes of plasma can be extracted from the patient in a non-invasive fashion and a diagnosis returned quickly.

6.3.iv Cellular Metabolites Reduce MCF7 Proliferation

D-Erythrose

D-erythrose appears to affect cell cycle early on by downregulation of cyclin C (required for transition into G₁; Giacinti and Giordano, 2006) and cyclin D, which pairs with CDK4 at G₁. Cyclin B1 and 2 are upregulated, but require c-myc to transition into M phase (Nakata et al., 2007), but this is downregulated so won't function. The same is true for cyclin A2 as it requires CDK1, which is downregulated. Cathepsin D is a mediator of IFN and TNF-induced apoptosis via p53 so upregulation indicates the cell cycle is halted (Deiss et al., 1996). Cyclins require a cognate cyclin-dependent kinase to function and vice-versa. This would indicate that D-erythrose negatively affects parts of the G₁/S transition of MCF7; the large downregulation of genes, such as CCND2, would indicate that this transition is not able complete as normal. The continued downregulation of genes in S and M phases will further prevent cell cycle completion (figure 6-18). Taking previous results into account, where Ki67 is decreased, it can be seen that this metabolite slows the cell cycle in MCF7 (table 6-2).

The anti-tumour mechanism of D-erythrose may be associated with the unique bioenergetic metabolism of cancer cells. Differing from normal cells, cancer cells mostly depend on glycolysis rather than mitochondrial oxidative phosphorylation to produce energy, even in the presence of ample oxygen. The increased dependency upon glycolysis is a hallmark of cancer cell metabolism, and gives rise to enhanced lactate production (Kroemer and Pouyssegur, 2008). The final products of D-erythrose metabolism are carbon dioxide and water (Batt et al., 1960). This excess carbon dioxide can then be converted to carbonic acid by carbonic

anhydrase (Wang and Wei, 2010). In addition, the increased lactate production in cancer cells leads to lactic acid-induced acidosis. Once the intracellular pH becomes too low the cell will die. Patra and Hay (2014) provide evidence that D-erythrose can markedly suppress the growth of colon carcinoma, inhibit tumor cell invasion and increase tumor cell apoptosis, without any observed toxic effects *in vivo*. This supports the findings in this study that D-erythrose inhibits MCF7 proliferation and migration, despite the evidence to suggest it does not appear to increase cellular adhesion (table 6-2).

L-Methionine

L-methionine appears to affect MCF7 cell cycle genes less than erythrose, but key genes are still downregulated: Cyclin D2, with corresponding CDk4 upregulated in a minor way; MAPK8 and BCL2L2 are downregulated showing the methionine is reducing apoptosis; ORC3 is required for DNA synthesis (Scholefield et al., 2011) and c-myb for G2/M transition with cyclin B1/2. Whilst some genes are upregulated the fold change from MCF7 cultured in DMEM alone is negligible. 3D Samples largely failed with only a few samples giving a result most likely due to the low RNA concentration recovered from spheroids - had to normalise to methionine treated cells at 3 ng/ μ L.

The anti-tumour mechanism of L-methionine may be associated with the increased source of methyl groups for DNA methylation. L-methionine downregulates p53 gene expression (Kim and Park, 2003). Mutations in the p53 gene can cause it to switch from a tumour suppressor to an oncogene (Muller, P.A. and Vousden, 2013). Upregulation in G₁/S phase of the cell cycle will prevent aberrant DNA replication, but gain-of-function mutants will allow oncogenic mutations to propagate. Through downregulating mutant p53, L-methionine can impede cell cycle progression. This can be seen in the fluidigm study (figure 6-21) as several

genes within G1 phase are greatly downregulated in the presence of L-methionine, which will negatively affect progression through the cell cycle.

Kim and Park (2003) show that dietary increase of L-methionine can protect DNA damage by carcinogenic compounds through methylation. PLU-1 is a H3K4 demethylase and knockdown of this protein leads to repression of cell proliferation in MCF7 (Yamane et al., 2007). This suggests that DNA methylation can negatively affect BCC proliferation. Providing the cell with excess L-methionine provides an excess of methyl donor groups, which can then be used for DNA methylation.

6.4 Conclusion

Breast cancer cell metastasis into the bone marrow niche involves a complex series of paracrine signalling and cell-cell interactions. However, here we showed that treating MFC7 cells with MSC-derived EVs alone slows cell migration and appears to initiate an epithelial cell phenotype. This suggests that MSC-derived EVs contribute to the net loss in tumourigenicity of invading BCCs, allowing them to engraft within the BM in a cycling quiescent state, ultimately resulting in anti-cancer drug resistance. It is evident that both EVs and microvesicles are present; these are trafficked out of the cell in different ways and as such their contents may also be different. Whilst there is some evidence in support of the role of microRNAs in initiating dormancy (Vallabhaneni et al., 2015; Wu et al., 2017), further research into the cargo of both populations of EVs is necessary; namely, which proteins and small molecules/metabolites may be involved in BCC dormancy. It is clear that MSC-derived EVs have a negative effect upon MCF7 proliferation and cause an increase in

'stemness', however, it is still not clear whether there is one major component of those EVs having this effect, or whether it is a combination of all the separate biomolecules working in concert to provide the same result. Some small molecules contained within these MSC-derived EVs have separately been implicated in reducing cancer cell proliferation and results shown in this study suggest that both D-erythrose and L-methionine have a negative effect upon MCF7 proliferation. The precise mode of action of these small molecules remains unclear and further work would need to be done to elucidate this. Molecules contained within EVs are able to bypass the usual modes of entry into a cell so if allowed access into the BCCs without passing through receptors may change their effect.

7 Final Discussion

7.1 Project Summary

As outlined in chapter 1, this project aimed to model the BM environment in a way that allows investigation into the potential influences that encourage BCCs to enter into a dormant or recurrent state. There is a clear research and clinical need to model these states as the prevalence of breast cancer still remains high and metastasis to the bone marrow, with cancer dormancy and subsequent recurrence, is a major factor of breast cancer fatality. This study has made progress towards this goal and key achievements are described below:

- Bone marrow 3D model. A spheroid culture system was adopted for 3D cell culture. In order to progress through the project, consistent and reproducible cell spheroids were required. Through investigating different cell seeding densities, spheroids were generated which were appropriate for use in the project. Electron microscopy was utilised to assess the cell-cell contacts within the 3D structure and allowed for the identification of strong intercellular bonds through filopodia.
- Breast cancer cell (BCC) line: Two different BCC lines were initially assessed in culture, MCF7 and MDA-MB-231. Following studies in monolayer and 3D spheroid culture, it was determined that the cell line MCF7 would be better for use in this project. Spheroids generated using MDA-MB-231 did not remain intact once removed from the magnetic source, where cells migrated away from the central mass, so could not be reliably used over long periods of time to model dormancy. MCF7 cells are a well-established cell line that are representative of epithelial-type breast cancers, making them more adherent to one another, allowing the formation of spheroids

that could be sustained for more than a few hours as was the case with MDA-MB-231 spheroids.

- Cytokine profile changes in MSC/BCC spheroid co-culture: Cytokines released into the environment during co-culture of BCC spheroids with MSC spheroids were analysed using antibody arrays. As reported in chapter 4, changes in cytokines within the co-culture environment will promote both migration and proliferation of cells. This determined that co-culturing the cells changed their cytokine profile, demonstrating how the presence of BCCs in the BM may react to MSC-derived cytokines and vice versa, together altering the BM chemistry.
- BCC recurrence in the BM model: The role of two specific cytokines secreted by MSCs during the co-culture study, IL-6 and TGF β , were investigated with a view towards their influence on BCCs spheroids. Control 3D BCC spheroids, without cytokines, appeared less active, slowing the cell cycle through analysis of gene expression, but the addition IL-6 and TGF β reverted this phenotype, generating a more active cell which migrated away from the spheroid mass into the 3D type I collagen environment.
- Potential BCC dormancy in response to MSC-derived EVs: Cytokines only form part of the cell-cell communication network. In order to examine other candidates, fractionated MSC-conditioned culture medium was used; each fraction as incubated with MCF7 cells. These fractions indicated how a wide range of effects can be produced by signalling molecules of different molecular weights. Whilst the smaller cytokines induced migration, the larger fractions slowed cell movement and allowed spheroids to remain intact over time. Extracellular vesicles (EVs) are within this large fraction and were subsequently isolated, purified and used to challenge MCF7 cells in both 2D and 3D culture. Results suggested the EVs can alter MCF7 cell

adhesion, migration and proliferation, potentially having a role in BCC dormancy.

7.2 Potential Applications for the *in vitro* Bone Marrow Model

The 3D collagen type I bone marrow model has been demonstrated to be capable of maintaining spheroid viability and morphology over 7 days. It is a simple, effective model for testing the influence of external factors on both MSC and MCF7 cell behaviour, in terms of migration and activity. The study within this thesis only looked at a limited number of variables within the MSC-BCC relationship. There is much scope for further work using this model in investigation of BCC behaviour. For example, the model could be used to assess BCC migration into a BM environment, to assess mechanisms of entry and homing towards resident cells, such as MSCs. Alternatively, BCC recurrence and exit from the environment could be studied. Some of these applications are summarised below.

7.2.i MSC-BCC Signalling and Communication

Whilst cell-cell signalling was assessed within this study, only a small subset of signalling molecules were analysed. Two key cytokines were assessed, IL-6 and TGF β , but as noted in chapter 4, many other cytokines play a role in MSC-BCC communication. The array used within the study in chapter 4 analysed 23 different cytokines; several of which were clearly altered in co-culture. RANTES, MCP-1 and many interleukins were present in higher volumes in co-culture. These could be further assessed to determine if they are altered within the

MSC/BCC co-culture environment in much the same was IL-6 and TGF β were assessed. .

When considering MSC-derived EVs, this thesis focused on the potential that metabolites may play in BCC migration and proliferation. However, it would also be interesting to determine which miRs are present in the EVs. MiRs play an important role in MSC/BCC signalling, the model could be used to assess what miRs are present and what their role is in either dormancy or recurrence.

The BCC line MCF7 was selected for use within this study, but other *in vitro* models have utilised different types of BCCs (Marlow et al., 2013; Imamura et al., 2015). There is no limitation to the cell line used within this *in model*, as such different kinds of breast cancer, indeed any cancer, can be modelled in the same environment to study how this effects interactions with MSCs in the BM. For example, prostate cancer is also known to preferentially metastasise to the bone marrow (Taichman et al., 2002; Shiozawa et al., 2011), thus the model would be applicable for further investigation.

Tests done *in vivo* may present a physiological environment, but it is equally important to remove as many factors from the native conditions in order to understand how BCCs affect cells in close proximity. This model focussed on the interaction between MSCs and BCCs, but could equally be used to understand the signalling effects of other cell types resident within the BM, such as HSCs and macrophages. Whilst many of these interactions may be indirect through the effects BCCs have upon cells such as MSCs, it is possible that invading BCCs directly interact with these other cell types, whether through paracrine signalling or cell-cell contact.

7.2.ii EV Isolate and Cargo

The use of EVs within chapter 6 was limited by the ability to harvest them. This is a difficult process that requires large amounts of cells from which to obtain the EVs. There are papers emerging which use bioreactor cultures for EV harvesting (Guerreiro et al., 2018; (Palviainen et al.,2019).These use cells cultured within a 3D membrane, which a media collection port to allow access to cell secretions. One such bioreactor, the CELLine AD 1000 is currently being tested in our labs to assess EV generation and harvesting. The cells, in this case MCF7 cells, grow throughout the membrane and generate EV numbers well in excess of corresponding tissue culture flask cells (figure 7.1). Such bioreactors will be adopted for use in future studies in our labs.

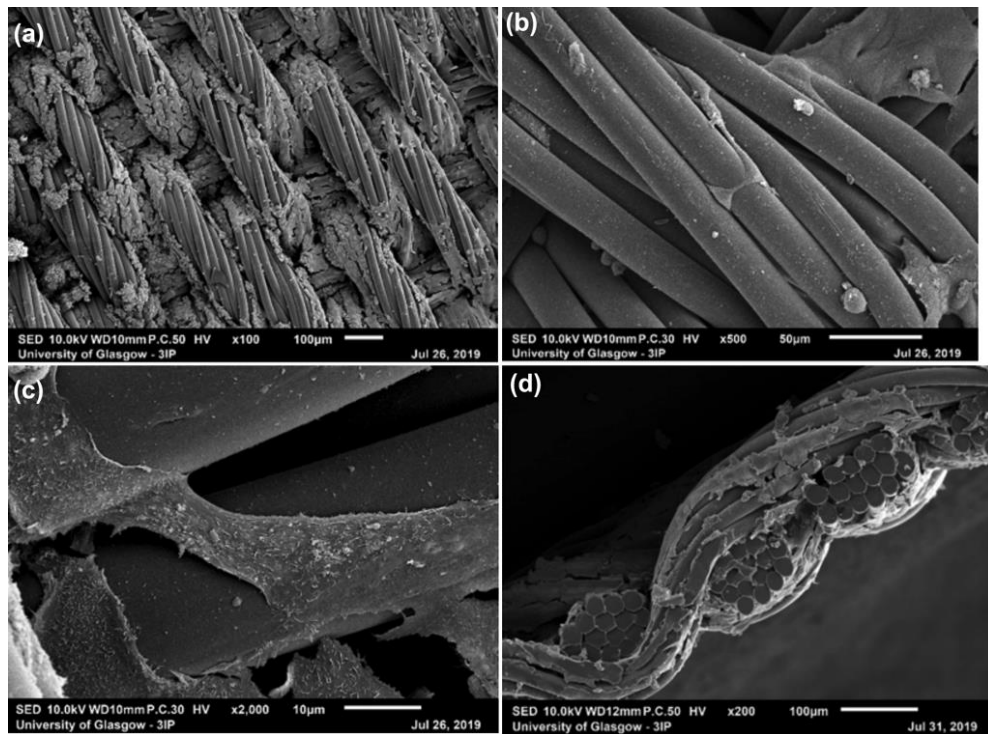


Figure 7-1 Scanning electron microscopy images of MCF7 cells cultured within the CELLine bioreactor. A) Overview of the interaction seen between the cells and the cellulose membrane, B & C) Clusters of cells attached on the membrane. C) A cross section of the membrane showing cells intermingling with the membrane fibers.

MSCs used for EV harvesting were simply cultured in monolayer, it is possible that what these cells package into their EVs may differ from cells cultured in 3D spheroids. It would therefore be useful to use the 3D BM model to culture MSC spheroids and harvest any EVs secreted into the environment. The volume of EVs harvested from a 3D culture environment will be much lower than those harvested from cells cultured in monolayer, so better purification methods would need to be explored to achieve good EV yields. As previously reported in chapter 6, other methods for harvesting EVs exist besides the one used here. The use of polyethylene glycol to precipitate out EVs is widely used as it prevents high speed centrifugation potentially damaging delicate vesicles, but brings with it the possibility of a lower purity sample.

In addition, the EV cargo may differ if the MSCs are treated differently - for example cultured in a 'diseased' or injured environment. The 3D model can again be used to simulate such conditions; indeed it has been used previously to replicate an injury, by culturing in a Transwell over a scratched monolayer of osteoblasts or chondrocytes (mimicking tissue injury) (Lewis et al., 2016).

Syn and colleagues (2016) studied EVs derived from tumour cells. These EVs were found to be pro-EMT and their contents will promote further growth of recipient tumour cells. Targeting the formation of these EVs will prevent this. The model could then be used to test agents that might block the formation or reception of EVs. If the contents can be elucidated and how the cells package them into EVs, methods to prevent this can be developed.

7.2.iii Pharmaceutical Screening

Research into breast cancer dormancy within the BM is increasing and *in vivo* studies are commonly performed to assess the effect of drugs on a more complex system. Bearing the 3Rs in mind, the use of mice is an expensive and time-consuming process, so the possibility of an *in vitro* model that appropriately mimics the BM would be invaluable. Although this model is simple, it presents the opportunity to be used as a drug testing platform, for example to be used to assess the effects of cancer drugs upon BCC growth and behaviour. The model successfully mimics the behaviour of BCCs in a 3D environment and can be achieved in a 6, 12, 24 48 or 96-well plate, so a large number of tests can be done simultaneously. Wenzel and colleagues (2014) utilised 3D multicellular spheroids to test large drug libraries and target cell death pathways. This model could then be used to test drugs that might induce dormancy or affect already dormant cells as current chemotherapies are unable to affect these cells.

Incorporating more physiological conditions such as mimicking tissue vasculature using microfluidics may further enhance the functionality of the model. In addition, the addition of immune cells would more closely resemble the *in vivo* BM environment chemistry. New pharmaceuticals could then be assessed for their effects upon the dormant BCCs as one feature of these cells is their resistance to many current chemotherapies (Mitra et al., 2015).

7.3 Limitations of the Model

7.3.i Additional Bone Marrow Cells Types

The *in vitro* model used within this study has many advantages, however, it is not without limitations. The simplicity of the model is advantageous, but is also a major limitation; the BM environment *in vivo* comprises many cell types, which are not included in this model. HSCs reside close to MSCs and will certainly be involved in and maintaining the BM microenvironment (Weber and Calvi, 2010; Morrison and Scadden, 2014). In addition, MSCs within the BM are able to differentiate into other cells types on demand. Tests done with this model are short term tissue culture tests and do not allow the MSCs enough time to differentiate further, which may be an outcome of co-culture with BCCs.

Cancer-associated fibroblasts are an important component of the tumour stroma *in vivo*, these cells are derived from MSCs (Lu et al., 2015). Immune cells are also a large factor in clearance of invading BCCs that enter the BM (Jiang and Shapiro, 2014). The absence of these also restricts the study of dormancy and how BCCs may affect the potential of local immune cells to remove threats from the environment.

When considering other cell types, such as those found in niche zones in the BM, both osteoblasts (endosteal niche) and endothelial (niche) cells were incorporated into the model, but the addition of each cell type made the triple-culture practically difficult; each cell type ideally requires a different culture medium so using DMEM alone affects division and impairs the physiological response expected from these additional cells.

7.3.ii Modelling Disease Conditions

The model used within this study only recreated one condition. Many patients who possess dormant BCCs within their BM may be advanced in age. As such, it is reasonable to assume their BM environment is not 'healthy' and likely to be osteoporotic. These conditions change the BM chemistry from that of a healthy patient. Osteoporosis is a disease characterised by systemic bone loss and destruction of the bone microstructure, causing fragility of the bone mass (Savopoulos et al., 2011). Patients with osteoporosis have an increased risk of low-traumatic fractures (Muschitz et al., 2015), which would lead to an increase in repair processes within the BM environment, affecting the growth of the invading BCCs. Osteoporosis is linked to a shift in MSC differentiation from osteoblasts towards adipocyte formation in the BM. This shift is caused by the activation of the proliferative activated receptor (PPAR) γ 2 pathway, not the RUNX-2 pathway, in MSCs (Rosen and Bouxsein, 2006). The *in vitro* model could then be used to assess how these diseased MSCs interact with BCCs and adding in further cell types related with the disease state may provide more 'physiologically relevant' information on breast cancer dormancy and/or recurrence.

7.4 Conclusion

This thesis has added several novel pieces of information to the body of research focusing on breast cancer dormancy. As previously discussed, there has been research into breast cancer utilising 3D spheroids, however, this thesis presents the first spheroids produced using mNPs. This method of creating 3D breast cancer spheroids is simple to reproduce on a larger scale. Whilst there are methods of producing spheroids that do not require the addition of an agent such as mNPs to form the 3D structures, their presence is beneficial when tracking them. As they possess a fluorescent tag, it removes the need for an additional immunohistochemical stain and live spheroids can be easily visualised over a given time period. This was of particular use in this thesis to monitor cell migration over several days.

Additionally, how BCCs respond to their environment has been studied in this thesis. The main focus of the research was the relationship between incoming BCCs and MSCs residing in the bone marrow, however, the cytokine study chapter assessed how these BCCs can react to injury signals within their new environment. These cytokines associated with injury repair, in particular IL-6, are known to be released when tissue is damaged so that the remaining cells may repair any damaged areas by migrating into them and dividing, sealing any gaps that an injury might cause. This research indicated that quiescent BCCs were stimulated to move out into their environment, perhaps leading to further metastasis.

Finally, MSC-derived EVs were assessed to determine their effect on BCCs. This is a growing area of research and the contents of these EVs are of particular interest as they are able to bypass any cell transport systems that may restrict access to the small molecules contained within. These MSC-derived EVs led to BCCs becoming quiescent; halting the cell cycle and reducing migration into their environment. Further research into these MSC-derived EVs would be of

interest to the study of dormancy; not only what is contained within the EVs, but how the environmental conditions might affect what small molecules MSCs package into them.

The research carried out within this thesis attempted to further understand breast cancer dormancy and recurrence within the BM environment through the interactions of BCCs with MSCs using spheroid culture. It was generally noted that MSC and BCC paracrine signalling was affected by co-culture. This in turn resulted in changes in cell migration, with potential links to EMT instigation, and changes in cell cycle, with potential links to dormancy/recurrence.

7.4.i Recommendations for Future Work

- Further investigate BCC spheroids and how size might affect gene expression.
- Create diseased BM model to assess the effect upon BCC spheroids.
- Introduce immune cells into the model to assess how the presence of BCCs changes their behaviour.
- Investigate cell signalling, quiescence, differentiation and migration when cultured for longer time points.
- Characterise the levels of cytokines secreted into the environment during co-culture and attempt to identify the source, whether BCC or MSC.
- Further examine the cell cycle, to determine whether RNA changes are observed downstream.
- Further study the contents of MSC EVs - does treatment change the cargo? If so, use these different sources of MSC EVs to assess their effects upon BCCs.

REFERENCES

1. Adorno, M., Cordenonsi, M., Montagner, M., Dupont, S., Wong, C., Hann, B., Solari, A., Bobisse, S., Rondina, M.B., Guzzardo, V. and Parenti, A.R., 2009. A Mutant-p53/Smad complex opposes p63 to empower TGF β -induced metastasis. *Cell*, 137(1), pp.87-98.
2. Aguirre-Ghiso, J.A., 2007. Models, mechanisms and clinical evidence for cancer dormancy. *Nature Reviews Cancer*, 7(11), p.834.
3. Almalki, S.G. and Agrawal, D.K., 2016. Effects of matrix metalloproteinases on the fate of mesenchymal stem cells. *Stem cell research & therapy*, 7(1), p.129.
4. Amable, P.R., Teixeira, M.V.T., Carias, R.B.V., Granjeiro, J.M. and Borojevic, R., 2014. Protein synthesis and secretion in human mesenchymal cells derived from bone marrow, adipose tissue and Wharton's jelly. *Stem cell research & therapy*, 5(2), p.53.
5. American Cancer Society. 2017. *Types of Breast Cancer*. [ONLINE] Available at: <https://www.cancer.org/cancer/breast-cancer/understanding-a-breast-cancer-diagnosis/types-of-breast-cancer.html>. [Accessed 3 October 2018].
6. Anthony DC and Bryan A. Regulation of hematopoietic stem cells by bone marrow stromal cells. *Trends Immun*, 35, 2014.
7. Anton, K., Banerjee, D. and Glod, J., 2012. Macrophage-associated mesenchymal stem cells assume an activated, migratory, pro-inflammatory phenotype with increased IL-6 and CXCL10 secretion. *PLoS one*, 7(4), p.e35036.
8. Antoni, D., Burckel, H., Josset, E. and Noel, G., 2015. Three-dimensional cell culture: a breakthrough in vivo. *International journal of molecular sciences*, 16(3), pp.5517-5527.
9. Arihiro, K., Oda, H., Kaneko, M. and Inai, K., 2000. Cytokines facilitate chemotactic motility of breast carcinoma cells. *Breast Cancer*, 7(3), pp.221-230.
10. Baksh, D., Song, L. and Tuan, R.S., 2004. Adult mesenchymal stem cells: characterization, differentiation, and application in cell and gene therapy. *Journal of cellular and molecular medicine*, 8(3), pp.301-316.
11. Bara, J.J., Richards, R.G., Alini, M. and Stoddart, M.J., 2014. Concise review: Bone marrow-derived mesenchymal stem cells change phenotype following in vitro culture: implications for basic research and the clinic. *Stem cells*, 32(7), pp.1713-1723.
12. Bartosh, T.J., Ylöstalo, J.H., Mohammadipoor, A., Bazhanov, N., Coble, K., Claypool, K., Lee, R.H., Choi, H. and Prockop, D.J., 2010. Aggregation of human mesenchymal stromal cells (MSCs) into 3D spheroids enhances their antiinflammatory properties. *Proceedings of the National Academy of Sciences*, 107(31), pp.13724-13729.

13. Batt RD, Dickens F and Williamson DH: Tetrose metabolism 2. The utilization of tetroses and tetrutols by rat tissues. *Biochem J* 77: 281-294, 1960.
14. Bell, H.S., Whittle, I.R., Walker, M., Leaver, H.A. and Wharton, S.B., 2001. The development of necrosis and apoptosis in glioma: experimental findings using spheroid culture systems. *Neuropathology and applied neurobiology*, 27(4), pp.291-304.
15. Benton, G., DeGray, G., Arnaoutova, I., Kleinman, H.K. and George, J., 2015, August. High throughput triculture: A breast cancer spheroid model for drug screening. In *Cancer Research* (Vol. 75). 615 CHESTNUT ST, 17TH FLOOR, PHILADELPHIA, PA 19106-4404 USA: AMER ASSOC CANCER RESEARCH.
16. Berry, C.C. and Curtis, A.S., 2003. Functionalisation of magnetic nanoparticles for applications in biomedicine. *Journal of physics D: Applied physics*, 36(13), p.R198.
17. Bersini, S., Jeon, J.S., Dubini, G., Arrigoni, C., Chung, S., Charest, J.L., Moretti, M. and Kamm, R.D., 2014. A microfluidic 3D in vitro model for specificity of breast cancer metastasis to bone. *Biomaterials*, 35(8), pp.2454-2461.
18. Bhadriraju, K. and Chen, C.S., 2002. Engineering cellular microenvironments to improve cell-based drug testing. *Drug discovery today*, 7(11), pp.612-620.
19. Birbrair, A. and Frenette, P.S., 2016. Niche heterogeneity in the bone marrow. *Annals of the new York Academy of Sciences*, 1370(1), pp.82-96.
20. Birkedal-Hansen, H., Moore, W.G.I., Bodden, M.K., Windsor, L.J., Birkedal-Hansen, B., DeCarlo, A. and Engler, J.A., 1993. Matrix metalloproteinases: a review. *Critical Reviews in Oral Biology & Medicine*, 4(2), pp.197-250.
21. Bliss, S.A., Sinha, G., Sandiford, O.A., Williams, L.M., Engelberth, D.J., Guiro, K., Isenalumhe, L.L., Greco, S.J., Ayer, S., Bryan, M. and Kumar, R., 2016. Mesenchymal stem cell-derived exosomes stimulate cycling quiescence and early breast cancer dormancy in bone marrow. *Cancer research*, 76(19), pp.5832-5844.
22. Bonab, M.M., Alimoghaddam, K., Talebian, F., Ghaffari, S.H., Ghavamzadeh, A. and Nikbin, B., 2006. Aging of mesenchymal stem cell in vitro. *BMC cell biology*, 7(1), p.14.
23. Bonapace, L., Coissieux, M.M., Wyckoff, J., Mertz, K.D., Varga, Z., Junt, T. and Bentires-Alj, M., 2014. Cessation of CCL2 inhibition accelerates breast cancer metastasis by promoting angiogenesis. *Nature*, 515(7525), p.130. Chaffer, C.L. and Weinberg, R.A., 2011. A perspective on cancer cell metastasis. *science*, 331(6024), pp.1559-1564.

24. Brabletz, S. and Brabletz, T., 2010. The ZEB/miR-200 feedback loop—a motor of cellular plasticity in development and cancer?. *EMBO reports*, 11(9), pp.670-677.
25. Breast Cancer Now. 2016. Breast Cancer Facts. [ONLINE] Available at: https://breastcancer.org/about-breast-cancer/want-to-know-about-breast-cancer/breast-cancer-facts?gclid=EAlalQobChMI7YWYtd373QIViLTtCh3cFQZyEAAYASAAEgLz4_D_BwE. [Accessed 10 October 2018].
26. Brew, K., Dinakarpanian, D. and Nagase, H., 2000. Tissue inhibitors of metalloproteinases: evolution, structure and function. *Biochimica et Biophysica Acta (BBA)-Protein Structure and Molecular Enzymology*, 1477(1), pp.267-283.
27. Bruno, S. and Darzynkiewicz, Z., 1992. Cell cycle dependent expression and stability of the nuclear protein detected by Ki-67 antibody in HL-60 cells. *Cell proliferation*, 25(1), pp.31-40.
28. Buck, C.A. and Horwitz, A.F., 1987. Cell surface receptors for extracellular matrix molecules. *Annual review of cell biology*, 3(1), pp.179-205.
29. Bühring, H.J., Battula, V.L., Treml, S., Schewe, B., Kanz, L. and Vogel, W., 2007. Novel markers for the prospective isolation of human MSC. *Annals of the New York Academy of Sciences*, 1106(1), pp.262-271.
30. Burger, J.A. and Kipps, T.J., 2006. CXCR4: a key receptor in the crosstalk between tumor cells and their microenvironment. *Blood*, 107(5), pp.1761-1767.
31. Cancer.net Editorial Board. 2018. Breast Cancer - Metastatic: Statistics. [Online]. [4 December 2018]. Available from: <https://www.cancer.net/cancer-types/breast-cancer-metastatic/statistics>
32. Caplan, A.I. and Bruder, S.P., 2001. Mesenchymal stem cells: building blocks for molecular medicine in the 21st century. *Trends in molecular medicine*, 7(6), pp.259-264.
33. Carey, L.A., Perou, C.M., Livasy, C.A., Dressler, L.G., Cowan, D., Conway, K., Karaca, G., Troester, M.A., Tse, C.K., Edmiston, S. and Deming, S.L., 2006. Race, breast cancer subtypes, and survival in the Carolina Breast Cancer Study. *Jama*, 295(21), pp.2492-2502.
34. Casado-Díaz, A., Quesada-Gómez, J.M. and Dorado, G., 2016. Stem cell research and molecular markers in medicine.
35. Castellana, B., Aasen, T., Moreno-Bueno, G., Dunn, S.E. and y Cajal, S.R., 2015. Interplay between YB-1 and IL-6 promotes the metastatic phenotype in breast cancer cells. *Oncotarget*, 6(35), p.38239.
36. Cesarz, Z. and Tamama, K., 2016. Spheroid culture of mesenchymal stem cells. *Stem cells international*, 2016.

37. Chaffer, C.L., San Juan, B.P., Lim, E. and Weinberg, R.A., 2016. EMT, cell plasticity and metastasis. *Cancer and Metastasis Reviews*, 35(4), pp.645-654.
38. Chambers, K.F., Mosaad, E.M., Russell, P.J., Clements, J.A. and Doran, M.R., 2014. 3D cultures of prostate cancer cells cultured in a novel high-throughput culture platform are more resistant to chemotherapeutics compared to cells cultured in monolayer. *PloS one*, 9(11), p.e111029.
39. Chandrasekaran, S., Marshall, J.R., Messing, J.A., Hsu, J.W. and King, M.R., 2014. TRAIL-mediated apoptosis in breast cancer cells cultured as 3D spheroids. *PloS one*, 9(10), p.e111487.
40. Chen, C., Skog, J., Hsu, C.H., Lessard, R.T., Balaj, L., Wurdinger, T., Carter, B.S., Breakefield, X.O., Toner, M. and Irimia, D., 2010. Microfluidic isolation and transcriptome analysis of serum microvesicles. *Lab on a Chip*, 10(4), pp.505-511.
41. Chen, C., Tseng, P., Lo, W., Wang, F. and Lee, C., 2017. Comparing the impact of 3D bioreactor and 2D culture system on immunomodulation potency of Warton's jelly derived-MSC. *Cytherapy*, 19(5), p.S186.
42. Child, H.W., del Pino, P.A., De La Fuente, J.M., Hursthouse, A.S., Stirling, D., Mullen, M., McPhee, G.M., Nixon, C., Jayawarna, V. and Berry, C.C., 2011. Working together: the combined application of a magnetic field and penetratin for the delivery of magnetic nanoparticles to cells in 3D. *ACS nano*, 5(10), pp.7910-7919.
43. Cho, D.I., Kim, M.R., Jeong, H.Y., Jeong, H.C., Jeong, M.H., Yoon, S.H., Kim, Y.S. and Ahn, Y., 2014. Mesenchymal stem cells reciprocally regulate the M1/M2 balance in mouse bone marrow-derived macrophages. *Experimental & molecular medicine*, 46(1), p.e70.
44. Cho, E.H., Wendel, M., Luttmann, M., Yoshioka, C., Marrinucci, D., Lazar, D., Schram, E., Nieva, J., Bazhenova, L., Morgan, A. and Ko, A.H., 2012. Characterization of circulating tumor cell aggregates identified in patients with epithelial tumors. *Physical biology*, 9(1), p.016001.
45. Ciravolo, V., Huber, V., Ghedini, G.C., Venturelli, E., Bianchi, F., Campiglio, M., Morelli, D., Villa, A., Mina, P.D., Menard, S. and Filipazzi, P., 2012. Potential role of HER2-overexpressing exosomes in countering trastuzumab-based therapy. *Journal of cellular physiology*, 227(2), pp.658-667.
46. da Silva Meirelles, L., Caplan, A.I. and Nardi, N.B., 2008. In search of the in vivo identity of mesenchymal stem cells. *Stem cells*, 26(9), pp.2287-2299.
47. Dano K, Behrendt N, Hoyer-Hansen G, Johnsen M, Lund LR, Ploug M and Romer J: Plasminogen activation and cancer. *Thromb Haemost* 93: 676-681, 2005.

48. Davies, O.G., Cox, S.C., Williams, R.L., Tsaroucha, D., Dorrepaal, R.M., Lewis, M.P. and Grover, L.M., 2017. Annexin-enriched osteoblast-derived vesicles act as an extracellular site of mineral nucleation within developing stem cell cultures. *Scientific reports*, 7(1), p.12639.
49. Davies, P.F., Spaan, J.A. and Krams, R., 2005. Shear stress biology of the endothelium. *Annals of biomedical engineering*, 33(12), pp.1714-1718.
50. De Becker, A., Van Hummelen, P., Bakkus, M., Broek, I.V., De Wever, J., De Waele, M. and Van Riet, I., 2007. Migration of culture-expanded human mesenchymal stem cells through bone marrow endothelium is regulated by matrix metalloproteinase-2 and tissue inhibitor of metalloproteinase-3. *Haematologica*, 92(4), pp.440-449.
51. De Luca, A., Lamura, L., Gallo, M., Maffia, V. and Normanno, N., 2012. Mesenchymal stem cell-derived interleukin-6 and vascular endothelial growth factor promote breast cancer cell migration. *Journal of cellular biochemistry*, 113(11), pp.3363-3370.
52. Deiss, L.P., Galinka, H., Berissi, H., Cohen, O. and Kimchi, A., 1996. Cathepsin D protease mediates programmed cell death induced by interferon-gamma, Fas/APO-1 and TNF-alpha. *The EMBO journal*, 15(15), pp.3861-3870.
53. Del Fattore, A., Luciano, R., Saracino, R., Battafarano, G., Rizzo, C., Pascucci, L., Alessandri, G., Pessina, A., Perrotta, A., Fierabracci, A. and Muraca, M., 2016. Differential effects of extracellular vesicles secreted by mesenchymal stem cells from different sources on glioblastoma cells. *Expert opinion on biological therapy*, 15(4), pp.496-504.
54. Dent, R., Trudeau, M., Pritchard, K.I., Hanna, W.M., Kahn, H.K., Sawka, C.A., Lickley, L.A., Rawlinson, E., Sun, P. and Narod, S.A., 2007. Triple-negative breast cancer: clinical features and patterns of recurrence. *Clinical cancer research*, 13(15), pp.4429-4434.
55. Di, G.H., Liu, Y., Lu, Y., Liu, J., Wu, C. and Duan, H.F., 2014. IL-6 secreted from senescent mesenchymal stem cells promotes proliferation and migration of breast cancer cells. *PloS one*, 9(11), p.e113572.
56. Diel, I.J., Kaufmann, M., Goerner, R., Costa, S.D., Kaul, S. and Bastert, G., 1992. Detection of tumor cells in bone marrow of patients with primary breast cancer: a prognostic factor for distant metastasis. *Journal of clinical oncology*, 10(10), pp.1534-1539.
57. Dominici, M.L.B.K., Le Blanc, K., Mueller, I., Slaper-Cortenbach, I., Marini, F.C., Krause, D.S., Deans, R.J., Keating, A., Prockop, D.J. and Horwitz, E.M., 2006. Minimal criteria for defining

- multipotent mesenchymal stromal cells. The International Society for Cellular Therapy position statement. *Cytotherapy*, 8(4), pp.315-317.
58. Edmondson, R., Broglie, J.J., Adcock, A.F. and Yang, L., 2014. Three-dimensional cell culture systems and their applications in drug discovery and cell-based biosensors. *Assay and drug development technologies*, 12(4), pp.207-218.
59. Ehninger, A. and Trumpp, A., 2011. The bone marrow stem cell niche grows up: mesenchymal stem cells and macrophages move in. *Journal of Experimental Medicine*, 208(3), pp.421-428.
60. Eichelser, C., Stückrath, I., Müller, V., Milde-Langosch, K., Wikman, H., Pantel, K. and Schwarzenbach, H., 2014. Increased serum levels of circulating exosomal microRNA-373 in receptor-negative breast cancer patients. *Oncotarget*, 5(20), p.9650.
61. Eltoukhy, H.S., Sinha, G., Moore, C., Guiro, K. and Rameshwar, P., 2016. CXCL12-abundant reticular cells (CAR) cells: a review of the literature with relevance to cancer stem cell survival. *Journal of Cancer*, 4, p.e1004.
62. Fierro, F.A., Sierralta, W.D., Epuñan, M.J. and Minguell, J.J., 2004. Marrow-derived mesenchymal stem cells: role in epithelial tumor cell determination. *Clinical & experimental metastasis*, 21(4), pp.313-319.
63. Fisher, B., Carbone, P., Economou, S.G., Frelick, R., Glass, A., Lerner, H., Redmond, C., Zelen, M., Band, P., Katrych, D.L. and Wolmark, N., 1976. L-Phenylalanine mustard (L-PAM) in the management of primary breast cancer: a report of early findings. *New England Journal of Medicine*, 292(3), pp.117-122.
64. Fonseca, K.B., Maia, F.R., Cruz, F.A., Andrade, D., Juliano, M.A., Granja, P.L. and Barrias, C.C., 2013. Enzymatic, physicochemical and biological properties of MMP-sensitive alginate hydrogels. *Soft Matter*, 9(12), pp.3283-3292.
65. Frankel LB, Christoffersen NR, Jacobsen A, Lindow M, Krogh A, Lund AH. Programmed Cell Death 4 (PDCD4) Is an Important Functional Target of the MicroRNA miR-21 in Breast Cancer Cells. *J Biol Chem*. 2008; 238:1026-33. [PubMed: 17991735]
66. Frenette, P.S., Pinho, S., Lucas, D. and Scheiermann, C., 2013. Mesenchymal stem cell: keystone of the hematopoietic stem cell niche and a stepping-stone for regenerative medicine. *Annual review of immunology*, 31, pp.285-316.
67. Galipeau, J., Krampera, M., Barrett, J., Dazzi, F., Deans, R.J., DeBrujin, J., Dominici, M., Fibbe, W.E., Gee, A.P., Gimble, J.M. and Hematti, P., 2016. International Society for Cellular Therapy perspective on immune functional assays for mesenchymal stromal cells as potency release criterion for advanced phase clinical trials. *Cytotherapy*, 18(2), pp.151-159.
68. Gelao, L., Criscitiello, C., Fumagalli, L., Locatelli, M., Manunta, S., Esposito, A., Minchella, I., Goldhirsch, A. and

- Curigliano, G., 2013. Tumour dormancy and clinical implications in breast cancer. *Ecancermedicalscience*, 7.
69. Giacinti, C. and Giordano, A., 2006. RB and cell cycle progression. *Oncogene*, 25(38), p.5220.
70. Gong, L., Zhao, Y., Zhang, Y. and Ruan, Z., 2016. The macrophage polarization regulates MSC osteoblast differentiation in vitro. *Annals of Clinical & Laboratory Science*, 46(1), pp.65-71.
71. Graveel, C.R., Calderone, H.M., Westerhuis, J.J., Winn, M.E. and Sempere, L.F., 2015. Critical analysis of the potential for microRNA biomarkers in breast cancer management. *Breast cancer: targets and therapy*, 7, p.59.
72. Gregory, L.A., Ricart, R.A., Patel, S.A., Lim, P.K. and Rameshwar, P., 2011. microRNAs, gap junctional intercellular communication and mesenchymal stem cells in breast cancer metastasis. *Current cancer therapy reviews*, 7(3), pp.176-183.
73. Grellner, W., Georg, T. and Wilske, J., 2000. Quantitative analysis of proinflammatory cytokines (IL-1 β , IL-6, TNF- α) in human skin wounds. *Forensic science international*, 113(1), pp.251-264.
74. Groebe, K. and Mueller-Klieser, W., 1991. Distributions of oxygen, nutrient, and metabolic waste concentrations in multicellular spheroids and their dependence on spheroid parameters. *European biophysics journal*, 19(4), pp.169-181.
75. Guerreiro, E.M., Vestad, B., Steffensen, L.A., Aass, H.C.D., Saeed, M., Øvstebø, R., Costea, D.E., Galtung, H.K. and Søland, T.M., 2018. Efficient extracellular vesicle isolation by combining cell media modifications, ultrafiltration, and size-exclusion chromatography. *PloS one*, 13(9), p.e0204276.
76. Hannoush, E.J., Sifri, Z.C., Elhassan, I.O., Mohr, A.M., Alzate, W.D., Offin, M. and Livingston, D.H., 2011. Impact of enhanced mobilization of bone marrow derived cells to site of injury. *Journal of Trauma and Acute Care Surgery*, 71(2), pp.283-291.
77. Hartman, Z.C., Poage, G.M., Den Hollander, P., Tsimelzon, A., Hill, J., Panupinthu, N., Zhang, Y., Mazumdar, A., Hilsenbeck, S.G., Mills, G.B. and Brown, P.H., 2013. Growth of triple-negative breast cancer cells relies upon coordinate autocrine expression of the proinflammatory cytokines IL-6 and IL-8. *Cancer research*, 73(11), pp.3470-3480.
78. He, M., Crow, J., Roth, M., Zeng, Y. and Godwin, A.K., 2014. Integrated immunoisolation and protein analysis of circulating exosomes using microfluidic technology. *Lab on a Chip*, 14(19), pp.3773-3780.
79. He, X., Wang, H., Jin, T., Xu, Y., Mei, L. and Yang, J., 2016. TLR4 activation promotes bone marrow MSC proliferation and osteogenic differentiation via Wnt3a and Wnt5a signaling. *PLoS One*, 11(3), p.e0149876.

80. Heinrich, P.C., Behrmann, I., Serge, H.A.A.N., Hermanns, H.M., Müller-Newen, G. and Schaper, F., 2003. Principles of interleukin (IL)-6-type cytokine signalling and its regulation. *Biochemical journal*, 374(1), pp.1-20.
81. Her GJ, Wu HC, Chen MH, Chen MY, Chang SC, Wang TW. Control of three-dimensional substrate stiffness to manipulate mesenchymal stem cell fate toward neuronal or glial lineages. *Acta Biomater* 2013;9:5170- 5180.
82. Herrmann, J.L., Weil, B.R., Abarbanell, A.M., Wang, Y., Poynter, J.A., Manukyan, M.C. and Meldrum, D.R., 2011. IL-6 and TGF- α costimulate mesenchymal stem cell vascular endothelial growth factor production by ERK-, JNK-, and PI3K-mediated mechanisms. *Shock*, 35(5), pp.512-516.
83. Herschkowitz, J.I., Simin, K., Weigman, V.J., Mikaelian, I., Usary, J., Hu, Z., Rasmussen, K.E., Jones, L.P., Assefnia, S., Chandrasekharan, S. and Backlund, M.G., 2007. Identification of conserved gene expression features between murine mammary carcinoma models and human breast tumors. *Genome biology*, 8(5), p.R76.
84. Hirschhaeuser, F., Menne, H., Dittfeld, C., West, J., Mueller-Klieser, W. and Kunz-Schughart, L.A., 2010. Multicellular tumor spheroids: an underestimated tool is catching up again. *Journal of biotechnology*, 148(1), pp.3-15.
85. Holiday DL and Speirs V. Choosing the right cell line for breast cancer research. *Breast Cancer Res*, 2011. 13(14):215.
86. Holmgren, L., O'Reilly, M.S. and Folkman, J., 1995. Dormancy of micrometastases: balanced proliferation and apoptosis in the presence of angiogenesis suppression. *Nature medicine*, 1(2), p.149.
87. Hong, C.S., Funk, S., Muller, L., Boyiadzis, M. and Whiteside, T.L., 2016. Isolation of biologically active and morphologically intact exosomes from plasma of patients with cancer. *Journal of extracellular vesicles*, 5(1), p.29289.
88. Hong, J.K., Yun, J., Kim, H. and Kwon, S.M., 2015. Three-dimensional culture of mesenchymal stem cells. *Tissue Engineering and Regenerative Medicine*, 12(4), pp.211-221.
89. Horwood, N.J., 2016. Macrophage polarization and bone formation: a review. *Clinical reviews in allergy & immunology*, 51(1), pp.79-86.
90. Hu, C., Yong, X., Li, C., Lü, M., Liu, D., Chen, L., Hu, J., Teng, M., Zhang, D., Fan, Y. and Liang, G., 2013. CXCL12/CXCR4 axis promotes mesenchymal stem cell mobilization to burn wounds and contributes to wound repair. *Journal of Surgical Research*, 183(1), pp.427-434.
91. Imamura N., Toyoda, M., Kiyota, N., Takao, S., Kono, S., Nakatsura, T. and Minami, H., 2015. Comparison of 2D-and 3D-culture

- models as drug-testing platforms in breast cancer. *Oncology reports*, 33(4), pp.1837-1843.
92. Jiang, X. and Shapiro, D.J., 2014. The immune system and inflammation in breast cancer. *Molecular and cellular endocrinology*, 382(1), pp.673-682.
93. Joos, H., Wildner, A., Hogrefe, C., Reichel, H. and Brenner, R.E., 2013. Interleukin-1 beta and tumor necrosis factor alpha inhibit migration activity of chondrogenic progenitor cells from non-fibrillated osteoarthritic cartilage. *Arthritis research & therapy*, 15(5), p.R119.
94. Kalluri, R., 2016. The biology and function of exosomes in cancer. *The Journal of clinical investigation*, 126(4), pp.1208-1215.
95. Kang, Y., Siegel, P.M., Shu, W., Drobnjak, M., Kakonen, S.M., Cordón-Cardo, C., Guise, T.A. and Massagué, J., 2003. A multigenic program mediating breast cancer metastasis to bone. *Cancer cell*, 3(6), pp.537-549.
96. Karnoub, A.E., Dash, A.B., Vo, A.P., Sullivan, A., Brooks, M.W., Bell, G.W., Richardson, A.L., Polyak, K., Tubo, R. and Weinberg, R.A., 2007. Mesenchymal stem cells within tumour stroma promote breast cancer metastasis. *Nature*, 449(7162), p.557.
97. Kasimir-Bauer, S., Hoffmann, O., Wallwiener, D., Kimmig, R. and Fehm, T., 2012. Expression of stem cell and epithelial-mesenchymal transition markers in primary breast cancer patients with circulating tumor cells. *Breast Cancer Research*, 14(1), p.R15.
98. Katzenellenbogen, B.S., Kendra, K.L., Norman, M.J. and Berthois, Y., 1987. Proliferation, hormonal responsiveness, and estrogen receptor content of MCF-7 human breast cancer cells grown in the short-term and long-term absence of estrogens. *Cancer research*, 47(16), pp.4355-4360.
99. Ke, F., Zhang, L., Liu, Z., Liu, J., Yan, S., Xu, Z., Bai, J., Zhu, H., Lou, F., Wang, H. and Shi, Y., 2014. Autocrine Interleukin-6 Drives Skin-Derived Mesenchymal Stem Cell Trafficking via Regulating Voltage-Gated Ca²⁺ Channels. *Stem Cells*, 32(10), pp.2799-2810.
100. Kenny, P.A., Lee, G.Y., Myers, C.A., Neve, R.M., Semeiks, J.R., Spellman, P.T., Lorenz, K., Lee, E.H., Barcellos-Hoff, M.H., Petersen, O.W. and Gray, J.W., 2007. The morphologies of breast cancer cell lines in three-dimensional assays correlate with their profiles of gene expression. *Molecular oncology*, 1(1), pp.84-96.
101. Khalid, A., Wolfram, J., Ferrari, I., Mu, C., Mai, J., Yang, Z., Zhao, Y., Ferrari, M., Ma, X. and Shen, H., 2015. Recent advances in discovering the role of CCL5 in metastatic breast cancer. *Mini reviews in medicinal chemistry*, 15(13), pp.1063-1072.
102. Khmara, I., Koneracka, M., Kubovcikova, M., Zavisova, V., Antal, I., Csach, K., Kopcansky, P., Vidlickova, I., Csaderova, L., Pastorekova, S. and Zatovicova, M., 2017. Preparation of poly-L-lysine functionalized magnetic nanoparticles and their influence on

- viability of cancer cells. *Journal of Magnetism and Magnetic Materials*, 427, pp.114-121.
103. Khoon, M.C.S., 2015. Experimental models of bone metastasis: opportunities for the study of cancer dormancy. *Advanced drug delivery reviews*, 94, pp.141-150.
104. Kim, H.H. and Park, C.S., 2003. Methionine cytotoxicity in the human breast cancer cell line MCF-7. *In Vitro Cellular & Developmental Biology-Animal*, 39(3-4), p.117.
105. Kim, H.K., Song, K.S., Park, Y.S., Kang, Y.H., Lee, Y.J., Lee, K.R., Ryu, K.W., Bae, J.M. and Kim, S., 2003. Elevated levels of circulating platelet microparticles, VEGF, IL-6 and RANTES in patients with gastric cancer: possible role of a metastasis predictor. *European journal of cancer*, 39(2), pp.184-191.
106. Klein, T. and Bischoff, R., 2011. Physiology and pathophysiology of matrix metalloproteases. *Amino acids*, 41(2), pp.271-290.
107. Knüpfer, H. and Preiß, R., 2007. Significance of interleukin-6 (IL-6) in breast cancer (review). *Breast cancer research and treatment*, 102(2), pp.129-135.
108. Korah, R., Boots, M. and Wieder, R., 2004. Integrin $\alpha 5\beta 1$ promotes survival of growth-arrested breast cancer cells: an in vitro paradigm for breast cancer dormancy in bone marrow. *Cancer research*, 64(13), pp.4514-4522.
109. Korde, L.A., Doody, D.R., Hsu, L., Porter, P.L. and Malone, K.E., 2018. Bisphosphonate use and risk of recurrence, second primary breast cancer, and breast cancer mortality in a population-based cohort of breast cancer patients. *Cancer Epidemiology and Prevention Biomarkers*, 27(2), pp.165-173.
110. Kroemer, G. and Pouyssegur, J., 2008. Tumor cell metabolism: cancer's Achilles' heel. *Cancer cell*, 13(6), pp.472-482.
111. Kuhn, D.A., Vanhecke, D., Michen, B., Blank, F., Gehr, P., Petri-Fink, A. and Rothen-Rutishauser, B., 2014. Different endocytotic uptake mechanisms for nanoparticles in epithelial cells and macrophages. *Beilstein journal of nanotechnology*, 5, p.1625.
112. Kumar, S. and Weaver, V.M., 2009. Mechanics, malignancy, and metastasis: the force journey of a tumor cell. *Cancer and Metastasis Reviews*, 28(1-2), pp.113-127.
113. Lazennec, G. and Lam, P.Y., 2016. Recent discoveries concerning the tumor-mesenchymal stem cell interactions. *Biochimica et Biophysica Acta (BBA)-Reviews on Cancer*, 1866(2), pp.290-299.
114. Lee, J.K., Park, S.R., Jung, B.K., Jeon, Y.K., Lee, Y.S., Kim, M.K., Kim, Y.G., Jang, J.Y. and Kim, C.W., 2013. Exosomes derived from mesenchymal stem cells suppress angiogenesis by down-regulating VEGF expression in breast cancer cells. *PLoS one*, 8(12), p.e84256.

115. Leight, J.L., Alge, D.L., Maier, A.J. and Anseth, K.S., 2013. Direct measurement of matrix metalloproteinase activity in 3D cellular microenvironments using a fluorogenic peptide substrate. *Biomaterials*, 34(30), pp.7344-7352.
116. Lewis, E.E., Child, H.W., Hursthouse, A., Stirling, D., McCully, M., Paterson, D., Mullin, M. and Berry, C.C., 2015. The influence of particle size and static magnetic fields on the uptake of magnetic nanoparticles into three-dimensional cell-seeded collagen gel cultures. *Journal of Biomedical Materials Research Part B: Applied Biomaterials*, 103(6), pp.1294-1301.
117. Lewis, E.E.L., Wheadon, H., Lewis, N., Yang, J., Mullin, M., Hursthouse, A., Stirling, D., Dalby, M.J. and Berry, C.C., 2016. A quiescent, regeneration-responsive tissue engineered mesenchymal stem cell bone marrow niche model via magnetic levitation. *ACS nano*, 10(9), pp.8346-8354.
118. Lewis, N.S., Lewis, E.E., Mullin, M., Wheadon, H., Dalby, M.J. and Berry, C.C., 2017. Magnetically levitated mesenchymal stem cell spheroids cultured with a collagen gel maintain phenotype and quiescence. *Journal of tissue engineering*, 8, p.2041731417704428.
119. Li, T. and Wu, Y., 2011. Paracrine molecules of mesenchymal stem cells for hematopoietic stem cell niche. *Bone marrow research*, 2011.
120. Li, T.A.O., Zhang, C., DiNG, Y., Zhai, W.E.I., Liu, K.U.I., Bu, F.A.N., Tu, T.A.O., Sun, L., Zhu, W.E.I., Zhou, F. and Qi, W., 2015. Umbilical cord-derived mesenchymal stem cells promote proliferation and migration in MCF-7 and MDA-MB-231 breast cancer cells through activation of the ERK pathway. *Oncology reports*, 34(3), pp.1469-1477.
121. Li, Z., Zhou, Z. and Donahue, H.J., 2008. Alterations in Cx43 and OB-cadherin affect breast cancer cell metastatic potential. *Clinical & experimental metastasis*, 25(3), pp.265-272.
122. Liang, Z., Yoon, Y., Votaw, J., Goodman, M.M., Williams, L. and Shim, H., 2005. Silencing of CXCR4 blocks breast cancer metastasis. *Cancer research*, 65(3), pp.967-971.
123. Liu, S., Ginestier, C., Ou, S.J., Clouthier, S.G., Patel, S.H., Monville, F., Korkaya, H., Heath, A., Dutcher, J., Kleer, C.G. and Jung, Y., 2011. Breast cancer stem cells are regulated by mesenchymal stem cells through cytokine networks. *Cancer research*, 71(2), pp.614-624.
124. Logullo, A.F., Nonogaki, S., Pasini, F.S., De Toledo Osório, C.A.B., Soares, F.A. and Brentani, M.M., 2010. Concomitant expression of epithelial-mesenchymal transition biomarkers in breast ductal carcinoma: association with progression. *Oncology reports*, 23(2), pp.313-320.
125. Lu, Y., Liu, J., Liu, Y., Qin, Y., Luo, Q., Wang, Q. and Duan, H., 2015. TLR4 plays a crucial role in MSC-induced inhibition of NK

- cell function. *Biochemical and biophysical research communications*, 464(2), pp.541-547.
126. Lu, C., Sun, X., Sun, L., Sun, J., Lu, Y., Yu, X., Zhou, L. and Gao, X., 2013. Snail mediates PDGF-BB-induced invasion of rat bone marrow mesenchymal stem cells in 3D collagen and chick chorioallantoic membrane. *Journal of cellular physiology*, 228(9), pp.1827-1833.
127. Luker, K.E. and Luker, G.D., 2006. Functions of CXCL12 and CXCR4 in breast cancer. *Cancer letters*, 238(1), pp.30-41.
128. Lukovic, D., Stojkovic, M., Moreno-Manzano, V., Jendelova, P., Sykova, E., Bhattacharya, S.S. and Erceg, S., 2015. Concise review: reactive astrocytes and stem cells in spinal cord injury: good guys or bad guys?. *Stem Cells*, 33(4), pp.1036-1041.
129. Malladi, S., Macalinao, D.G., Jin, X., He, L., Basnet, H., Zou, Y., De Stanchina, E. and Massagué, J., 2016. Metastatic latency and immune evasion through autocrine inhibition of WNT. *Cell*, 165(1), pp.45-60.
130. Marcato, P., Dean, C.A., Giacomantonio, C.A. and Lee, P.W., 2011. Aldehyde dehydrogenase: its role as a cancer stem cell marker comes down to the specific isoform. *Cell cycle*, 10(9), pp.1378-1384.
131. Maeng, H.J., Kim, E.S., Chough, C., Joung, M., Lim, J.W., Shim, C.K. and Shim, W.S., 2014. Addition of amino acid moieties to lapatinib increases the anti-cancer effect via amino acid transporters. *Biopharmaceutics & drug disposition*, 35(1), pp.60-69.
132. Magdolenova, Z., Drlickova, M., Henjum, K., Rundén-Pran, E., Tulinska, J., Bilanicova, D., Pojana, G., Kazimirova, A., Barancokova, M., Kuricova, M. and Liskova, A., 2015. Coating-dependent induction of cytotoxicity and genotoxicity of iron oxide nanoparticles. *Nanotoxicology*, 9(sup1), pp.44-56.
133. Marlow, R., Honeth, G., Lombardi, S., Cariati, M., Hessey, S., Pipili, A., Mariotti, V., Buchupalli, B., Foster, K., Bonnet, D. and Grigoriadis, A., 2013. A novel model of dormancy for bone metastatic breast cancer cells. *Cancer research*, 73(23), pp.6886-6899.
134. Marriott, I., Gray, D.L., Tranguch, S.L., Fowler, V.G., Stryjewski, M., Levin, L.S., Hudson, M.C. and Bost, K.L., 2004. Osteoblasts express the inflammatory cytokine interleukin-6 in a murine model of *Staphylococcus aureus* osteomyelitis and infected human bone tissue. *The American journal of pathology*, 164(4), pp.1399-1406.
135. Masiakowski, P., Breathnach, R., Bloch, J., Gannon, F., Krust, A. and Chambon, P., 1982. Cloning of cDNA sequences of hormone-regulated genes from the MCF-7 human breast cancer cell line. *Nucleic acids research*, 10(24), pp.7895-7903.
136. Mathivanan, S., Fahner, C.J., Reid, G.E. and Simpson, R.J., 2011. ExoCarta 2012: database of exosomal proteins, RNA and lipids. *Nucleic acids research*, 40(D1), pp.D1241-D1244.

137. Matsumoto, A. and Nakayama, K.I., 2013. Role of key regulators of the cell cycle in maintenance of hematopoietic stem cells. *Biochimica et Biophysica Acta (BBA)-General Subjects*, 1830(2), pp.2335-2344.
138. Mattila, P.K. and Lappalainen, P., 2008. Filopodia: molecular architecture and cellular functions. *Nature reviews Molecular cell biology*, 9(6), pp.446-454.
139. Mattila, P.K. and Lappalainen, P., 2008. Filopodia: molecular architecture and cellular functions. *Nature reviews Molecular cell biology*, 9(6), pp.446-454.
140. Maxson, S., Lopez, E.A., Yoo, D., Danilkovitch-Miagkova, A. and LeRoux, M.A., 2012. Concise review: role of mesenchymal stem cells in wound repair. *Stem cells translational medicine*, 1(2), pp.142-149.
141. McDermott, S.P. and Wicha, M.S., 2010. Targeting breast cancer stem cells. *Molecular oncology*, 4(5), pp.404-419.
142. Meo M, Mani SA and Cristofanilli M: Molecular mechanisms of metastasis in breast cancer - clinical applications. *Nat Rev Clin Oncol* 7: 693-701, 2010.
143. Mehta, G., Hsiao, A.Y., Ingram, M., Luker, G.D. and Takayama, S., 2012. Opportunities and challenges for use of tumor spheroids as models to test drug delivery and efficacy. *Journal of Controlled Release*, 164(2), pp.192-204.
144. Melzer, C., Yang, Y. and Hass, R., 2016. Interaction of MSC with tumor cells. *Cell Communication and Signaling*, 14(1), p.20.
145. Meng, X., Vander Ark, A., Lee, P., Hostetter, G., Bhowmick, N.A., Matrisian, L.M., Williams, B.O., Miranti, C.K. and Li, X., 2016. Myeloid-specific TGF- β signaling in bone promotes basic-FGF and breast cancer bone metastasis. *Oncogene*, 35(18), p.2370.
146. Menon, L.G., Picinich, S., Koneru, R., Gao, H., Lin, S.Y., Koneru, M., Mayer-Kuckuk, P., Glod, J. and Banerjee, D., 2007. Differential gene expression associated with migration of mesenchymal stem cells to conditioned medium from tumor cells or bone marrow cells. *Stem cells*, 25(2), pp.520-528.
147. Mishima, S., Nagai, A., Abdullah, S., Matsuda, C., Taketani, T., Kumakura, S., Shibata, H., Ishikura, H., Kim, S.U. and Masuda, J., 2010. Effective ex vivo expansion of hematopoietic stem cells using osteoblast-differentiated mesenchymal stem cells is CXCL12 dependent. *European journal of haematology*, 84(6), pp.538-546.
148. Mishra, P.J., Mishra, P.J., Humeniuk, R., Medina, D.J., Alexe, G., Mesirov, J.P., Ganesan, S., Glod, J.W. and Banerjee, D., 2008. Carcinoma-associated fibroblast-like differentiation of human mesenchymal stem cells. *Cancer research*, 68(11), pp.4331-4339.
149. Mitra, A., Mishra, L. and Li, S., 2015. EMT, CTCs and CSCs in tumor relapse and drug-resistance. *Oncotarget*, 6(13), p.10697.

150. Morrison, S.J. and Scadden, D.T., 2014. The bone marrow niche for haematopoietic stem cells. *Nature*, 505(7483), p.327.
151. Muller, P.A. and Vousden, K.H., 2013. p53 mutations in cancer. *Nature cell biology*, 15(1), p.2.
152. Murphy, A.N., Unsworth, E.J. and Stetler-Stevenson, W.G., 1993. Tissue inhibitor of metalloproteinases-2 inhibits bFGF-induced human microvascular endothelial cell proliferation. *Journal of cellular physiology*, 157(2), pp.351-358.
153. Muschitz, C., Kocijan, R., Haschka, J., Pahr, D., Kaider, A., Pietschmann, P., Hans, D., Muschitz, G.K., Fahrleitner-Pammer, A. and Resch, H., 2015. TBS reflects trabecular microarchitecture in premenopausal women and men with idiopathic osteoporosis and low-traumatic fractures. *Bone*, 79, pp.259-266.
154. Nadig, R.R., 2009. Stem cell therapy-Hype or hope? A review. *Journal of conservative dentistry: JCD*, 12(4), p.131.
155. Nagase, H., Visse, R. and Murphy, G., 2006. Structure and function of matrix metalloproteinases and TIMPs. *Cardiovascular research*, 69(3), pp.562-573.
156. Nakata, Y., Shetzline, S., Sakashita, C., Kalota, A., Rallapalli, R., Rudnick, S.I., Zhang, Y., Emerson, S.G. and Gewirtz, A.M., 2007. c-Myb contributes to G2/M cell cycle transition in human hematopoietic cells by direct regulation of cyclin B1 expression. *Molecular and cellular biology*, 27(6), pp.2048-2058.
157. Newcomb, P.A., Trentham-Dietz, A. and Hampton, J.M., 2010. Bisphosphonates for osteoporosis treatment are associated with reduced breast cancer risk. *British journal of cancer*, 102(5), p.799.
158. NHS. 2016. *Breast Cancer*. [ONLINE] Available at: <https://www.nhs.uk/conditions/breast-cancer/>. [Accessed 3 October 2018].
159. Nozaki, S., Sledge Jr, G.W. and Nakshatri, H., 2000. Cancer cell-derived interleukin 1 α contributes to autocrine and paracrine induction of pro-metastatic genes in breast cancer. *Biochemical and biophysical research communications*, 275(1), pp.60-62.
160. Oh, N. and Park, J.H., 2014. Endocytosis and exocytosis of nanoparticles in mammalian cells. *International journal of nanomedicine*, 9(Suppl 1), p.51.
161. Ono, M., Kosaka, N., Tominaga, N., Yoshioka, Y., Takeshita, F., Takahashi, R.U., Yoshida, M., Tsuda, H., Tamura, K. and Ochiya, T., 2014. Exosomes from bone marrow mesenchymal stem cells contain a microRNA that promotes dormancy in metastatic breast cancer cells. *Sci. Signal.*, 7(332), pp.ra63-ra63.
162. Page-McCaw, A., Ewald, A.J. and Werb, Z., 2007. Matrix metalloproteinases and the regulation of tissue remodelling. *Nature reviews. Molecular cell biology*, 8(3), p.221.
163. Paik, S., Shak, S., Tang, G., Kim, C., Baker, J., Cronin, M., Baehner, F.L., Walker, M.G., Watson, D., Park, T. and Hiller, W.,

2004. A multigene assay to predict recurrence of tamoxifen-treated, node-negative breast cancer. *New England Journal of Medicine*, 351(27), pp.2817-2826.
164. Palviainen, M., Saari, H., Kärkkäinen, O., Pekkinen, J., Auriola, S., Yliperttula, M., Puhka, M., Hanhineva, K. and Siljander, P.R.M., 2019. Metabolic signature of extracellular vesicles depends on the cell culture conditions. *Journal of extracellular vesicles*, 8(1), p.1596669.
165. Pang, M.F., Georgoudaki, A.M., Lambut, L., Johansson, J., Tabor, V., Hagikura, K., Jin, Y., Jansson, M., Alexander, J.S., Nelson, C.M. and Jakobsson, L., 2016. TGF- β 1-induced EMT promotes targeted migration of breast cancer cells through the lymphatic system by the activation of CCR7/CCL21-mediated chemotaxis. *Oncogene*, 35(6), p.748.
166. Papaccio, F., Paino, F., Regad, T., Papaccio, G., Desiderio, V. and Tirino, V., 2017. Concise review: cancer cells, cancer stem cells, and mesenchymal stem cells: influence in cancer development. *Stem cells translational medicine*, 6(12), pp.2115-2125.
167. Patra, K.C. and Hay, N., 2014. The pentose phosphate pathway and cancer. *Trends in biochemical sciences*, 39(8), pp.347-354.
168. Peyvandi, S., Lan, Q., Lorusso, G. and Rüegg, C., 2019. Chemotherapy-induced immunological breast cancer dormancy: a new function for old drugs?. *J Cancer Metastasis Treat*, 5, p.44doi.
169. Phang, J.M., Liu, W., Hancock, C.N. and Fischer, J.W., 2016. Proline metabolism and cancer: emerging links to glutamine and collagen. *Current opinion in clinical nutrition and metabolic care*, 18(1), p.71.
170. Philipp, D., Suhr, L., Wahlers, T., Choi, Y.H. and Paunel-Görgülü, A., 2018. Preconditioning of bone marrow-derived mesenchymal stem cells highly strengthens their potential to promote IL-6-dependent M2b polarization. *Stem cell research & therapy*, 9(1), p.286.
171. Poste, G. and Fidler, I.J., 1980. The pathogenesis of cancer metastasis. *Nature*, 283(5743), p.139.
172. Potapova, I.A., Gaudette, G.R., Brink, P.R., Robinson, R.B., Rosen, M.R., Cohen, I.S. and Doronin, S.V., 2007. Mesenchymal stem cells support migration, extracellular matrix invasion, proliferation, and survival of endothelial cells in vitro. *Stem cells*, 25(7), pp.1761-1768.
173. Prada, I. and Meldolesi, J., 2016. Binding and fusion of extracellular vesicles to the plasma membrane of their cell targets. *International journal of molecular sciences*, 17(8), p.1296.
174. Pradhan, S., Sperduto, J.L., Farino, C.J. and Slater, J.H., 2018. Engineered In Vitro Models of Tumor Dormancy and Reactivation. *Journal of biological engineering*, 12(1), p.37.

175. Pratap, J., Wixted, J.J., Gaur, T., Zaidi, S.K., Dobson, J., Gokul, K.D., Hussain, S., Van Wijnen, A.J., Stein, J.L., Stein, G.S. and Lian, J.B., 2008. Runx2 transcriptional activation of Indian Hedgehog and a downstream bone metastatic pathway in breast cancer cells. *Cancer research*, 68(19), pp.7795-7802.
176. Pricola, K.L., Kuhn, N.Z., Haleem-Smith, H., Song, Y. and Tuan, R.S., 2009. Interleukin-6 maintains bone marrow-derived mesenchymal stem cell stemness by an ERK1/2-dependent mechanism. *Journal of cellular biochemistry*, 108(3), pp.577-588.
177. Psaila, B. and Lyden, D., 2009. The metastatic niche: adapting the foreign soil. *Nature Reviews Cancer*, 9(4), pp.285-293.
178. Quimby, J.M. and Borjesson, D.L., 2018. Mesenchymal stem cell therapy in cats: Current knowledge and future potential. *Journal of feline medicine and surgery*, 20(3), pp.208-216.
179. Radomski, A., Jurasz, P., Sanders, E.J., Overall, C.M., Bigg, H.F., Edwards, D.R. and Radomski, M.W., 2002. Identification, regulation and role of tissue inhibitor of metalloproteinases-4 (TIMP-4) in human platelets. *British journal of pharmacology*, 137(8), pp.1330-1338.
180. Rattigan, Y., Hsu, J.M., Mishra, P.J., Glod, J. and Banerjee, D., 2010. Interleukin 6 mediated recruitment of mesenchymal stem cells to the hypoxic tumor milieu. *Experimental cell research*, 316(20), pp.3417-3424.
181. Ren, G., Zhang, L., Zhao, X., Xu, G., Zhang, Y., Roberts, A.I., Zhao, R.C. and Shi, Y., 2008. Mesenchymal stem cell-mediated immunosuppression occurs via concerted action of chemokines and nitric oxide. *Cell stem cell*, 2(2), pp.141-150.
182. Resetkova, E., Reis-Filho, J.S., Jain, R.K., Mehta, R., Thorat, M.A., Nakshatri, H. and Badve, S., 2010. Prognostic impact of ALDH1 in breast cancer: a story of stem cells and tumor microenvironment. *Breast cancer research and treatment*, 123(1), pp.97-108.
183. Rey, F.M., Pontes, C.L., Rosales, R.R., Russo, J., Su, Y., Santucci-Pereira, J., Espreafico, E.M. and Tiezzi, D.G., 2018. The role of epithelial-to-mesenchymal transition on breast tumorigenesis cancer associated to mesenchymal stem cells.
184. Ridge SM et al. Mesenchymal stem cells: key players in cancer progression. *Mol. Cancer*. 2017.
185. Roesch, A., Vultur, A., Bogeski, I., Wang, H., Zimmermann, K.M., Speicher, D., Körbel, C., Laschke, M.W., Gimotty, P.A., Philipp, S.E. and Krause, E., 2013. Overcoming intrinsic multidrug resistance in melanoma by blocking the mitochondrial respiratory chain of slow-cycling JARID1B^{high} cells. *Cancer cell*, 23(6), pp.811-825.
186. Rofstad, E.K. and Sutherland, R.M., 1989. Growth and radiation sensitivity of the MLS human ovarian carcinoma cell line grown as multicellular spheroids and xenografted tumours. *British journal of cancer*, 59(1), p.28.

187. Romero-Moreno, R., Coughlin, T., Curtis, K., Dutta, S., Niebur, G. and Littlepage, L.E., 2018. CXCL5 is a master regulator of the dormancy switch to activate metastatic colonization of dormant breast cancer cells during bone metastasis.
188. Rosen, C.J. and Bouxsein, M.L., 2006. Mechanisms of disease: is osteoporosis the obesity of bone?. *Nature Reviews Rheumatology*, 2(1), p.35.
189. Roux, S. and Orcel, P., 2000. Bone loss: Factors that regulate osteoclast differentiation-an update. *Arthritis Research & Therapy*, 2(6), p.451.
190. Rucci, N. and Teti, A., 2010. Osteomimicry: how tumor cells try to deceive the bone. *Front Biosci (Schol Ed)*, 2, pp.907-915.
191. Sart, S., Tsai, A.C., Li, Y. and Ma, T., 2013. Three-dimensional aggregates of mesenchymal stem cells: cellular mechanisms, biological properties, and applications. *Tissue Engineering Part B: Reviews*, 20(5), pp.365-380.
192. Sasser, A.K., Mundy, B.L., Smith, K.M., Studebaker, A.W., Axel, A.E., Haidet, A.M., Fernandez, S.A. and Hall, B.M., 2007. Human bone marrow stromal cells enhance breast cancer cell growth rates in a cell line-dependent manner when evaluated in 3D tumor environments. *Cancer letters*, 254(2), pp.255-264.
193. Sasser, A.K., Sullivan, N.J., Studebaker, A.W., Hendey, L.F., Axel, A.E. and Hall, B.M., 2007. Interleukin-6 is a potent growth factor for ER- α -positive human breast cancer. *The FASEB Journal*, 21(13), pp.3763-3770.
194. Savopoulos, C., Dokos, C., Kaiafa, G. and Hatzitolios, A., 2011. Adipogenesis and osteoblastogenesis: trans-differentiation in the pathophysiology of bone disorders. *Hippokratia*, 15(1), p.18.
195. Scholefield, G., Veening, J.W. and Murray, H., 2011. DnaA and ORC: more than DNA replication initiators. *Trends in cell biology*, 21(3), pp.188-194.
196. Schuettpelz, L. and Link, D., 2013. Regulation of hematopoietic stem cell activity by inflammation. *Frontiers in immunology*, 4, p.204.
197. Scully, O.J., Bay, B.H., Yip, G. and Yu, Y., 2012. Breast cancer metastasis. *Cancer Genomics-Proteomics*, 9(5), pp.311-320.
198. Sempere, L., Keto, J. and Fabbri, M., 2017. Exosomal microRNAs in breast cancer towards diagnostic and therapeutic applications. *Cancers*, 9(7), p.71.
199. Sergina, N.V., Rausch, M., Wang, D., Blair, J., Hann, B., Shokat, K.M. and Moasser, M.M., 2007. Escape from HER-family tyrosine kinase inhibitor therapy by the kinase-inactive HER3. *Nature*, 445(7126), p.437. Tamplin OJ et al. Hematopoietic stem cell arrival triggers dynamic remodeling of the perivascular niche. *Cell*, 160, 2015.

200. Sheikhpour, E., Noorbakhsh, P., Foroughi, E., Farahnak, S., Nasiri, R. and Neamatzadeh, H., 2018. A survey on the role of interleukin-10 in breast cancer: a narrative. *Reports of biochemistry & molecular biology*, 7(1), p.30.
201. Shiozawa, Y., Pedersen, E.A., Havens, A.M., Jung, Y., Mishra, A., Joseph, J., Kim, J.K., Patel, L.R., Ying, C., Ziegler, A.M. and Pienta, M.J., 2011. Human prostate cancer metastases target the hematopoietic stem cell niche to establish footholds in mouse bone marrow. *The Journal of clinical investigation*, 121(4), pp.1298-1312.
202. Sica, A., Schioppa, T., Mantovani, A. and Allavena, P., 2006. Tumour-associated macrophages are a distinct M2 polarised population promoting tumour progression: potential targets of anti-cancer therapy. *European journal of cancer*, 42(6), pp.717-727.
203. Sinha, P., Clements, V.K. and Ostrand-Rosenberg, S., 2005. Interleukin-13-regulated M2 macrophages in combination with myeloid suppressor cells block immune surveillance against metastasis. *Cancer research*, 65(24), pp.11743-11751.
204. Smith, I.E., Walsh, G., Jones, A., Prendiville, J., Johnston, S., Gusterson, B., Ramage, F., Robertshaw, H., Sacks, N. and Ebbs, S., 1995. High complete remission rates with primary neoadjuvant infusional chemotherapy for large early breast cancer. *Journal of clinical oncology*, 13(2), pp.424-429.
205. Sohni, A. and Verfaillie, C.M., 2013. Mesenchymal stem cells migration homing and tracking. *Stem cells international*, 2013.
206. Song, X., Xie, S., Lu, K. and Wang, C., 2015. Mesenchymal stem cells alleviate experimental asthma by inducing polarization of alveolar macrophages. *Inflammation*, 38(2), pp.485-492.
207. Soria, G. and Ben-Baruch, A., 2008. The inflammatory chemokines CCL2 and CCL5 in breast cancer. *Cancer letters*, 267(2), pp.271-285.
208. Soule, H.D., et al., A human cell line from a pleural effusion derived from a breast carcinoma. *J Natl Cancer Inst*, 1973. 51(5): p. 1409-16
209. Souza, G.R., Molina, J.R., Raphael, R.M., Ozawa, M.G., Stark, D.J., Levin, C.S., Bronk, L.F., Ananta, J.S., Mandelin, J., Georgescu, M.M. and Bankson, J.A., 2010. Three-dimensional tissue culture based on magnetic cell levitation. *Nature nanotechnology*, 5(4), pp.291-296.
210. Sozzani, S., Luini, W., Molino, M., Jilek, P., Bottazzi, B., Cerletti, C., Matsushima, K. and Mantovani, A., 1991. The signal transduction pathway involved in the migration induced by a monocyte chemotactic cytokine. *The Journal of Immunology*, 147(7), pp.2215-2221.
211. Spaeth, E.L., Dembinski, J.L., Sasser, A.K., Watson, K., Klopp, A., Hall, B., Andreeff, M. and Marini, F., 2013. Correction: Mesenchymal Stem Cell Transition to Tumor-Associated Fibroblasts

- Contributes to Fibrovascular Network Expansion and Tumor Progression. *PLoS one*, 8(3).
212. Sridharan, R., Cameron, A.R., Kelly, D.J., Kearney, C.J. and O'Brien, F.J., 2015. Biomaterial based modulation of macrophage polarization: a review and suggested design principles. *Materials Today*, 18(6), pp.313-325.
213. Standal, T., Borset, M. and Sundan, A., 2004. Role of osteopontin in adhesion, migration, cell survival and bone remodeling. *Exp Oncol*, 26(3), pp.179-84.
214. Sullivan, N.J., Sasser, A.K., Axel, A., Vesuna, F., Raman, V., Ramirez, N., Oberyszyn, T.M. and Hall, B.M., 2009. Interleukin-6 induces an epithelial-mesenchymal transition phenotype in human breast cancer cells. *Oncogene*, 28(33), p.2940.
215. Susan G Komen Breast Cancer Foundation. 2018. TREATMENTS FOR METASTATIC BREAST CANCER. [Online]. [4 December 2018]. Available from: <https://ww5.komen.org/BreastCancer/RecommendedTreatmentsforMetastaticBreastCancer.html>
216. Syn, N., Wang, L., Sethi, G., Thiery, J.P. and Goh, B.C., 2016. Exosome-mediated metastasis: from epithelial-mesenchymal transition to escape from immunosurveillance. *Trends in pharmacological sciences*, 37(7), pp.606-617.
217. Taichman, R.S., Cooper, C., Keller, E.T., Pienta, K.J., Taichman, N.S. and McCauley, L.K., 2002. Use of the stromal cell-derived factor-1/CXCR4 pathway in prostate cancer metastasis to bone. *Cancer research*, 62(6), pp.1832-1837.
218. Tang, B., Vu, M., Booker, T., Santner, S.J., Miller, F.R., Anver, M.R. and Wakefield, L.M., 2003. TGF- β switches from tumor suppressor to prometastatic factor in a model of breast cancer progression. *The Journal of clinical investigation*, 112(7), pp.1116-1124.
219. Tivari, S., Lu, H., Dasgupta, T., De Lorenzo, M.S. and Wieder, R., 2018. Reawakening of dormant estrogen-dependent human breast cancer cells by bone marrow stroma secretory senescence. *Cell Communication and Signaling*, 16(1), pp.1-18.
220. Thind, A. and Wilson, C., 2016. Exosomal miRNAs as cancer biomarkers and therapeutic targets. *Journal of extracellular vesicles*, 5(1), p.31292.
221. Tomita, H., Tanaka, K., Tanaka, T. and Hara, A., 2016. Aldehyde dehydrogenase 1A1 in stem cells and cancer. *Oncotarget*, 7(10), p.11018.
222. Tong, J.G., Valdes, Y.R., Barrett, J.W., Bell, J.C., Stojdl, D., McFadden, G., McCart, J.A., DiMattia, G.E. and Shepherd, T.G., 2015. Evidence for differential viral oncolytic efficacy in an in vitro model of epithelial ovarian cancer metastasis. *Molecular Therapy-Oncolytics*, 2, p.15013.

223. Travers, M.T., Gow, I.F., Barber, M.C., Thomson, J. and Shennan, D.B., 2004. Indoleamine 2, 3-dioxygenase activity and L-tryptophan transport in human breast cancer cells. *Biochimica et Biophysica Acta (BBA)-Biomembranes*, 1661(1), pp.106-112.
224. Tripathi, C., Tewari, B.N., Kanchan, R.K., Baghel, K.S., Nautiyal, N., Shrivastava, R., Kaur, H., Bhatt, M.L.B. and Bhadauria, S., 2014. Macrophages are recruited to hypoxic tumor areas and acquire a pro-angiogenic M2-polarized phenotype via hypoxic cancer cell derived cytokines Oncostatin M and Eotaxin. *Oncotarget*, 5(14), p.5350.
225. Tsai, A.C., Liu, Y., Yuan, X. and Ma, T., 2015. Compaction, fusion, and functional activation of three-dimensional human mesenchymal stem cell aggregate. *Tissue Engineering Part A*, 21(9-10), pp.1705-1719.
226. Ullah, I., Subbarao, R.B. and Rho, G.J., 2015. Human mesenchymal stem cells-current trends and future prospective. *Bioscience reports*, 35(2), p.e00191.
227. Vallabhaneni, K.C., Penfornis, P., Dhule, S., Guillonneau, F., Adams, K.V., Mo, Y.Y., Xu, R., Liu, Y., Watabe, K., Vemuri, M.C. and Pochampally, R., 2016. Extracellular vesicles from bone marrow mesenchymal stem/stromal cells transport tumor regulatory microRNA, proteins, and metabolites. *Oncotarget*, 6(7), p.4953.
228. Van Deun, J., Mestdagh, P., Sormunen, R., Cocquyt, V., Vermaelen, K., Vandesompele, J., Bracke, M., De Wever, O. and Hendrix, A., 2014. The impact of disparate isolation methods for extracellular vesicles on downstream RNA profiling. *Journal of extracellular vesicles*, 3(1), p.24858.
229. Velasco-Velázquez, M.A., Homsí, N., De La Fuente, M. and Pestell, R.G., 2012. Breast cancer stem cells. *The international journal of biochemistry & cell biology*, 44(4), pp.573-577.
230. Vickers, P.J., Dickson, R.B., Shoemaker, R. and Cowan, K.H., 1988. A multidrug-resistant MCF-7 human breast cancer cell line which exhibits cross-resistance to antiestrogens and hormone-independent tumor growth in vivo. *Molecular Endocrinology*, 2(10), pp.886-892. 163.
231. Vishal, M., Swetha, R., Thejaswini, G., Arumugam, B. and Selvamurugan, N., 2017. Role of Runx2 in breast cancer-mediated bone metastasis. *International journal of biological macromolecules*, 99, pp.608-614.
232. Walker, N.D., Patel, J., Munoz, J.L., Hu, M., Guiro, K., Sinha, G. and Rameshwar, P., 2016. The bone marrow niche in support of breast cancer dormancy. *Cancer letters*, 380(1), pp.263-271.
233. Wang, J., Loberg, R. and Taichman, R.S., 2006. The pivotal role of CXCL12 (SDF-1)/CXCR4 axis in bone metastasis. *Cancer and Metastasis Reviews*, 25(4), pp.573-587.

234. Wang, L., Li, Y., Chen, X., Chen, J., Gautam, S.C., Xu, Y. and Chopp, M., 2002. MCP-1, MIP-1, IL-8 and ischemic cerebral tissue enhance human bone marrow stromal cell migration in interface culture. *Hematology*, 7(2), pp.113-117.
235. Wang, X. and Wei, Y., 2010. Erythrocytes kill cancer cells in vitro and inhibit tumor growth in vivo.
236. Waterman, R.S., Tomchuck, S.L., Henkle, S.L. and Betancourt, A.M., 2010. A new mesenchymal stem cell (MSC) paradigm: polarization into a pro-inflammatory MSC1 or an immunosuppressive MSC2 phenotype. *PloS one*, 5(4), p.e10088.
237. Weber, J.M. and Calvi, L.M., 2010. Notch signaling and the bone marrow hematopoietic stem cell niche. *Bone*, 46(2), pp.281-285.
238. Weigelt, B., Peterse, J.L. and Van't Veer, L.J., 2005. Breast cancer metastasis: markers and models. *Nature reviews cancer*, 5(8), p.591.
239. Welton, J.L., Webber, J.P., Botos, L.A., Jones, M. and Clayton, A., 2015. Ready-made chromatography columns for extracellular vesicle isolation from plasma. *Journal of extracellular vesicles*, 4(1), p.27269.
240. Wendt MK, Taylor MA, Schiemann BJ and Schiemann WP: Down-regulation of epithelial cadherin is required to initiate metastatic outgrowth of breast cancer. *Mol Biol Cell* 22: 2423- 2235, 2011.
241. Weng, Y.S., Tseng, H.Y., Chen, Y.A., Shen, P.C., Al Haq, A.T., Chen, L.M., Tung, Y.C. and Hsu, H.L., 2019. MCT-1/miR-34a/IL-6/IL-6R signaling axis promotes EMT progression, cancer stemness and M2 macrophage polarization in triple-negative breast cancer. *Molecular cancer*, 18(1), p.42.
242. Wenzel, C., Riefke, B., Gründemann, S., Krebs, A., Christian, S., Prinz, F., Osterland, M., Golfier, S., Råse, S., Ansari, N. and Esner, M., 2014. 3D high-content screening for the identification of compounds that target cells in dormant tumor spheroid regions. *Experimental cell research*, 323(1), pp.131-143.
243. Wilder, P.T., Weber, D.J., Winstead, A., Parnell, S., Hinton, T.V., Stevenson, M., Giri, D., Azemati, S., Olczak, P., Powell, B.V. and Odebode, T., 2018. Unprecedented anticancer activities of organorhenium sulfonate and carboxylato complexes against hormone-dependent MCF-7 and hormone-independent triple-negative MDA-MB-231 breast cancer cells. *Molecular and cellular biochemistry*, 441(1-2), pp.151-163.
244. Wu, J., Qu, Z., Fei, Z.W., Wu, J.H. and Jiang, C.P., 2017. Role of stem cell-derived exosomes in cancer. *Oncology letters*, 13(5), pp.2855-2866.

245. Wu, J., Qu, Z., Fei, Z.W., Wu, J.H. and Jiang, C.P., 2017. Role of stem cell-derived exosomes in cancer. *Oncology letters*, 13(5), pp.2856-2866.
246. Xu, Q., Wang, L., Li, H., Han, Q., Li, J., Qu, X., Huang, S. and Zhao, R.C., 2012. Mesenchymal stem cells play a potential role in regulating the establishment and maintenance of epithelial-mesenchymal transition in MCF7 human breast cancer cells by paracrine and induced autocrine TGF- β . *International journal of oncology*, 41(3), pp.959-968.
247. Yagi, H., Soto-Gutierrez, A., Kitagawa, Y. and Yarmush, M.L., 2012. Mesenchymal Stem Cell Therapy: Immunomodulation and Homing Mechanisms. In *Stem Cells and Cancer Stem Cells, Volume 8* (pp. 91-104). Springer Netherlands.
248. Yamane, K., Tateishi, K., Klose, R.J., Fang, J., Fabrizio, L.A., Erdjument-Bromage, H., Taylor-Papadimitriou, J., Tempst, P. and Zhang, Y., 2007. PLU-1 is an H3K4 demethylase involved in transcriptional repression and breast cancer cell proliferation. *Molecular cell*, 25(6), pp.801-812.
249. Yan, X.L., Fu, C.J., Chen, L., Qin, J.H., Zeng, Q., Yuan, H.F., Nan, X., Chen, H.X., Zhou, J.N., Lin, Y.L. and Zhang, X.M., 2012. Mesenchymal stem cells from primary breast cancer tissue promote cancer proliferation and enhance mammosphere formation partially via EGF/EGFR/Akt pathway. *Breast cancer research and treatment*, 132(1), pp.153-164.
250. Yáñez-Mó, M., Siljander, P.R.M., Andreu, Z., Bedina Zavec, A., Borràs, F.E., Buzas, E.I., Buzas, K., Casal, E., Cappello, F., Carvalho, J. and Colás, E., 2016. Biological properties of extracellular vesicles and their physiological functions. *Journal of extracellular vesicles*, 4(1), p.27066.
251. Yang EV, Bane CM, MacCallum RC, Kiecolt-Glaser JK, Malarkey WB, Glaser R. 2002. Stress-related modulation of matrix metalloproteinase expression. *J Neuroimmunol* 133:144 -150.
252. Yin, J.J., Selander, K., Chirgwin, J.M., Dallas, M., Grubbs, B.G., Wieser, R., Massagué, J., Mundy, G.R. and Guise, T.A., 1999. TGF- β signaling blockade inhibits PTHrP secretion by breast cancer cells and bone metastases development. *The Journal of clinical investigation*, 103(2), pp.197-206.
253. Yoon, M.K., Mitrea, D.M., Ou, L. and Kriwacki, R.W., 2012. Cell cycle regulation by the intrinsically disordered proteins p21 and p27.
254. Yoshitake, F., Itoh, S., Narita, H., Ishihara, K. and Ebisu, S., 2008. Interleukin-6 directly inhibits osteoclast differentiation by suppressing receptor activator of NF- κ B signaling pathways. *Journal of biological chemistry*, 283(17), pp.11535-11540.
255. Yu, Y., Xiao, C.H., Tan, L.D., Wang, Q.S., Li, X.Q. and Feng, Y.M., 2014. Cancer-associated fibroblasts induce epithelial-

- mesenchymal transition of breast cancer cells through paracrine TGF- β signalling. *British journal of cancer*, 110(3), p.724.
256. Zhang, X.H.F., Giuliano, M., Trivedi, M.V., Schiff, R. and Osborne, C.K., 2013. Metastasis dormancy in estrogen receptor-positive breast cancer. *Clinical Cancer Research*, 19(23), pp.6389-6397.
257. Zhang, X.H.F., Wang, Q., Gerald, W., Hudis, C.A., Norton, L., Smid, M., Foekens, J.A. and Massagué, J., 2009. Latent bone metastasis in breast cancer tied to Src-dependent survival signals. *Cancer cell*, 16(1), pp.67-78.
258. Zhou, X., Li, T., Chen, Y., Zhang, N., Wang, P., Liang, Y., Long, M., Liu, H., Mao, J., Liu, Q. and Sun, X., 2019. Mesenchymal stem cell derived extracellular vesicles promote the in vitro proliferation and migration of breast cancer cells through the activation of the ERK pathway. *International journal of oncology*, 54(5), pp.1843-1852.
259. Zimmermann, J. and McDevitt, T.C., 2018. Engineering the 3D MSC Spheroid Microenvironment to Enhance Immunomodulation. *Cytotherapy*, 20(5), p.S106.